A new analytical framework for tidal propagation in estuaries

A new analytical framework for tidal propagation in estuaries

Proefschrift

door

Huayang Cai

Master of Science in Physical Geography, Sun Yat-sen University, Guangzhou,
China
geboren te in Jinjiang, Fujian Province, China.

Dit proefschrift is goedgekeurd door de promotor:

Prof. dr. ir. H.H.G. Savenije

Samenstelling promotiecommissie:

Rector Magnificus,   voorzitter
Prof. dr. ir. H.H.G. Savenije,   Technische Universiteit Delft, promotor
Prof. dr. ir. Z.B. Wang,   Technische Universiteit Delft
Prof. dr. ir. J.A. Roelvink,   UNESCO-IHE Institute for Water Education
Prof. dr. ir. W.S.J. Uijttewaal, Technische Universiteit Delft
Prof. dr. H.E. de Swart,   University of Utrecht
Prof. dr. Leo C. van Rijn,   Deltares and University of Utrecht
Dr. M. Toffolon,   University of Trento
Prof. dr. ir. J.C. Winterwerp,   Technische Universiteit Delft, reservelid

To my parents

Preface

Most of the analytical theory developed to date for tidal wave propagation in a prismatic or convergent estuary requires linearization of the St. Venant equations, i.e., neglecting the inertial term, linearizing the friction term. The basic assumption then is that the tidal elevation and velocity can be described by simple harmonic waves, where the tidal amplitude and velocity amplitude vary exponentially along the estuary axis. The second fundamental assumption made for deriving analytical solution is that the tidally averaged flow depth and the friction is constant when tide propagates landward. Conversely, *Savenije* [1998, 2001, 2005, 2012] derived analytical solution based on the nonlinearized St. Venant equations in a Lagrangean reference frame, using the assumption that the water particle moves according to a simple harmonic. This theory leads to an analytical expression for the tidal damping by subtracting high water (HW) and low water (LW) envelopes that retained both the quadratic velocity in the numerator and the periodic variation of the hydraulic radius in the denominator. This thesis builds on this theory, refines it and compares it to other approaches. The first challenge was to compare the linear and quasi-nonlinear models. Fortunately, it appears that all the analytical approaches can be cast in the form of a set of four implicit dimensionless equations for the phase lag, the velocity amplitude, the damping, and the wave celerity (see Chapter 2). To explore different analytical models, a common theoretical framework has been proposed and the results show that the main difference between the examined models lies in the treatment of the friction term (see Chapter 3).

The second challenge was to analyse the asymptotic behaviour of the tidal damping, which is nonexistent in the linear theory since the tidal amplitude approaches zero for a damped wave and infinity for an amplified wave. A new explicit expression for the tidal amplitude as a function of distance has been proposed, where an asymptotic solution exists when distance approaches infinity, reflecting the balance between friction and channel convergence (see Chapter 4).

The investigation of how river discharge affects tidal damping is the third challenge in this thesis. The numerical simulations indicate that the residual water level slope can have a substantial influence on tidal damping when including the river discharge. However, this factor is seldom taken into account in analytical analysis. The analytical framework developed in Chapter 3 has been extended to account for the effect of river discharge, in which an iterative analytical method has been adopted to include the influence of the residual water level slope (Chapter 5).

It should be noted that the method presented in this thesis is not meant to replace linear theory since in practice all the analytical methods perform approximately well. The main purpose is to enhance our understanding of tidal wave propagation in estuaries and to provide a consistent analytical tool to describe this process. In this respect, the proposed method could be valuable from both the

scientific and practical point of view.

Huayang Cai
Delft, February 2014

Notation

The following symbols are used in this thesis:

a	convergence length of cross-sectional area [L]
$\overline{A}$	tidally averaged cross-sectional area of flow [L^2]
$\overline{A_0}$	tidally averaged cross-sectional area at the estuary mouth [L^2]
b	convergence length of width [L]
$\overline{B}$	width [L]
$\overline{B_0}$	tidally averaged width at the estuary mouth [L]
B_s	storage width [L]
c	wave celerity [L/T]
c_0	celerity of a frictionless wave in a prismatic channel [L/T]
c_{HW}	wave celerity at HW [L/T]
c_{LW}	wave celerity at LW [L/T]
d	convergence length of depth [L]
D	longitudinal dispersion coefficient [L^2/T]
D_0	longitudinal dispersion coefficient at the estuary mouth [L^2/T]
f	friction factor accounting for the difference in friction at HW and LW [-]
f_L	friction factor used for the derivation of linear damping equation [-]
F	quadratic friction term [-]
F	mass flux [M/T]
F_D	Dronkers' friction term accounting for river discharge [-]
F_G	Godin's friction term accounting for river discharge [-]
F_H	Hybrid friction term accounting for river discharge [-]
F_L	Lorentz's friction term accounting for river discharge [-]
$\widehat{F}_S$	effective friction term obtained with a Lagrangean-based approach [-]
g	acceleration due to gravity [L/T^2]
G_0, G_1, G_2, G_3	Godin's coefficients accounting for river discharge [-]
h	cross-sectional average depth [L]
$\overline{h}$	tidal average depth [L]
h_{ideal}	ideal depth [L]
$h_{critical}$	critical depth [L]
h_{HW}	depth at HW [L]
h_{LW}	depth at LW [L]
I_r	water level residual slope due to the density gradient [-]
H	tidal range [L]
I	tidally averaged water level slope [-]
I_b	bottom slope [-]
K	Manning-Strickler friction factor [L$^{1/3}$/T]
$\widehat{K}$	Van der Burgh's coefficient [-]

L	estuary length [L]
L	salt intrusion length [L]
L^*	salt intrusion length [-]
L_0, L_1	Lorentz's coefficients accounting for river discharge [-]
p_0, p_1, p_2, p_3	Chebyschev coefficients accounting for river discharge [-]
Q_f	river discharge [L^3/T]
Q	tidal discharge [L^3/T]
r_s	storage width ratio [-]
S	steady state salinity [M/L^3]
S^*	steady state salinity [-]
S_0	steady state salinity at the estuary mouth [M/L^3]
t	time [T]
t^*	time [-]
T	tidal period [T]
U	cross-sectional average flow velocity [L/T]
U^*	cross-sectional average flow velocity [-]
U_{HW}	tidal velocity at HW [L/T]
U_{LW}	tidal velocity at LW [L/T]
U_t	tidal velocity [L/T]
U_r	river velocity [L/T]
$U^{'}$	the maximum possible velocity in Godin's approach [L/T]
V_{HW}	velocity at HW [L/T]
V_{LW}	velocity at LW [L/T]
V	Lagrangean velocity for a moving particle [L/T]
x	distance from the estuary mouth [L]
x^*	distance from the estuary mouth [-]
z	tidal water level variation [L]
α	weight of the linearized friction term [-]
β	tidal Froude number [-]
γ	estuary shape number [-]
γ_b	estuary shape number accounting for width convergence [-]
γ_d	estuary shape number accounting for depth convergence [-]
Γ	damping parameter of quasi-nonlinear model [-]
Γ_L	damping parameter of linear model [-]
Γ_D	damping parameter of Dronkers' model [-]
Γ_G	damping parameter of Godin's model [-]
Γ_H	damping parameter of hybrid model [-]
δ	damping number [-]
δ_H	damping gradient [1/L]
ε	phase lag between HW and HWS (or LW and LWS) [-]
ζ	tidal amplitude to depth ratio [-]
ζ_{inf}	asymptotic tidal amplitude to depth ratio [-]
η	tidal amplitude [L]
η^*	tidal amplitude [-]
η_0	tidal amplitude at the estuary mouth [L]

θ	dimensionless term accounting for wave celerity not being equal at HW and LW [-]
κ	coefficient that include the effect of time-dependent depth in the friction term [-]
φ_z	phase of water level [-]
φ_U	phase of velocity [-]
λ	celerity number [-]
μ	velocity number [-]
μ_0	velocity number at the seaward boundary [-]
υ	tidal velocity amplitude [L/T]
υ^*	tidal velocity amplitude [-]
υ_{inf}	asymptotic velocity amplitude [L/T]
χ	friction number [-]
χ_0	reference friction number [-]
$\widehat{\chi_0}$	friction number at the seaward boundary [-]
ω	tidal frequency [1/T]
Δ	error term [1/L]
Δ'	error term [1/L]
Δx	length step [L]

Superscript/subscript

x^*	dimensionless variable
$\overline{x}$	tidally averaged variable
x_0	variable at the estuary mouth

Abbreviations:

LWS	Low water slack
HWS	High water slack
LW	Low water
HW	High water
TA	Tidal average

Contents

1

Introduction

Estuaries are of primary importance to humankind due to the fact that they are usually prominent locations for ports, industry, agriculture, recreation and urban development. In recent years, there has been an increasing concern about environmental degradation in estuaries as a result of human interventions, such as dredging for navigation, land reclamation, dam construction and fresh water withdrawal, which in turn has led to growing demands for developing rapid assessment techniques that assist policy maker and managers to make considered decisions for the protection and management of estuarine environment. However, before predictions about hydraulic responses to future changes can be made with any confidence, there is need to achieve an adequate understanding of tidal wave propagation in estuaries. Hence, in this thesis we restrict our attention to the development of physical understanding of tidal dynamics in estuaries, which are essential to assess the effects of these human interventions.

In particular, we focus on the tidal wave propagation in convergent estuaries, where the cross-sectional area varies as an exponential function along the estuary axis. This kind of estuarine geometry, observed in coastal plain estuaries all over the world including such widely-studied tidal estuaries as the Scheldt in the Netherlands, Thames in the U.K. and Delaware in the U.S.A., is similar to the shape of an ideal estuary as described by *Pillsbury* [1956a,b] and *Langbein* [1963], where there is no tidal damping (i.e., constant tidal amplitude and velocity amplitude) and the topographic convergence is just sufficient to balance the friction. If the effect of convergence is stronger than the effect of friction, the wave is amplified; if friction is stronger than convergence, the wave is damped.

1.1. Formulation of the Problem

The generic geometry of the idealized tidal channel of interest to this thesis is shown in Figure 1.1. We consider a tidal channel with varying width and depth and investigate the propagation of the tidal wave along an estuary with a fixed

bed, where the flow is mainly concentrated in a rectangular cross section, with a possible presence of lateral storage areas, described by the storage width ratio $r_S = B_S/\overline{B}$, i.e., the ratio between the storage width B_S and the stream width $\overline{B}$ (hereafter overbars denote tidal averages). The along channel variation in tidally averaged width $\overline{B}$ and depth $\overline{h}$ is assumed to be exponentially convergent[e.g. *Savenije*, 2005, 2012]:

$$\overline{B} = \overline{B_0} \exp\left(-\frac{x}{b}\right), \qquad \overline{h} = \overline{h_0} \exp\left(-\frac{x}{d}\right), \tag{1.1}$$

where x is the longitudinal coordinate directed landward, $\overline{B_0}$ and $\overline{h_0}$ are the tidally averaged width and depth at the estuary mouth, b and d are the convergence length of the width and depth, respectively. Similarly the tidally averaged cross-sectional area $\overline{A}$ can be expressed as

$$\overline{A} = \overline{A_0} \exp\left(-\frac{x}{a}\right), \tag{1.2}$$

where $\overline{A_0}$ is the cross-sectional area at the mouth and a is the convergence length for cross-sectional area, respectively, and the subscript 0 relates to the reference value at the estuary mouth. Since $\overline{A} = \overline{Bh}$ the relationship between these convergence lengths is $a = bd/(b + d)$.

We assume that the system is forced by a simple harmonic tidal wave (e.g., M_2) in the seaward boundary, with a possible presence of constant river discharge Q_f from the upstream boundary. In Figure 1.1b we see that the water levels along the estuary remain between two envelopes: one for high water (HW) and the other for low water (LW). It is worth noting that the mean water level does not coincide with mean sea level everywhere along the estuary due to the nonlinear terms from mass and momentum equations [*Vignoli et al.*, 2003].

1.2. Objective of This Thesis

The objective of this thesis is to enhance our understanding of tidal propagation in estuaries and to provide an analytical instrument to describe the tidal propagation process in a convergent estuary. The proposed analytical solutions are transparent and practical, allowing a quantitative and qualitative assessment of human interventions (e.g., dredging, flow reduction) on tidal dynamics. Moreover, they are rapid assessment techniques that enable the users to set up a simple model and to understand the functioning of the system with a minimum of information required.

It is important to note that there already exists a number of analytical solutions for tidal dynamics in estuaries (see Chapter 2 for a review). In this thesis we derive an analytical solution that differs from these earlier studies:

1. We concentrate on one dominant tidal constituent (e.g., M_2) without overtides (i.e, neglecting any tidal distortion), but develop an analytical model for reproducing the most relevant features of the tidal wave along the estuary (i.e., tidal amplitude, velocity amplitude, wave celerity, relative phase between elevation and velocity).

(a)

Tide

Storage areas Q_f

$\overline{B}_0$ $\overline{B}$ B_S

planimetric view

(b)

HW envelope

Mean water level

Ocean   River

Mean sea level

$\overline{h}_0$ $\overline{h}$ LW envelope

altimetric view

x

Figure 1.1: Sketch of an estuary: (a) planimetric view; (b) altimetric view.

It should be noted that the linear analytical solutions developed to date all concentrated on the propagation of one dominant tidal constituent (e.g., M_2), where the solutions for the tidal elevation (Z) and cross-sectionally averaged tidal velocity (U) at any location can be expressed by:

$$Z(x,t) = \eta(x)\cos(\omega t - kx), \quad U(x,t) = v(x)\cos(\omega t - kx - \phi), \quad (1.3)$$

where x is longitudinal coordinate measured in landward direction from the estuary mouth, t is time, η and v are the tidal elevation and velocity amplitude, ω and k are tidal frequency and wavenumber, and ϕ is the relative phase between tidal elevation and velocity. This means that the linear solutions only reproduce the tidal dynamics along the estuary for a single harmonic tidal constituent. However, as tide propagates along the estuary overtides can be generated due to the nonlinear terms in continuity and momentum equations [*Parker*, 1991].

On the contrary, in this thesis, building on earlier works by *Savenije* [1998,

1

2001, 2005, 2012], the analytical solutions are derived based on the full non-linearized St. Venant equations in a Lagrangean reference frame. The fundamental assumption we made for the flow characteristics is that the instantaneous flow velocity V for a moving particle can be described by a simple harmonic wave:

$$V = v(x)\sin(\omega t), \tag{1.4}$$

Based on this assumption, the mass and momentum equations can be rewritten in a Lagrangean way and are solved for the instance of high water (HW) and low water (LW), where a nonlinear damping equation can be obtained by subtracting HW and LW envelopes that retained both the quadratic velocity in the numerator and the periodic variation of the hydraulic radius (approximated by the depth) in the denominator. As a results, the derived analytical solutions aim at enabling to reproduce the most relevant features of the tidal wave along the estuary, which accounts for the nonlinear effects in the St Venant equations (e.g., overtides).

2. We adopt a multi-reach approach for accounting for the along-channel variations of friction and depth.

In linear theory, we also note that the solutions are usually derived for the entire estuary with an effective friction coefficient (i.e., hydraulic drag coefficient) and a constant averaged depth. This is mainly due to the fact that they have to neglect any variation of the friction and averaged depth when solving a second-order differential equation for one of the two unknowns in St Venant equations. However, in principle the friction along an estuary is a function of tidal amplitude and tidally averaged depth. The classical linear solution is valid locally or for a short reach where the friction and depth could be assumed constant. Hence a multi-reach approach has been adopted to follow variations of the estuarine sections along the estuary.

In this thesis, we demonstrated that analytical solutions to the one-dimensional St. Venant equations for the tidal hydrodynamics in convergent unbounded estuaries with negligible river discharge can be cast in the form of a set of four implicit dimensionless equations for phase lag, velocity amplitude, damping, and wave celerity, as a function of two localized parameters describing friction and convergence. With obtained damping gradient $\mathrm{d}\eta/\mathrm{d}x$, a tidal amplitude η_1 at a distance Δx (e.g., 1 km) upstream can be calculated by simple explicit integration of the damping number:

$$\eta_1 = \eta_0 + \frac{\mathrm{d}\eta}{\mathrm{d}x}\Delta x. \tag{1.5}$$

This process is repeated until the solutions for the whole estuary are obtained.

3. We develop an analytical model that takes into account the effect of river discharge and residual water level slope due to nonlinear friction.

1

It is noted that most of the analytical solutions for tidal dynamics were derived based on the assumption that the river discharge is negligible compared to the amplitude of the tidal discharge. This is not a restrictive assumption in the downstream part of an estuary since the cross-sectional area is large compared to the cross-sectional area in river [*Horrevoets et al.*, 2004]. However, as river discharge gains importance (such as in the upstream part of an estuary or during flood season), an analytical model that includes the effect of river discharge is required for further understanding of tidal process.

In this thesis we also extend the validity of the analytical model for tidal dynamics by including the effect of river discharge within a consistent framework. It is observed that the residual water level slope can have a substantial influence on tidal wave propagation when the effect of river discharge is remarkable (e.g., in Yangtze estuary)[*Cai et al.*, 2014]. An iterative analytical method has been developed to account for this factor, which significantly improves the model performance.

1.3. Outline of This Thesis

In this Chapter we briefly introduce the formulation of the problem and define the objective of this study. It also highlights the main differences between the proposed analytical model and the previous linear theory developed to date. The main results of the present thesis is divided into five parts: the similarity of the linear analytical solutions developed so far (Chapter 2), the new analytical framework for understanding tidal damping (Chapter 3), the asymptotic behaviour of tidal damping (Chapter 4), the influence of river discharge on tidal propagation (Chapter 5) and developing a coupled analytical model for analysing salt intrusion (Chapter 6). And conclusions and future research are drawn in Chapter 7.

In Chapter 2 a brief derivation of the localized linear solutions is presented, where four dimensionless equations are derived directly from the mass and momentum equations. We also compare analytical solutions of a wide range of authors and compare them within one consistent framework.

Chapter 3 presents one consistent analytical framework for understanding tidal damping in estuaries. A general solution procedure is proposed for the set of governing analytical equations expressed in dimensionless form. The different analytical solutions are then tested against fully nonlinear numerical results for a wide range of parameters and a new analytical expression for the tidal damping is derived. The new accurate relationship for the tidal damping is then exploited for a classification of estuaries. Finally, the new model is used to investigate the effect of depth variations on the tidal dynamics in 23 real estuaries, highlighting the usefulness of the analytical method to assess the influence of human interventions (e.g. by dredging) and global sea-level rise on the estuarine environment.

In Chapter 4 we investigate the asymptotic behaviour of tidal damping in the new analytical framework presented in Chapter 3. An explicit solution for the longitudinal tidal damping is proposed, in order to study the asymptotic behaviour when the friction is balanced by the channel convergence. The model is subsequently used

1

to explore the influence of deepening on tidal wave propagation and the asymptotic behaviour as increasing depth is studied.

Chapter 5 shows an extended analytical framework for tidal wave propagation when accounting for the effect of river discharge. We highlight the importance of residual water level slope on tidal wave propagation when including the effect of river discharge. The analytical solutions are compared with numerical results and the data from Modaomen and Yangtze estuaries are used to validate the new method.

In Chapter 6 we have developed a coupled analytical model (i.e., combining salt intrusion and hydrodynamics models) for analysing salt intrusion in estuaries. The coupled model has been applied to six estuaries in Malaysia, where we did measurements from June to August 2012 and February to March 2013 during the dry season at spring tide.

In Chapter 7 we summarize the main results from this thesis and elaborate on the possible future research.

2

Comparing different analytical solutions for tidal dynamics in convergent estuaries

Analytical solutions to the one-dimensional St. Venant equations for tidal hydrodynamics in convergent infinite estuaries with negligible river discharge can be cast in the form of a set of four implicit dimensionless equations for phase lag, velocity amplitude, damping, and wave celerity in terms of two independent parameters (describing friction and convergence). This method allows one to make comparisons among different analytical approaches by rewriting the solutions in this form. In this paper, classical and more recent formulations are compared, showing that the solutions correspond to each other apart from specific simplifications. The envelope method that subtracts the envelope expressions at high water and low water can be used to derive damping equations by exploiting different friction approximations for the friction term, which results in as many analytical solutions, and thereby building one consistent theoretical framework. Analysis of the asymptotic behaviour of the equations shows that an equilibrium tidal amplitude exists reflecting the balance between friction and channel convergence.

2.1. Introduction

Knowledge of tidal dynamics is essential to analyze the effect of human interventions, such as dredging for navigation, fresh water withdrawal, and design of regulation structures, in estuaries. Analytical tools are invaluable tools to assess the impact of such interventions as they provide direct insight in cause-effect relations that are generally nonlinear. Over time, a range of 1-D analytical solutions of

the tidal dynamics equations have been derived by: *Hunt* [1964], *Dronkers* [1964], *Ippen* [1966], *Jay* [1991], *Friedrichs and Aubrey* [1994], *Lanzoni and Seminara* [1998], *Savenije* [1992a, 1998, 2001, 2005, 2012], *Prandle* [2003], *Savenije and Veling* [2005], *Souza and Hill* [2006], *Savenije et al.* [2008], *Friedrichs* [2010], *Toffolon and Savenije* [2011], *Van Rijn* [2011], *Cai et al.* [2012a] and *Winterwerp and Wang* [2013]. The aim of this chapter is to compare all these analytical solutions that try to reproduce the main dynamics of tidal wave propagation along the estuary within one consistent theoretical framework. As a result, we aim to provide insight into the effects of tidal forcing and geometry on estuarine dynamics.

All analytical solutions in convergent estuaries developed to date invariably require assumptions to simplify the nonlinear set of St. Venant equations. Most researchers linearized the St. Venant equations by neglecting the inertial term, density term in the momentum equation and linearizing the friction term. For a simple harmonic wave, they also assumed that the tidal amplitude and velocity amplitude are damped or amplified exponentially along the estuary axis. It was demonstrated by *Cai et al.* [2012a] that many of the linear solutions are in fact identical since they solved the same set of differential equations by using the same assumptions. Unlike most researchers who derived the solutions in an Eulerian frame, *Savenije* [1998, 2001, 2005, 2012] derived expressions for the envelope curves of high water (HW) and low water (LW) in a Lagrangean reference frame to arrive at a tidal damping equation that retained the quadratic dependence of friction on velocity as well as the effect of the periodic variation of the hydraulic radius (we will term this as the 'envelope method' because of its peculiar derivation). After scaling the St. Venant equations, *Toffolon et al.* [2006] derived four dimensionless equations reflecting the phase lag, the tidal damping, and wave propagation and provided a fully explicit solution for tidal wave propagation by solving the set of four implicit equations. The approach was further developed by *Cai et al.* [2012a], who used different approximations to the friction term in the momentum equation and ended up with various damping equations using the envelope method.

Of course, analytical approaches to describe a real complex estuarine system comprise several limitations, like for instance the highly simplified geometry of the cross-section, the idealized planimetric shape, the assumption of small tidal amplitude, the neglect of Coriolis force and density gradients. Nevertheless, the advantages are many. First of all, the analytical equations provide direct insight into the effect of model forcing and geometry on system performance (e.g., to assess the effects of dredging on tidal dynamics). Second, they form a simple and rapid assessment tool in the preparation of a more complex numerical modeling exercise (e.g., to assess the possible outcome of a numerical model or to design the model setup). Finally, they can be very useful in setting up a monitoring program and to identify the most effective density and location of the monitoring network.

The chapter is organized as follows. In the next section, we describe the basic equations for the analytical solutions. In section 2.3, a general derivation of the classical linear solutions in convergent estuaries is presented and it is shown that the solutions can be obtained by solving a set of four implicit equations. A comparison of the different linear solutions is presented in section 2.4. In section 2.5 we presented

the quasi-nonlinear approach and hybrid solutions using the envelope method. In section 2.6 we analyze the asymptotic behavior of solutions reflecting the balance between friction and convergence. Finally, conclusions are drawn in section 2.7.

2.2. Formulation of the Problem

We consider a tidal channel with varying width and depth and investigate the propagation of the tidal wave along an estuary with a fixed bed. The conceptual sketch of the geometry of the idealized tidal channel is presented in Figure 2.1, together with a simplified picture of the periodic oscillations of water level and velocity defining the phase lag. In order to derive a simple analytical solution, we assume that the flow is concentrated in a main rectangular cross-section, with possible presence of lateral storage areas, described by the storage width ratio $r_s = B_s/\overline{B}$, i.e., the ratio between the storage width B_s and the stream width $\overline{B}$ (see Figure 2.1).
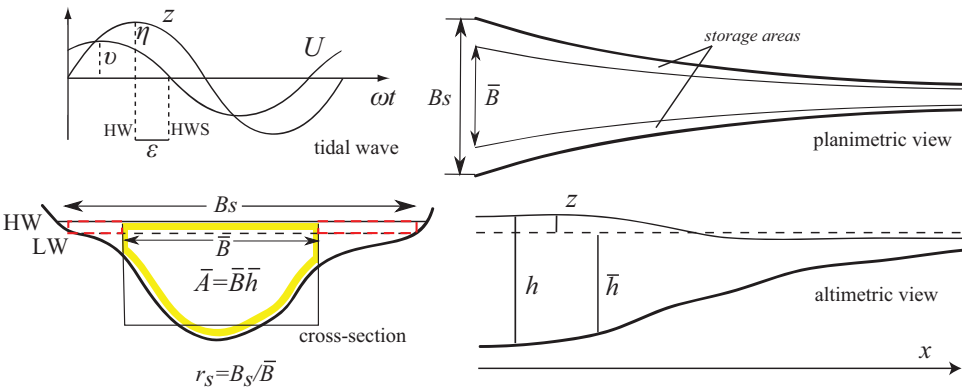
Figure 2.1: Sketch of the geometry of the idealized tidal channel and notation: tidal oscillations of water level z and velocity U and definition of the phase lag ε; definition of the equivalent rectangular cross-section of width $\overline{B}$, and of the total width B_s including storage areas; planimetric view of the estuary with storage areas; lateral view showing instantaneous and tidally averaged depth. Figure modified from *Savenije et al.* [2008].

The basic one-dimensional equations describing the tidal dynamics in an estuary are the continuity and momentum equations [e.g., *Savenije*, 2005], which read:

$$\frac{\partial U}{\partial t} + U\frac{\partial U}{\partial x} + g\frac{\partial h}{\partial x} + gI_b + gF + \frac{gh}{2\rho}\frac{\partial \rho}{\partial x} = 0\,, \tag{2.1}$$

$$r_s\frac{\partial z}{\partial t} + U\frac{\partial z}{\partial x} + h\frac{\partial U}{\partial x} - \frac{hU}{a} = 0\,, \tag{2.2}$$

where t is the time, U is the cross-sectional average flow velocity, h is the flow depth, g is the acceleration due to gravity, I_b is the bottom slope, ρ is the water density, z is the free surface elevation, a is the convergence length of cross-sectional area

2

defined in (1.2) and F is the friction term. The friction term is widely represented by:

$$F = \frac{U|U|}{K^2 h^{4/3}},\tag{2.3}$$

where K is the Manning-Strickler friction coefficient. The density gradient described by the last term in the left-hand side of equation (2.1) is often disregarded, but in the method of *Savenije et al.* [2008] it is retained.

The system is forced by a sinusoidal tidal wave with a tidal period T and a frequency $\omega = 2\pi/T$. As the wave propagates into the estuary, it has a wave celerity c, an amplitude of the tidal water level variation η, a tidal velocity amplitude v, and a phase lag ε, defined as the phase difference between high water (HW) and high water slack (HWS), or between low water (LW) and low water slack (LWS) due to the assumption of a simple harmonic solution (see Figure 2.1). For a simple harmonic wave, $\epsilon = \pi/2 - (\varphi_z - \varphi_U)$, where φ_z is the phase of water level and φ_U the phase of the tidal velocity. After scaling the continuity and momentum equations (2.1) and (2.2), five dimensionless variables can be found: the estuary shape number γ (representing the effect of depth and width convergence), the friction number χ (describing the role of the frictional dissipation), the velocity number μ (the actual velocity scaled with the frictionless value in a prismatic channel), the celerity number λ (the ratio between the theoretical frictionless celerity in a prismatic channel and the actual wave celerity), and the damping number for tidal amplitude δ (a dimensionless description of the increase, $\delta > 0$, or decrease, $\delta < 0$, of the tidal wave amplitude along the estuary) [*Toffolon et al.*, 2006; *Savenije et al.*, 2008], where γ and χ are the independent variables, while $\varepsilon, \mu, \lambda, \delta$ are the dependent variables. For further details on the scaling factors and the resulting dimensionless equations, readers can refer to *Savenije et al.* [2008]. These dimensionless variables are defined as:

$$\gamma = \frac{c_0}{\omega a},\tag{2.4}$$

$$\chi = r_s f \frac{c_0}{\omega \overline{h}} \zeta,\tag{2.5}$$

$$\mu = \frac{1}{r_s} \frac{v\overline{h}}{\eta c_0},\tag{2.6}$$

$$\lambda = \frac{c_0}{c},\tag{2.7}$$

$$\delta = \frac{1}{\eta} \frac{d\eta}{dx} \frac{c_0}{\omega},\tag{2.8}$$

where c_0 is the classical wave celerity of a frictionless progressive wave, $\overline{h}$ is the tidal average depth of flow, f is the dimensionless friction factor and ζ is the dimensionless tidal amplitude defined as:

$$c_0 = \sqrt{g\bar{h}/r_s},\tag{2.9}$$

$$f = \frac{g}{K^2\bar{h}^{-1/3}}\left[1-\left(\frac{4}{3}\zeta\right)^2\right]^{-1},\tag{2.10}$$

$$\zeta = \frac{\eta}{\bar{h}}.\tag{2.11}$$

In equation (2.10), the periodic effect of depth variation during the tidal cycle has been taken into account through the factor indicated between square brackets, which results from the subtraction of the envelopes at HW and LW. This additional friction factor is a property of the envelope method [e.g., *Savenije*, 2005], which traditional linearization methods do not have. For small value of tidal amplitude to depth ratio ($\zeta \ll 1$), this property is less important.

2.3. The Classical Linear Solutions

2.3.1. Basic Equations

The tidal dynamics in an alluvial estuary with possible presence of intertidal flats may be approximated by the following linearized equations [e.g. *Toffolon and Savenije*, 2011]:

$$r_S\frac{\partial h}{\partial t} + U\frac{\partial h}{\partial x} + h\frac{\partial U}{\partial x} + \frac{hU}{B}\frac{dB}{dx} = 0,\tag{2.12}$$

$$\frac{\partial U}{\partial t} + g\frac{\partial z}{\partial x} + F_L = 0,\tag{2.13}$$

where g the gravity acceleration and F_L is the linearized friction term using Lorentz's method [*Lorentz*, 1926]. The linearization of friction term is widely represented by:

$$F_L = \frac{8}{3\pi}f_L\frac{v}{\bar{h}}U,\tag{2.14}$$

where f_L is a dimensionless friction factor, defined as:

$$f_L = \frac{g}{K^2\bar{h}^{-1/3}},\tag{2.15}$$

It should be noted that the water level variation can be expressed as $z = h - \bar{h}$. In the case of small tidal amplitude (i.e., $z \ll \bar{h}$), it is possible to find:

$$U\frac{\partial h}{\partial x} = U\frac{\partial\left(z+\bar{h}\right)}{\partial x} = U\frac{\partial z}{\partial x} + \frac{\bar{h}U}{\bar{h}}\frac{\partial\bar{h}}{\partial x} \approx U\frac{\partial z}{\partial x} + \frac{hU}{\bar{h}}\frac{\partial\bar{h}}{\partial x},\tag{2.16}$$

where the last equality only applies for small value of $z/\bar{h}$. Substituting equation (2.16) into (2.12) and making use of equation (1.2), the following equation is obtained:

$$r_S\frac{\partial z}{\partial t} + U\frac{\partial z}{\partial x} + h\frac{\partial U}{\partial x} - \frac{hU}{a} = 0,\tag{2.17}$$

which has the advantage that the depth convergence is implicitly taken into account by the convergence of the tidally averaged cross-sectional area. The nonlinear term $U \partial z / \partial x$ is negligible with respect to the following term in the case of small tidal amplitude. Thus equation (2.17) finally modifies into

$$r_S \frac{\partial z}{\partial t} + h \frac{\partial U}{\partial x} - \frac{hU}{a} = 0. \tag{2.18}$$

2.3.2. Scaling the Equations

We introduce a scaling on equations (2.13) and (2.18), similar to that used by *Savenije et al.* [2008], to derive the dimensionless equations, the asterisk superscript denoting dimensionless variables:

$$U^* = U/v_0, h^* = h/\overline{h}, z^* = z/\eta_0, x^* = x \frac{2\pi}{L}, t^* = t \frac{2\pi}{T}, \tag{2.19}$$

where η_0 and v_0 are the tidal amplitude and velocity amplitude at the estuary mouth, L is the wavelength and T is the tidal period. Note that the scaling of tidal flow velocity and water level fluctuation are slightly different from the scaling used by *Savenije et al.* [2008] because they are scaled with the corresponding values at the estuary mouth. For an infinite length estuary, the velocity amplitude and the tidal amplitude are proportional:

$$\frac{1}{v} \frac{\partial v}{\partial x} = \frac{1}{\eta} \frac{\partial \eta}{\partial x}, \tag{2.20}$$

which implies that the ratio of the velocity amplitude to the tidal amplitude is constant:

$$\frac{v}{\eta} = \frac{v_0}{\eta_0}. \tag{2.21}$$

Making use of the assumption (2.21), equations (2.13) and (2.18) may then be rewritten as:

$$\frac{\partial U^*}{\partial t^*} + \left(\frac{g \eta T}{vL} \right) \frac{\partial z^*}{\partial x^*} + \left(\frac{8}{3\pi} \frac{v T f_L}{2\pi \overline{h}} \right) U^* = 0, \tag{2.22}$$

$$\frac{\partial z^*}{\partial t^*} + \left(\frac{\overline{h} v T}{\eta L r_S} \right) h^* \frac{\partial U^*}{\partial x^*} - \left(\frac{\overline{h} v T}{2\pi \eta a r_S} \right) h^* U^* = 0. \tag{2.23}$$

The real scales of velocity amplitude v and the wavelength L are scaled with the corresponding values for a frictionless tidal wave in a channel with zero convergence (U_0, L_0) as a reference:

$$v = U_0 \mu, \tag{2.24}$$

$$L = L_0 / \lambda, \tag{2.25}$$

where the dimensionless velocity number μ and celerity number λ are defined in (2.6) and (2.7), respectively.

For the case of frictionless estuary with zero convergence, the velocity amplitude U_0 and the wavelength L_0 are:

$$U_0 = \zeta c_0 r_S, \tag{2.26}$$

$$L_0 = c_0 T. \tag{2.27}$$

Assuming $h^* = 1$ (i.e., $h = \bar{h}$) in the continuity equation (2.23), then the dimensionless equations (2.22) and (2.23) read:

$$\frac{\partial U^*}{\partial t^*} + \frac{\lambda}{\mu} \frac{\partial z^*}{\partial x^*} + \frac{8}{3\pi} \mu \chi U^* = 0, \tag{2.28}$$

$$\frac{\partial z^*}{\partial t^*} + \mu \lambda \frac{\partial U^*}{\partial x^*} - \mu \gamma U^* = 0, \tag{2.29}$$

where the dimensionless parameters χ and γ have been introduced as the friction number (2.5) and estuary shape number (2.4), respectively.

2.3.3. Analytical Solutions of the Linearized Equations

Concentrating on the propagation of one predominant tidal constituent (e.g., M_2), the solution can be expressed as:

$$U^* = V^* \exp(it^*), z^* = A^* \exp(it^*), \tag{2.30}$$

where V^*, A^*, and i are the complex amplitude of the velocity, the complex amplitude of the tidal elevation, and the unit imaginary number $\sqrt{-1}$, respectively.

Substituting equation (2.30) into (2.28) and (2.29) yields:

$$iV^* + \frac{\lambda}{\mu} \frac{\partial A^*}{\partial x^*} + \frac{8}{3\pi} \chi \mu V^* = 0, \tag{2.31}$$

$$iA^* + \mu \lambda \frac{\partial V^*}{\partial x^*} - \mu \gamma V^* = 0. \tag{2.32}$$

We introduce the well-known fundamental solutions for a simple harmonic wave, i.e., assuming a solution that is the real part of:

$$A^*(x^*) = \exp(\delta x^*/\lambda) \exp(-ix^*), \tag{2.33}$$

$$V^*(x^*) = \exp(\delta x^*/\lambda) \exp[-i(x^* + \varphi)], \tag{2.34}$$

where ϕ is the relative phase between tidal elevation and velocity. Substituting equations (2.33) and (2.34) into equations (2.28) and (2.29) gives the following for momentum and continuity:

$$\frac{\exp(i\varphi)}{\mu} = \frac{-\lambda + 8\mu\chi\delta/(3\pi)}{-\lambda^2 - \delta^2} + i \frac{\delta + 8\mu\chi\lambda/(3\pi)}{-\lambda^2 - \delta^2}, \tag{2.35}$$

$$\frac{\exp(i\varphi)}{\mu} = \lambda + i(\delta - \gamma). \tag{2.36}$$

One can separately balance the real and imaginary parts to derive:

$$\frac{-\lambda + 8\mu\chi\delta/(3\pi)}{-\lambda^2 - \delta^2} = \lambda, \tag{2.37}$$

$$\frac{\delta + 8\mu\chi\lambda/(3\pi)}{-\lambda^2 - \delta^2} = \delta - \gamma. \tag{2.38}$$

Multiplying equation (2.37) by λ and equation (2.38) by δ, and adding them together, we end up with:

$$\lambda^2 = 1 - \delta(\gamma - \delta). \tag{2.39}$$

Similarly, multiplying equation (2.37) by δ and equation (2.38) by λ, and adding them together, we obtain the following equation:

$$\delta = \frac{\gamma}{2} - \frac{4}{3\pi}\frac{\chi\mu}{\lambda}. \tag{2.40}$$

Using the identity $\exp(i\phi) = \cos(\phi) + i\sin(\phi)$, the phase of velocity relative to elevation is seen from equation (2.36) to be:

$$\tan(\varphi) = \frac{\delta - \gamma}{\lambda}. \tag{2.41}$$

From equation (2.36) it also follows that:

$$\mu = \cos(\varphi)/\lambda = \sin(\varphi)/(\delta - \gamma). \tag{2.42}$$

The phase lag between high water slack (HWS) and high water (HW) (or low water slack (LWS) and low water (LW)) for a simple harmonic wave is $\epsilon = \pi/2 + \phi$, such that equations (2.41) and (2.42) can be rearranged respectively to become

$$\tan(\epsilon) = \frac{\lambda}{\gamma - \delta}, \tag{2.43}$$

$$\mu = \frac{\sin(\epsilon)}{\lambda} = \frac{\cos(\epsilon)}{\gamma - \delta}. \tag{2.44}$$

We can see that equations (2.43) and (2.44) are derived from the continuity equation, while equations (2.39) and (2.40) are obtained from the combination of continuity and momentum equations.

Equations (2.39), (2.40), (2.43) and (2.44) represent a set of four implicit equations, which can be solved by an iterative numerical method (e.g., a simple Newton-Raphson method). Making use of the trigonometric equation $[\cos(\epsilon)]^{-2} = 1 + [\tan(\epsilon)]^2$, equations (2.43) and (2.44) can be combined to eliminate the variable ϵ to give:

$$(\gamma - \delta)^2 = \frac{1}{\mu^2} - \lambda^2. \tag{2.45}$$

Then the four equations reduce to three. Table 2.1 presents the linear solutions for the general case as well as for some particular cases: frictionless ($\chi = 0$, both with subcritical convergence, $\gamma < 2$, and supercritical convergence, $\gamma \geq 2$), constant cross section ($\gamma = 0$) and ideal estuary ($\delta = 0$). Similar results are derived by *Toffolon and Savenije* [2011]. Figure 2.2 shows the variation of the dependent dimensionless parameters obtained by solving the set of equations (2.39), (2.40) and (2.45) as a function of the estuary shape number γ and the friction number χ.

Table 2.1: Classical linear solutions of tidal wave propagation

Case	Phase lag $\tan(\epsilon)$	Scaling μ	Damping δ	Celerity λ^2
General	$\lambda/(\gamma-\delta)$	$\sin(\epsilon)/\lambda = \cos(\epsilon)/(\gamma-\delta)$	$\gamma/2 - 4\chi\mu/(3\pi\lambda)$	$1-\delta(\gamma-\delta)$
Frictionless ($\gamma < 2$)	$\sqrt{4/\gamma^2 - 1}$	1	$\gamma/2$	$1 - \gamma^2/4$
Frictionless ($\gamma \geq 2$)	0	$(\gamma - \sqrt{\gamma^2-4})/2$	$(\gamma - \sqrt{\gamma^2-4})/2$	0
Constant cross section	$-\lambda/\delta$	$\sin(\epsilon)/\lambda = -\cos(\epsilon)/\delta$	$-4\chi\mu/(3\pi\lambda)$	$1+\delta^2$
Ideal estuary	$1/\gamma$	$\sqrt{1/(1+\gamma^2)} = 3\pi\gamma/(8\chi)$	0	1

2.4. Similarity of Different Linear Solutions

Hunt's approach

Hunt [1964] was one of the first to consider tidal wave propagation in estuaries characterized by width convergence with constant or variable depth. It is worth noting that equations (2.31) and (2.32) can be combined into a single, second-order differential equation and rearranged to form separate expressions for either A^* or V^*. The expressions for the tidal amplitude A* and velocity amplitude V* are then as follows:

$$\frac{\partial^2 A^*}{\partial x^{*2}} - \frac{\gamma}{\lambda}\frac{\partial A^*}{\partial x^*} + \frac{1 - i\widehat{\chi}}{\lambda^2}A^* = 0, \tag{2.46}$$

$$\frac{\partial^2 V^*}{\partial x^{*2}} - \frac{\gamma}{\lambda}\frac{\partial V^*}{\partial x^*} + \frac{1 - i\widehat{\chi}}{\lambda^2}V^* = 0, \tag{2.47}$$

with

$$\widehat{\chi} = 8\chi\mu/(3\pi). \tag{2.48}$$

Equations (2.46) and (2.47) can be solved if the coefficients are constant. This means that we have to neglect any variation of the parameters γ, λ, and $\widehat{\chi}$ along the longitudinal coordinate x^*. Since equations (2.46) and (2.47) are identical except dependent variable, we can solve either of them analytically, leading to:

$$c_1 \exp\left[\left(\gamma/2 + \sqrt{\gamma^2/4 - 1 + i\widehat{\chi}}\right)x^*/\lambda\right] + c_2 \exp\left[\left(\gamma/2 - \sqrt{\gamma^2/4 - 1 + i\widehat{\chi}}\right)x^*/\lambda\right], \tag{2.49}$$

where c_1 and c_2 are two constants.

For an infinite length estuary with no landward boundary condition, applying the seaward boundary condition $A^* = 1$ at $x^* = 0$, the solution is then given by:

$$c_1 = 0, c_2 = 1, \tag{2.50}$$

which suggests that there is no reflective wave.

The expressions for the main dependent dimensionless parameters have been derived by *Toffolon and Savenije* [2011] and can be summarized as follows:

$$\tan(\varphi) = \frac{\gamma\kappa + 2\kappa^2}{\widehat{\chi}}, \tag{2.51}$$

$$\mu = \frac{1}{\sqrt{1 + \gamma\kappa + 2\kappa^2}}, \tag{2.52}$$

2
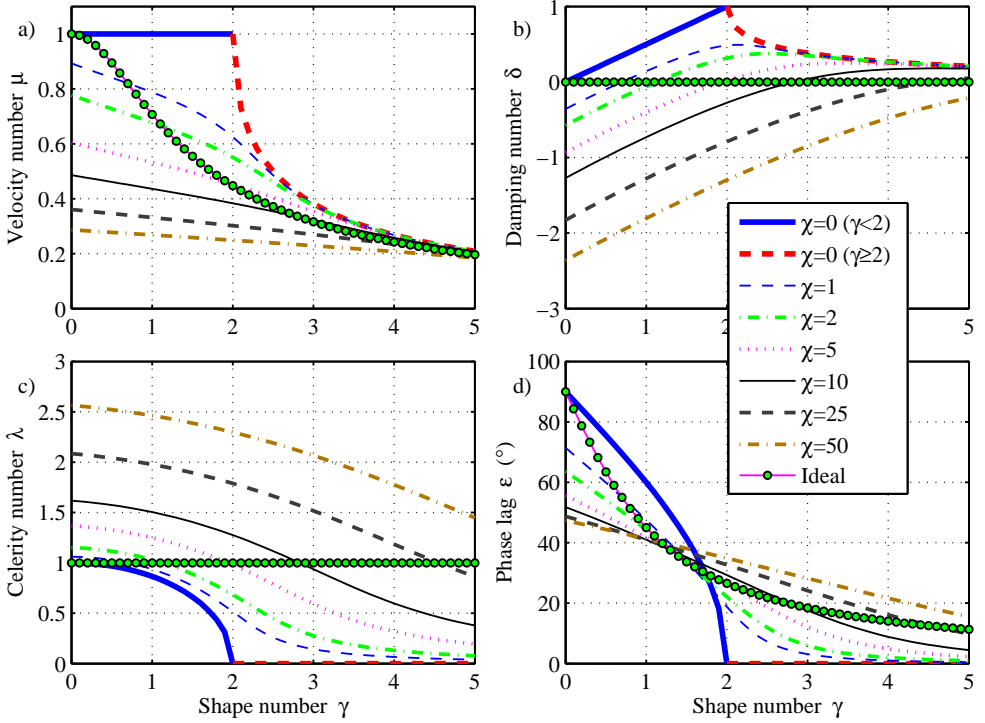
Figure 2.2: Relationship between the main dimensionless parameters and the estuary shape number γ obtained by solving equations (2.38), (2.39) and (2.44) for different values of the friction number χ.

$$\delta = \frac{\gamma}{2} - \kappa, \tag{2.53}$$

$$\lambda^2 = \kappa^2 + \Gamma, \tag{2.54}$$

with

$$\kappa = \sqrt{\frac{\Omega - \Gamma}{2}}, \Omega = \sqrt{\Gamma^2 + \widehat{\chi}^2}, \Gamma = 1 - \left(\frac{\gamma}{2}\right)^2. \tag{2.55}$$

It is important to note that equations (2.51)–(2.54) are implicit equations because of $\widehat{\chi}$ as a function of μ. Unlike *Toffolon and Savenije* [2011] who made use of an iterative refinement to determine the friction, Hunt assumed $\widehat{\chi}$ as a constant ($\widehat{\chi} = \chi$). Consequently, Hunt's solution can be directly obtained from equations (2.51)–(2.54), which corresponds to the model of "lin0" by *Toffolon and Savenije* [2011].

The analytically determined dimensionless parameters, both without and with an iterative procedure to determine the friction, are presented in Figure 2.3. It can be seen that the deviation between the model assuming constant friction and the

model using an iterative refinement to determine the correct friction becomes large as friction increases.
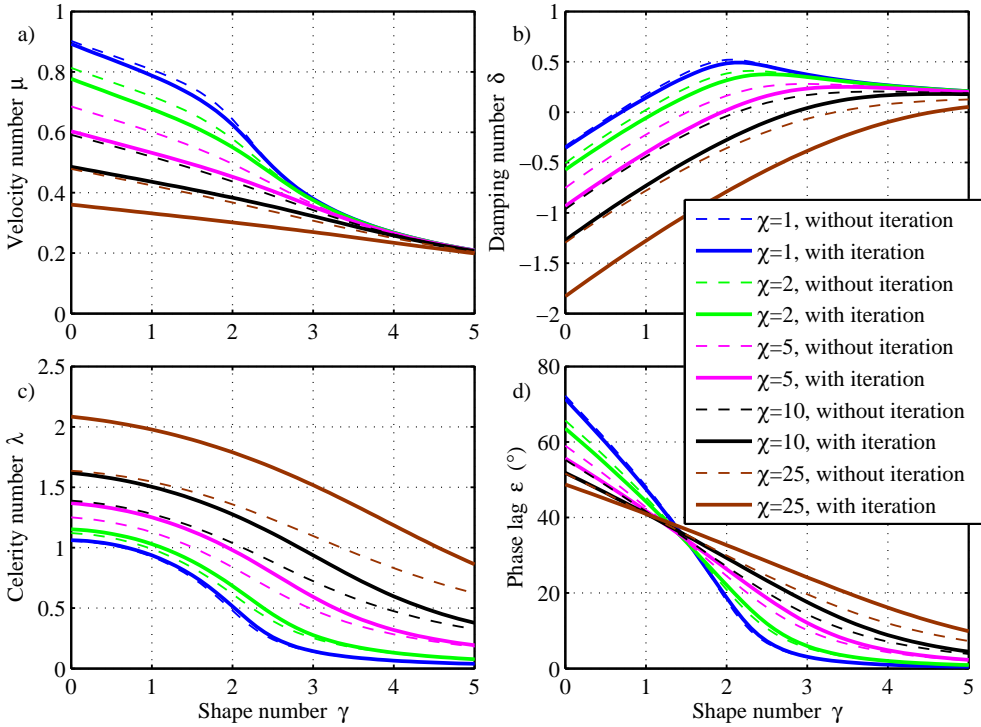
Figure 2.3: The main dimensionless parameters obtained with different analytical models. The dashed lines represent the model using constant friction ($\hat{\chi}=\chi$), while the drawn lines indicate the model exploiting an iterative procedure to determine the friction.

Analytical solutions for exponentially converging channels with constant depth derived by *Prandle and Rahman* [1980] and *Prandle* [1985] have large similarities with Hunt's approach with regard to considering constant friction.

Pillsbury's approach

Pillsbury [1956a,b] provided a particular solution for an 'ideal' estuary, where the tidal amplitude, velocity amplitude and depth are uniform through the entire channel. In this case, the width reduces in an upstream direction as an exponential function:

$$\overline{B} = \overline{B_0} \exp[-kx \cot(\epsilon)], \tag{2.56}$$

and the velocity amplitude v and wave celerity c are given by:

$$v = \frac{\eta g}{c} \sin(\epsilon), c = \frac{\omega}{k} = \sqrt{g\overline{h}}. \tag{2.57}$$

After some algebra and making use of the dimensionless parameters, equations (2.56) and (2.57) appear to be identical to (1.1) and (2.44) for an ideal estuary (see Table 2.1). In an ideal estuary, the increase in tidal amplitude due to channel convergence in width is just sufficient to balance the tidal damping due to friction [*Langbein*, 1963].

Ippen's approach

Ippen [1966] derived analytical solutions of the linearized St. Venant equations for a prismatic estuary (i.e., constant depth and width) both with and without friction. In a frictionless, prismatic channel of rectangular cross-section, the one-dimensional St. Venant equations for tidal elevation (H) reduce to a basic wave equation:

$$\frac{\partial^2 z}{\partial t^2} = c_0 \frac{\partial^2 z}{\partial x^2}.$$

(2.58)

For an estuary of infinite length, equation (2.58) produces a progressive wave solution with $c = c_0$ (hence $\lambda = 1$) and the relative phase between tidal elevation and velocity is 0 (hence $\epsilon = \pi/2$). Without considering the effect of channel convergence and friction, the system becomes an ideal estuary (hence $\delta = 0$) and the velocity amplitude is given by $\upsilon = (\eta/\bar{h})c_0$ (hence $\mu = 1$). As a result, we can see that Ippen's analytical solution for a frictionless, prismatic channel of infinite length corresponds to the frictionless solution presented in Table 2.1 in the case of $\gamma = 0$.

Ippen [1966] also provided solutions to (2.58) for channel closed at one end, characterized by incident and reflected waves of equal amplitude. The result is a standing wave of maximum amplitude at antinodes and of zero amplitude at nodes. However, the relative phase between tidal elevation and velocity can be shown to be close to 90° time angle in many short estuaries without the need to explicitly include a classical reflected wave [*Hunt*, 1964; *Wright et al.*, 1973]. In fact, as shown in Table 2.1 and Figure 2.2, it is possible to predict realistic solutions in these short estuaries using a single incident wave without the explicit presence of a reflected wave by including both friction and the channel convergence of the cross-sectional area.

Ippen [1966] then used Green's Law [*Green*, 1837] to examine tides in channels of gradually varying cross-section. In particular, the solution of tidal amplitude for the channel of constant depth with exponential variation of width is given by:

$$\eta = \eta_0 \exp\left(\frac{1}{2a}x\right),$$

(2.59)

which corresponds to the damping equation in the frictionless ($\gamma < 2$) case presented in Table 2.1. However, *Ippen* [1966] did not provide the solutions of velocity amplitude, wave celerity and phase lag, which are presented in Table 2.1.

In his review of tidal dynamics in estuaries, *Ippen* [1966] also discussed the more 'realistic' case of tidal wave propagation in a prismatic channel which includes the effect of friction. In a channel of infinite length, the tidal amplitude decays

exponentially along the estuary axis where the damping number δ is described by:

$$\left(\frac{\omega}{c_0}\right)^2 = \left(\frac{\omega}{c}\right)^2 - \left(-\delta\frac{\omega}{c_0}\right)^2,$$ (2.60)

which is the celerity equation for the constant cross-section channel presented in Table 2.1. Substitution of equation (2.60) into the following equation

$$\frac{g}{\omega}\frac{8}{3\pi}\frac{\upsilon}{K^2\overline{h}^{-4/3}} = \tan(-2\varphi) = -2\frac{\delta\omega/c_0}{\omega/c}\frac{1}{1 - \left[(\delta\omega/c_0)/(\omega/c)\right]},$$ (2.61)

yields the damping equation of constant cross-section channel presented in Table 2.1. The phase of velocity relative to elevation is described by:

$$\tan(-\varphi) = (\delta\omega/c_0)/(\omega/c),$$ (2.62)

and the velocity amplitude is given by:

$$\upsilon = \frac{\eta}{h}c_0\frac{\omega/c_0}{\sqrt{(-\delta\omega/c_0)^2 + (\omega/c)^2}},$$ (2.63)

which correspond to the phase lag equation and scaling equation of constant cross-section channel presented in Table 2.1, respectively.

Jay's approach

Jay [1991] revisited Green's law on tidal propagation in strongly convergent by including the effects of friction, channel convergence, finite amplitude, river flow and tidal flats adjacent to the main channel. Two analytical solutions were then derived: the former applied to weakly dissipative estuaries where the effects of acceleration and topographic convergence are dominant over friction in determining the complex wave number; the latter concerns strongly dissipative estuaries where friction controls the wave number. Both solutions change character at the defined "critical convergence" such that the effect of acceleration and topography balanced exactly in his wavenumber equation [*Jay*, 1991, equation 22]. In this case, the complex wave number is given to lowest order by:

$$q = \frac{\omega}{c} + i\frac{1}{\eta}\frac{d\eta}{dx},$$ (2.64)

with

$$\frac{\omega}{c} = -\frac{1}{\eta}\frac{d\eta}{dx} = \frac{\omega}{c_0\sqrt{2\omega K^2\overline{h}^{-4/3}/(pg\upsilon)}},,$$ (2.65)

where the coefficient p is derived from the Tschebyschev coefficient, and the velocity amplitude is scaled as:

$$\upsilon = \frac{\eta}{h}c_0.$$ (2.66)

Substituting the dimensionless parameters presented in Section 3 into equations (2.64)-(2.66) gives to the following solutions:

$$\delta = -\lambda, \lambda = \sqrt{p\chi\mu/2}, \mu = 1. \tag{2.67}$$

Friedrichs' approach

Friedrichs and Aubrey [1994] considered tidal propagation in strongly convergent estuaries and provided simple first and second order analytical solutions, which diverge markedly from classical views of co-oscillating tides. The solution of the first order is of negligible amplification for the tidal wave and has a relative phase between velocity and elevation of 90 degree time angle, in which the velocity amplitude and wave celerity are given by:

$$v = a\omega\eta/\overline{h}, \tag{2.68}$$

$$c = \omega/k = \frac{3\pi}{8}\frac{c_0^2 \overline{h}}{fva}, \tag{2.69}$$

The first order solutions for velocity amplitude (2.68) and wave celerity (2.69) were then used in the derivation of second-order solution, where the dominant tidal component is a uni-directional wave with an amplitude that is exponentially modulated. The amplitude growth factor is presented as follows:

$$\frac{1}{\eta}\frac{d\eta}{dx}\frac{c}{\omega} = \frac{3\pi}{8}\frac{\omega\overline{h}}{fv} - \frac{\omega a}{c} = \frac{\omega a}{c}\left[\left(\frac{c}{c_0}\right)^2 - 1\right], \tag{2.70}$$

while the phase lag between HW and HWS is given by:

$$\epsilon = \frac{\omega}{c}a. \tag{2.71}$$

Making use of the dimensionless parameters defined in Section 3, equations (2.68)–(2.71) can be scaled resulting in the following set of dimensionless equations:

$$\mu = 1/\gamma, \lambda = 8\mu\chi/(3\pi\gamma), \lambda^2 = 1 - \gamma\delta, \epsilon = \lambda/\gamma. \tag{2.72}$$

After some algebra, (2.72) can be cast in the form of analytical solutions of the four dependent parameters (μ, δ, λ and ϵ) as functions of the shape number γ and friction number χ:

$$\mu = 1/\gamma, \delta = \left(-64\chi^2 + 9\gamma^4\pi^2\right)/\left(9\gamma^5\pi^2\right), \lambda = (8\chi)/(3\gamma^2\pi), \epsilon = (8\chi)/(3\gamma^3\pi). \tag{2.73}$$

It is worth noting that the set of equations (2.72) is a simplified version of our linearized solutions with vanishing amplification (small δ) and strong convergence of cross-sectional area (big γ, hence small ϵ), because *Friedrichs and Aubrey* [1994] used perturbation analysis where the scaled equations are simplified by neglecting higher-order terms. The analytically computed dependent dimensionless parameters based on equation (2.73) as a function of estuary shape number γ is shown

in Figure 2.4. We can see that, as the shape number γ increases, the solutions (2.73) suggests that the velocity number μ, celerity number λ and the phase lag ϵ decrease until zero is reached asymptotically, while the damping number is approaching zero. The asymptotic case is identical to a frictionless standing wave system (see Table 2.1).
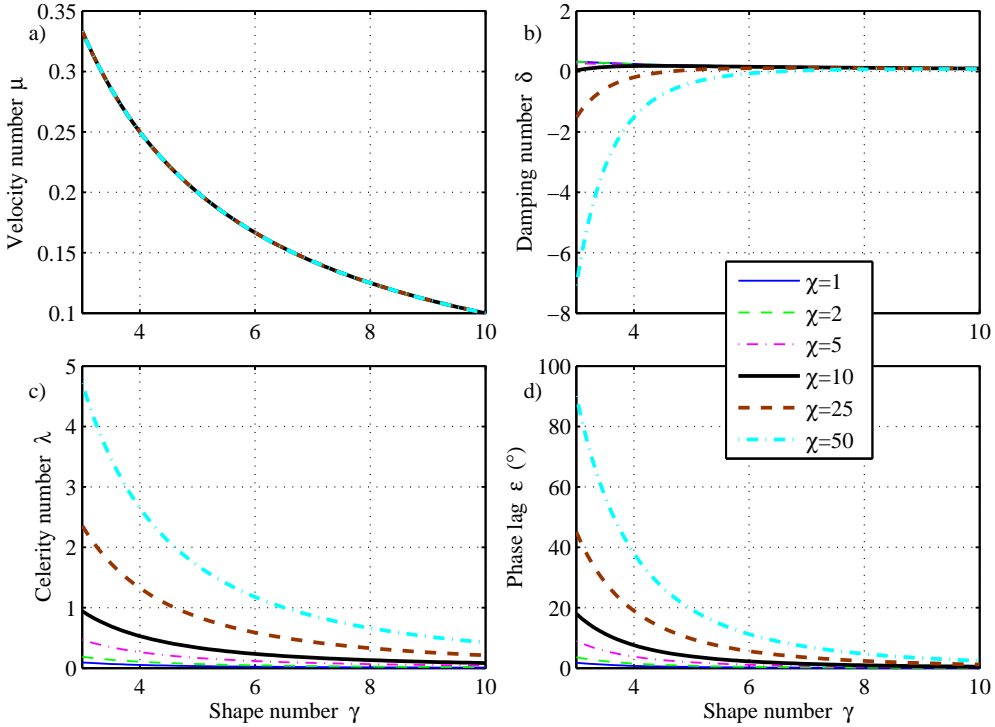
Figure 2.4: Variation of the dimensionless parameters obtained with equation (2.72) as a function of estuary shape number γ for given values of friction number χ.

Friedrichs [2010] again used perturbation analysis to simplify the governing equations for a wide range of channelized estuaries. In particular, he solved the linearized St. Venant equations by including the effect of width convergence based on the assumption that the tidal amplitude and velocity amplitude along the estuary axis can be described by exponential functions. The general solutions can be described by the following four dimensional equations:

$$\frac{c^2}{(gh/r_S)} = \frac{3\pi}{8} \frac{\omega \overline{h}}{f\upsilon} \left(\frac{c}{a\omega} - 2\frac{1}{\eta}\frac{\mathrm{d}\eta}{\mathrm{d}x}\frac{c}{\omega} \right), \tag{2.74}$$

$$\frac{c^2}{(gh/r_S)} = 1 + \frac{c}{\omega a}\frac{1}{\eta}\frac{\mathrm{d}\eta}{\mathrm{d}x}\frac{c}{\omega} - \left(\frac{1}{\eta}\frac{\mathrm{d}\eta}{\mathrm{d}x}\frac{c}{\omega} \right)^2, \tag{2.75}$$

$$\varphi = -\arctan\left(\frac{c}{\omega a} - \frac{1}{\eta}\frac{d\eta}{dx}\frac{c}{\omega}\right),, \tag{2.76}$$

$$v_0 = \frac{g\eta_0}{c}\left|\frac{i - \left(\frac{\omega}{c}\frac{1}{\eta}\frac{d\eta}{dx}\right)^{-1}}{i + \frac{8fv}{3\pi\omega\overline{h}}}\right|. \tag{2.77}$$

Substitution of the dimensionless parameters defined in Section 3 into equations (2.74)–(2.76)yields the damping equation, celerity equation and phase lag equation for the general case presented in Table 2.1. However, equation (2.77) is not the scaling equation as we expected due to the complex number in the right-hand side. In fact, following the derivation used by *Friedrichs* [2010, pp. 47-48] and using the identity $\exp(i\phi) = \cos(\phi) + i\sin(\phi)$, it is possible to derive:

$$v_0 = \frac{r_s\eta_0 c\cos(\varphi)}{\overline{h}} = r_s\eta_0 c\sin(\varphi)\left/\left[\overline{h}\left(\frac{1}{\eta}\frac{d\eta}{dx}\frac{c}{\omega} - \frac{c}{\omega a}\right)\right]\right., \tag{2.78}$$

which is the scaling equation as presented in Table 2.1.

Lanzoni's approach

Lanzoni and Seminara [1998] revisited the one-dimensional tidal propagation in convergent estuaries considering four limit cases identified by the relative strength of channel convergence and ratio of friction to local inertia. For weakly dissipative and weakly convergent estuaries, the dominant tidal component reduces to a progressive wave in a frictionless prismatic channel, where the velocity is in phase with free surface elevation (i.e., $\epsilon = \pi/2$). In this case, the solution for the tidal amplitude along the estuary is given by:

$$\eta = \eta_0\frac{\exp[x/(2a)]}{1 - 8fva/\left(3\pi c_0\overline{h}\right) + 8fva/\left(3\pi c_0\overline{h}\right)\exp[x/(2a)]}. \tag{2.79}$$

Making use of scaling equation for velocity amplitude $v = \zeta c_0$ (implying $\mu = \lambda = 1$)and dimensionless parameters defined in Section 3, equation (2.79) reduces to:

$$\eta^* = \frac{\exp[x^*\gamma/(2\lambda)]}{1 - 8\chi/(3\pi\gamma) + [8\chi/(3\pi\gamma)]\exp[x^*\gamma/(2\lambda)]}, \tag{2.80}$$

with

$$\eta^* = \eta/\eta_0. \tag{2.81}$$

One can easily observe that an equilibrium tidal amplitude η^*_{inf} exists when the distance approaches infinity, which reads:

$$\eta^*_{inf} = \frac{3\pi\gamma}{8\chi}. \tag{2.82}$$

In weakly dissipative and moderately or strongly convergent estuaries, they derived the following form of solutions:

$$\frac{1}{\eta}\frac{d\eta}{dx}\frac{\omega}{c_0} = \frac{1}{2a}, \tag{2.83}$$

$$\frac{\omega}{c} = \frac{\sqrt{4\omega^2 a^2/c_0^2 - 1}}{2a}, \tag{2.84}$$

$$\tan(\epsilon) = \sqrt{4\omega^2 a^2/c_0^2 - 1}, \tag{2.85}$$

$$\frac{v}{\zeta \omega a} = \frac{c_0}{\omega a}, \tag{2.86}$$

which can be rewritten by using the dimensionless parameters defined in Section 3 and give rise to the solutions:

$$\delta = \gamma/2, \lambda = \sqrt{1 - \gamma^2/4}, \tan \epsilon = \sqrt{4/\gamma^2 - 1}, \mu = 1, \tag{2.87}$$

which corresponds with the frictionless case ($\gamma < 2$) presented in Table 2.1. For the cases of strongly dissipative and weakly convergent estuaries and strongly dissipative and strongly convergent estuaries, *Lanzoni and Seminara* [1998] did not derive the analytical solutions due to the nonlinearity of the friction term.

Prandle's approach

Prandle [2003, 2004] proposed localized analytical solutions for the particular case of a synchronous (i.e., ideal) estuary with strongly convergent triangular cross-sections and a predominant (M_2) tidal constituent. He also assumed a constant estuary depth to width ratio and introduced a cross-sectional slope defined as $\tan(\alpha) = 2\bar{h}/B$. Noting that for a triangular cross-section $\bar{A} = 0.5\bar{B}\bar{h}$, then the convergence of cross-sectional area is given by:

$$\frac{1}{\bar{A}}\frac{\partial \bar{A}}{\partial x} = \frac{1}{\bar{h}^2/\tan(\alpha)}\frac{\partial\left[\bar{h}^2/\tan(\alpha)\right]}{\partial x} = \frac{1}{\bar{h}}\frac{\partial \bar{h}}{\partial x}. \tag{2.88}$$

The solution for the wave celerity corresponds to the propagation of an unbounded inviscid wave (in water depth $\bar{h}/2$). In this case the solutions are described by the following equations:

$$\tan(-\varphi) = -1.33\chi\mu = 2\frac{1}{\bar{h}}\frac{\partial \bar{h}}{\partial x}\frac{c}{\omega}, \tag{2.89}$$

$$v = \eta g/\left[c\sqrt{1 + \left(\frac{8}{3\pi}\chi\mu\right)^2}\right], \tag{2.90}$$

$$c = \sqrt{g\bar{h}/2}, \tag{2.91}$$

where the factor 1.33 in equation (2.89) is derived from the linearization of the quadratic velocity term in the momentum equation for a triangular cross-section. Equations (2.89)–(2.91) can be solved for v and $\partial\bar{h}/\partial x$, and by integrating $\partial\bar{h}/\partial x$, it is possible to obtain the values of depth along the estuary.

Substitution of the dimensionless parameters in equations (2.89)–(2.91) yields the following set of equations:

$$\tan(\epsilon) = 2/\gamma = 1/(1.33\mu\chi), \mu = \sqrt{1/(1 + 4\gamma^2)}, \lambda = 1, \qquad (2.92)$$

which are slightly different from our solutions for the ideal estuary (see Table 2.1) due to the triangular cross-section shape.

Van Rijn' s approach

Van Rijn [2011] derived the analytical solutions for tidal wave propagation in both prismatic and converging channels, where the main tidal dynamics can be explicitly described by two independent parameters, i.e., the width convergence and Lorentz' s friction factor. The solution is an exponential damped/amplified wave due to the balance between channel convergence and friction. The solutions are given by:

$$\tan(-\varphi) = \frac{c}{\omega}\left[\frac{1}{2b} + \frac{1}{\sqrt{2}}\frac{\omega}{c_0}\sqrt{-1 + \left(\frac{c_0}{2\omega b}\right)^2 + \sqrt{\left[-1 + \left(\frac{c_0}{2\omega b}\right)^2\right]^2 + \left(\frac{8fv}{3\pi\overline{h}\omega}\right)^2}}\right],$$
$$(2.93)$$

$$v = -\left(\eta/\overline{h}\right)c\cos(-\varphi), \qquad (2.94)$$

$$-\frac{1}{\eta}\frac{d\eta}{dx} = -\frac{1}{2b} + \frac{1}{\sqrt{2}}\frac{\omega}{c_0}\sqrt{-1 + \left(\frac{c_0}{2\omega b}\right)^2 + \sqrt{\left[-1 + \left(\frac{c_0}{2\omega b}\right)^2\right]^2 + \left(\frac{8fv}{3\pi\overline{h}\omega}\right)^2}}, \quad (2.95)$$

$$c = \frac{\omega}{k} = \omega/\left[\frac{1}{2b} - \frac{1}{\sqrt{2}}\frac{\omega}{c_0}\sqrt{1 - \left(\frac{c_0}{2\omega b}\right)^2 + \sqrt{\left[-1 + \left(\frac{c_0}{2\omega b}\right)^2\right]^2 + \left(\frac{8fv}{3\pi\overline{h}\omega}\right)^2}}\right], \quad (2.96)$$

which can be scaled by the dimensionless parameters defined in Section 3 and lead to four dimensionless equations:

$$\tan(\epsilon) = \lambda/(\gamma - \delta), \qquad (2.97)$$

$$\mu = \sin(\epsilon)/\lambda, \qquad (2.98)$$

$$\delta = \frac{\gamma}{2} - \frac{1}{\sqrt{2}}\sqrt{-(1 - \gamma^2/4) + \sqrt{(1 - \gamma^2/4)^2 + \left(\frac{8}{3\pi}\chi\mu\right)^2}}, \qquad (2.99)$$

$$\lambda^2 = 1 - \delta(\gamma - \delta). \qquad (2.100)$$

After some algebra, it is possible to rewrite equation (2.99) as:

$$\delta = \frac{\gamma}{2} - \frac{4}{3\pi}\frac{\chi\mu}{\lambda}. \qquad (2.101)$$

We can see that the solutions (2.98)-(2.101) are identical to the general case of linear solutions that presented in Table 2.1.

Meanwhile, *Van Rijn* [2011] also proposed a semi-analytical (because it should be coupled with his linear solution) solution of the energy equation:

$$2\frac{\mathrm{d}\eta}{\mathrm{d}x} = \frac{1}{b}\eta - \frac{8}{3\pi}\frac{fv^2}{g\overline{h}\cos(-\varphi)},\tag{2.102}$$

which includes the effect of quadratic (nonlinear) bottom friction as he mentioned. However, using the dimensionless parameters and noting that $\cos(\phi) = \sin(\epsilon) = \mu\lambda$, the solution of (2.102) becomes equation (2.101), which means that it is still identical to its linear solution.

Toffolon's approach

Toffolon and Savenije [2011] revisited the classical linear solution for tidal propagation in convergent estuaries (with width and depth convergence) based on complex functions. Moreover, it is shown how the solution can be improved by exploiting an iterative refinement of the linearized bottom friction and by subdividing the estuary in multiple reaches.

The analytical solution is given explicitly by the set of equations (2.51)–(2.55) as presented in Hunt's approach. The refinement process based on iteratively calculating the correct value of $\widehat{\chi}$ based on the estimated μ is described in *Toffolon and Savenije* [2011]. Here it suffices to say that plugging the set of equations (2.55) into equations (2.51)–(2.54) yields equations (2.97)–(2.100), which suggests that Toffolon's solutions are also identical to the linear solution (general case) presented in Table 2.1.

Winterwerp's approach

The solution presented by *Winterwerp and Wang* [2013] is identical to the solution proposed by *Van Rijn* [2011] and *Toffolon and Savenije* [2011]. It should be noted that the wave number k defined in their paper is a complex, where the real part represents the real wave number ω/c while the imaginary part represents the damping gradient $\frac{1}{\eta}\frac{\mathrm{d}\eta}{\mathrm{d}x}$. We are able to rewrite their solutions with dimensionless parameters presented in Section 3:

$$\frac{1}{2}\left[2\sqrt{(4r_s/\gamma^2 - 1)^2 + (4r_s\widehat{\chi}/\gamma^2)^2} + 2(4r_s/\gamma^2 - 1)\right]^{1/2} = \frac{2}{\gamma}\lambda,\tag{2.103}$$

$$1 - \frac{1}{2}\left[2\sqrt{(4r_s/\gamma^2 - 1)^2 + (4r_s\widehat{\chi}/\gamma^2)^2} - 2(4r_s/\gamma^2 - 1)\right]^{1/2} = \frac{2}{\gamma}\delta,\tag{2.104}$$

$$\mu = \sqrt{\frac{\lambda^2 + \delta^2}{1 + \widehat{\chi}^2}},\tag{2.105}$$

$$\tan(-\varphi) = \frac{\delta - \gamma}{\lambda}.\tag{2.106}$$

It can be seen from equations (2.103)–(2.106) that they are just slightly different expressions of the analytical solutions (general case) presented in Table 2.1. However, instead of using an iterative procedure to determine the correct velocity scale υ, they assumed a constant friction parameter $\hat{\chi}$ along the estuary. Neither did they use a multi-reach approach to account for the variation of the longitudinal depth.

2.5. The Quasi-nonlinear and Hybrid Approaches

As shown in the previous section, analytical solutions developed to date concentrated on linear models, usually neglecting the inertial term, linearized the friction term and assuming a constant friction and average flow depth. *Savenije* [1998, 2001], however, followed another approach based on a Langrangean reference frame and derived an analytical expression for the tidal damping (i.e., the damping equation) that retained the nonlinear friction term (i.e., the quadratic velocity and the periodic variation of the hydraulic radius). We termed this as "envelope method" due to the fact that the damping equation was obtained by subtracting the envelope curves of HW and LW. A detailed description of the envelope method to derive the damping equations for different friction formulations is presented in Appendixes A.2 and A.3. On the basis of this envelope method, *Toffolon et al.* [2006] and *Savenije et al.* [2008] derived a fully explicit solution for the tidal wave propagation by solving four equations, i.e., phase lag, scaling, damping, and celerity equations, where the phase lag and scaling equations were derived by *Savenije* [1992a, 1993a] from the mass balance equation by a Lagrangean approach, while the celerity equation was derived by *Savenije and Veling* [2005] with the method of characteristics.

Recently, *Cai et al.* [2012a] presented one consistent theoretical framework for tidal wave propagation building on the previous works by *Toffolon et al.* [2006] and *Savenije et al.* [2008]. It was demonstrated by *Cai et al.* [2012a] that different friction formulations can be used in the envelope method to arrive at an equal number of damping equations (see Table 2.2). These equations are explained in detail in *Savenije* [2012] and are similar to the ones described in Appendixes A.2 and A.3. Subsequently, the different damping equations can be combined with phase lag, scaling, and celerity equations to form the solutions of the hydraulic equations. In general, the main classes of the solutions are: (1) quasi-nonlinear solution with nonlinear friction term [*Savenije et al.*, 2008]; (2) linear solution with Lorentz's linearization [*Lorentz*, 1926]; (3) Dronkers' solution with higher order formulation for quadratic velocity [*Dronkers*, 1964]; (4) hybrid solution characterized by a weighted average of Lorentz's linearization, with weight 1/3, and the nonlinear friction term, with weight 2/3 [*Cai et al.*, 2012a]. It is worth noting that in this framework we used a different definition for the dimensionless friction factor:

$$f = f_L\left[1 - (4\zeta/3)^2\right]^{-1}, \tag{2.107}$$

where the last term stems from the subtraction between HW and LW envelopes, which accounts for the periodic variation of the hydraulic radius in the denominator

of the friction term.

Table 2.2: A new analytical framework for tidal wave propagation

Model	Friction term	Damping equation	References
Quasi-nonlinear	$U\lvert U\rvert/(K^2 h^{4/3})$	$\delta = \gamma/2 - \chi\mu^2/2$	Appendix A.1
Linear	$8\upsilon U/(3\pi K^2 \overline{h}^{4/3})$	$\delta = \gamma/2 - 4\chi\mu/(3\pi\lambda)$	Appendix A.2
Dronkers	$16\upsilon^2[U/\upsilon + 2(U/\upsilon)^3]/(15\pi K^2 \overline{h}^{4/3})$	$\delta = \gamma/2 - 8\chi\mu/(15\pi\lambda) - 16\chi\mu^3\lambda/(15\pi)$	Appendix A.3
Hybrid	$2U\lvert U\rvert/(3K^2 h^{4/3}) + 8\upsilon U/(9\pi K^2 h^{4/3})$	$\delta = \gamma/2 - 4\chi\mu/(9\pi\lambda) - \chi\mu^2/3$	*Savenije* [2012, 84–89]

Figures 2.5–2.8 illustrate the response of the velocity number, the damping number, the celerity number, and the phase lag obtained with different analytical models (see Table 2.2) as a function of friction number χ and estuary shape number γ. The range of χ (0—50) and γ (0—5) values covered is representative of most estuaries. It can be seen from Figures 2.5–2.8 that all methods are identical for a frictionless wave. Since there exists two families of solutions in the quasi-nonlinear model [*Savenije et al.*, 2008], we can clearly see that the dimensionless scale of velocity μ flips suddenly when the friction reaches its critical value, defined as the threshold condition for the transition from the mixed tidal wave (first family of solution, $0 < \epsilon < 2/\pi$) to the"apparently standing wave" (second family, $\epsilon = 0$) (see Figure 2.5). On the contrary, the other three methods (i.e., the hybrid, linear and Dronkers' models) provide a continuous solution with a smooth transition.

It is important to recognize that the solutions for the dependent dimensionless parameters μ, δ, λ and ϵ are local because they are obtained by solving four implicit equations that depend only on local (fixed position) quantities (i.e., the local tidal amplitude to depth ratio ζ, the local estuary shape number γ and the local friction number χ). In order to reproduce the correct wave behavior along the estuary, a multi-reach approach has to be used to follow along-channel variations of the estuarine sections, where the whole estuary is subdivided into multiple reaches. With the obtained damping number δ, it is possible to calculate a tidal amplitude η_1 at a distance Δx (e.g., 1 km) upstream by simple explicit integration of the damping number:

$$\eta_1 = \eta_0 + \frac{\mathrm{d}\eta}{\mathrm{d}x}\Delta x = \eta_0 + \frac{\eta_0\omega\delta}{c_0}\Delta x. \tag{2.108}$$

To demonstrate the capability of the proposed multi-reach approach, Figure 2.9 compares the longitudinal variations of tidal amplitude and velocity amplitude as well as the control parameters (friction number χ and shape number γ) for different depth profile along the estuary (d=infinite, d=150 km or d=-150 km). It should be noted that for the convergent depth there exists a maximum value for χ due to the opposite effect of depth reduction. On the other hand, for the prismatic channel with diverging depth we can see that the tidal amplitude and velocity amplitude consistently decrease because of frictional dissipation and diverging depth.

2.6. Asymptotic Behaviour of the Solutions

The present method, exploiting a multi-reach approach, differs from earlier studies [e.g. *Hunt*, 1964; *Ippen*, 1966; *Friedrichs and Aubrey*, 1994; *Van Rijn*, 2011] in

2
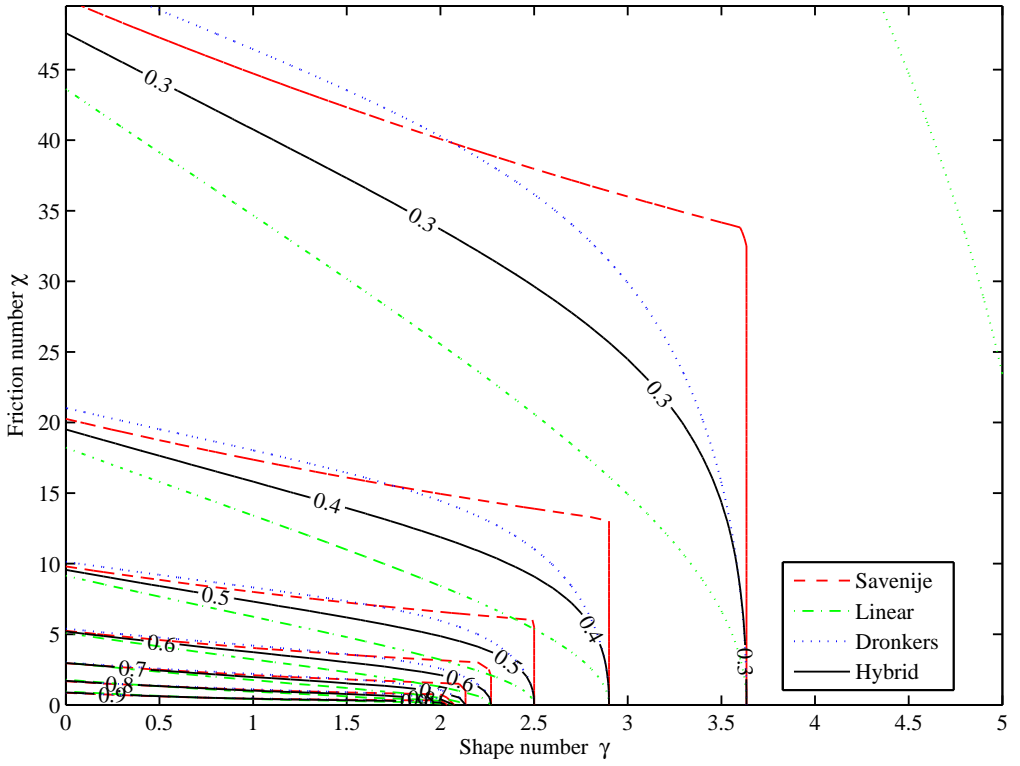
Figure 2.5: Contour plot of the velocity number μ in the $\gamma - \chi$ plane obtained with different analytical approaches.

exploring localized dynamics in terms of tidal amplitude to depth ratio as opposed to seeking whole-estuary solutions. It was demonstrated by *Cai and Savenije* [2013] that the exponential damping for the whole-estuary is only valid for an ideal estuary or for the case of frictionless. This is due to the fact that for these two cases the damping number δ is assumed to be constant (hence constant friction χ, velocity μ, celerity λ, and phase lag ϵ). In particular, the classical exponential solutions for tidal amplitude and velocity amplitude can be described as:

$$\eta^* = \exp(x^*\delta/\lambda), v^* = \exp(x^*\delta/\lambda). \tag{2.109}$$

with

$$v^* = v/v_0. \tag{2.110}$$

It can be seen from equation (2.109) that both tidal amplitude and velocity amplitude approach zero for a damped wave and infinity for an amplified wave. On the contrary, *Cai and Savenije* [2013] found that an asymptotic solution exists due to the balance between friction and channel convergence and derived a fully explicit equation for tidal amplitude (as a function of distance) from the damping equation,
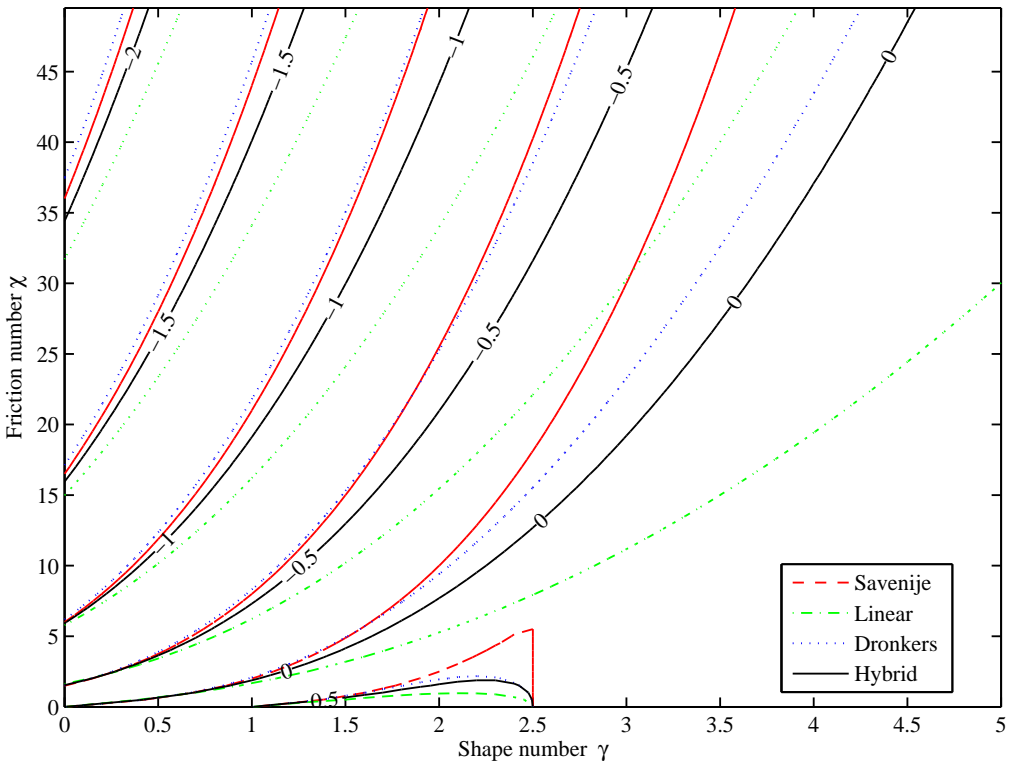
Figure 2.6: Contour plot of the damping number δ in the $\gamma - \chi$ plane obtained with different analytical approaches.

which can be expressed as:

$$\eta^* = \frac{\eta^*_{\text{inf}}}{1 - \left(1 - \eta^*_{\text{inf}}\right)\exp\{-\gamma\mu^2 x^*/[\lambda(1 + \mu^2)]\}}, \tag{2.111}$$

where η^*_{inf} is the asymptotic solution of tidal amplitude when the distance approaches infinity and depends on the specific damping equation (see Table 2.2). Table 3 presents the analytical expressions that reflect the balance between friction and channel convergence, which are derived by setting $\delta = 0$ in the damping equation. The localized asymptotic solutions for tidal amplitude derived from different damping equations are also presented in Table 2.3, where the subscript Q, L, D, and H stand for the corresponding analytical models. The reason that the asymptotic solutions are local is due to the fact that they are obtained by assuming that the friction factor f, the phase lag ϵ, the wave celerity c, the tidally averaged depth $\bar{h}$, and the ratio of the velocity amplitude to the tidal amplitude v/η are constant.

Figure 2.10 illustrates the asymptotic behaviour of tidal amplitude when distance approaches infinity where the friction is balanced by the channel convergence for

2
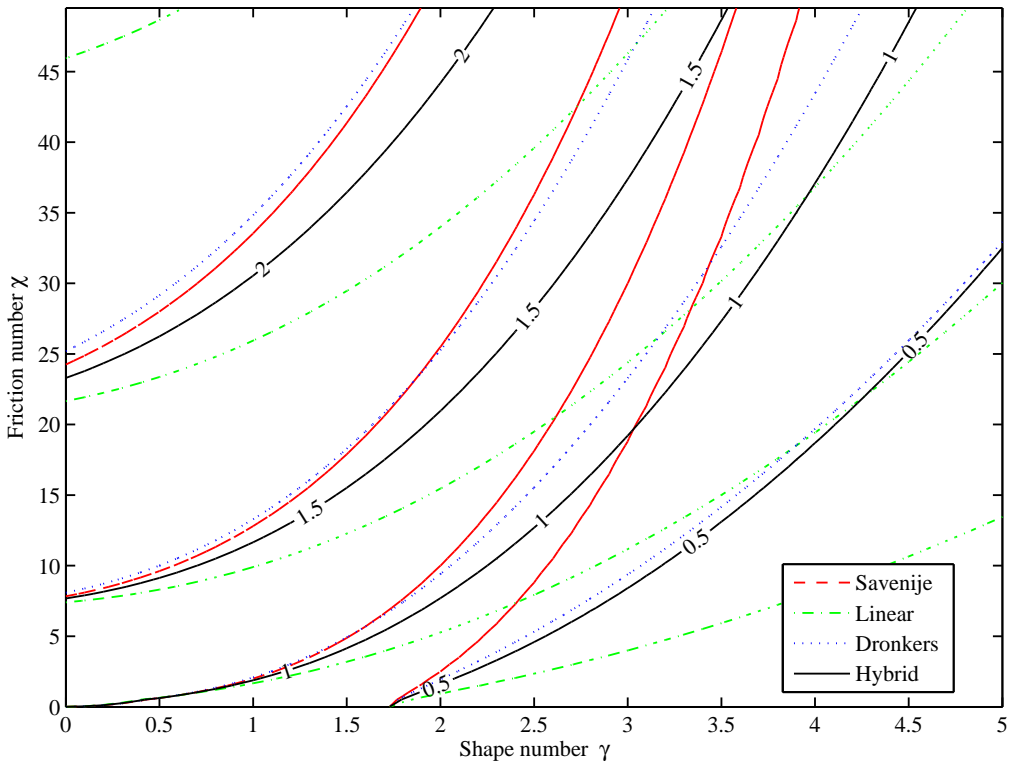
Figure 2.7: Contour plot of the celerity number λ in the $\gamma - \chi$ plane obtained with different analytical approaches.

different values of the estuary shape number γ. Although in reality the estuary is too short to achieve an equilibrium tidal amplitude, the explicit equation (2.107) does provide new insight into the tidal damping in convergent estuaries when compared with the simple exponential damping equation (2.109).

2.7. Conclusions

In this chapter we present a general derivation of linear solution for tidal wave propagation in convergent estuaries without land boundary (i.e., infinite length channel) based on a Eulerian reference frame using the assumption that the tidal elevation and velocity can be described by simple harmonic waves. The derivation results in four implicit equations, i.e., the phase lag, the scaling, the linear damping, and the celerity equation, which can be solved by simple numerical method. It is demonstrated that most of the analytical solutions developed to date have large similarity to the proposed linear solutions with four explicit equations, except the analytical approach proposed by *Savenije* [1998, 2001, 2005, 2012], *Savenije et al.* [2008] who derived the solutions in a Lagrangean reference frame while retaining
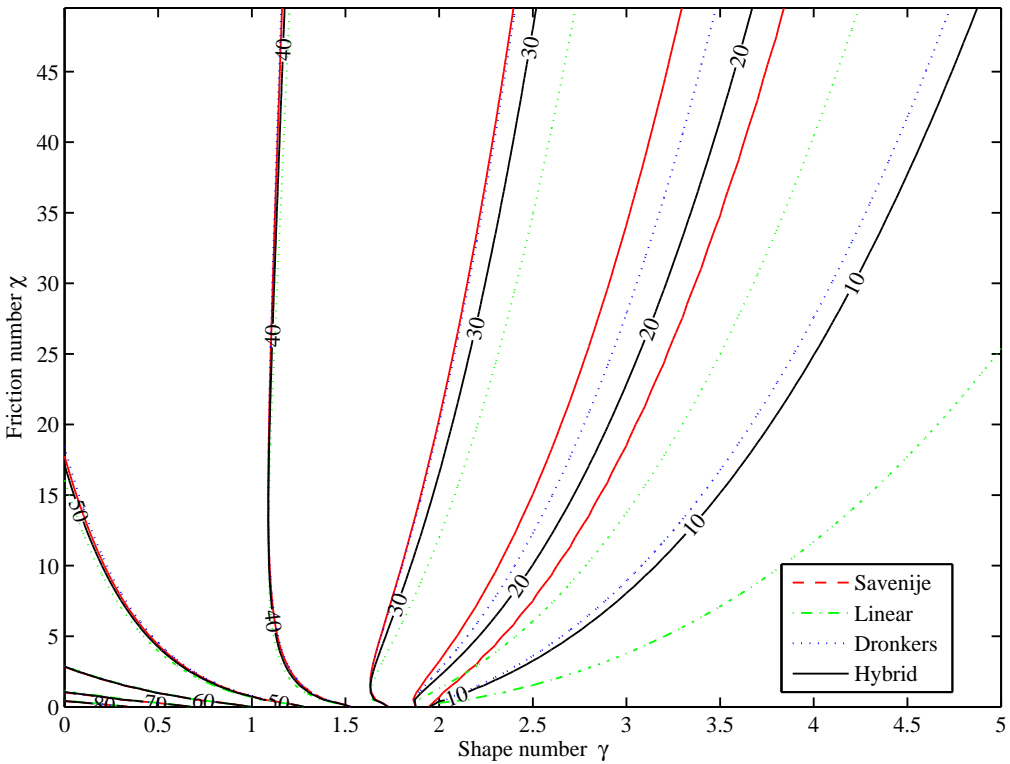
Figure 2.8: Contour plot of the phase lag ϵ in the $\gamma - \chi$ plane obtained with different analytical approaches.

the inertial term and nonlinear friction term in the momentum equation. In general, it is possible to classify the linear solutions into four types: 1) linear solution assuming constant friction, such as *Hunt* [1964], *Prandle and Rahman* [1980], *Prandle* [1985], *Friedrichs* [2010]; 2) linear solution exploiting an iterative procedure to determine the correct velocity amplitude υ in the Lorentz's linearization, such as *Van Rijn* [2011]; 3) linear solution that accounts for the longitudinal variation of friction and depth by subdividing the entire estuary in short reaches over which the friction number χ and averaged depth are considered constant, such as *Toffolon and Savenije* [2011]. 4) linear solution that is obtained by solving four implicit equations and the longitudinal behavior is reproduced by a multi-reach approach, such as the method presented in section 3 and the linear model proposed by *Cai et al.* [2012a].

The analytical framework developed by *Cai et al.* [2012a] enables comparison among a wide range of analytical approaches. Four classes of analytical solutions are identified and the main difference lies in the treatment of the friction term using different friction approximations. They are quasi-nonlinear model with nonlinear
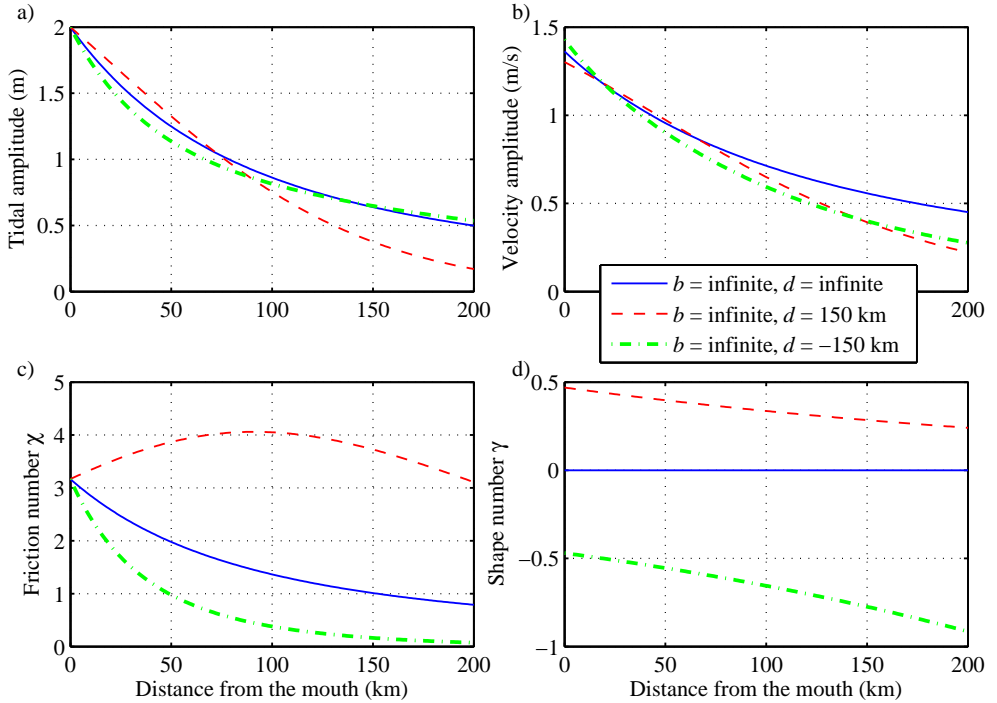
Figure 2.9: Comparison of the main dimensional parameters as well as their control parameters under different depth profile scenarios. The drawn line represents prismatic channel with horizontal bed (d= infinite). The dashed line denotes prismatic channel with convergent depth (d= 150 km), while the dashed-dotted line for prismatic channel with diverging depth (d= -150 km).

friction term, linear model with Lorentz's linearization, Dronkers' model with third order formulation for the friction term, and hybrid model characterized by 2/3 of the nonlinear friction term and 1/3 of the Lorentz's linearization. It is important to recognize that a multi-reach approach should be applied in order to reproduce the correct behavior of tidal dynamics along the estuary. The asymptotic behavior of these analytical solutions was further investigated by *Cai and Savenije* [2013] where equilibrium tidal amplitude was found that reflects the balance between friction and channel convergence.

Table 2.3: Summary of the asymptotic solutions for different analytical models

Model	Balance between friction χ and channel convergence γ	Localized asymptotic solution
Quasi-nonlinear	$\chi = \gamma(\gamma^2 + 1)$	$\eta^*_{inf\_Q} = \gamma/(\chi_0 \mu^2 \lambda^2)$
Linear	$\chi = 3\pi\gamma\sqrt{\gamma^2 + 1}/8$	$\eta^*_{inf\_L} = 3\pi\gamma/(8\chi_0 \mu\lambda)$
Dronkers	$\chi = \left[15\pi\gamma(\gamma^2 + 1)^{3/2}\right]/[16(\gamma^2 + 3)]$	$\eta^*_{inf\_D} = 15\pi\gamma/(16\chi_0 \mu\lambda + 32\chi_0 \mu^3 \lambda^3)$
Hybrid	$\chi = \gamma/\left\{8/(9\pi\sqrt{1 + \gamma^2}) + 2/[3(1 + \gamma^2)]\right\}$	$\eta^*_{inf\_H} = \gamma/\left[8\chi_0 \mu\lambda/(9\pi) + 2\chi_0 \mu^2 \lambda^2/3\right]$
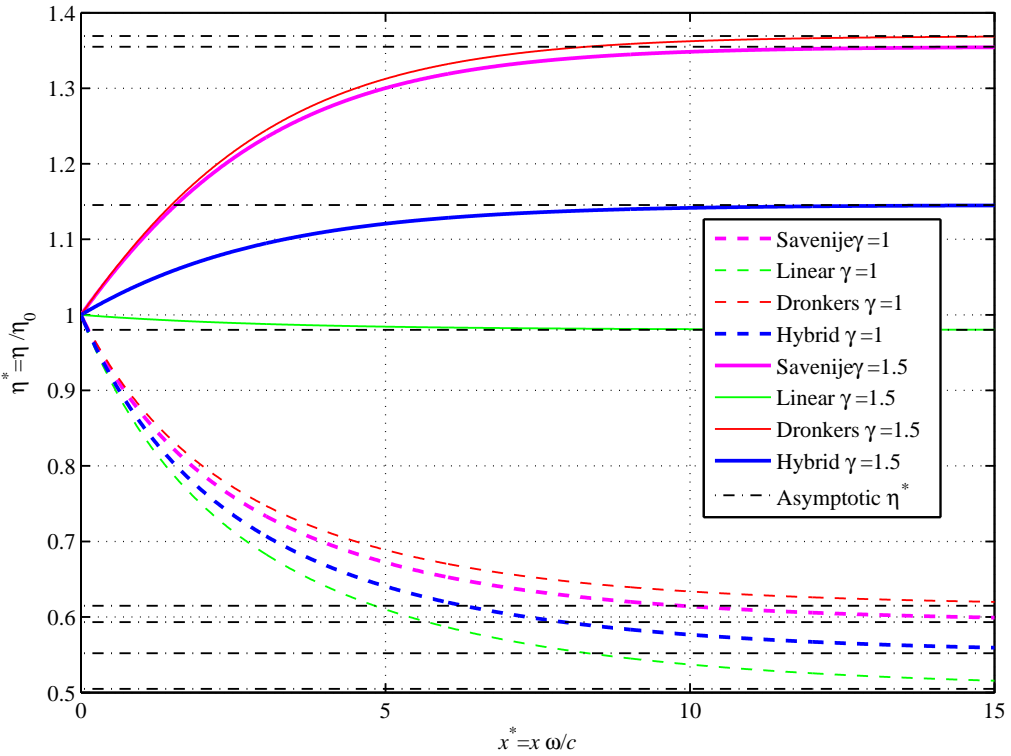
Figure 2.10: Longitudinal variation of the dimensionless tidal amplitude along the estuary obtained with the explicit equation (2.110) using different analytical models for different values of the estuary shape number γ with ζ=0.1, K=30 m$^{1/3}$s^{-1}, r_S=1. The dot-dashed lines represent the asymptotic solution of tidal amplitude.

3

A new analytical framework for assessing the effect of sea-level rise and dredging on tidal damping in estuaries

This chapter explores different analytical solutions of the tidal hydraulic equations in convergent estuaries. Linear and quasi-nonlinear models are compared for given geometry, friction, and tidal amplitude at the seaward boundary, proposing a common theoretical framework and showing that the main difference between the examined models lies in the treatment of the friction term. A general solution procedure is proposed for the set of governing analytical equations expressed in dimensionless form, and a new analytical expression for the tidal damping is derived as a weighted average of two solutions, characterized by the usual linearized formulation and the quasi-nonlinear Lagrangean treatment of the friction term. The different analytical solutions are tested against fully nonlinear numerical results for a wide range of parameters, and compared with observations in the Scheldt estuary. Overall, the method compares best with the numerical solution and field data. The new accurate relationship for the tidal damping is then exploited for a classification of estuaries based on the distance of the tidally averaged depth from the ideal depth (relative to vanishing amplification) and the critical depth (condition for maximum amplification). Finally, the model is used to investigate the effect of depth variations on the tidal dynamics in 23 real estuaries, highlighting the usefulness of the analytical method to assess the influence of human interventions (e.g. by dredging) and global sea-level rise on the

estuarine environment.

3.1. Introduction

Recently, *Toffolon and Savenije* [2011] proposed a modified linear model and compared it with the quasi-nonlinear model of *Savenije et al.* [2008], suggesting that the discontinuous behavior (i.e., with two families of solutions) and the transition toward a standing wave (i.e., the wave celerity tending toward infinity) predicted by the latter model do not happen in reality. Interestingly, numerical simulations (see section 3.3.2) indicate that the two models approach the numerical results from a different side, i.e., the modified linear model overestimates the tidal damping while the quasi-nonlinear model underestimates it, and it appears that a weighted average of the two comes close to the numerical results. In this chapter, a comparison is made between different linear and quasi-nonlinear models building a common theoretical framework based on which a new analytical model is derived. We pay particular attention to the effect of different formulations of the friction term, leading to different expressions for tidal damping.

The chapter is arranged as follows. In the next section, we present the quasi-nonlinear solution of tidal wave propagation in convergent estuaries. The comparison between the quasi-nonlinear model and the linear model is presented in section 3.3. In section 3.4, the performance of the new analytical model is shown and compared with analytical solutions by *Savenije et al.* [2008], *Toffolon and Savenije* [2011] and Dronkers' approach [*Dronkers*, 1964]. The new model is subsequently applied in the Scheldt estuary and compared with the solution of a numerical model. In section 3.5, a new classification of estuaries and the effect of depth variations on tidal dynamics in 23 real estuaries are presented. Finally, conclusions are drawn in section 3.6.

3.2. Quasi-nonlinear model

Savenije et al. [2008] derived four dimensionless equations based on the equations for the phase lag [*Savenije*, 1992a, 1993a], for tidal damping [*Savenije*, 1998, 2001], and for wave propagation [*Savenije and Veling*, 2005]:

$$\delta = \frac{\gamma}{2} - \frac{1}{2}\chi\mu^2, \tag{3.1}$$

$$\mu = \frac{\sin(\varepsilon)}{\lambda} = \frac{\cos(\varepsilon)}{\gamma - \delta}, \tag{3.2}$$

$$\tan(\varepsilon) = \frac{\lambda}{\gamma - \delta}, \tag{3.3}$$

$$\lambda^2 = 1 - \delta(\gamma - \delta). \tag{3.4}$$

The damping equation (3.1) reflects the relative balance between the convergence of banks and friction and can be rewritten as:

$$\gamma - \delta = \frac{\gamma + \chi\mu^2}{2},\tag{3.5}$$

which is greater than 0 for any convergent estuary ($\gamma > 0$), showing that the tidal wave amplification (δ) cannot be larger than the estuary shape number γ. The scaling equation (3.2) shows that the velocity amplitude is determined by the ratio between the phase lag ε and the combined effect of friction and convergence as expressed in (3.5). The phase lag equation (3.3) highlights that a standing wave ($\varepsilon = 0$) is characterized by an infinite wave celerity ($\lambda \to 0$) and that friction tends to move the system far from this asymptotic condition. On the other hand, a progressive wave ($\varepsilon = \pi/2$) is obtained only when the difference between γ and δ (3.5) is vanishingly small, i.e., when both friction and convergence are negligible. The celerity equation (3.4) shows that tidal wave propagation is closely related with the longitudinal amplitude variation (amplification or damping): recalling the positive value of (3.5), it is easy to see that the actual celerity c is larger than the reference value c_0 for amplified conditions, while it decreases with damping. It is worth noting that this set of equations corresponds to the case of an infinitely long channel, where the effect of the landward boundary condition can be neglected [*Toffolon and Savenije*, 2011]. Also it is worth noting that in the derivation of both the damping and the celerity equation, the density term in the momentum balance equation was taken into account, but that this term dropped out in both the envelope method [*Savenije*, 1998, 2001] and the method of characteristics [*Savenije and Veling*, 2005] used for their derivation. Hence the density term has no impact on the tidal damping nor the wave celerity (only indirectly, it leads to a residual water level slope). The scaling equation and the phase lag equation result from the mass balance equation and hence are also not affected by the density term.

3.3. Comparison between Linear and Quasi-nonlinear Solutions

3.3.1. Difference in Damping Equation

Recently, *Toffolon and Savenije* [2011] and *Van Rijn* [2011] revisited the linear solution for estuarine hydrodynamics by taking into account the effects of the width and depth convergence. In this section we compare these modified linear solutions with the quasi-nonlinear analytical solution proposed by *Savenije et al.* [2008], with specific focus on the damping equation (Table 3.1). Basically, *Toffolon and Savenije* [2011] and *Van Rijn* [2011] exploited the same method, linearizing the friction term (both the velocity variation $U|U|$ and the variation of the depth h) and neglecting the inertial term $U\partial U/\partial x$ and the density term $gh/(2\rho)\partial\rho/\partial x$ in the momentum balance equation. The set of obtained equations was then solved using complex functions. These functions were considered as a local approximation of the solution in a multi-reach system by *Toffolon and Savenije* [2011], who also showed a more reliable solution can be obtained by iteratively refining the Lorentz' constant in the friction term. On the other hand, *Van Rijn* [2011] concentrated on the solution of

the whole estuary, but derived a damping equation based on energy considerations as well. Another distinct difference is that the solution proposed by *Savenije et al.* [2008] is intrinsically local, i.e., it is expressed in terms of point-to-point values of the parameters provided that the information about the tidal amplitude is transferred only in the landward direction by means of the damping equation, while the other two linearized solutions (which potentially account also for the landward boundary condition) can be used in this way by neglecting the effect of the reflected wave.

3

Table 3.1: Comparison of different approaches to tidal damping equation.

Model	Method	Landward b.c.	$U\partial U/\partial x$ and $gh/(2\rho)\partial\rho/\partial x$	Friction term	Damping equation
Savenije et al. [2008]	Subtracting high water and low water envelopes	Neglected	Considered	Quadratic velocity, time-variable depth	$\delta = \frac{\gamma}{2} - \frac{1}{2}\chi\mu^2$
Toffolon and Savenije [2011], *Van Rijn* [2011]	Considering the amplitude of complex function	Neglected (but possibly considered)	Neglected	Linearized, time-invariant depth	$\delta = \frac{\gamma}{2} - \frac{1}{\sqrt{2}}\sqrt{\Gamma + \sqrt{\Gamma^2 + \left(\frac{8}{3\pi}\chi\mu\right)^2}}$ (T1) $\Gamma = \frac{\gamma^2}{4} - 1$
Van Rijn [2011]	Energy-based approach	Neglected	Neglected	Linearized, time-invariant depth	$\delta = \frac{\gamma}{2} - \frac{4}{3\pi}\frac{\chi\mu}{\lambda}$ (T2)

It is worth noting that, after some algebra, it is possible to demonstrate that the two damping equations (T1) and (T2) in Table 3.1 are identical, which means that the analytical solution proposed by *Van Rijn* [2011], both with the linear and the energy-based approach, can be cast into the same set of four nonlinear equations using the dimensionless parameters defined in section 3.2. The dimensionless equations obtained are similar to equations (3.1)-(3.4), but with a different damping equation:

$$\delta = \frac{\gamma}{2} - \frac{4}{3\pi}\frac{\chi\mu}{\lambda}. \tag{3.6}$$

Since *Van Rijn* [2011]'s model is characterized by Lorentz's linearization [*Lorentz*, 1926] of the friction term F:

$$F_L = \frac{8}{3\pi}\frac{\upsilon}{K^2\bar{h}^{-4/3}}U, \tag{3.7}$$

it is interesting to analyze the effect of using Lorentz's assumption in the derivation of the damping equation (3.1) with the envelope method. This is done in Appendix A.2, following the procedure proposed by *Savenije* [2005] and considering the linearized friction term, instead of the quasi-nonlinear friction term, in the momentum equation. The result is that we obtain the same linear tidal damping equation as in (3.6), demonstrating that *Van Rijn* [2011]'s model coincides with the linearized version of *Savenije et al.* [2008].

Replacing the quasi-nonlinear damping equation (3.1) with equation (3.6), a new system of four analytical equations is obtained, namely (3.6), (3.2), (3.3) and (3.4). In contrast to the quasi-nonlinear system, which has an explicit solution,

this set of equations can only be solved by an iterative numerical method (e.g., a simple Newton-Raphson method). Figure 3.1 shows the variation of the dependent dimensionless parameters obtained with the different approaches as a function of the estuary shape number γ and the friction number χ. We can see that the results obtained using (3.6) coincide fully with the solutions provided by *Van Rijn* [2011] and *Toffolon and Savenije* [2011]. Hence, the only difference between the quasi-nonlinear [*Savenije et al.*, 2008] and modified linear models [*Toffolon and Savenije*, 2011; *Van Rijn*, 2011] is the friction term in the damping equation.
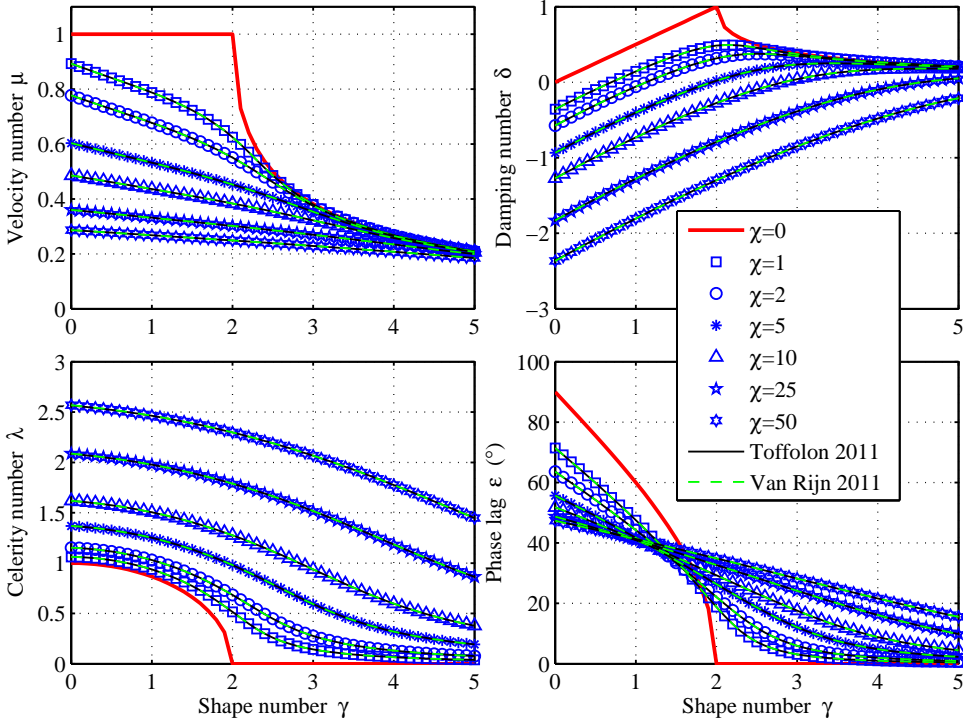
Figure 3.1: Relationship between the main dimensionless parameters and the estuary shape number γ (2.4) obtained by solving equation (3.6) in combination with equations (3.3), (3.2), and (3.4) for different values of the friction number χ (2.5). The drawn black and dashed green lines represent the solutions obtained by *Toffolon and Savenije* [2011] and *Van Rijn* [2011], respectively.

More precisely, the damping equation of *Savenije et al.* [2008] differs from the linearized damping equation by a factor that depends on the phase lag ε, as becomes clear by substituting (3.2) into (3.1):

$$\delta = \frac{\gamma}{2} - \frac{1}{2} \frac{\chi \mu}{\lambda} \sin(\varepsilon). \tag{3.8}$$

Equations (3.6) and (3.8) are formally identical if $\sin(\varepsilon) = 8/(3\pi) \approx 0.85$, implying

a value of the phase lag of approximately 58° (2 hours for an M2 tide).

Dronkers [1964, p. 302] suggested an interesting higher order formulation for the friction term (see also *Cartwright* [1968]), leading to results that are comparable to those obtained using the fully nonlinear formulation for the friction term. *Dronkers* [1964] took account of over-tide generation by including a third order term (cubic velocity) in the friction term, while also assuming that U is a periodic function with zero mean:

$$F_D = \frac{16}{15\pi} \frac{v^2}{K^2 \overline{h}^{-4/3}} \left[\frac{U}{v} + 2\left(\frac{U}{v}\right)^3 \right]. \tag{3.9}$$

Note that this equation did not account for the time variable depth in the friction term. In our symbols the expression for the tidal damping using Dronkers' friction term would read (see Appendix A.3):

$$\delta = \frac{\gamma}{2} - \frac{8}{15\pi} \frac{\chi\mu}{\lambda} - \frac{16}{15\pi} \chi\mu^3\lambda. \tag{3.10}$$

Equation (3.10), when combined with equations (3.2), (3.3) and (3.4), forms a new set of nonlinear equations, which can be solved iteratively.

It is worth noting that the different methods use different definitions of the dimensionless friction factor f (i.e., equation (2.10)). The Lorentz's linearization and Dronkers' method consider a time-invariant depth in the friction term, which is the same as taking ζ=0 in (2.10), i.e., $f = g/\left(K^2 \overline{h}^{-1/3}\right)$.

3.3.2. Performance of Different Analytical Models

In order to investigate the performance of the analytical solutions, they have been compared with a fully nonlinear numerical solution of the governing equations (2.1) and (2.2). The numerical model [*Toffolon et al.*, 2006] is based on the explicit MacCormack method, which is second order accurate both in space and in time. A total variation diminishing (TVD) filter is applied to avoid spurious oscillations, especially when the wave steepens because of frictional or geometrical effects.

Since we focus on the tidal damping in this paper, in this section we present a comparison between the values of the dimensionless damping number δ estimated using analytical methods against the fully nonlinear numerical results. We consider a wide range of parameters (with $1 \leq \gamma \leq 3$, $0.1 \leq \zeta \leq 0.3$, 10 m$^{1/3}$s$^{-1} \leq K \leq 50$ m$^{1/3}$s^{-1} and $\overline{h}$=10 m) covering a wide spectrum of tidal channels. In order to present dimensionless results, distance x is scaled by the frictionless wavelength in prismatic channels:

$$x^* = \frac{\omega}{c_0} x \tag{3.11}$$

Figure 3.2 shows the performance of the different analytical models at a single position $x^* = 0.426$ (corresponding to 30 km for a 10 m deep estuary). Both the linear [*Toffolon and Savenije*, 2011] and the quasi-nonlinear [*Savenije et al.*, 2008] solution behave reasonably well, but none of them is fully correct for a finite

amplitude wave. It appears that Dronkers' approach lies closest to the numerical solution, and that *Savenije et al.* [2008] and *Toffolon and Savenije* [2011] have a consistent bias from the numerical solution. The former method underestimates the tidal damping, while the latter overestimates it.
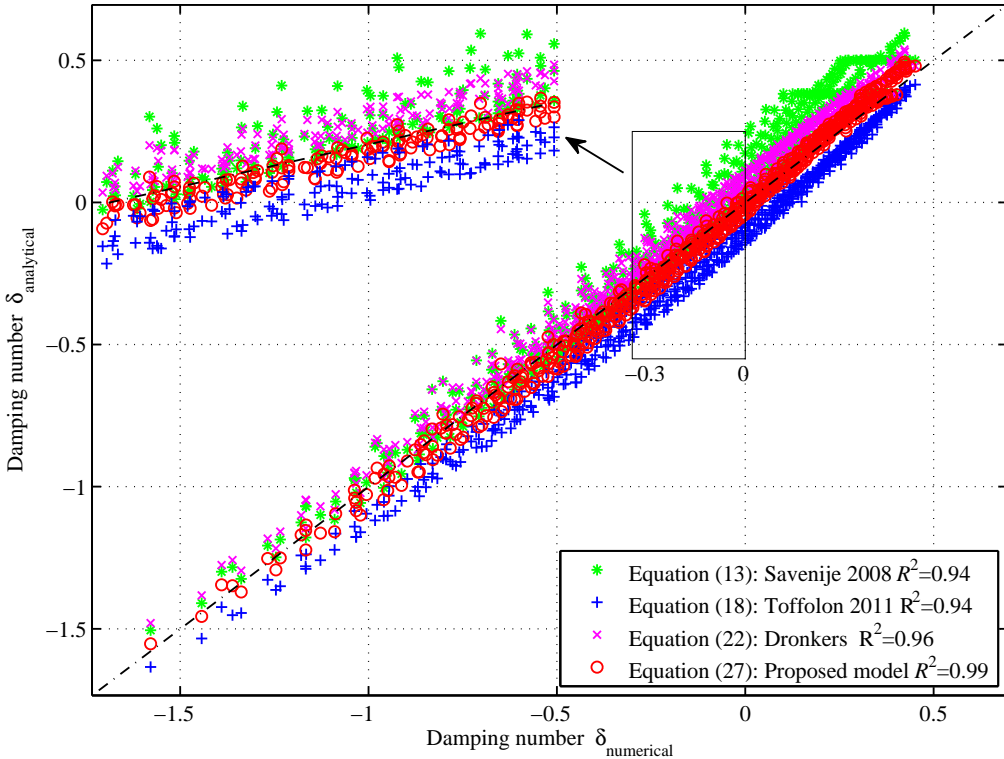
Figure 3.2: Tidal damping δ at $x^* = 0.426$ obtained with four different analytical models (new damping equation (3.15), Dronkers' equation (3.10), *Savenije et al.* [2008], *Toffolon and Savenije* [2011]), compared to numerical results. R^2 is the coefficient of determination, which provides an estimate of the average deviation of the estimates of the different analytical models from the assumed correct value (numerical model): the closer R^2 is to unit, the better is the model.

The reason for this behavior lies in the different simplifications used in the friction term F. *Toffolon and Savenije* [2011] used Lorentz's linearization (3.7), which is based on the equal energy dissipated by linear and quadratic friction during a tidal cycle (assuming a sinusoidal tide). On the other hand, working within an original Lagrangean-based approach, *Savenije et al.* [2008] obtained the effective friction $\widehat{F}_S$ acting over a tidal cycle by subtracting the high water (HW) and low water (LW) envelopes, leading to:

$$\widehat{F}_S = \frac{1}{2}\left[\frac{U_{HW}^2}{K^2\left(\overline{h} + \eta_{HW}\right)^{4/3}} + \frac{U_{LW}^2}{K^2\left(\overline{h} - \eta_{LW}\right)^{4/3}}\right],\tag{3.12}$$

where the two velocities at HW and LW follow from:

$$U_{HW} \approx v\sin(\varepsilon), \qquad U_{LW} \approx -v\sin(\varepsilon).\tag{3.13}$$

3

These approaches (linearized and quasi-nonlinear), which are correct for the strictly linear case where the tidal wave is a simple harmonic, yield opposite biases in the damping equation for finite-amplitude waves.

This behavior can be clearly seen from Figure 3.3, which compares the friction effectively acting during a tidal cycle considering the different options. The damping in the three standard Eulerian approaches (see also *Vignoli et al.* [2003]) is based on the definition of a tidally average friction term $\langle|F|\rangle = T^{-1}\int_T |F|\, \mathrm{d}t$, where F is estimated as follows: the fully nonlinear definition from (2.3) (blue line), Lorentz's linearization F_L from (3.7) (red dashed line), and Dronkers' relationship F_D from (3.9) (black dash-dot line). On the contrary, Savenije's Lagrangean approach (3.12) directly provides the effective friction $\widehat{F}_S$ (green dashed line), which can be consistently compared with the previous ones. All quantities used in Figure 3.3 are obtained by the numerical model, so the only difference is the approximation used for the friction term. The comparison suggests that the tidally averaged friction term obtained with Lorentz's linearization overestimates the friction along the estuary, while *Savenije et al.* [2008] model tends to underestimate it. In the middle, the third-order approximation by *Dronkers* [1964] is very close to the complete nonlinear friction.

As a whole, the two approaches to calculate the frictional dissipation (i.e., using the linearized friction term or the average of HW and LW values) consistently have an opposite bias. Because of this, it is attractive to explore if the 'true' damping can be obtained by taking the weighted average of equations (3.6) and (3.8):

$$\delta = \frac{\gamma}{2} - \alpha\frac{4}{3\pi}\frac{\chi\mu}{\lambda} - (1-\alpha)\frac{1}{2}\chi\mu^2.\tag{3.14}$$

For different weights of the linearized friction term α (from 0 to 1), it is possible to compare the values of δ obtained by equation (3.14) with the damping observed in the numerical results for the same wide range of parameters as for Figure 3.2. Figure 3.4 presents the optimum weight α with its standard error at different locations along the estuary and the corresponding coefficient of determination R^2. We can see that the optimum weight α becomes stable from $x^* \simeq 0.35$ onward and that the equilibrium weight for α is about 1/3. The fact that the weight is approximately 1 (corresponding to the linearized friction) near the estuary mouth is the result of the imposed harmonic boundary condition without overtides, which is consistent with the linear assumption. The stable values of α that develops in the landward direction indicates that the wave adjusts its shape toward an equilibrium shape.

Assuming $\alpha = 1/3$, the optimized damping equation hence reads:
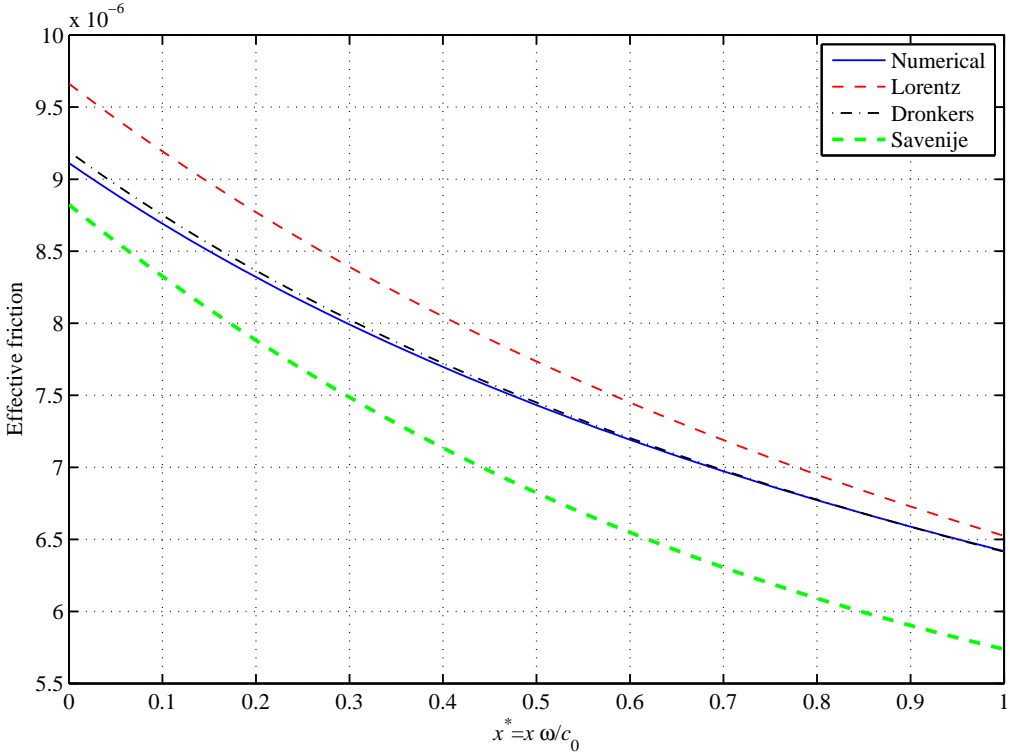
Figure 3.3: Comparison of the tidally averaged friction term $<|F|>$ computed with different formulations of the friction term: fully nonlinear (2.3) (blue line), Lorentz's linearization (3.7) (red dashed line), Dronkers' expansion (3.9) (black dash-dot line); and for Savenije's effective friction $\hat{F}_S$ (3.12) (green dashed line). All estimates are based on variables obtained from numerical results ($\gamma=1$, $\zeta=0.1$, $K=30$ m$^{1/3}s^{-1}$ and $\bar{h}=10$ m).

$$\delta = \frac{\gamma}{2} - \frac{4}{9\pi}\frac{\chi\mu}{\lambda} - \frac{\chi\mu^2}{3}. \tag{3.15}$$

This equation is very similar to Dronkers' equation (3.10), which can be rearranged using (3.2) in the following form:

$$\delta = \frac{\gamma}{2} - \frac{2}{5}\frac{4}{3\pi}\frac{\chi\mu}{\lambda} - \frac{32}{15\pi}\sin(\varepsilon)\frac{1}{2}\chi\mu^2. \tag{3.16}$$

Similarly to (3.14), the last two terms of equation (3.16) can be seen as a combination of (3.6) and (3.8), whereby the weights of the linearized and nonlinear models imply $\alpha = 0.4$ and $1 - \alpha = 0.68\sin(\varepsilon)$, which is satisfied if $\sin(\varepsilon) \simeq 0.88$, a value similar to the one derived from (3.8).

By iteratively solving the set of four analytical equations (3.2), (3.3), (3.4) and (3.15), we have obtained a new analytical solution for the dimensionless parameters

3
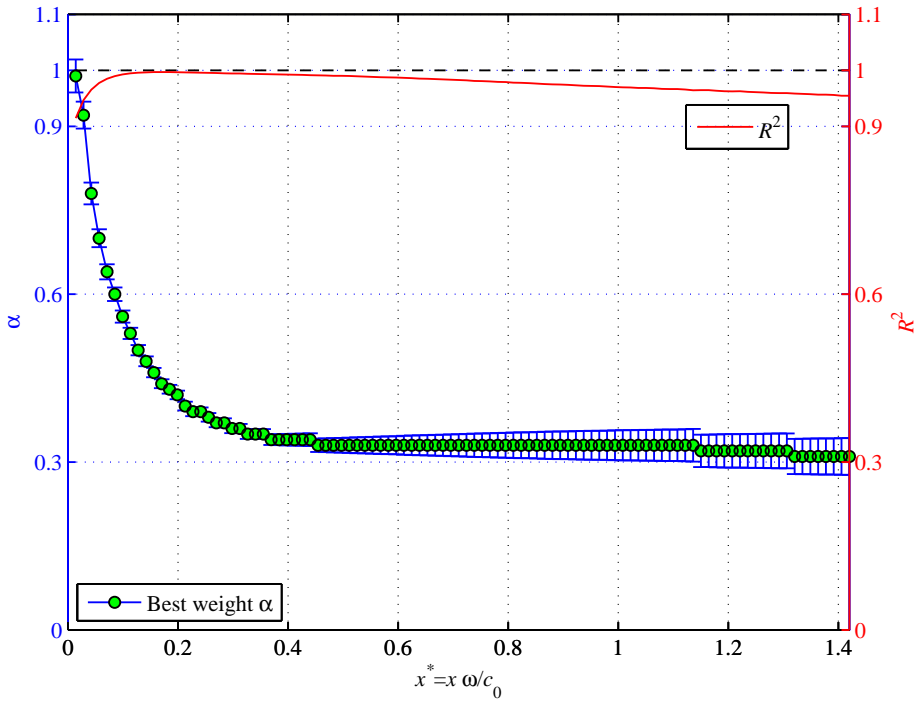
Figure 3.4: Optimum weight of the linearized friction term α with its standard error along the estuary axis and the corresponding coefficient of determination R^2.

μ, δ, λ, and ε. The damping number δ has been compared with the other solutions in Figure 3.2, and we can see that the agreement of equations (3.10) and (3.15) with the numerical model is very good, but the latter obtains the best result with the highest coefficient of determination $R^2 = 0.99$. Moreover, as we can see from Figure 3.5, where different versions of analytical solutions are compared with numerical results, the proposed new damping equation obtains the best result with the highest coefficient of determination R^2 along the estuary axis, except near the mouth of the estuary where the modified linear model [*Toffolon and Savenije*, 2011] achieves the best result due to the purely harmonic wave imposed at the seaward boundary.

Apparently, by combining the two approaches of *Toffolon and Savenije* [2011] and *Savenije et al.* [2008], we have obtained a more accurate analytical model, which is closer to the fully nonlinear numerical solution.
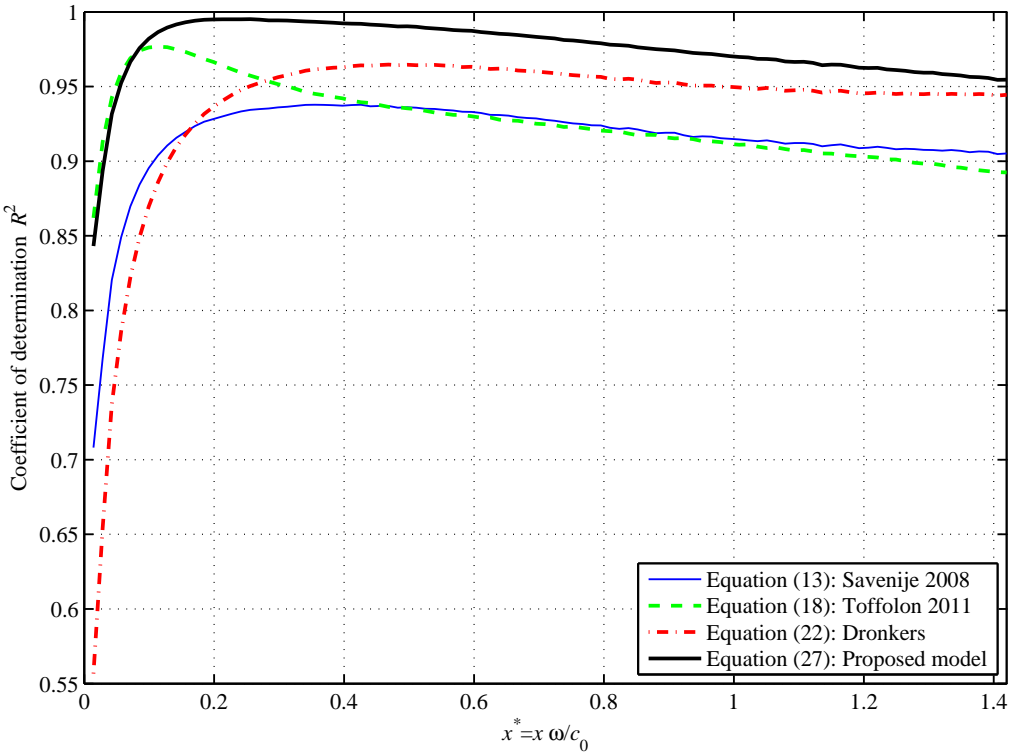
Figure 3.5: Longitudinal variation of the coefficient of determination R^2 between numerical model and different analytical models for a wide range of parameters with $1 \leq \gamma \leq 3$, $0.1 \leq \zeta \leq 0.3$, $10 \text{ m}^{1/3}\text{s}^{-1} \leq K \leq 50 \text{ m}^{1/3}\text{s}^{-1}$ and $\overline{h} = 10 \text{ m}$.

3.4. Behavior of the New Set of Equations

3.4.1. General Performance

Figures 3.6-3.9 present the solution of the velocity number, the damping number, the celerity number, and the phase lag obtained with the different analytical models as a function of γ and χ. In these graphs, the blue symbols represent the new method using equation (3.15), whereas the dashed red lines represent the solution of *Savenije et al.* [2008], the drawn black lines the solution of *Toffolon and Savenije* [2011], and the dashed-dotted green lines the solution with Dronkers' friction term. Unlike the equation of *Savenije et al.* [2008], which had two families of solutions for mixed and standing waves, both the new solution and the solutions of *Toffolon and Savenije* [2011] and Dronkers' approach provide continuous solutions in the transition zone of critical convergence [*Jay*, 1991] where γ is close to 2. In the new model, a clear separation between the subcritical and the supercritical cases exists only for vanishing friction ($\chi = 0$).

Comparing the new model with the other three models, we can see in Figures

3.6-3.9 that three zones can be distinguished. For small values of γ (weakly convergent estuaries), the main dimensionless parameters (μ, δ, λ and ε) obtained with the new model are closer to the linear solution of *Toffolon and Savenije* [2011]. In the transition zone where critical convergence occurs in the model of Savenije et al. (2008), the result is about the average of *Savenije et al.* [2008] and *Toffolon and Savenije* [2011]. For larger values of γ (the strongly convergent estuaries), we can see that the new solution is closer to the frictionless case. Moreover, it appears that Dronkers' solution is very close to our new solution for an amplified wave with bigger γ, while it is similar to *Savenije et al.* [2008] for waves with $\gamma < 2$. For an ideal estuary (where friction balances convergence), the four methods are identical.
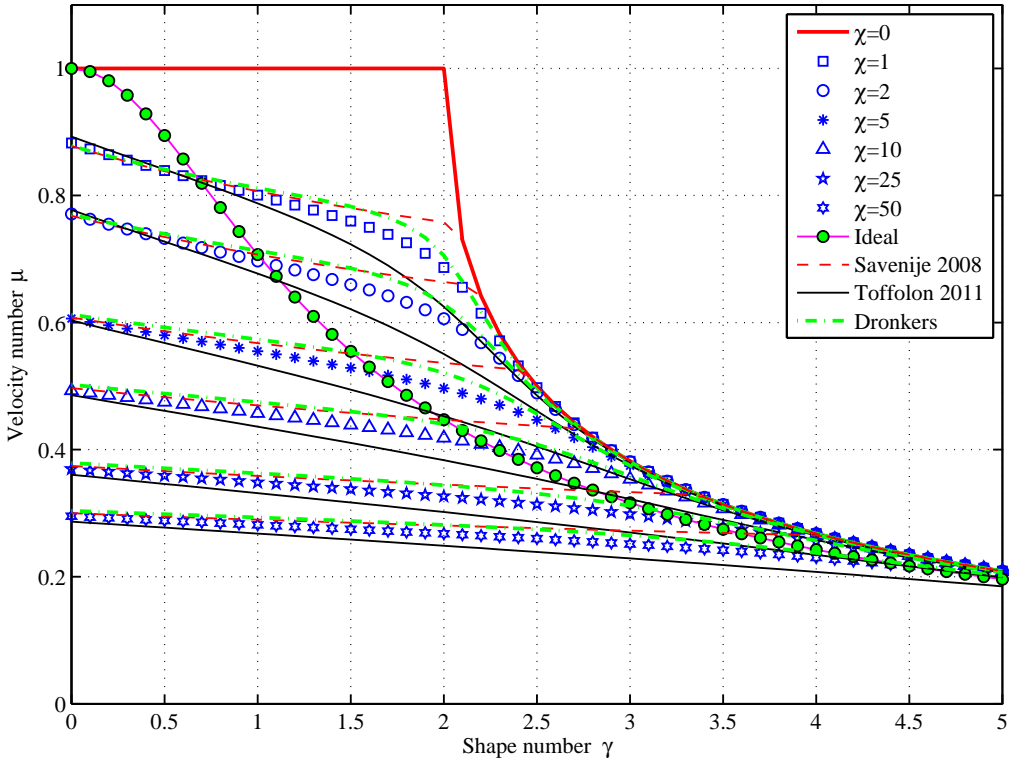
Figure 3.6: Relationship between the velocity number μ (2.6) and the estuary shape number γ (2.4) for different values of the friction number χ (2.5). The blue symbols indicate the new model exploiting equation (3.15). The red drawn line represents the frictionless estuary ($\chi=0$). The dashed red lines, drawn black lines, and dashed-dotted green lines represent the solutions obtained by *Savenije et al.* [2008], *Toffolon and Savenije* [2011], and Dronkers' approach, respectively. The green round symbols indicate the ideal estuary ($\mu = \sqrt{\frac{1}{1+\gamma^2}}$).
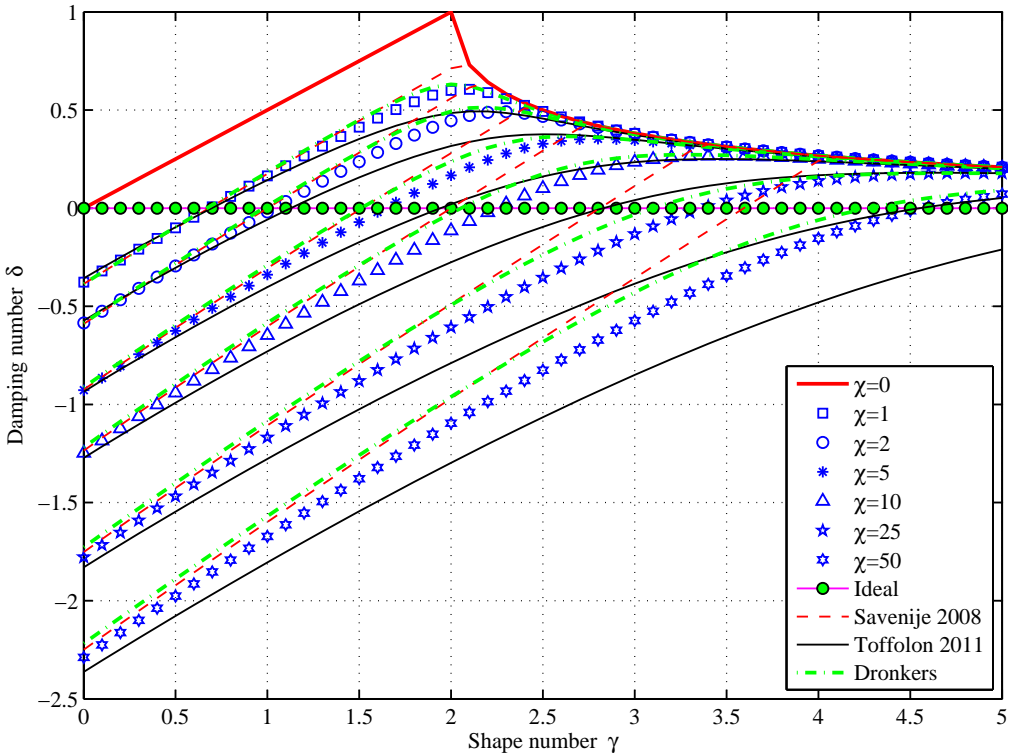
Figure 3.7: Relationship between the damping number δ (2.8) and the estuary shape number γ (2.4) for different values of the friction number χ (2.5). The symbols are as in Figure 3.6. The ideal estuary is defined by $\delta = 0$.

3.4.2. Application to the Scheldt Estuary

For given geometry, friction, and tidal amplitude at the downstream boundary, the dimensional values of the tidal amplitude η, the velocity amplitude υ, the wave celerity c, and the phase lag ε can be computed by using the analytical model presented in section 3.3. We have applied the new equation to the geometry of the Scheldt estuary, assuming a convergence length for the cross-sectional area $a = 27$ km (see also *Horrevoets et al.* [2004]). Until 110 km from the mouth of the estuary the flow depth is approximately constant ($\bar{h} = 11$ m), while more landward the depth reduces gradually to 2.6 m (assumed estuary length $L = 200$ km). At the estuary mouth ($x = 0$ m), we assume a harmonic tide characterized by a tidal amplitude $\eta_0 = 2.3$ m (spring tide) and a tidal period $T = 44400$ s.

The four analytical models have been compared with observations made in the Scheldt estuary during spring tide on 14-15 June 1995. The different models can be made to fit the observations if a suitable friction coefficient is used. However, this calibration provided significantly different values of the Manning-Strickler coefficient: $K = 32$ m$^{1/3}$s^{-1} for *Savenije et al.* [2008]'s model, $K = 33$ m$^{1/3}$s^{-1} for Dronkers'

3
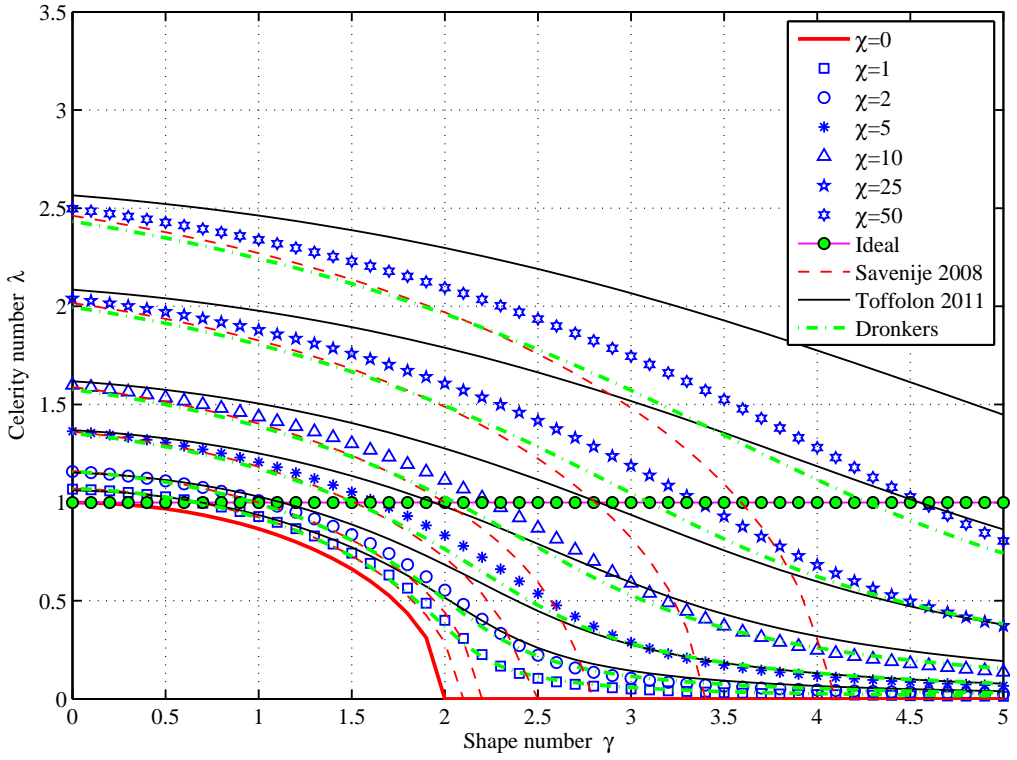
Figure 3.8: Relationship between the celerity number λ (2.7) and the estuary shape number γ (2.4) for different values of the friction number χ (2.5). The symbols are as in Figure 3.6. The ideal estuary is defined by $\lambda=1$.

approach, $K=39$ m$^{1/3}$s^{-1} for the present model, and $K=46$ m$^{1/3}$s^{-1} for *Toffolon and Savenije* [2011]'s model. Apparently the differences introduced by using different friction formulations can be compensated by decreasing or increasing the friction coefficient. Therefore, the different analytical models have also been compared with a 1D numerical model in the Scheldt estuary. The calibrated Manning-Strickler friction coefficient K used in the numerical model (38 m$^{1/3}$s^{-1}) appears to be almost the same as the friction coefficient of the new model (39 m$^{1/3}$s^{-1}), which is to be expected since the new damping equation (3.15) was obtained by calibration of K against numerical solutions. In Figure 3.10, all models use the same friction coefficient $K=38$ m$^{1/3}$s^{-1}. It can be clearly seen that the quasi-nonlinear model [*Savenije et al.*, 2008] and Dronkers' method underestimate the tidal damping while the linear model [*Toffolon and Savenije*, 2011] overestimates it. The reason for the overestimation of the travel time at LW in the landward part in both the analytical and numerical models is due to the neglect of river discharge and the high tidal amplitude to depth ratio.

Finally, the tidal characteristics of the Scheldt estuary, as computed with the new
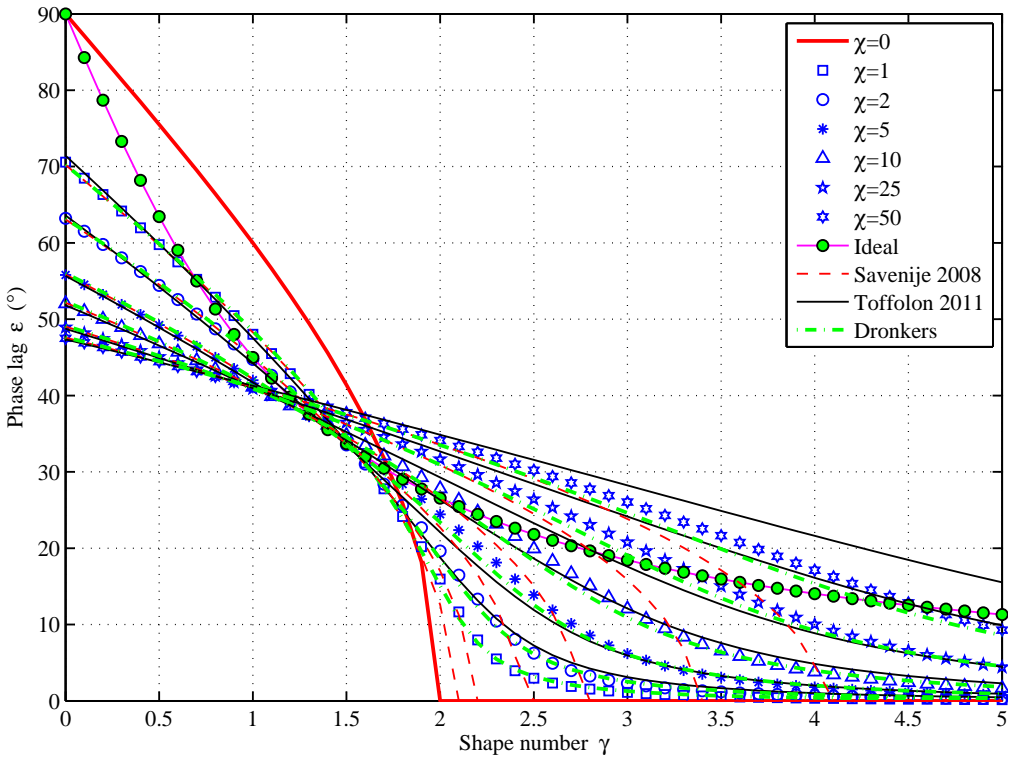
Figure 3.9: Relationship between the phase lag ε and the estuary shape number γ (2.4) for different values of the friction number χ (2.5). The symbols are as in Figure 3.6. The ideal estuary is defined by $\varepsilon = \arctan(1/\gamma)$.

model, are presented in diagrams for the velocity number, damping number, celerity number and phase lag. In Figure 3.11, the Scheldt estuary is represented by red line segments. Next to the segments, the distance from the estuary mouth in kilometers is written, indicating the length over which a segment is representative. We can see that in the Scheldt the seaward part (0-110 km) has a vertical line segment with a constant estuary shape number (this is due to the constant convergence length and depth assumed over that reach). At the inflection point, at 110 km, the tidal wave comes near to a standing wave, but unlike in the method of *Savenije et al.* [2008], this does not happen in the new method. Further upstream the pattern becomes irregular due to shallowing.

3.5. Results

3.5.1. Classification of Estuary

Estuaries can be classified on the basis of their water balance, geomorphology, vertical structure of salinity, or hydrodynamics [*Valle-Levinson*, 2010]. The interac-

3
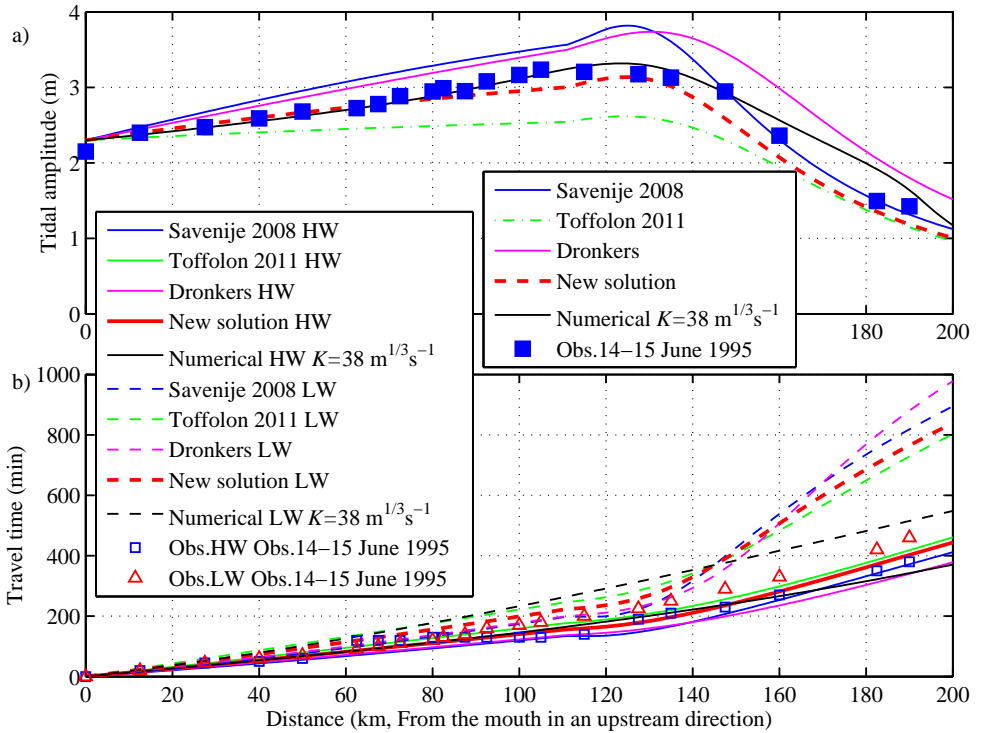
Figure 3.10: Comparison between different analytical models, numerical solution and field data: (a) tidal amplitude, and (b) travel time at HW and LW in the Scheldt estuary observed on 14-15 June 1995.

tion between tidal wave propagation and the geomorphology of the estuary is an important factor for characterizing the type of estuary [*Dyer*, 1997]. *Savenije et al.* [2008] suggest that the classification of estuaries can be based on the result of the imbalance between topographic convergence (i.e., the shape number γ) and friction (i.e., the friction number χ). If convergence is stronger than friction, the wave is amplified; if friction is stronger than convergence, the wave is damped; if their impact is equal, the tidal range is constant and the estuary is indicated as "ideal". In the following, we show that the classification of estuaries can be based on the comparison between tidally averaged depth $\bar{h}$ and ideal depth h_{ideal} which is defined as the depth corresponding to an ideal estuary obtained keeping all the other characteristic quantities (say, tidal amplitude at the mouth, convergence length, friction coefficient) fixed. In particular, an estuary can be characterized as amplified when $\bar{h} > h_{ideal}$, while it is a damped estuary for $\bar{h} < h_{ideal}$, and an ideal estuary for $\bar{h} = h_{ideal}$.

The marginal condition for tidal wave amplification is easily set by posing $\delta = 0$ (hence $\lambda = 1$ and $\tan(\epsilon) = 1/\lambda$). The resulting relationship between the friction
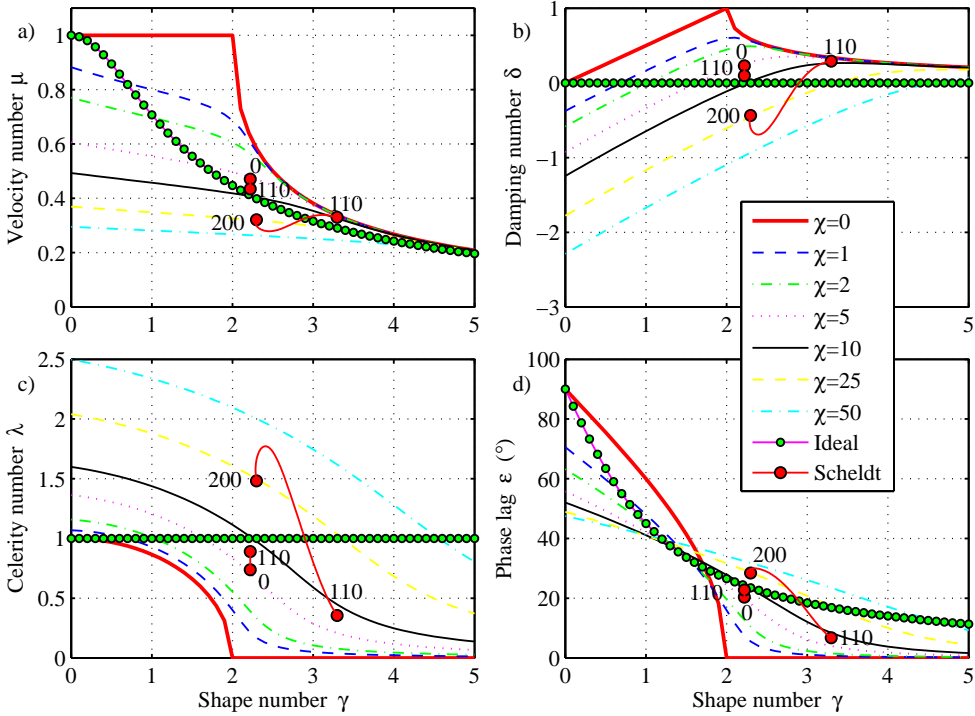
Figure 3.11: Positioning of the Scheldt estuary (red circles) in: (a) velocity number diagram, (b) damping number diagram, (c) celerity number, and (d) phase lag diagram. The numbers at the inflection points indicate the distance from the estuary mouth (in kilometers). The background shows the lines of the new model with different values of the friction number χ (2.5). The drawn line with dots represents the ideal estuary.

number χ and the shape number γ in the current model is:

$$\chi = \frac{\gamma}{\frac{8}{9\pi}\sqrt{\frac{1}{\gamma^2+1}} + \frac{2}{3(\gamma^2+1)}} ,$$

(3.17)

where, substituting (2.5) into (2.10), the friction number reads:

$$\chi = r_s \frac{g c_0}{K^2 \omega \bar{h}^{-4/3}\left[1 - (4\zeta/3)^2\right]} \zeta .$$

(3.18)

In the case of a small tidal amplitude to depth ratio ζ, equation (3.18) corresponds to the definition by *Toffolon et al.* [2006] and *Toffolon and Savenije* [2011].

Substitution of equation (3.17) into equation (3.18) yields the expressions of the ideal depth h_{ideal} as a function of tidal amplitude η, frequency ω, convergence length a, and friction K:

$$h_{ideal} = f(\eta, \omega, a, K). \tag{3.19}$$

It is easy to solve equation (3.19) by a simple numerical algorithm, e.g., Newton's iteration method, since the convergence is usually fast. Figure 3.12 shows the tidally averaged reference depth $\bar{h}$, the ideal depth h_{ideal} calculated by equation (3.19), and the critical depth $h_{critical}$ introduced in the next section. The classification of some estuaries in the world, based on the relative quantity $(\bar{h} - h_{ideal})/\bar{h}$ to assess the magnitude of amplification or damping, is presented in Table 3.2. It can be seen from Figure 3.12 that most of the estuaries, such as Bristol Channel, Outer Bay of Fundy, Scheldt and St. Lawrence, are significantly amplified estuaries because of the bigger positive relative difference between tidally averaged depth and ideal depth, while Fraser, Ord, Gambia, Pungue, Lalang, Tha Chin, and Chao Phya can be classified as damped estuaries due to negative relative difference. Finally, it is easy to see that Gironde, Hudson, Potomac, Maputo are very close to an ideal estuary. The correspondence of this classification with field observations is consistent, as confirmed by the references indicated in Table 3.2. The earlier studies of *Toffolon et al.* [2006] and *Savenije et al.* [2008] showed that the estuarine classification can be based on two dimensionless parameters γ and χ. Although results are obviously consistent, the present study yields a dimensional classification system.

Table 3.2: Characteristic values of alluvial estuaries and classification.

No.	Estuary [1]	T hour	η_0 m	$\bar{h}$ m	a km	K m$^{1/3}$s^{-1}	ζ −	γ −	χ −	h_{ideal} m	$(\bar{h} - h_{ideal})/\bar{h}$ −	$h_{critical}$ m	Type	Ref.[2]
1	Bristol Channel	12.4	2.6	45	65	33	0.06	2.30	0.48	14.9	0.67	37	Over-amplified	1
2	Columbia	12.4	1	10	25	38	0.10	2.81	2.21	4.7	0.53	9	Over-amplified	2
3	Deltaware	12.5	0.64	5.8	40	51	0.11	1.35	2.21	4.8	0.18	13	Amplified	3
4	Elbe	12.4	2	10	42	43	0.20	1.68	3.79	8.4	0.16	18	Amplified	4
5	Fraser	12.4	1.5	9	215	31	0.17	0.31	6.28	28.0	-2.11	370	Damped	1
6	Gironde	12.4	2.3	10	44	38	0.23	1.60	5.52	9.8	0.02	20	Close to ideal	5
7	Hudson	12.4	0.69	9.2	140	67	0.08	0.48	0.58	8.9	0.03	157	Close to ideal	1
8	Ord	12	2.5	4	15.2	50	0.63	2.83	54.5	4.5	-0.11	7	Damped	6
9	Outer Bay of Fundy	12.4	2.1	60	230	33	0.04	0.75	0.23	31.7	0.47	424	Amplified	1
10	Potomac	12.4	0.65	6	54	56	0.11	1.01	1.75	5.6	0.07	23	Close to ideal	1
11	Scheldt	12.4	1.9	10.5	27	39	0.18	2.67	3.35	6.2	0.41	11	Amplified	7
12	Severn	12.4	3	15	41	40	0.20	2.10	3.09	10.0	0.33	19	Amplified	8
13	St. Lawrence	12.4	2.5	70	183	44	0.04	1.02	0.11	23.8	0.66	267	Amplified	1
14	Tees	12	1.5	7.5	5.5	36	0.20	10.7	6.62	2.3	0.69	1	Over-amplified	9
15	Thames	12.3	2	8.5	25	31	0.24	2.57	9.94	6.9	0.19	12	Amplified	7
16	Gambia	12.4	0.6	8.7	121	42	0.07	0.54	1.43	11.2	-0.29	117	Damped	7
17	Pungue	12.4	3	4.3	20	31	0.70	2.31	341	6.9	-0.60	11	Damped	7
18	Lalang	12.4	1.5	10.6	217	40	0.14	0.33	2.73	23.0	-1.17	378	Damped	7
19	Tha Chin	12.4	1.35	5.3	87	34	0.25	0.59	13.47	14.3	-1.69	59	Damped	7
20	Incomati	12.4	0.5	3	42	50	0.17	0.92	6.14	4.6	-0.53	14	Damped	7
21	Limpopo	12.4	0.55	7	50	43	0.08	1.18	1.82	5.9	0.15	20	Amplified	7
22	Maputo	12.4	1.4	3.6	16	48	0.39	2.64	17.0	3.4	0.06	6	Close to ideal	7
23	Chao Phya	12.4	0.9	8	109	35	0.11	0.58	3.55	13.9	-0.74	94	Damped	7

[1] Data are modified from *Toffolon et al.* [2006], where data in columns L_b and C_h were listed in a wrong way due to editing mistakes.
[2] Reference where the classification is confirmed: 1, *Prandle* [1985]; 2, *Giese and Jay* [1989]; 3, *Friedrichs and Aubrey* [1994]; 4, *Savenije et al.* [2008]; 5, *Allen et al.* [1980]; 6, *Wright et al.* [1973]; 7, *Savenije* [1992a]; 8, *Uncles* [1981]; 9, *Lewis and Lewis* [1987].

3.5.2. Effect of Depth Variations on Tidal Dynamics in Real Estuaries

The relatively simple analytical solution proposed in this paper is powerful to obtain first-order estimates of the consequences of estuary geometry variations:
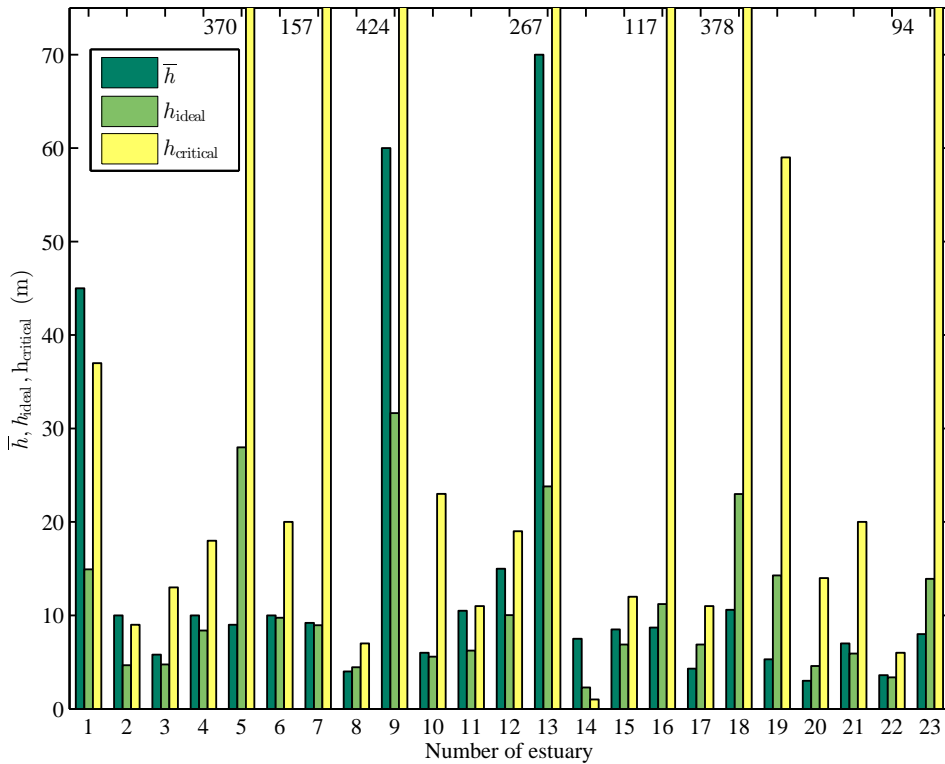
Figure 3.12: Values of the characteristic depths for the estuaries presented in Table 3.2: tidally averaged depth $\overline{h}$, ideal depth h_{ideal} from (3.19), critical depth $h_{critical}$ obtained by the condition (3.20). Bar for $h_{critical}$ are truncated and higher values are indicated by numbers. The physical meaning is as follows: if $\overline{h} > h_{ideal}$ the estuary is amplified ($\overline{h} < h_{ideal}$ implying damping); if $\overline{h} > h_{critical}$ the estuary is over-amplified.

it is a useful practical tool for management purposes, since it provides a rapid assessment of the tidal behavior of an estuary in response to external or internal modifications.

In particular, intensive dredging along the estuary, which changes the estuary topography, has a measurable impact on the tidal propagation and the damping through the variation of the depth. In addition, it has a direct relation to salt intrusion and storm surge propagation into the estuary. Also sea-level rise can modify the tidally averaged depth $\overline{h}$, thus producing effects that are qualitatively similar to those of dredging. *Church and White* [2006] estimated an increase of global sea-level ranging from 0.28 to 0.34 m from 1990 to 2100 based on the multi-century sea-level records, while projections for UK estuaries exceed 0.5 m at the end of the century for high emissions scenarios considering also vertical land movement [*Lowe*, 2009].

To demonstrate the potential of the analytical method to evaluate the effect

3

of deepening, we applied a depth increase of 3 m to the estuaries listed in Table 3.2. For simplicity, we assume that the tidal amplitude at the estuary mouth is unchanged by deepening. It is worth noting that *Garrett and Greenberg* [1977] showed how a change of tidal amplitude at the open boundary may be estimated and used to correct predictions of changes in tidal dynamics that might be brought about by the structures, such as tidal power development. Table 3.3 shows the effect of this deepening on tidal amplitude η, velocity amplitude v, wave celerity c, and phase lag ε at two fixed positions in the estuaries (x=0 and x=50 km). We can see that the response of these quantities to an increase of the depth is quite variable from case to case, while the wave celerity is always increased with larger depth. It is attractive to assess the influence of increasing depth on tidal variables through the diagrams of the velocity number μ, the damping number δ, the celerity number λ, and the phase lag ε (see Figures 3.6-3.9) as a function of γ and χ. Since the shape number γ is increased with depth, what we need to do is to determine the influence of depth on the friction number χ according to equation (3.18). At the mouth of estuary (x=0), it is easy to estimate the influence of dredging on tidal variables keeping the tidal amplitude constant: the friction number χ is decreased and the shape number γ increases due to larger depths.

Table 3.3: Variation of tidal amplitude $\Delta\eta$, velocity amplitude Δv, wave celerity Δc, and phase lag $\Delta\varepsilon$ at two locations after an increase of the average depth of 3 m.

No.	Estuary	$\Delta\eta$ (m)		Δv (m/s)		Δc (m/s)		$\Delta\varepsilon$ (°)	
		x=0	x=50 km	x=0	x=50 km	x=0	x=50 km	x=0	x=50 km
1	Bristol Channel	0	-0.05	-0.06	-0.09	105.49	91.87	-0.83	-1.06
2	Columbia	0	-0.09	-0.11	-0.17	110.36	92.33	-2.40	-3.46
3	Deltaware	0	0.18	-0.05	0.06	3.27	2.69	-7.90	-7.70
4	Elbe	0	0.33	-0.05	0.07	4.36	3.29	-7.21	-6.39
5	Fraser	0	0.19	0	0.09	0.84	0.48	2.23	1.45
6	Gironde	0	0.40	-0.04	0.11	3.06	2.30	-5.80	-5.22
7	Hudson	0	0.05	-0.06	-0.02	0.25	0.24	1.72	1.26
8	Ord	0	1.29	-0.12	0.13	24.10	11.62	-24.27	-15.11
9	Outer Bay of Fundy	0	0.01	-0.02	-0.02	0.13	0.13	-0.17	-0.16
10	Potomac	0	0.15	-0.05	0.06	1.38	1.21	-2.42	-3.24
11	Scheldt	0	-0.07	-0.19	-0.24	52.22	40.48	-5.77	-7.55
12	Severn	0	0.19	-0.12	-0.05	14.23	9.54	-8.28	-7.40
13	St. Lawrence	0	0	-0.02	-0.02	0.24	0.24	-0.53	-0.51
14	Tees	0	-0.04	-0.05	-0.05	878.26	841.05	-0.06	-0.07
15	Thames	0	0.31	-0.14	-0.04	17.64	11.65	-11.85	-10.78
16	Gambia	0	0.07	-0.03	0.02	0.55	0.44	2.22	1.25
17	Pungue	0	1.55	0.37	0.38	3.94	1.40	-17.2	-8.35
18	Lalang	0	0.15	-0.02	0.06	0.65	0.42	2.78	1.90
19	Tha Chin	0	0.34	0.02	0.17	1.20	0.59	0.40	-0.68
20	Incomati	0	0.27	-0.03	0.16	1.88	1.23	-4.08	-5.68
21	Limpopo	0	0.11	-0.03	0.04	1.84	1.61	-4.00	-4.39
22	Maputo	0	0.50	-0.27	-0.09	36.4	23.7	-19.6	-17.8
23	Chao Phya	0	0.14	-0.02	0.06	0.88	0.59	1.55	0.56

The effect of deepening on tidal dynamics is not linear: in same cases deepening leads to amplification while in others it leads to a reduction of the tidal amplitudes. Figure 3.13 shows the variation of the velocity amplitude as a result of deepening by 3 m (a) and a more modest increase of 0.3 m (b) for the same locations x=0 and x=50 km. In Figure 3.13a, corresponding to a depth increase of 3 m, it can be seen that the velocity at the estuary mouth is generally decreased as a result of dredging except in the Fraser, Pungue, and Tha Chin, while the velocity at x=50 km

increases with depth for most of the estuaries. Whether the velocity is increased or not depends on the position of the new values of γ and χ in the graph for the velocity number (Figure 3.6). The extremely high celerity in the Tees (see Table 3.3, No. 14) is attributed to the strong convergence of the estuary ($\gamma=10.72$), where a standing wave develops and the celerity tends to infinite. A similar behavior can be noticed in Figure 3.13b for the smaller depth increase (0.3 m), although some exceptions indicate that the behavior is not monotonic and that the trend of velocity amplification or reduction can change during the deepening process (for instance, in the Ord, Severn, Thames and Maputo, indicated by No. 8, 12, 15 and 22, respectively).
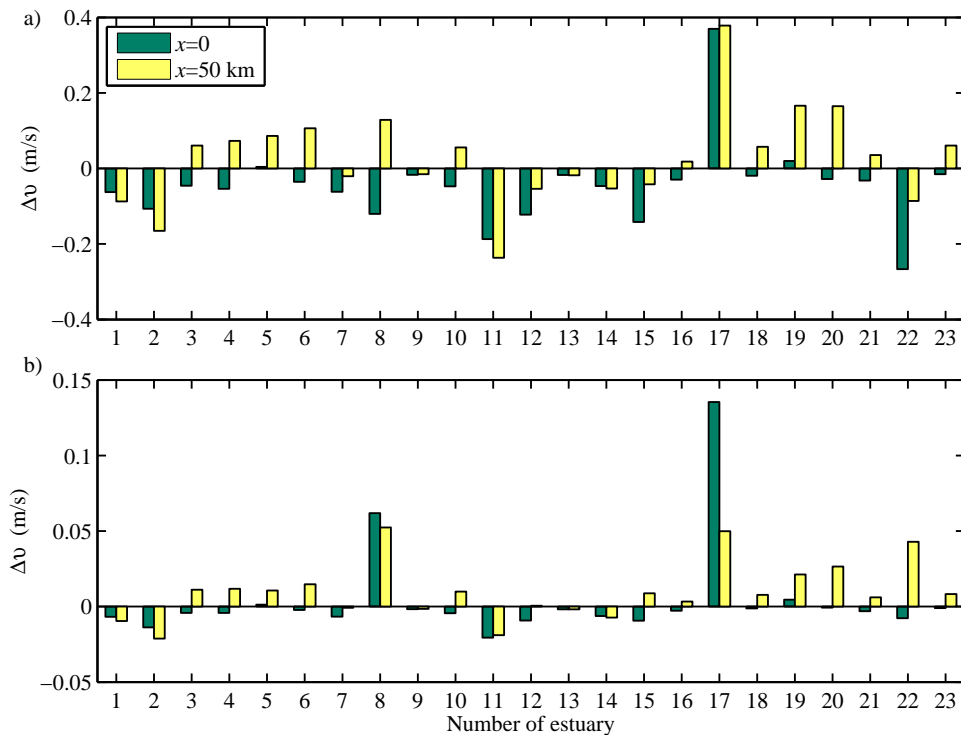
Figure 3.13: Change of the velocity amplitude at the estuary mouth ($x=0$) and at $x=50$ km for:(a) a large increase of the average depth of 3 m, due to dredging; (b) a modest increase of 0.3 m, in agreement with projected sea-level rise for 2100.

Another interesting result we see in Table 3.3 (deepening of 3 m) is that the tidal amplitude (at $x=50$ km) increases in most of the estuaries, but that the strongly amplified estuaries experience a reduction of the amplitude: e.g., Bristol Channel, Columbia, Scheldt and Tees. This is unusual since it is generally accepted that the tidal wave is further amplified as a result of the reduced friction induced by larger depth [e.g., *Luo et al.*, 2007; *Cai et al.*, 2012b]. To illustrate this phenomenon, we

present the trajectory of the damping number δ with increasing depth in Figure 3.14. It can be seen that the damping numbers of Bristol Channel, Columbia, Scheldt and Tees (No. 1, 2, 11 and 14; note that the position of Scheldt is different from that in Figure 3.11, where spring tide conditions were considered instead of mean tide) are actually decreasing with larger depth. We see that a depth increase only leads to increased amplification (larger δ) until a maximum value is reached at a critical depth $h_{critical}$ defined by the condition:

3
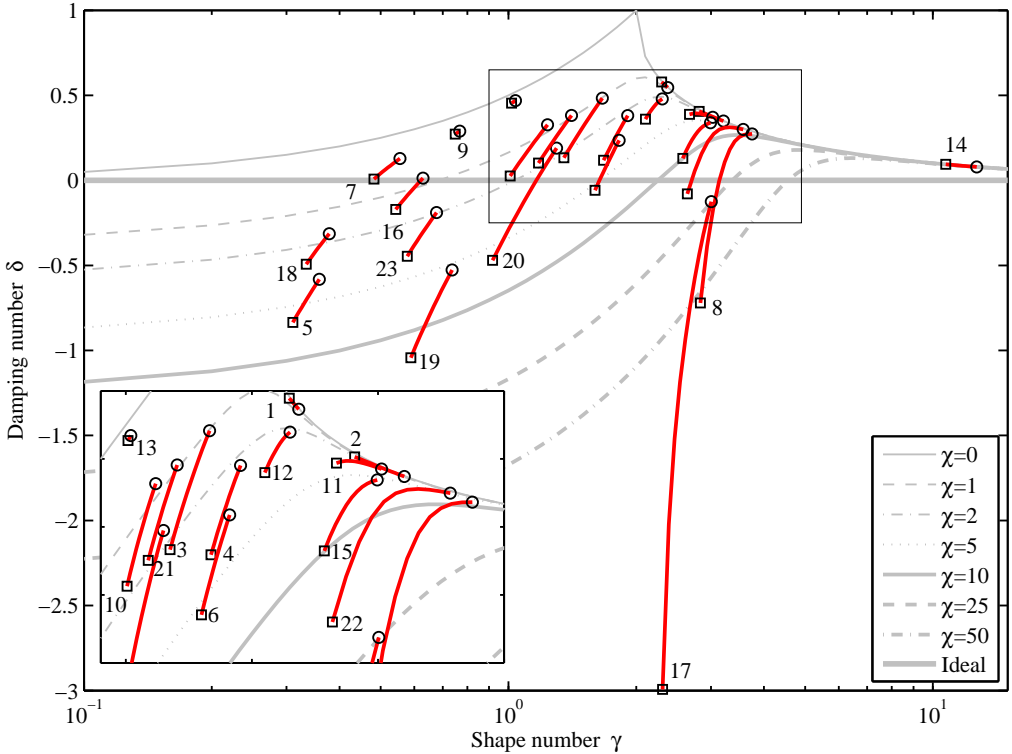
Figure 3.14: Positioning of the estuaries in Table 3.2 in the damping number diagram. The black square symbols indicate the initial position before dredging, while the black circle symbols represent the final position after increasing the depth by 3 m. The red segments indicate the trajectories in the (γ, δ) plane. The gray lines indicate the analytical solutions of the new model for different values of the friction number χ (2.5).

$$\frac{\partial \delta}{\partial \bar{h}} = 0 . \qquad (3.20)$$

A further increase of the depth leads to a reduction of the amplification until the ideal condition ($\delta=0$) is reached asymptotically. A similar equation was derived by *Savenije et al.* [2008] for critical convergence (i.e., equation 43 therein), which approximately corresponds to condition (3.20). The critical convergence was the

threshold beyond which the tidal wave acted as a standing wave. We see something similar here. However, unlike the discontinuous behavior predicted by *Savenije et al.* [2008], switching from one wave type to another, the current model provides a continuous solution.

We term estuaries having a depth $\overline{h} > h_{critical}$ as 'over-amplified', a condition typical of strongly convergent (large γ) and relatively weekly dissipative (small χ) estuaries, where increasing the depth reduces the amplification. It is possible to identify this critical depth $h_{critical}$ by changing the depth over a wide range of values in our analytical model until it satisfies condition (3.20): the calculated values are shown in Table 3.2. Figure 3.12 shows the comparison between the tidally averaged depth $\overline{h}$ and the critical depth $h_{critical}$: by comparing the difference between the green and yellow bar, we are able to determine whether an estuary is over-amplified (e.g., Bristol Channel, Columbia, and Tees, indicated by No. 1, 2 and 14, respectively) or not. Generally, with this figure, we are capable of predicting the influence of depth variations on tidal dynamics. This is particularly useful when assessing the influence of human interventions in estuary topography (e.g., dredging) or global sea-level rise on tidal propagation in estuaries, as it influences the aquatic environmental of an estuary and the potential use of water resources.

In Figure 3.14, we also see that the variation of the damping number in the Bristol Channel, Outer Bay of Fundy, and St. Lawrence (No. 1, 9 and 13, respectively) is very small. This is due to the fact that the tidally averaged depth $\overline{h}$ in these estuaries is very large while the shape number γ, which is increased by dredging, does not change much.

3.6. Conclusions

In this paper we revisited the analytical approach for tidal hydrodynamics proposed by *Savenije et al.* [2008] by introducing a new tidal damping equation, which is similar to the equation that uses the friction formulation proposed by *Dronkers* [1964]. Reworking this quasi-nonlinear solution, we are able to accurately reproduce the main dynamics of tidal wave propagation along estuary channels. We have also demonstrated that the linear models of *Toffolon and Savenije* [2011] and *Van Rijn* [2011] and the quasi-nonlinear model of *Savenije et al.* [2008] can be readily combined within one consistent theoretical framework, i.e., by solving the same set of equations with different formulations for the friction term. Exploring the difference between the quasi-nonlinear model [*Savenije et al.*, 2008] and the modified linear models proposed by *Toffolon and Savenije* [2011] and *Van Rijn* [2011], we found that the main difference lies in the friction term: the linear model exploits a linear damping equation resulting from a linearized friction term [*Lorentz*, 1926], while the quasi-nonlinear model retains the fully nonlinear friction term, with quadratic velocity and varying depth, but assuming a simple harmonic to determine the tidal velocity at HW and LW. An important difference between the quasi-nonlinear friction term and Dronkers' friction term lies in the fact that Dronkers' friction term does not account for tidally varying depth, while the quasi-nonlinear term does. Another difference is that the approach by *Savenije et al.* [2008] im-

plicitly accounts for the density term, while the other methods neglect the density effect. This has no implications because, as was shown by *Savenije* [2005], the density term cancels out in the derivation of the damping and celerity equations. We further note that the effect of river discharge can, in principle, be incorporated in the present model through a modified formulation, as proposed in *Cai et al.* [2012b].

We have compared the performance of the different analytical models with a fully nonlinear numerical model. The comparison indicates that *Savenije et al.* [2008] and *Toffolon and Savenije* [2011] models approach the numerical results from opposite sides (under/overestimating friction). A weighted average of the two comes very close to the numerical results, the optimum weight of the linearized friction term being 1/3, and 2/3 of the quasi-nonlinear friction term. We tested the equations in a real case, the Scheldt estuary, which has strong convergence (overall with γ values above 2, which is the region where the methods show the largest difference). Overall, the new method preforms best against field data and numerical results.

The new model proposed in this paper not only overcomes the unrealistically discontinuous behavior predicted by *Savenije et al.* [2008], but also improves on accuracy compared with linear models as by *Toffolon and Savenije* [2011]. This is important when assessing the influence of depth increase on tidal dynamics in real estuaries (e.g., because of human interventions, by dredging, or sea-level rise). For this purpose, we provided two threshold criteria: the ideal depth h_{ideal} (condition for vanishing damping) and the critical depth $h_{critical}$ (condition for maximum amplification). As a result, we could classify estuaries into three types on the basis of the tidally averaged depth $\overline{h}$ compared with h_{ideal}: damped ($\overline{h} < h_{ideal}$), amplified ($\overline{h} > h_{ideal}$), and approximately ideal ($\overline{h} \simeq h_{ideal}$). Moreover, an estuary can be characterized as over-amplified when it has a depth larger than the $h_{critical}$: in this case, a further increase of the depth reduces the tidal wave amplification.

4

Asymptotic behavior of tidal damping in alluvial estuaries

Tidal wave propagation can be described analytically by a set of four implicit equations, i.e., the phase lag equation, the scaling equation, the damping equation, and the celerity equation. It is demonstrated that this system of equations has an asymptotic solution for an infinite channel, reflecting the balance between friction and channel convergence. Subsequently, explicit expressions for the tidal amplitude and velocity amplitude are derived, which are different from the generally assumed exponential damping equation that follows from linearizing the friction term. Analysis of the asymptotic behavior demonstrates that exponential damping of the tidal amplitude is only correct for a frictionless wave or an ideal estuary (no damping). However, in estuaries with modest damping (near ideal) it provides a reasonable approximation. In natural estuaries there is generally a need to take account of local variability of e.g. depth and friction, by subdividing the estuary into multiple reaches. This is illustrated with an example of the Scheldt estuary, which has been gradually deepened for navigation purpose over the last half-century. The analytical model is used to study the effect of this deepening on the tidal dynamics in the main navigation channel, demonstrating that the navigation channel will become 'over-amplified' when it reaches a depth larger than the critical depth. In the case of over-amplification, a further increase of the depth reduces the amplification until critical convergence (condition for a frictionless standing wave) is reached asymptotically. Finally, based on the ratio between the tidal amplitude at the seaward boundary and the asymptotic tidal amplitude, estuaries can be classified into damped, amplified or ideal estuaries, which is illustrated with 23 real estuaries.

4.1. Introduction

In the previous chapter, we proposed a general analytical framework to simulate tidal wave propagation, which allowed the comparison of different analytical approaches mentioned above and concluded that the main difference between these models lies in the treatment of the friction term. It appeared that linear solutions, such as those by *Toffolon and Savenije* [2011] or *Van Rijn* [2011], based on the classical Lorentz linearization [*Lorentz*, 1926] for the friction term, are identical, although they used a different solution method. It was shown by *Cai et al.* [2012a] that a hybrid combination of the traditional linearized approach [e.g., *Toffolon and Savenije*, 2011] and the envelope method [e.g., *Savenije et al.*, 2008] provides the most accurate predictive results. However, although they provided an explicit solution for tidal damping, they were not yet able to write the tidal amplitude and velocity amplitude as explicit functions of distance. In this chapter, we provide a new explicit solution for the tidal amplitude. Furthermore we demonstrate that, in contrast with what is generally believed, the tidal amplitude has an asymptotic solution. Classical methods, assuming exponential damping, either lead to an infinite amplitude (when amplified), or a zero amplitude (when damped), but here we show that the asymptotic solution corresponds with the amplitude of an ideal estuary.

The chapter is organized as follows. First a comparison between classical solutions and those developed by *Savenije et al.* [2008], *Toffolon and Savenije* [2011] and *Cai et al.* [2012a] is presented in section 4.2. In section 4.3, a fully explicit solution of the tidal damping equation is developed, leading to an explicit equation for the tidal amplitude. In section 4.4, the upstream and downstream asymptotic behavior is explored based on the obtained explicit solution. In section 4.5, the model is compared to observations in the Scheldt estuary, which over the last half century has been substantially deepening with drastic implications for the tidal dynamics. The asymptotic solution is subsequently used to classify 23 real estuaries in the world. Finally, conclusions are drawn in section 4.6.

4.2. Comparison of Models

Table 4.1 presents one consistent theoretical framework for the solution of the one-dimensional hydrodynamic equations for tidal wave propagation as provided by *Cai et al.* [2012a] [based on *Toffolon et al.*, 2006; *Savenije et al.*, 2008] (see also chapter 3). *Cai et al.* [2012a] showed that different friction formulations can be used in the envelope method to arrive at an equal number of analytical solutions. In general, the main classes of the solutions are: (1) quasi-nonlinear solution with nonlinear friction term [*Savenije et al.*, 2008], (2) modified linear solution with Lorentz's linearization [*Lorentz*, 1926], (3) hybrid solution characterized by a weighted average of Lorentz's linearization, with weight 1/3, and the nonlinear friction term, with weight 2/3 [*Cai et al.*, 2012a]. And the solutions can be obtained by solving four implicit equations, i.e.,: the phase lag equation (T1), scaling equation (T2), celerity equation (T3), and damping equation (T4a, T4b, or T4c), where δ is the damping number (a dimensionless description of the amplification ($\delta > 0$) or damping

($\delta < 0$) of the tidal wave amplitude along the estuary), μ the velocity number (the actual velocity scaled with the frictionless value in a prismatic channel), γ the estuary shape number (representing the effect of cross-sectional convergence), χ the friction number (describing the role of the frictional dissipation), and λ the celerity number (the ratio between the theoretical frictionless celerity in a prismatic channel and the actual wave celerity). The dimensionless variables of these equations are presented in Table 4.2. The analytical solutions for some particular cases, including: constant cross-section ($\gamma=0$), frictionless channel ($\chi=0$, both with subcritical convergence ($\gamma <2$) and supercritical convergence ($\gamma \geq 2$)) and ideal estuary ($\delta=0$), are also presented in Table 4.1. For a frictionless or an ideal estuary, all methods are identical.

Table 4.1: Analytical framework for tidal wave propagation [*Cai et al.*, 2012a]

Case		Phase lag $\tan(\epsilon)$	Scaling μ	Celerity λ^2	Damping δ
General	Quasi-nonlinear	$\lambda/(\gamma - \delta)$	$\cos(\epsilon)/(\gamma - \delta)$	$1 - \delta(\gamma - \delta)$	$\gamma/2 - \chi\mu^2/2$ (T4a)
	Modified linear				$\gamma/2 - 4\chi\mu/(3\pi\lambda)$ (T4b)
	Hybrid	(T1)	(T2)	(T3)	$\gamma/2 - 4\chi\mu^2/(9\pi\lambda) - \chi\mu^2/3$ (T4c)
Constant cross-section	Quasi-nonlinear	$-\lambda/\delta$	$-\cos(\epsilon)/\delta$	$1 + \delta^2$	$-\chi\mu^2/2$
	Modified linear				$-4\chi\mu/(3\pi\lambda)$
	Hybrid				$-4\chi\mu^2/(9\pi\lambda) - \chi\mu^2/3$
Frictionless ($\gamma < 2$)		$\sqrt{4/\gamma^2 - 1}$	1	$1 - \gamma^2/4$	$\gamma/2$
Frictionless ($\gamma \geq 2$)		0	$(\gamma - \sqrt{\gamma^2 - 4})/2$	0	$(\gamma - \sqrt{\gamma^2 - 4})/2$
Ideal estuary		$1/\gamma$	$\sqrt{1/(1 + \gamma^2)}$	1	0

Savenije et al. [2008] showed that these equations (corresponding with quasi-nonlinear model in Table 4.1) can be solved explicitly, with two families of solutions. The first family consists of a mixed tidal wave with $0 < \epsilon < \pi/2$, while the second family consists of an "apparently standing" wave ($\epsilon = 0$). Recently, *Toffolon and Savenije* [2011] modified the classical linearized solution for tidal hydrodynamics in convergent channels by exploiting an iterative procedure to determine friction and a multi-reach approach (corresponding with modified linear model in Table 4.1). It was demonstrated by *Cai et al.* [2012a] that the modified linear model overestimates the tidal damping while the quasi-nonlinear model underestimates it, and the hybrid model provides the best predictions when compared with numerical results. Figure 4.1 describes the variation of the main dependent dimensionless parameters as a function of shape number γ and friction number χ, obtained with different analytical models. Unlike the discontinuous behaviour (i.e., with two families of solutions) and the transition towards a standing wave (i.e., the wave celerity approaching infinity) predicted by *Savenije et al.* [2008], both linear and hybrid models provide a continuous solution in the transition zone of critical convergence [*Jay*, 1991] where γ is close to 2. This is important since it enables the linear and hybrid models to be applicable in the zones where convergence exceeds critical convergence.

It is important to note that the two independent variables γ and χ depend on the tidally averaged depth $\bar{h}$ and tidal amplitude to depth ratio ζ, respectively. In Figure 4.1 we adopted a multi-reach approach in which the damping number δ is integrated in short reaches over which the estuary shape number γ and friction number χ are considered constant. This is done by simple explicit integration of the linear differential equation over a distance Δx (e.g., 1 km), leading to a tidal amplitude at

Table 4.2: The definition of dimensionless parameters

Dimensionless parameters	
Independent	Dependent
	Velocity number
	$\mu = v/(r_S \zeta c_0) = v\bar{h}/(r_S \eta c_0)$
Tidal amplitude at the downstream boundary	Damping number
$\zeta_0 = \eta_0/\bar{h}$	$\delta = \mathrm{d}\eta c_0/(\eta \mathrm{d}x\omega)$
Estuary shape	Celerity number
$\gamma = c_0/(\omega a)$	$\lambda = c_0/c$
Reference friction number	Phase lag
$\chi_0 = r_S g c_0/(K^2 \omega \bar{h}^{-4/3})$	$\epsilon = \pi/2 - (\varphi_z - \varphi_U)$
or	Tidal amplitude
Friction number at the downstream boundary	$\zeta = \eta/\bar{h}$
$\widehat{\chi_0} = \chi_0 \zeta_0 \left[1 - (4\zeta_0/3)^2\right]^{-1}$	
	Friction number
	$\chi = \chi_0 \zeta \left[1 - (4\zeta/3)^2\right]^{-1} = r_S f c_0 \zeta/\left(\omega \bar{h}\right)$

4

a distance Δx upstream, which is repeated for the whole estuary [*Savenije et al.*, 2008]. It should be noted that similar multi-reach approaches for the representation of topography and friction have been commonly used in literature [e.g., *Jay and Flinchem*, 1997; *Toffolon and Savenije*, 2011].

The classical analytical solution to tides in infinite channels assumes the tidal wave to be exponentially damped (or amplified) as it progresses into the estuary [e.g., *Hunt*, 1964; *Ippen*, 1966; *Friedrichs and Aubrey*, 1994; *Friedrichs*, 2010; *Van Rijn*, 2011], where the tidal amplitude and velocity amplitude, rewritten in our notation, are given by:

$$\eta = \eta_0 \exp(x\delta\omega/c_0), \tag{4.1}$$

$$v = v_0 \exp(x\delta\omega/c_0), \tag{4.2}$$

where η_0, v_0 represent the tidal amplitude and velocity amplitude at the estuary mouth, respectively.

Although widely applied, it can be shown that this assumption is only valid if the friction number χ is constant along the estuary axis (i.e., $\chi = \chi_0$), where χ_0 is the friction number calculated at the estuary mouth. This can be seen from Figure 4.2, which shows the dimensionless tidal amplitude η^* as a function of dimensionless distance x^*, using the quasi-nonlinear method of *Savenije et al.* [2008], indicated by (Q), modified linear method of *Toffolon and Savenije* [2011], indicated by (M), and hybrid method of *Cai et al.* [2012a], indicated by (H). It can be seen that these solutions only coincide with the classical equation if we use a constant friction number χ (indicated by a, b and c), where the definitions of η^* and x^* are:

$$\eta^* = \eta/\eta_0, \qquad x^* = x\omega/c_0. \tag{4.3}$$

It is worth noting that in the modified linear model the authors also used exponential damping, but that as a result of the iterative multi-reach approach with
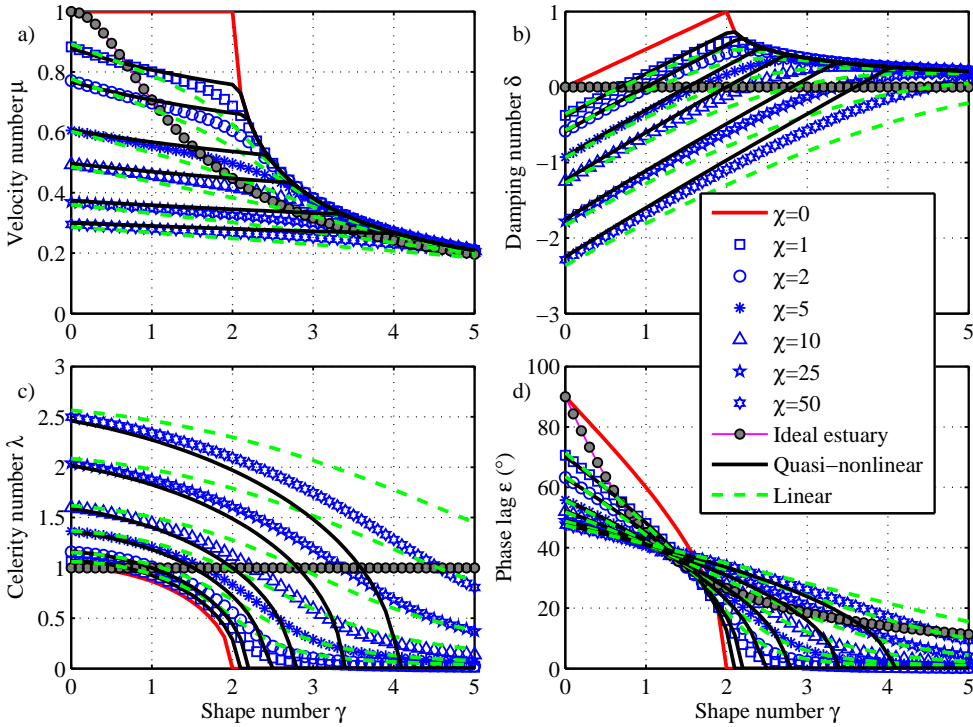
Figure 4.1: Main dimensionless parameters (the velocity number μ (a), damping number δ (b), celerity number λ (c) and phase lag ϵ (d) obtained with various analytical relationships as a function of estuary shape number γ for different values of friction number χ. The gray symbols represent the ideal estuary (see Table 4.1).

variable friction, the error made by assuming exponential damping was small (the linear model being a good first order approximation).

An important difference between the classical solution and the quasi-nonlinear approach is that the latter results in an equilibrium amplitude as an asymptotic solution when approaching infinity, whereas the classical solution approaches zero for a damped wave and infinity for an amplified wave. This asymptotic solution implies that the flow adapts itself to the shape of the estuary until it has the same properties as an ideal estuary, with a constant friction and tidal amplitude.

The condition of an ideal estuary (no damping) is easily set by imposing $\delta=0$ whereafter the relationship between the friction number χ and the shape number γ in the hybrid model becomes (see T4c in Table 4.1):

$$\chi = \gamma / \left\{ 8 / \left(9\pi \sqrt{1+\gamma^2} \right) + 2 / \left[3 \left(1+\gamma^2 \right) \right] \right\} . \tag{4.4}$$

In the quasi-nonlinear model this relationship reads (see T4a in Table 4.1):

4
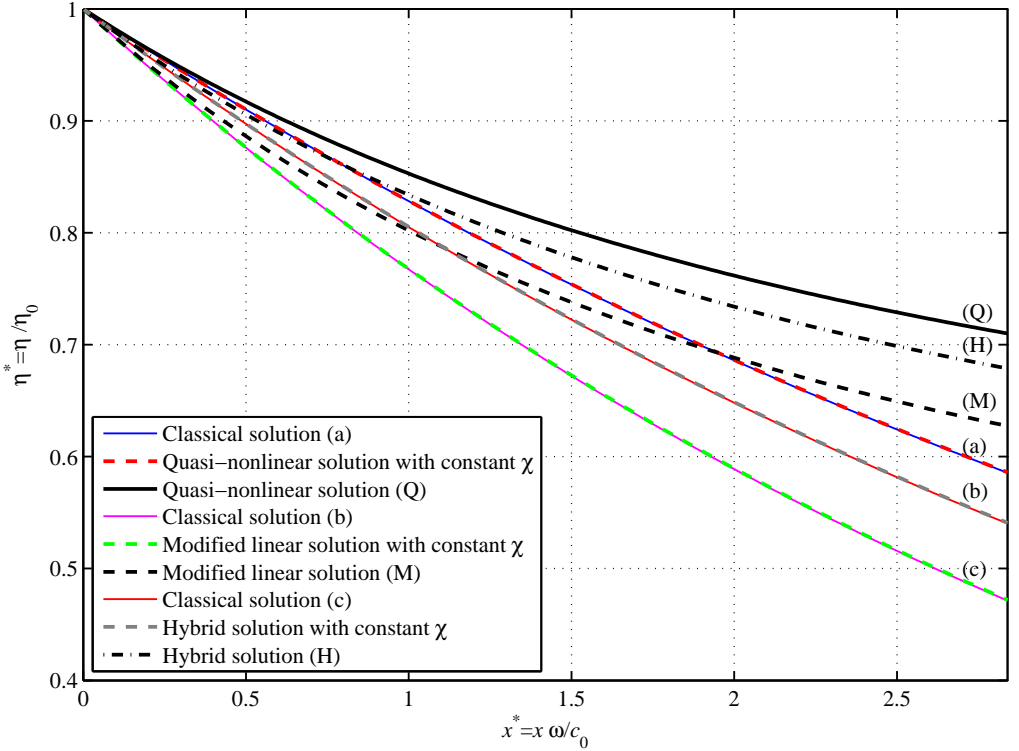
Figure 4.2: Longitudinal variation of tidal amplitude obtained with quasi-nonlinear (Q), modified linear (M) and hybrid (H) models applying constant and variable friction number for $\gamma=1$, $\zeta_0=0.1$, $K=30$ m$^{1/3}$s^{-1}. For comparison, the three classical solutions have been calculated with the boundary conditions for δ_0 corresponding to the quasi-nonlinear model (a), the modified linear model (b), and the hybrid model (c).

$$\chi = \gamma(\gamma^2 + 1). \tag{4.5}$$

Similarly, in the linearized model it reads (see T4b in Table 4.1):

$$\chi = 3\pi\gamma\sqrt{\gamma^2 + 1}/8. \tag{4.6}$$

It is worth noting that these methods use different definitions of the dimensionless friction factor f (i.e., equation (2.10)) incorporated in the friction number χ. The Lorentz's linearization considers a time-invariant depth in the friction term, which is the same as taking $\zeta=0$ in (2.10), i.e., $f \approx g/\left(K^2\bar{h}^{-1/3}\right)$ [*Toffolon et al.*, 2006; *Toffolon and Savenije*, 2011].

Using the definition of the friction number χ (see Table 4.2) in equation (4.4) yields the expression of the asymptotic tidal amplitude for the hybrid model [*Cai et al.*, 2012a]:

$$\eta_{\text{inf}} = \frac{-9m_1 + 3\sqrt{9m_1^2 + 64m_2^2}}{32m_2}\overline{h},\tag{4.7}$$

$$m_1 = r_s g c_0,\tag{4.8}$$

$$m_2 = \gamma K^2 \overline{h}^{-4/3} \omega / \left\{ 8/\left(9\pi\sqrt{1+\gamma^2}\right) + 2/[3(1+\gamma^2)] \right\}.\tag{4.9}$$

For small tidal amplitude to depth ratio ($\zeta \ll 1$), so that $f \approx g/\left(K^2\overline{h}^{-1/3}\right)$, equation (4.4) can be simplified whereby χ is linear in ζ. As a result, equation (4.7) modifies into:

$$\eta_{inf} \approx m_2 \overline{h}/m_1.\tag{4.10}$$

The relationship found for the quasi-nonlinear model is similar to equation (4.10) with only a different expression for m_2:

$$m_2 = \gamma(\gamma^2 + 1)K^2\overline{h}^{-4/3}\omega.\tag{4.11}$$

Similarly, the expression of m_2 for the linear model reads:

$$m_2 = 3\pi\gamma\sqrt{\gamma^2 + 1}K^2\overline{h}^{-4/3}\omega/8.\tag{4.12}$$

An example of the asymptotic solutions of these models is given in Figure 4.3 (the Matlab scripts are provided as auxiliary material[1]). We can see that the three solutions only differ in the parameter m_2 (i.e., $8\sqrt{1+\gamma^2}/(9\pi) + 2/3$ for the quasi-nonlinear model and $\pi/(4\sqrt{1+\gamma^2}) + 1/3$ for the modified linear model), resulting in a slightly different asymptotic value.

4.3. Explicit Solution to the Tidal Damping Equation

In principle, the explicit solution to the tidal damping equation can be derived for all three analytical models, i.e., quasi-nonlinear, modified linear and hybrid models. In the following we focus on the hybrid model since it provides the best predictive results [*Cai et al.*, 2012a]. The derivation for the other models are summarized in the Appendixes A.4 and A.5.

For an infinite length estuary and assuming that the freshwater discharge is small compared to tidal discharge, *Cai et al.* [2012a] derived an expression for tidal damping or amplification through the envelope method:

$$\frac{1}{\eta}\frac{d\eta}{dx}\left[1 + \frac{g\eta}{cv\sin(\epsilon)}\right] = \frac{1}{a} - \frac{2}{3}f\frac{v}{hc}\left[\frac{4}{3\pi} + \sin(\epsilon)\right],\tag{4.13}$$

[1]Auxiliary materials are available in the online version at http://onlinelibrary.wiley.com/doi/10.1002/2013JC008772/suppinfo

4
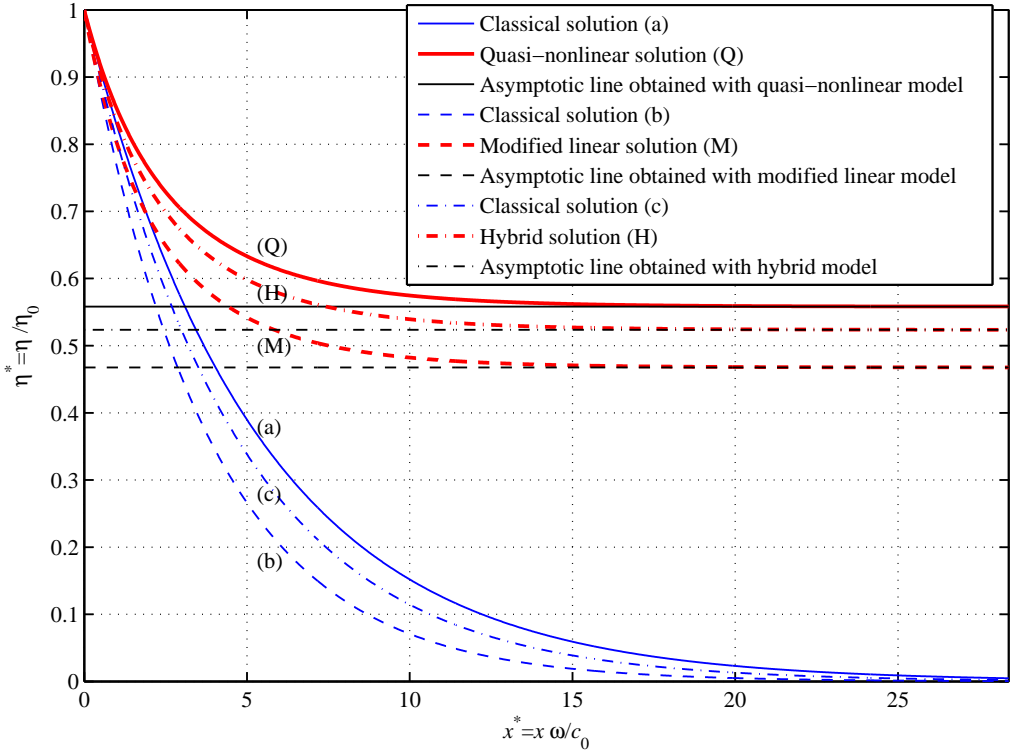
Figure 4.3: Longitudinal variation of tidal amplitude obtained with quasi-nonlinear (Q), modified linear (M) and hybrid (H) models for $\gamma=1$, $\zeta_0=0.1$, $K=30$ m$^{1/3}$s^{-1}. The black lines represent the corresponding asymptotic lines obtained with equation (4.7). The blue lines represent the classical solutions for the three different boundary conditions of δ_0 corresponding with the quasi-nonlinear model (a), the modified linear model (b), and the hybrid model (c).

which is identical to the dimensionless damping equation (T4c) for δ in Table 4.1.

Until now, the tidal amplitude and velocity amplitude variation along the estuary axis were obtained by step-wise numerical integration of the damping number δ. Here, we revisit the analytical approach proposed by *Cai et al.* [2012a] and derive an explicit analytical solution of the tidal damping equation, requiring the following assumptions:

1. A constant friction factor: f

2. A constant phase lag: ϵ

3. A constant wave celerity: c

4. A constant depth: $\bar{h}$

5. The velocity amplitude and tidal amplitude are proportional: $\dfrac{1}{\upsilon}\dfrac{\partial \upsilon}{\partial x} = \dfrac{1}{\eta}\dfrac{\partial \eta}{\partial x}$

The last assumption implies that the ratio of the velocity amplitude to the tidal amplitude is constant, which applies to estuaries of infinite length [*Savenije et al.*, 2008]:

$$\frac{\upsilon}{\eta} = \frac{\upsilon_0}{\eta_0} . \tag{4.14}$$

This relationship is valid for long coastal plain estuaries, which was demonstrated to be correct by *Savenije* [1992a, 1993a] based on numerical simulations in a wide range of convergent estuaries. Moreover, as a result of the multi-reach approach, e.g. to account for variability in the geometry, a potential error resulting from this assumption is small.

To simplify equation (4.13), two parameters are introduced:

$$\psi = 1 + \frac{g\eta}{c\upsilon \sin \epsilon} = 1 + \frac{g\eta_0}{c\upsilon_0 \sin \epsilon} = 1 + \frac{1}{\mu_0^2} , \tag{4.15}$$

$$\beta = \frac{2}{3} f \frac{\upsilon_0}{\bar{h}c} \left[\frac{4}{3\pi} + \sin(\epsilon) \right] . \tag{4.16}$$

which are constant under the above assumptions. It can be shown that $\psi \geq 2$ since $0 < \mu_0 \leq 1$ [*Savenije et al.*, 2008], while $\beta > 0$.

Substitution of equations (4.14)-(4.16) into equation (4.13) leads to:

$$\frac{d\eta^*}{dx} = \frac{\eta^*}{\psi a}(1 - a\beta\eta^*) . \tag{4.17}$$

It can be seen from equation (4.17) that convergence and friction are in balance if $\eta^* = 1/(a\beta)$, which is the case of an ideal estuary where there is no tidal damping or amplification. In fact, there are two situations where there is no damping. The first one is the trivial situation where $\eta^* = 0$, and the other is where $\eta^* = 1/(a\beta)$.

With $\eta_0^* = 1$ at $x = 0$, integration yields an explicit solution for the tidal amplitude:

$$\eta^* = \frac{1}{a\beta + (1 - a\beta) \exp\left[-x/(\psi a)\right]} = \frac{\eta_{inf}^*}{1 - \left(1 - \eta_{inf}^*\right) \exp\left[-x/(\psi a)\right]} , \tag{4.18}$$

where the infinite tidal amplitude $\eta_{inf}^* = 1/(a\beta)$ and the damping scale ψa are constants.

Introducing the dimensionless parameters used in Table 4.2, equation (4.18) can be rewritten as:

$$\eta^* = \frac{\gamma/\left[8\widehat{\chi_0}\mu_0\lambda/(9\pi) + 2\widehat{\chi_0}\mu_0^2\lambda^2/3\right]}{1 - \{1 - \gamma/\left[8\widehat{\chi_0}\mu_0\lambda/(9\pi) + 2\widehat{\chi_0}\mu_0^2\lambda^2/3\right]\} \exp\left[-\gamma\mu_0^2 x^*/(1 + \mu_0^2)\right]} . \tag{4.19}$$

Subsequently, the solutions of tidal amplitude η and velocity amplitude υ are:

$$\eta = \eta_0 \eta^*, \tag{4.20}$$

$$v = \frac{r_s c_0 \mu_0}{\overline{h}} \eta = \frac{r_s c_0 \mu_0}{\overline{h}} \eta_0 \eta^*, \tag{4.21}$$

where equation (4.21) has been obtained from the definition of the velocity number in Table 4.2.

Figure 4.4 presents the computed tidal amplitude along the estuary for the case of modest convergence (γ=0.5) resulting in a damped tidal wave, and for the case of strong convergence (γ=2), resulting in an amplified wave. The drawn lines correspond with the new explicit equation (4.19) whereas the dashed lines correspond with the classical exponential equation (4.1). It can be seen clearly that the two approaches have the same asymptote at x^*=0, but that the difference lies in the asymptote when x^* approaches infinity. With equation (4.1) the tidal amplitude approaches zero for a damped wave and infinity for an amplified wave, whereas equation (4.19) has an asymptotic tidal amplitude that reflects the balance between friction and channel convergence. However, for an estuary with constant cross section (i.e., γ=0 without channel convergence) equation (4.19) is no longer applicable, but continuous damping leads to an asymptote of $\eta_{inf}^* = 0$.

4.4. Asymptotic Behavior of the Damping Equation
4.4.1. Upstream asymptotic behavior

In the asymptotic situation with no river discharge, the infinite dimensionless tidal amplitude η_{inf}^* reads:

$$\eta_{\text{inf}}^* = \frac{1}{\alpha\beta} = \gamma \Big/ \Big[8\widehat{\chi_0}\mu_0\lambda/(9\pi) + 2\widehat{\chi_0}\mu_0^2\lambda^2/3 \Big]$$

$$= \gamma \Big/ \Big[8\widehat{\chi_0}\mu_I\lambda_I/(9\pi) + 2\widehat{\chi_0}\mu_I^2\lambda_I^2/3 \Big] = \frac{\chi_I}{\widehat{\chi_0}}, \tag{4.22}$$

where the last step in (4.22) follows from using the expressions for χ in equation (4.4) and for μ_0 and λ of an ideal estuary [*Cai et al.*, 2012a]:

$$\mu_I^2 = \frac{1}{1+\gamma^2}, \qquad \lambda_I = 1, \tag{4.23}$$

where the subscript I stands for the ideal estuary. This implies that in the upstream asymptotic situation the amplitude tends to an ideal estuary with constant amplitude. If $\eta_{inf}^* > 1$ (or $\chi_I > \widehat{\chi_0}$, $\alpha\beta < 1$), then the estuary is amplified; if $\eta_{\text{inf}}^* < 1$ (or $\chi_I < \widehat{\chi_0}$, $\alpha\beta > 1$), then it is damped; and if $\eta_{\text{inf}}^* = 1$ (or $\chi_I = \widehat{\chi_0}$, $\alpha\beta = 1$), the estuary is ideal.

Using (4.4) for χ of an ideal estuary, the amplitude then becomes:
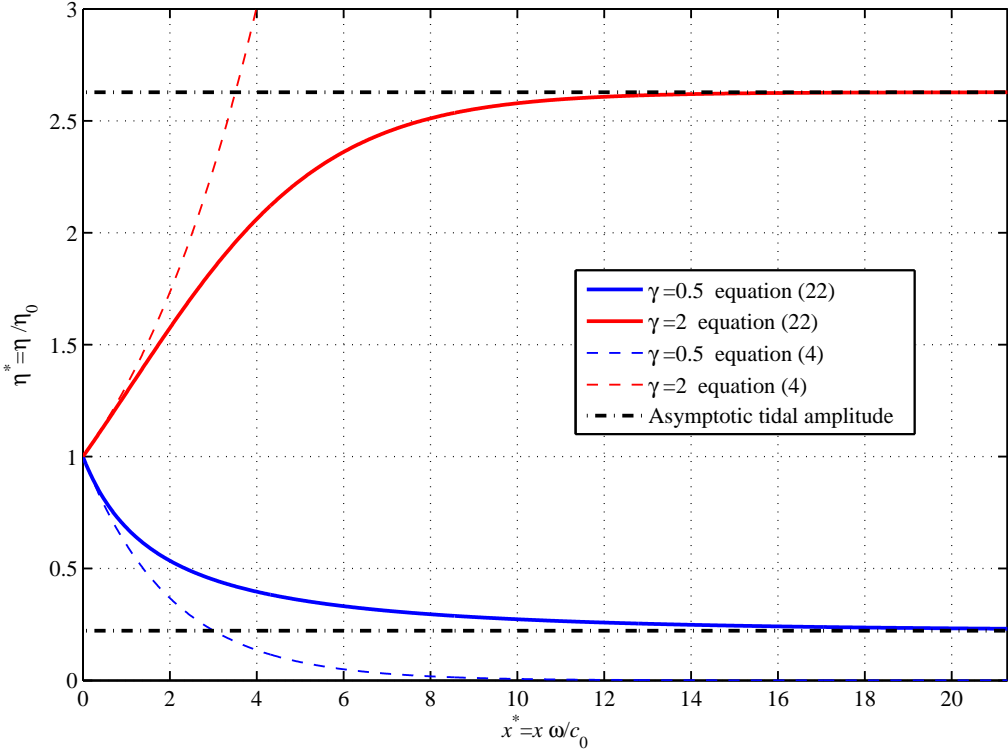
Figure 4.4: Comparison of longitudinal tidal amplitude between the proposed explicit equation (4.19) and the classical equation (4.1), for strong ($\gamma=2$) and modest ($\gamma=0.5$) convergence with $\zeta_0=0.1$, $K=30$ m$^{1/3}$s^{-1}.

$$\eta_{inf} = \frac{\chi_I}{\widehat{\chi_0}}\eta_0 = \frac{\gamma/\left\{8/\left(9\pi\sqrt{1+\gamma^2}\right)+2/\left[3(1+\gamma^2)\right]\right\}}{\widehat{\chi_0}}\eta_0$$

$$= \frac{\omega}{c_0}\frac{\overline{h}^{-2}}{r_s f}\gamma/\left\{8/\left(9\pi\sqrt{1+\gamma^2}\right)+2/\left[3(1+\gamma^2)\right]\right\}, \qquad (4.24)$$

or

$$\zeta_{inf} = \frac{\overline{h}}{a}\frac{1}{r_s f\left\{8/\left(9\pi\sqrt{1+\gamma^2}\right)+2/\left[3(1+\gamma^2)\right]\right\}}, \qquad (4.25)$$

which is an expression that only depends on the geometry and the friction, and is independent on the boundary conditions. The caveat is that the equation applies to long (infinite) estuaries where we may assume that $\frac{1}{\upsilon}\frac{\partial \upsilon}{\partial x} = \frac{1}{\eta}\frac{\partial \eta}{\partial x}$. We can see

that in deep convergent estuaries (with large γ), this can lead to a large equilibrium amplitude. Equation (4.24) is the same as equation (4.10) for small value of ζ, where equation (2.10) is reduced to $f \approx g/\left(K^2 \overline{h}^{-1/3}\right)$. Using the scaling equation (T2) in Table 4.1 together with (4.23) yields the expression for the asymptotic velocity amplitude:

$$v_{inf} = \frac{\overline{h}}{a} \frac{c_0}{f\left\{8/(9\pi) + 2/\left[3\sqrt{1+\gamma^2}\right]\right\}} \,. \tag{4.26}$$

It is interesting to note that if an estuary is long enough, the system will adjust itself until the condition of the ideal estuary is achieved. This is an indication that the ideal estuary is the energetically stable state of an estuary to which the forces of nature converge. Also note that the variables in these equations are all independent variables related to the geometry and the friction, and hence that the asymptotic state is independent of the tidal forcing.

4.4.2. Downstream asymptotic behavior

Near the estuary mouth, we can also look at the asymptotic behavior. To what extent is the damping exponential? We can approach the longitudinal damping/amplification of the tidal amplitude by a Taylor series:

$$\eta^* \approx \eta_0^* + \frac{d\eta_0^*}{dx}x + \frac{d^2\eta_0^*}{dx^2}\frac{x^2}{2} + \dots \, . \tag{4.27}$$

On the basis of (4.17) we can determine the second derivative of η^*:

$$\frac{d^2\eta^*}{dx^2} = \frac{1}{(\psi a)^2}\left[2a^2\beta^2\eta^{*3} - 3a\beta\eta^{*2} + \eta^*\right]. \tag{4.28}$$

Substitution of (4.17) and (4.28) into (4.27) with $\eta_0^* = 1$ yields:

$$\eta^* \approx 1 + (1 - a\beta)\frac{x}{\psi a} + \frac{1}{2}(2a^2\beta^2 - 3a\beta + 1)\left(\frac{x}{\psi a}\right)^2 + \dots \tag{4.29}$$

In a region close enough to the mouth where $x < \psi a$, we can see that the damping or amplification behaves as a linear function of x. If $a\beta$ is very small, then the slope is $1/(\psi a)$. For large values of $a\beta$, the gradient becomes negative and the steeper it gets, the less linear the behavior. A small value of $a\beta$ occurs in deep and strongly converging estuaries, which are generally amplified. Hence we see that amplification is often linear, as is the case in the Scheldt [*Savenije*, 2001]. The region where amplification is linear may extend over quite some distance into the estuary. The nonlinear effect only becomes apparent when we move further upstream. In contrast, we see that the process of damping is never linear but closer to an exponential function.

It is interesting to compare the above Taylor series with the Taylor series of the classical exponential damping equation (4.1). We can develop the exponential equation in a Taylor series as well (making use of (4.17)):

$$\eta^* \approx 1 + (1 - a\beta) \frac{x}{\psi a} + \frac{1}{2}(1 - a\beta)^2 \left(\frac{x}{\psi a}\right)^2 + \dots . \qquad (4.30)$$

We can then see that the first two terms are the same, but that the higher order terms are different. Figure 4.5 compares the factors of the second order terms. We can see from Figure 4.5 that the two expressions are only the same in two situations: the ideal estuary (where $a\beta = 1$) and the frictionless wave (where $a\beta = 0$). The first case is trivial, because in the ideal case there is no damping, while the second case is an unrealistic case. As a result, the exponential damping assumption is only acceptable if the estuary is near ideal (almost no damping or amplification), or has very low friction. In the next section we shall show that in real estuaries the use of the classical equation can lead to substantial errors.
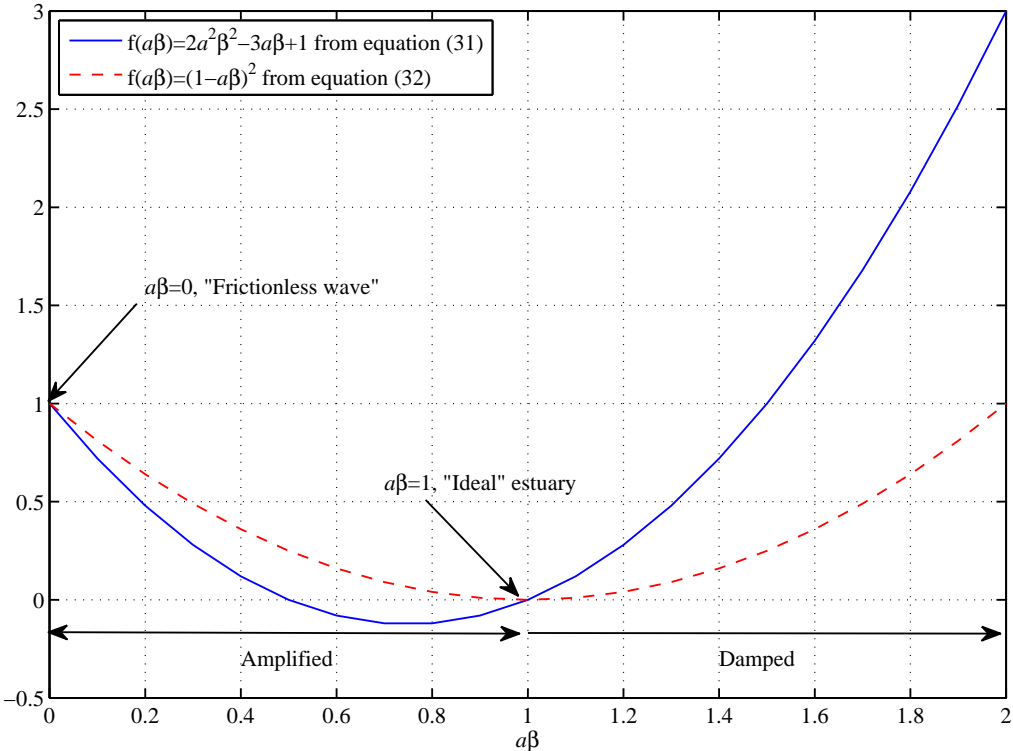
Figure 4.5: Comparison of the Taylor expansion between the new (4.29) and the classical (4.30) damping equations.

4.5. Results

4.5.1. Accounting for Local Variability

The depth, celerity, phase lag and friction of an estuary are seldom considered constant along the estuary axis. To follow along-channel variations of the estuary geometry or friction, we can split the channel into a series of reaches with different (but constant) friction, phase lag, celerity, depth, etc. [e.g., *Souza and Hill*, 2006; *Savenije et al.*, 2008; *Toffolon and Savenije*, 2011; *Cai et al.*, 2012a]. Since we derived the explicitly analytical solution for tidal propagation based on only the seaward boundary condition, it can be readily applied in a multi-reach model moving the origin of the axis for every reach.

For given geometry, friction and tidal amplitude at the seaward boundary η_0, we are able to compute the shape number γ and the friction number at the estuary mouth $\widehat{\chi_0}$. We thereby assume constant values of μ, λ, ϵ within each reach (calculated at the origin of each reach), which can be computed by solving the set of equations in *Cai et al.* [2012a]. Unlike *Cai et al.* [2012a] who solved the longitudinal tidal amplitude by numerical integration of the damping number δ over a length step Δx, we calculate the tidal amplitude variation along the estuary axis directly from the new equation (4.19). The use of the explicit equation (4.19) leads to an updated tidal amplitude η_1 (hence friction number χ_1) at a distance interval Δx (e.g., 1 km) upstream, which is repeated for the whole estuary.

For the case of negligible river discharge, it is customary that classical studies [e.g., *Hunt*, 1964; *Ippen*, 1966; *Friedrichs and Aubrey*, 1994; *Friedrichs*, 2010; *Van Rijn*, 2011] use the exponential function (4.1) to describe the longitudinal variation of the tidal amplitude along the estuary axis. It is important to note that in these studies the damping number, the celerity number and the phase lag are assumed to be constant for the entire estuary reach. The two undetermined parameters (i.e., the Manning-Strickler friction coefficient K and the storage width ratio r_S) are subsequenlty calibrated by comparing the computed results against observations of tidal amplitude and travel time of the tidal wave. While the damping/amplification is sensitive to both friction and storage width ratio, the wave celerity is specifically sensitive to the r_S. The method presented here differs from these earlier studies in that we derive local solutions depending on the local tidal amplitude to depth ratio ζ, which enables the model to take account of along-channel variations of the estuary geometry (e.g., the depth and the storage width ratio) or the friction. The whole estuary can be divided into multiple reaches of length Δx (e.g., 1 km) with constant depth and friction while the variable tidal amplitude is obtained by the explicit equation (4.19). The same method can be applied using the classical linear solutions [see, for instance, *Toffolon and Savenije*, 2011].

Incorporating the new explicit equation (4.19) into a multi-reach approach with $\Delta x = 1$ km, the Hybrid model [*Cai et al.*, 2012a] has been applied to the Scheldt estuary. The total length of the estuary is about 180 km from the estuary mouth at Vlissingen to the estuary head near Gent (closed by a weir). The annual observations of tidal amplitude and travel time at HW and LW along the Scheldt between 1955 – 2006 have been used to calibrate and verify the model. The cross-sectional area of the estuary can be well represented by an exponential function (1.2) with

a convergence length a=27 km in the seaward part ($0 - 90$ km) and a=18 km ($90 - 180$ km) in the upstream part [see also *Horrevoets et al.*, 2004]. The reduction of the convergence length is due to the shallowing, whereby the upstream part has experienced less dredging. Until 90 km from the estuary mouth (x= 0 km, Vlissingen) it is observed that the flow depth is approximately constant, while more landward the depth gradually reduces (until about 3 m) as the estuary becomes more riverine in character. Table 4.3 presents the geometric and flow characteristics as well as the calibrated parameters, including the storage width ratio r_S and Manning-Strickler coefficient K on which the computation is based. During the examined period (1955 – 2006), according to the cross-sectional survey, the annually averaged depth of the seaward part (x= 0 – 90 km) was deepened from 10.5 m to 12.3 m.

Table 4.3: Parameters used for analytical models in the Scheldt estuary (1955 – 2006)

Reach (km)	Convergence length a (km)	Averaged depth $\bar{h}$ (m)	Tidal amplitude at Vlissingen η_0 (m)	Storage width ratio r_S	Manning-Strickler coefficient K (m$^{1/3}$s^{-1})
$0 - 90$	27	$10.5 - 12.3$	$1.87 - 1.96$	$1.5 - 1.9$	39
$90 - 180$	18	$5.4 - 6$		$1.3 - 1.5$	20

In Figures 4.6 and 4.7, the analytically computed tidal amplitudes are compared with the observations along the Scheldt estuary. We can see that the correspondence with observed values is good, both in the seaward part (x= 0 – 90 km) where the depth is close to constant and in the landward part (x= 90 – 180 km) where the depth gradually reduces. The model fits the observations with constant values of Manning-Strickler coefficient, i.e., 39 m$^{1/3}$s^{-1} in the seaward part and 20 m$^{1/3}$s^{-1} in the landward part, respectively (see Table 4.3). It is worth noting that the calibrated friction coefficient in the upstream part is rather small (K=20 m$^{1/3}$s^{-1}, hence big friction), which is due to the neglect of river discharge in the equations. The neglect of river discharge can be compensated by increasing the friction [*Cai et al.*, 2012b]. Further work will be needed to include the effect of river discharge in this model.

To demonstrate the practical importance of the proposed multi-reach method, Figure 4.8 compares the performance of two analytical models (both with fine (#1, #2) and coarse (#3, #4) discretization) applied to the Scheldt estuary, compared against annual observations of tidal amplitude and travel time for HW and LW in 2000 (the Matlab scripts are provided as auxiliary material). The models #1 and #2 use a multi-reach approach with a small length step Δx=1 km, #1 adopting the explicit equation (4.19) and #2 the exponential damping equation (4.1) for the tidal amplitude, respectively. Models #3 and #4 use a large length step (i.e., 90 km in the seaward part x=0 – 90 km and 30 km in the upstream part x=90 – 180 km), making use of the explicit equation (4.19) and the exponential damping equation (4.1), respectively. The damping number δ in the exponential equation (4.1) was estimated by the hybrid model of *Cai et al.* [2012a]. All models use the same roughness values as presented in Table 4.3. It can be seen from Figure 4.8 that the performance of model #1 and model #2 is almost identical for small length step, which indicates that equation (4.1) is a good first order approximation of the
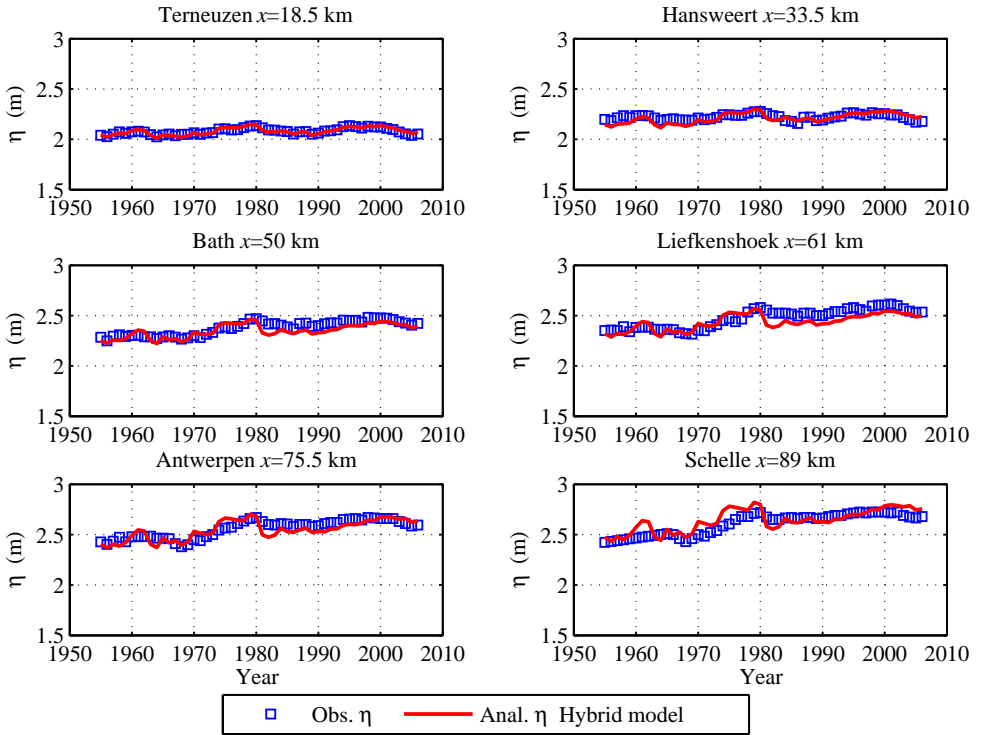
Figure 4.6: Comparison between the analytically computed tidal amplitude and measurements in the seaward part (0 − 90 km) of the Scheldt estuary at different locations.

proposed explicit equation (4.19) as long as Δx is small. For the model of #3, the correspondence with observed tidal amplitude is surprisingly good even using large length steps. The reason why the fit is not perfect is because in #3 f is rather constant, whereas it is ζ-dependent to cater for the tidal depth variability in the denominator of the friction term. In model #3 we have to assume that f remains constant over a reach. Model #4 is less accurate for larger length steps. This is because the new method has asymptotic values both for amplified and damped conditions, whereas the classical method tends to infinity for an amplified wave and to zero for a damped wave. For the travel times, the methods do not differ much. It is worth noting that model #4 can be made to fit observations, but only by adjusting the roughness values for the different reaches. It would have required a larger roughness coefficient in the downstream part and a smaller roughness in the upstream part to fit the observations.
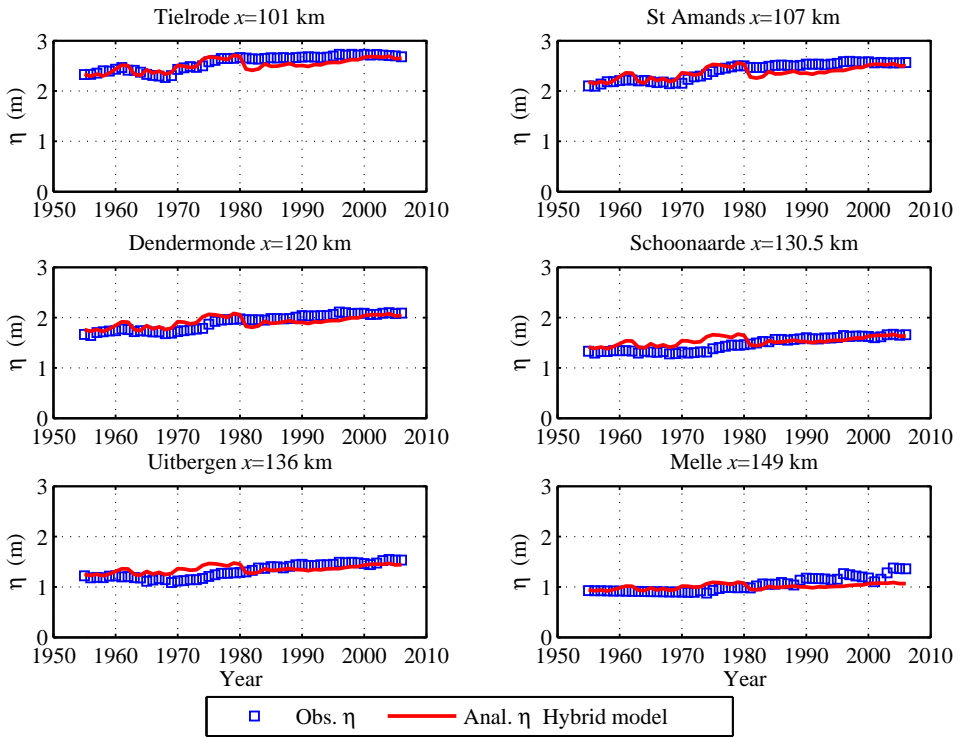
Figure 4.7: Comparison between the analytically computed tidal amplitude and measurements in the upstream part (90 − 180 km) of the Scheldt estuary at different locations.

4.5.2. Over-amplification Induced by Deepening

The tidal amplitude along the Scheldt estuary can be well simulated by the analytical model, which suggests that the analytical solution presented in this paper is a very powerful instrument to assess the possible influence of human interference in the estuarine system, such as dredging and deepening of navigation channels. During the past century, the navigation channel to the port of Antwerp in Belgium was deepened several times and at present it is maintained by annual dredging. Due to the effect of depth increase, the tidal amplitude and wave celerity have greatly increased over the last half-century. However, tidal amplification is not a straightforward function of depth. There appears to be a critical depth, which causes maximum amplification, beyond which the amplification is reduced as the wave gradually assumes the properties of a standing wave. To minimize the environmental impacts of tidal wave amplification, we need to fully understand the non-linear relationship between deepening and tidal amplification. The new analytical equation (4.19) is an excellent tool for this. Since they provide direct insight into the threshold, the asymptotic value and the functional relationship that governs
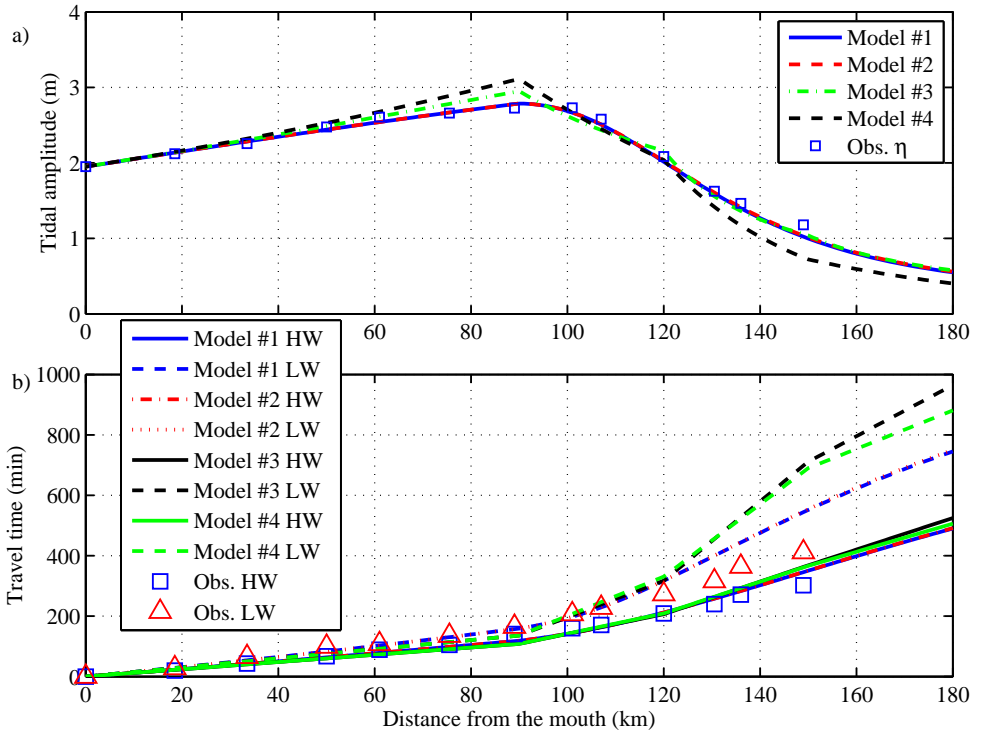
Figure 4.8: Comparison between different analytical models and observations: (a) tidal amplitude, and (b) travel time at HW and LW in the Scheldt estuary observed in 2000. Models #1 (using equation (4.19))and #2 (using equation (4.1)) make use of multi-reach approach with small length step $\Delta x= 1$ km, while models #3 (using equation (22)) and #4 (using (4.1)) use large length steps $\Delta x=90$ km (in the seaward part $x=0 - 90$ km) and 30 km (in the landward part $x= 90 - 180$ km).

amplification.

To evaluate the effect of deepening on tidal dynamics in the Scheldt estuary, various computations have been made under different depths (ranging from 5m to 25 m) using the proposed hybrid analytical model and the 1D numerical model [as described in *Toffolon et al.*, 2006] with the same tidal amplitude at the seaward boundary (1.9 m corresponding with the annual average tidal amplitude between 1955 and 2006) and fixed storage width ratio of 1.6 (estimated by fitting the average annual tidal observations during $1955 - 2006$). Figure 4.9 shows the effect of deepening on the tidal damping/amplification ratio (η/η_0) at different locations along the primary navigation channel ($0 - 90$ km). We can see that the analytically computed values are in good agreement with the measured tidal amplification ratio at the different stations. The results of the numerical model are also shown in Figure 4.9. In general, the correspondence between the analytical model and the numerical model is good, although the analytical results are slightly overestimated

for averaged depth between 12 m and 18 m and more so in the upstream part. This is due to the deformation of the wave which the analytical model does not consider. The analytical model shows that tidal damping ($\eta/\eta_0 < 1$) occurs for a depth smaller than about 7 m due to the dominant effect of friction, while the wave becomes amplified ($\eta/\eta_0 > 1$) for a depth larger than 7 m when the convergence is stronger than friction. We can demonstrate that a depth increase only leads to increased amplification (larger η/η_0) until a maximum value is reached at a critical depth $\overline{h}_{critical}$ defined by the condition

$$\frac{\partial \eta}{\partial \overline{h}} = 0\,. \tag{4.31}$$
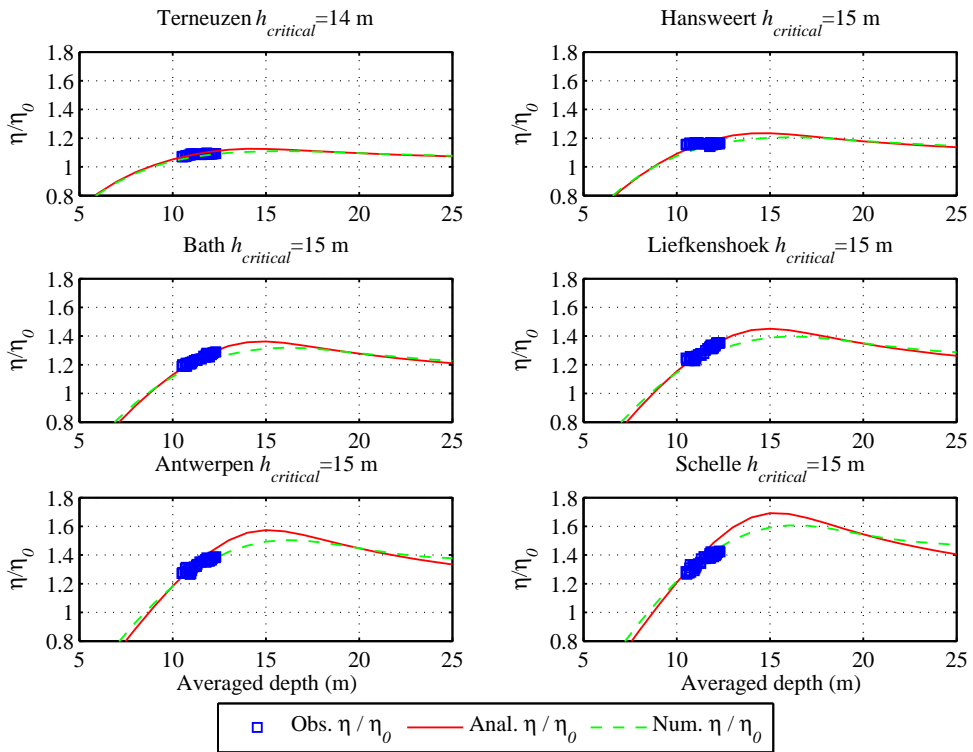
Figure 4.9: Observed tidal amplification ratio as function of averaged depth along the primary navigation channel in the Scheldt estuary, compared to the amplification computed with the hybrid model (continuous lines) and the 1D numerical model (dashed lines).

For the quasi-nonlinear model, this condition for maximum amplification is similar to the one defined by *Savenije et al.* [2008] as the threshold for the critical convergence at which the tide switches from mixed wave to the "apparently standing" wave (the wave is not a formally standing wave generated by the superimposition

of incident and reflected waves; rather it is an incident wave that mimics a standing wave having a phase difference of 90 ° between water level and velocity and a wave celerity tending to infinity). Rewriting their equation (44a) for the critical shape number γ_c as a function of $\bar{h}_{critical}$ leads to:

$$\bar{h}_{critical} = r_S \gamma_c^2 \omega^2 a^2/g, \qquad \gamma_c = \frac{1}{3\chi}\left(m_1/2 - 1 + (24\chi^2 + 2)/m_1\right),$$

$$m_1 = \left[108\chi^4 + 288\chi^2 - 8 + \sqrt{432\chi^2(\chi^2 - 2)^2(27\chi^2 - 4)}\right]^{1/3}. \qquad (4.32)$$

This value based on critical convergence rather than on the critical depth defined by (4.31) provides a slightly smaller value of $\bar{h}_{critical}$. It is worth noting that the system flips suddenly to a frictionless standing wave after reaching maximum amplification (i.e., $\bar{h} \geq \bar{h}_{critical}$) due to the discontinuous transition to a standing wave predicted by *Savenije et al.* [2008].

It is worth noting that the critical convergence defined by *Jay* [1991] is the rate at which the topographic convergence is balanced by the effect of acceleration, where the estuary shape number $\gamma=2$, which is the same value as obtained by our hybrid model for a frictionless wave system.

The tidal amplification ratio reduces for a depth larger than the critical depth, i.e. about 15 m for the main navigational channel. And it can be seen from Figure 4.9 that the maximum amplification increases in landward direction, from about 1.1 in Terneuzen to 1.7 in Schelle. *Cai et al.* [2012a] classified estuaries having a depth $\bar{h} > \bar{h}_{critical}$ as 'over-amplified', where increasing the depth reduces the tidal amplification. The same phenomenon of 'over-amplification' was observed by *Van Rijn* [2011] using an energy-based method, which in fact is identical to the linear solution. Instead of using a multi-reach implementation (as described by section 5.1), *Van Rijn* [2011] obtained the longitudinal tidal amplitude by applying the exponential equation (4.1).

Since the hybrid model consists of four implicit equations (see Table 4.1), the reaction of tidal wave propagation to the deepening cannot be observed directly from these equations. To illustrate the effect of deepening in the Scheldt estuary (0 − 90 km), we present the trajectory of the four main dimensionless parameters as function of averaged depth ($5 \leq \bar{h} \leq 25$ m) in Figure 4.10. We can see that the velocity number and the damping number increase until a maximum value is reached. A further increase of the depth reduces the tidal amplification (both tidal amplitude and velocity amplitude) until critical convergence is reached asymptotically, where the celerity number and the phase lag approach zero (see Figure 4.10cd), corresponding with a frictionless standing wave system. For the case of critical convergence, the solutions are identical to those obtained by the *Savenije et al.* [2008] for the second family of solution ("apparently standing" wave) and the solutions are completely determined by the convergence alone, i.e.,

$$\lambda = \epsilon = 0, \qquad \mu = \delta = (\gamma - \sqrt{\gamma^2 - 4})/2. \qquad (4.33)$$
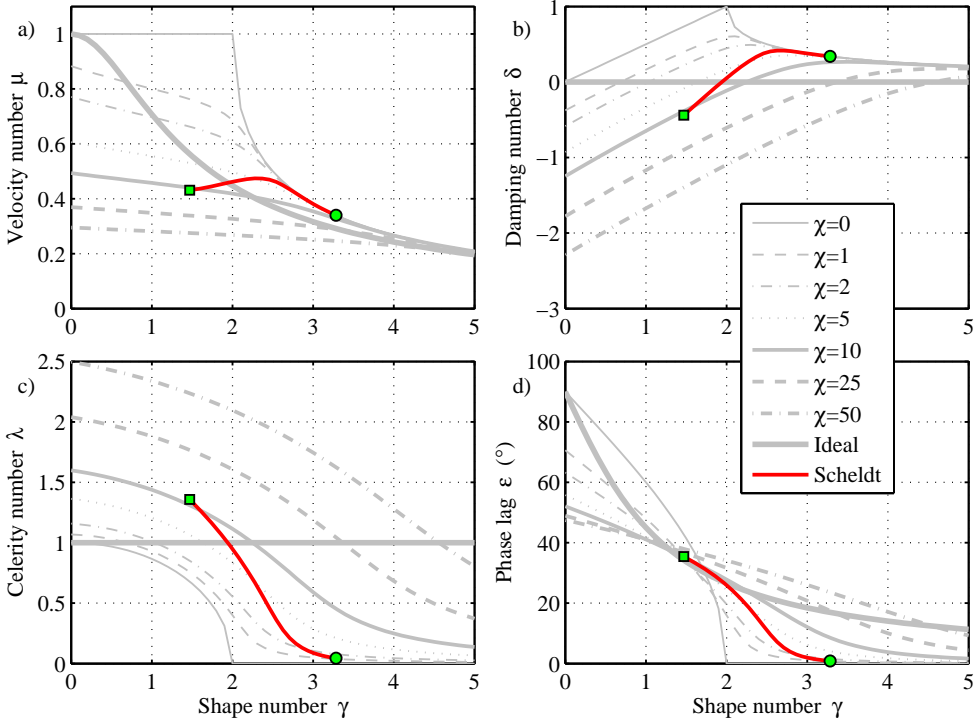
Figure 4.10: Trajectories of the main dimensionless parameters as function of averaged depth in the Scheldt estuary ($0 - 90$ km, red segments) in: (a) velocity number diagram, (b) damping number diagram, (c) celerity number diagram, and (d) phase lag diagram. The green square symbols indicate the initial position with averaged depth of 5 m, while the green circle symbols represent the final position with averaged depth of 25 m. The background shows the lines of the hybrid model with different values of the friction number χ.

When the estuary shape number γ goes to infinity (e.g, $\bar{h}$ approaches infinity), we can see that both μ and δ approach zero asymptotically. From a physical point of view, we can derive from the dimensional damping equation (4.13) that if depth is increased (hence friction becomes smaller), the friction term on the right-hand side, i.e. $2fv[4/(3\pi) + \sin(\epsilon)]/(3\bar{h}c)$, becomes smaller, leading to more amplification. However, the term contained in the parenthesis on the left-hand side, i.e. $1 + g\eta/(cv\sin(\epsilon)) = 1 + 1/\mu^2$, becomes larger with increasing depth, leading to less amplification. The term $1/\mu^2$ reflects the ratio of gravity to acceleration and only becomes dominant for small values of μ. The maximum amplification stems from the trade off between these terms.

In Figure 4.11 we present the analytical values of the velocity amplitude and tidal amplitude as well as their corresponding dimensionless numbers (velocity number and damping number) as a function of the averaged depth at Bath (x=50 km). As

the depth increases, both the velocity amplitude and tidal amplitude increase until a maximum value is reached at critical depth. The critical depth for the velocity amplitude and the velocity number are about 12 m, while the critical depth for the tidal amplitude is about 15 m, which is slightly smaller than the critical depth of the damping number at 16 m depth. These differences follow directly from the definitions of δ and μ as function of depth (see Table 4.2).
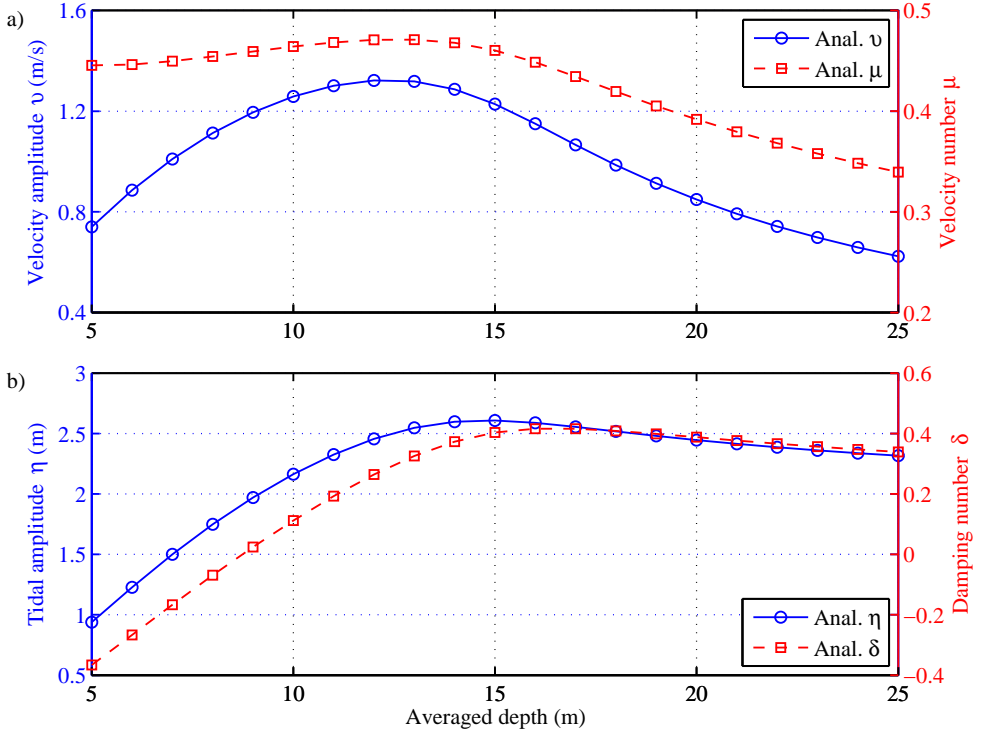
Figure 4.11: The velocity amplitude as well as the velocity number (a) and the tidal amplitude along with the damping number (b) as function of averaged depth at Bath (x=50 km) in the Scheldt estuary.

4.5.3. Classification of Estuary

The asymptotic tidal amplitudes η_{inf} and velocity amplitude υ_{inf} of a selection of estuaries are shown in Table 4.4, where η_{inf} is calculated with equation (4.7) while υ_{inf} is computed with equation (4.26). Qualitatively, we can determine whether an estuary is amplified or damped by comparing the difference between the tidal amplitude at the estuary mouth η_0 and the asymptotic (or ideal) tidal amplitude η_{inf}. For amplified estuaries where $\eta_0 < \eta_{inf}$ ($a\beta < 1$), such as Bristol Channel, Columbia, Outer Bay of Fundy, Scheldt, Severn, St. Lawrence, and Tees, a larger asymptotic tidal amplitude η_{inf} and velocity amplitude υ_{inf} is obtained. For damped

estuaries where $\eta_0 > \eta_{inf}$ ($a\beta > 1$), like Fraser, Ord, Gambia, Pungue, Lalang, Tha Chin, Incomati, and Chao Phya, we can see η_{inf} and v_{inf} achieve a lower asymptotic value. We can also see that the Gironde, Hudson, Potomac, and Maputo are very close to ideal estuaries with $\eta_{inf} \approx \eta_0$ ($a\beta \approx 1$).

Table 4.4: Characteristic values of alluvial estuaries and classification

Number	Estuary [1]	$T(hour)$	η_0 (m)	$\bar{h}$ (m)	a (km)	K (m$^{1/3}$ s^{-1})	ζ	γ	$a\beta$	η_{inf} (m)	v_{inf} (m/s)	Type
1	Bristol Channel	12.4	2.6	45	65	33	0.06	2.3	0.1	25.09	12.16	Amplified
2	Columbia	12.4	1	10	25	38	0.1	2.81	0.22	4.63	1.54	Amplified
3	Deltaware	12.5	0.64	5.8	40	51	0.11	1.35	0.68	0.94	0.47	Amplified
4	Elbe	12.4	2	10	42	43	0.2	1.68	0.76	2.64	2.68	Amplified
5	Fraser	12.4	1.5	9	215	31	0.17	0.31	17.16	0.09	0.13	Damped
6	Gironde	12.4	2.3	10	44	38	0.23	1.6	1.16	1.99	2.4	Close to ideal
7	Hudson	12.4	0.69	9.2	140	67	0.08	0.48	0.96	0.72	0.46	Close to ideal
8	Ord	12	2.5	4	15.2	50	0.63	2.83	1.46	1.71	2.23	Damped
9	Outer Bay of Fundy	12.4	2.1	60	230	33	0.04	0.75	0.21	9.91	6.73	Amplified
10	Potomac	12.4	0.65	6	54	56	0.11	1.01	0.91	0.71	0.42	Close to ideal
11	Scheldt	12.4	1.9	11	27	39	0.17	2.16	0.56	3.39	3.23	Amplified
12	Severn	12.4	3	15	41	40	0.2	2.1	0.48	6.24	6.51	Amplified
13	St. Lawrence	12.4	2.5	70	183	44	0.04	1.02	0.09	28.88	18.95	Amplified
14	Tees	12	1.5	7.5	5.5	36	0.2	10.72	0.28	5.44	0.87	Amplified
15	Thames	12.3	2.7	8.9	24	51	0.3	2.32	0.69	3.92	5.21	Amplified
16	Gambia	12.4	0.62	8.7	121	64	0.07	0.48	1.21	0.51	0.35	Damped
17	Pungue	12.4	3	4.3	20	33	0.7	2.11	5.42	0.55	1.18	Damped
18	Lalang	12.4	1.5	10.6	217	70	0.14	0.33	2.31	0.65	0.89	Damped
19	Tha Chin	12.4	1.2	5.3	87	50	0.23	0.56	6.95	0.17	0.26	Damped
20	Incomati	12.4	1.35	3	42	63	0.45	0.75	10.62	0.13	0.3	Damped
21	Limpopo	12.4	0.55	7	50	43	0.08	1.18	0.73	0.75	0.32	Amplified
22	Maputo	12.4	1.4	3.6	16	70	0.39	2.41	0.87	1.61	1.56	Close to ideal
23	Chao Phya	12.4	0.9	8	109	51	0.11	0.51	2.95	0.31	0.31	Damped

[1] Data are modified from *Cai et al.* [2012a].

4.5.4. Application to real estuaries

Figures 4.12 and 4.13 show longitudinal computations applied to the Scheldt, Thames, Pungue, Lalang, Tha Chin, Incomati, Maputo, and Chao Phya estuaries where tidal damping observations were available. Details on the geometric parameters used for these calculation are shown in the supporting information[2]. It can be seen from Figures 4.12 and 4.13 that the model fits the observed tidal amplitude very well and the estimated asymptotic tidal amplitude (4.24) is in good agreement with the observations. The fact that the Lalang shows larger amplitude upstream is due to an increasing depth in the upstream direction [*Savenije*, 1992b]. On the other hand, the strong upstream damping in the Scheldt and Thames is due to upstream shallowing. The jump in the asymptotic value near $x^* = 1.7$ (Scheldt) and $x^* = 1.3$ (Thames) is due to the change of the convergence length, which generates an almost standing wave over a short distance before the depth reduction further upstream again reduces the asymptotic amplitude.

It is worth noting that the proposed hybrid analytical model is able to accurately reproduce the main tidal hydrodynamics by following along-channel variation of estuarine sections (e.g., the depth). For instance, Figure 4.12a shows the computed and measured tidal amplitude along the Scheldt estuary, even in the upstream part, where the depth gradually reduces. We can see that the seaward part ($0 - 90$ km) can be classified as amplified, with a large asymptotic tidal amplitude, while the

[2]Auxiliary materials are available in the online version at http://onlinelibrary.wiley.com/doi/10.1002/2013JC008772/suppinfo

4
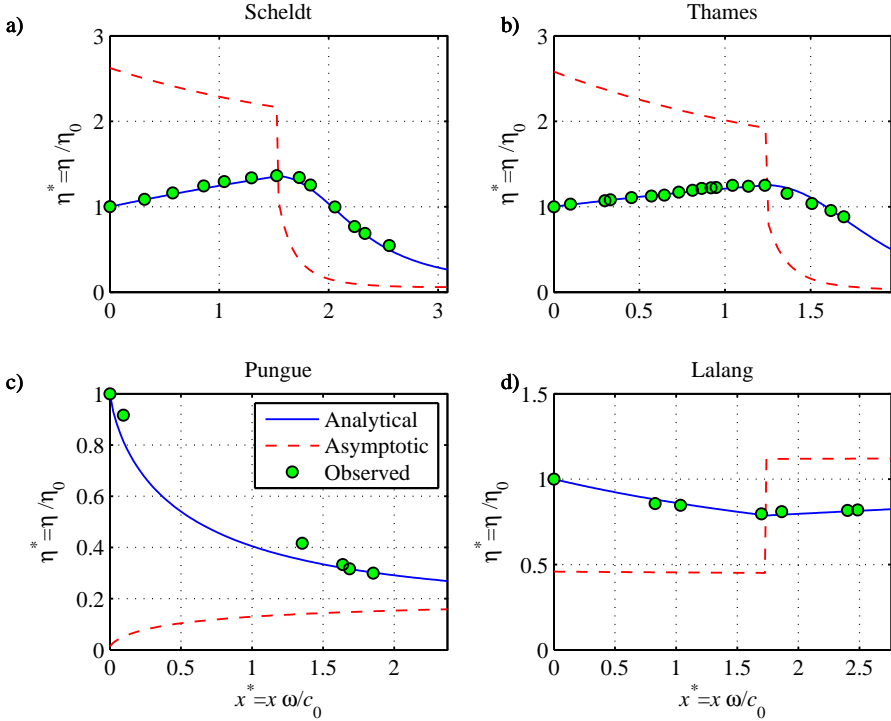
Figure 4.12: Observed and computed longitudinal variation of tidal amplitude in selected estuaries (a: Scheldt; b: Thames; c: Pungue; d: Lalang). The red dashed line represents the asymptotic tidal amplitude obtained with equation (4.24) as a function of the locally observed geometry.

upstream part $(90 - 180 \text{ km})$ is significantly damped with a much smaller asymptotic tidal amplitude.

4.6. Conclusions

In this chapter we have presented fully explicit expressions for tidal amplitude and velocity amplitude along the estuary axis. The derived equations provide direct insight into the hydrodynamics of estuaries. The solutions depend on two parameters, i.e., the shape number γ and the friction number at the estuary mouth $\widehat{\chi_0}$. These simple expressions can be easily incorporated in the model proposed by *Cai et al.* [2012a] with a multi-reach technique, i.e., subdividing the estuary into multiple reaches. The multi-reach implementation enables the analytical model to take account of local variability (e.g., the depth or friction) and performs much better than the classical exponential equation (4.1) applied to the entire estuary (i.e., single reach).

We have compared the performance between the classical linear solution and
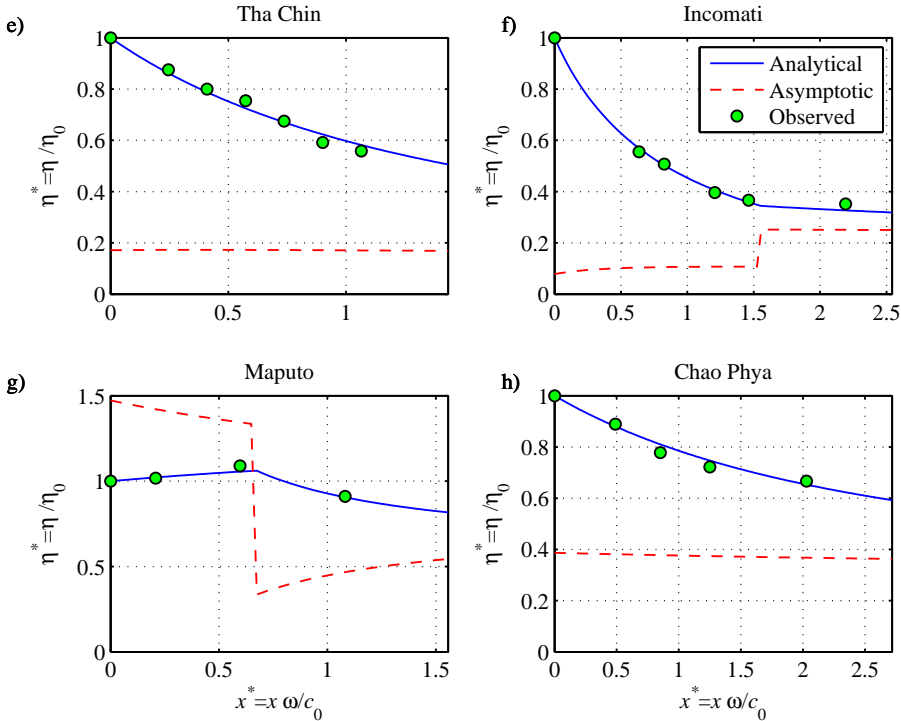
Figure 4.13: Observed and computed longitudinal variation of tidal amplitude in selected estuaries (e: Tha Chin; f: Incomati; g: Maputo; h: Chao Phya). The red dashed line represents the asymptotic tidal amplitude obtained with equation (4.24) as a function of the locally observed geometry.

those proposed by *Savenije et al.* [2008], *Toffolon and Savenije* [2011] and *Cai et al.* [2012a]. It is found that exponential damping is only valid when assuming a constant friction number χ along the estuary axis, which in fact implies a constant amplitude, and hence an ideal estuary. The more realistic situation is that estuaries converge towards an asymptote where the impact of convergence is balanced by friction.

We have also shown that the upstream asymptotic state is basically independent of tidal forcing, which indicates that an estuary adjusts the tidal amplitude to the estuary shape until it has the same properties as in an ideal estuary with spatially constant parameters. For the downstream asymptotic behavior of the damping equation, it has been shown that damping/amplification is linear in a region close to the estuary mouth, particularly in the case of amplification, such as in the seaward part of the Scheldt estuary. The nonlinear effect only becomes significant in the upper reaches of the estuary. The analysis of the downstream asymptotic behavior of tidal damping demonstrates that the classical exponential damping equation (4.1) is only valid when there is almost no damping or amplification (which is trivial) or

for a frictionless wave (which is unrealistic).

The analytical solutions are compared with half a century of observations in the Scheldt estuary, which was substantially deepened over that period. The correspondence with observations is very good. The analytical model has subsequently been applied to investigate the effect of further deepening on the tidal dynamics. Interestingly, there is a critical depth beyond which the amplification is reduced until critical convergence (frictionless and standing wave system) is reached asymptotically. Finally, the asymptotic behavior can be used to classify estuaries as damped, amplified or ideal by comparing the tidal amplitude at the estuary mouth with that of an ideal estuary.

4

5

Linking the river to the estuary: influence of river discharge on tidal damping

The effect of river discharge on tidal damping in estuaries is explored within the framework of four implicit equations, i.e., the phase lag, the scaling, the damping and the celerity equation. In this framework it is possible to show that river discharge affects tidal damping primarily through the friction term. It appears that the residual slope due to nonlinear friction can have a substantial influence on tidal wave propagation when including the effect of river discharge. An iterative analytical method is proposed to include this effect, which significantly improved model performance in the upper reaches of an estuary. The application to the Modaomen and Yangtze estuaries demonstrates that the proposed analytical model is able to describe the main tidal dynamics with realistic roughness values in the upper part of the estuary where the ratio of river flow to tidal flow amplitude is substantial, while a model with negligible river discharge can be made to fit observations only with unrealistically high roughness values.

5.1. Introduction

The natural variability of river flow into estuaries is greatly modified by human activities, such as dam construction, flow diversion and freshwater withdrawal. These activities impact on tidal damping and tidal wave propagation. In addition, they influence salt intrusion and even storm surge propagation into an estuary [*Zhang et al.*, 2011, 2012; *Cai et al.*, 2012b]. Hence, understanding the effect

of river discharge on tidal hydraulics is important. Most studies on the analytical solution of tidal wave propagation neglect the effect of river discharge, such as *Hunt* [1964], *Dronkers* [1964], *Ippen* [1966], *Friedrichs and Aubrey* [1994], *Savenije* [1998, 2001], *Lanzoni and Seminara* [1998], *Prandle* [2003], *Savenije et al.* [2008], *Toffolon and Savenije* [2011], *Van Rijn* [2011] and *Cai et al.* [2012a]. Only few studies analysed the influence of river discharge on tidal wave propagation in estuaries. Of these, most authors used perturbation analysis, where the scaled equations are simplified by neglecting higher order terms, generally discarding the advective acceleration term and linearizing the friction term [e.g., *Dronkers*, 1964; *Leblond*, 1978; *Godin*, 1985, 1999; *Jay*, 1991]. Others used a regression model to determine the relationship between river discharge and tide [*Jay et al.*, 2011; *Kukulka and Jay*, 2003]. In contrast, *Horrevoets et al.* [2004] and *Cai et al.* [2012b] provided analytical solutions of tidal damping accounting for the effect of river discharge without simplifying the equations, based on the envelope method originally developed by *Savenije* [1998].

The treatment of the nonlinear friction term is key to finding an analytical solution for tidal hydrodynamics. The nonlinearity of the friction term has two sources: the quadratic stream velocity in the numerator and the variable hydraulic radius in the denominator [*Parker*, 1991]. The classical linearization of the friction term was first obtained by *Lorentz* [1926] who, disregarding the variable depth, equated the dissipation by the linear friction over the tidal cycle to that of the quadratic friction. An extension to include river discharge was provided by *Dronkers* [1964]. In this seminal work, he derived a higher order formulation using Chebyshev polynomials, both with and without river discharge, resulting in a close correspondence with the quadratic velocity. *Godin* [1991, 1999] showed that quadratic velocity can be well approximated by using only the first and third order terms of the non-dimensional velocity. However, none of the above linearizations took into account the effect of the periodic variation of the hydraulic radius (to the power $4/3$ in the Manning–Strickler formulation) in the denominator of the friction term. On the other hand, *Savenije* [1998], using the envelope method (see Appendix A.6), obtained a damping equation that takes account of both the quadratic velocity and the time-variable hydraulic radius in the denominator.

This chapter builds on a variety of previous publications on analytical approaches to tidal wave propagation and damping. A first attempt to include the effect of river discharge by *Horrevoets et al.* [2004] used the quasi-nonlinear method of *Savenije* [2001], assuming constant velocity amplitude, wave celerity and phase lag. *Cai et al.* [2012b] applied this model to the Modaomen estuary. In the present paper we make use of the analytical framework for tidal wave propagation by *Cai et al.* [2012a], but including for the first time the effect of river discharge in a hybrid model that performs better. Moreover, fully analytical equations accounting for four spatial variables (velocity amplitude, tidal amplitude, wave celerity and phase lag) of tidal propagation are now presented demonstrating that the effect of river discharge is similar to that of friction. In addition, building on the research by *Vignoli et al.* [2003] on nonlinear frictional residual effects on tidal propagation, the influence of residual slope on tidal wave propagation has been taken into account, which

significantly improved performance, especially in the upstream part of estuaries where the effect of river discharge is considerable.

In the following section, we present the damping equations that take account of river discharge. The method to include the residual slope in the analytical solution is reported in Section 5.3. Section 5.4 presents a comparison of the different analytical approaches and a sensitivity analysis. The model is subsequently compared against the fully nonlinear numerical results and applied to two real estuaries where the effect of the river discharge is apparent in the upstream part of the estuary. The paper closes off with conclusions in Section 5.5.

5.2. New Damping Equations Accounting for the Effect of River Discharge

In the following, we extend the validity of the damping equations by introducing the effect of river discharge into the different approximations of the friction term.

In a Lagrangean approach, we assume that the water particle moves according to a simple harmonic wave and the influence of river discharge on tidal velocities is not negligible. As a result, the instantaneous flow velocity V for a moving particle is made up of a steady component U_r, created by the discharge of freshwater, and a time-dependent component U_t, contributed by the tide:

$$V = U_t - U_r, \qquad U_t = v\sin(\omega t), \qquad U_r = Q_f/\overline{A}, \qquad (5.1)$$

where Q_f is the freshwater discharge, directed against the positive x-direction.

The dimensionless river discharge ϕ is defined as:

$$\phi = \frac{U_r}{v}. \qquad (5.2)$$

We show the procedure for including the effect of river discharge within the envelope method in Appendix A.6.

For a more concise notation, we refer to a general formulation of the damping parameter of the form:

$$\delta = \frac{\mu^2}{1 + \mu^2\beta}\left(\gamma\theta - \chi\mu\lambda\Gamma\right), \qquad (5.3)$$

where we introduce the dimensionless parameters β, θ, and Γ. Both β and θ are equal to unity if $\phi = 0$. The parameter β corrects the tidal Froude number $\mu^2 = [v/(c_0 r_s \zeta)]^2$ [*Savenije et al.*, 2008] for the influence of river discharge:

$$\beta = \theta - r_s\zeta\frac{\phi}{\mu\lambda}. \qquad (5.4)$$

The correction factor θ accounts for the wave celerity not being equal at HW and LW, which depends on ϕ by:

$$\theta = 1 - \left(\sqrt{1+\zeta} - 1\right)\frac{\phi}{\mu\lambda}. \qquad (5.5)$$

This parameter has a value smaller than unity, but is close to unity as long as $\zeta \ll 1$ although $\mu\lambda = \sin(\epsilon)$ is also less than 1. In practical applications, we can typically assume $\theta \approx 1$, but this is not a necessary assumption in our method. Finally, the parameter Γ depends on the specific approach, as it is discussed in the next sections.

5.2.1. The Quasi-nonlinear Approach

Savenije et al. [2008] presented a fully analytical solution for tidal wave propagation without linearizing the friction term through the envelope method. The method was termed quasi-nonlinear because it still made use of a regular harmonic function to describe the flow velocity. *Horrevoets et al.* [2004] introduced the effect of river discharge in the quasi-nonlinear model. Using the dimensionless parameters presented in Table 4.2, *Cai et al.* [2012b] developed this solution into a general expression for tidal damping, where two zones are distinguished depending on the value of ϕ defined by equation (5.2).

In the tide-dominated zone, where $\phi < \mu\lambda$, the parameter Γ introduced in equation (5.3) reads

$$\Gamma = \mu\lambda\left[1 + \frac{8}{3}\zeta\frac{\phi}{\mu\lambda} + \left(\frac{\phi}{\mu\lambda}\right)^2\right],\tag{5.6}$$

while in the river discharge-dominated zone, where $\phi \geq \mu\lambda$, it becomes

$$\Gamma = \mu\lambda\left[\frac{4}{3}\zeta + 2\frac{\phi}{\mu\lambda} + \frac{4}{3}\zeta\left(\frac{\phi}{\mu\lambda}\right)^2\right].\tag{5.7}$$

5.2.2. Lorentz's Approach

The Fourier expansion of the product $U|U|$ in the friction term is [*Dronkers*, 1964, 272–275]:

$$U|U| = \frac{1}{4}L_0 v^2 + \frac{1}{2}L_1 v U_t,\tag{5.8}$$

where the expressions of coefficients L_0 and L_1 when $0 < \phi < 1$ are:

$$L_0 = [2 + \cos(2\alpha)]\left(2 - \frac{4\alpha}{\pi}\right) + \frac{6}{\pi}\sin(2\alpha),\tag{5.9}$$

$$L_1 = \frac{6}{\pi}\sin(\alpha) + \frac{2}{3\pi}\sin(3\alpha) + \left(4 - \frac{8\alpha}{\pi}\right)\cos(\alpha),\tag{5.10}$$

with

$$\alpha = \arccos(-\phi),\tag{5.11}$$

where $\pi/2 < \alpha < \pi$ because ϕ is positive. In case $\phi \geq 1$,

$$L_0 = -2 - 4\phi^2,\quad L_1 = 4\phi,\tag{5.12}$$

while the case of $\phi=1$ (i.e., $U_r = v$) corresponds with $\alpha = \pi$ and leads to $L_0 = -6$ and $L_1 = 4$.

As a result, the development of the Lorentz's friction term accounting for the effect of river discharge reads:

$$F_{\mathrm{L}} = \frac{1}{K^2 \overline{h}^{4/3}} \left(\frac{1}{4} L_0 v^2 + \frac{1}{2} L_1 v U_t \right),$$ (5.13)

where the subscript L stands for Lorentz.

If the river discharge is negligible, i.e., $U_r = 0$ and $\alpha = \pi/2$, equation (5.13) reduces to the classical Lorentz linearization and hence $L_0 = 0$ and $L_1 = 16/(3\pi)$:

$$F_{\mathrm{L}} = \frac{8}{3\pi} \frac{v}{K^2 \overline{h}^{4/3}} U_t.$$ (5.14)

With the envelope method, making use of friction term equation (5.13), it is possible to derive the parameter Γ in the damping equation (5.3) (see Appendix A.6):

$$\Gamma_{\mathrm{L}} = \frac{L_1}{2}.$$ (5.15)

Extending Lorentz's solution with the periodic variation of the depth in the denominator of the friction term (i.e., $K^2 h^{4/3}$) is also possible. The resulting expression is reported in Table 5.1, where $\kappa = 1$ yields the time-dependent case, while equation (5.12) is recovered by setting $\kappa = 0$.

Table 5.1: Comparison of the terms in the damping equation (5.3) for different analytical methods. The effect of the time-dependent depth in the friction term for Lorentz's, Dronkers' and Godin's method is accounted for by setting $\kappa=1$ in the expressions for Γ, whereas $\kappa=0$ describes the time-independent case.

Model[(1)]	Friction term	Γ without river discharge ($\phi = 0$)	Γ with river discharge ($\phi > 0$), introducing $\psi = \phi/(\mu\lambda)$	
Savenije[a,b,c,d]	$\frac{U\|U\|}{K^2 h^{4/3}}$	$\mu\lambda$	$\begin{cases} \mu\lambda\left(1 + \frac{8}{3}\zeta\psi + \psi^2\right) & (\psi < 1) \\ \mu\lambda\left(\frac{4}{3}\zeta + 2\psi + \frac{4}{3}\zeta\psi^2\right) & (\psi \geq 1) \end{cases}$	T1
Lorentz[e]	$\frac{1}{K^2 h^{4/3}}\left(\frac{L_0}{4}v^2 + \frac{L_1}{2}vU_t\right)$	$8/(3\pi)$	$\frac{L_1}{2} - \kappa\zeta\frac{L_0}{3\mu\lambda}$	T2
Dronkers[f]	$\frac{1}{K^2 h^{4/3}}(p_0 v^2 + p_1 vU + p_2 U^2 + p_3 U^3/v)$	$\frac{16}{15\pi} + \frac{32}{15\pi}(\mu\lambda)^2$	$\begin{cases} \frac{1}{\pi}\{-p_0\frac{4\kappa\zeta}{3\mu\lambda} + p_1\left(1 + \frac{4}{3}\kappa\zeta\psi\right) \\ \quad -2p_2\phi\left[1 + \frac{2}{3}\kappa\zeta\left(\frac{1}{\psi} + \psi\right)\right] \\ \quad +p_3\phi^2\left[3 + \frac{1}{\psi^2} + 4\kappa\zeta\left(\frac{1}{\psi} + \frac{\psi}{3}\right)\right]\} \end{cases}$	T3
Godin[g]	$\frac{16}{15\pi}\frac{U'^2}{K^2 h^{4/3}}\left[\frac{U}{U'} + 2\left(\frac{U}{U'}\right)^3\right]$	$\frac{16}{15\pi} + \frac{32}{15\pi}(\mu\lambda)^2$	$G_0 + G_1(\mu\lambda)^2 + \kappa\zeta\left(G_2\mu\lambda + \frac{G_3}{\mu\lambda}\right)$	T4
Hybrid[h]	$\frac{2}{3}\frac{U\|U\|}{K^2 h^{4/3}} + \frac{1}{3}\frac{1}{K^2 h^{4/3}}\left(\frac{L_0}{4}v^2 + \frac{L_1}{2}vU_t\right)$	$\frac{2}{3}\mu\lambda + \frac{8}{9\pi}$	$\begin{cases} \frac{2}{3}\mu\lambda\left(1 + \frac{8}{3}\zeta\psi + \psi^2\right) + \frac{L_1}{6} - \frac{L_0}{9}\frac{\zeta}{\mu\lambda} & (\psi < 1) \\ \frac{2}{3}\mu\lambda\left(\frac{4}{3}\zeta + 2\psi + \frac{4}{3}\zeta\psi^2\right) + \frac{L_1}{6} - \frac{L_0}{9}\frac{\zeta}{\mu\lambda} & (\psi \geq 1) \end{cases}$	T5
		$\beta = 1, \quad \theta = 1$	$\beta = \theta - r_S\zeta\psi, \quad \theta \approx 1$	

[(1)] [a] Savenije [1998]; [b] Horrevoets et al. [2004]; [c] Savenije et al. [2008]; [d] Cai et al. [2012b]; [e] Lorentz [1926]; [f] Dronkers [1964]; [g] Godin [1991, 1999]; [h] Cai et al. [2012a]

We also tested higher order formulations of the friction term, such as proposed by *Dronkers* [1964] and *Godin* [1991, 1999], which we implemented in the envelope method arriving at tidal damping equations accounting for river discharge. For further details on these damping equations, readers can refer to the Supplement[1] (see also Table 5.1).

[1] Auxiliary materials are available in the online version at http://www.hydrol-earth-syst-sci.net/18/287/2014/hess-18-287-2014-supplement.pdf

5.2.3. Hybrid Method

Cai et al. [2012a] showed that a linear combination of the traditional Lorentz approach [e.g., *Toffolon and Savenije*, 2011] with the quasi-nonlinear approach [e.g., *Savenije et al.*, 2008] gives good predictive results. In this study, we expand this method to account for river discharge. Consequently, the new nonlinear friction term reads:

$$F_{\mathrm{H}} = \frac{2}{3}F + \frac{1}{3}F_{\mathrm{L}} = \frac{1}{K^2 h^{4/3}}\left[\frac{2}{3}U|U| + \frac{1}{3}\left(\frac{L_0}{4}v^2 + \frac{L_1}{2}vU_t\right)\right], \qquad (5.16)$$

where the subscript H stands for hybrid. Applying the envelope method with this friction formulation, we are able to derive a new river discharge dependent damping equation:

$$\Gamma_{\mathrm{H}} = \frac{2}{3}\Gamma + \frac{1}{3}\Gamma_{\mathrm{L}}, \qquad (5.17)$$

where Γ_{L} is given by T2 (see Table 5.1) with $\kappa = 1$, and Γ by either equation (5.6) or (5.7) in the downstream tide-dominated zone ($\phi < \mu\lambda$) or in the upstream river discharge-dominated zone ($\phi \geq \mu\lambda$), respectively.

5.3. Influence of Nonlinear Friction on the Averaged Water Level

The tidally averaged free surface elevation does not coincide with mean sea level along the estuary due to the nonlinear frictional effect on averaged water level, even if river discharge is negligible [*Vignoli et al.*, 2003]. *Vignoli et al.* [2003] derived an analytical expression for the mean free surface elevation (see Appendix A.7):

$$\overline{z}(x) = -\int_0^x \frac{\overline{V|V|}}{K^2 h^{4/3}}\,dx, \qquad (5.18)$$

which is also valid when accounting for the effect of river discharge (the overbar denotes the average over the tidal period).

A fully nonlinear one-dimensional numerical model accounting for river discharge has been used to investigate the effects of the friction term on the tidally averaged water level. The numerical model uses an explicit MacCormack scheme and is second order accurate both in space and time [*Toffolon et al.*, 2006]. As a simple case, we considered a channel with horizontal bed, where the width is assumed to decrease exponentially in landward direction as:

$$\overline{B} = \overline{B_{\mathrm{min}}} + \left(\overline{B_0} - \overline{B_{\mathrm{min}}}\right)\exp(-x/b), \qquad (5.19)$$

where $\overline{B_{\mathrm{min}}}$ is imposed to keep a minimum width when the convergence is strong and the estuary is long. The length of the estuary is 2000 km. In the landward part, we imposed a slight bed slope and higher friction in order to reduce spurious reflections due to the landward boundary condition.

Figure 5.1 presents a comparison between the numerically calculated tidally averaged water level and the values obtained from equation (5.18), both with (5000 m^3s^{-1}) and without river discharge. For simplicity, we calculated the tidally averaged friction using the Eulerian velocity U rather than the Langranean velocity V with (5000 m^3s^{-1}) and without river discharge. It can be seen from Figure 5.1 that the correspondence between them is reasonable. The deviation is mainly due to the fact that we calculated the tidally averaged friction using the Eulerian velocity U, instead of integrating the Lagrangean velocity V as in equation (5.18). We can see from Figure 5.1 that due to river discharge the residual water level slope is significantly increased, suggesting that the residual effects on the averaged water level is particularly important when river discharge is substantial.
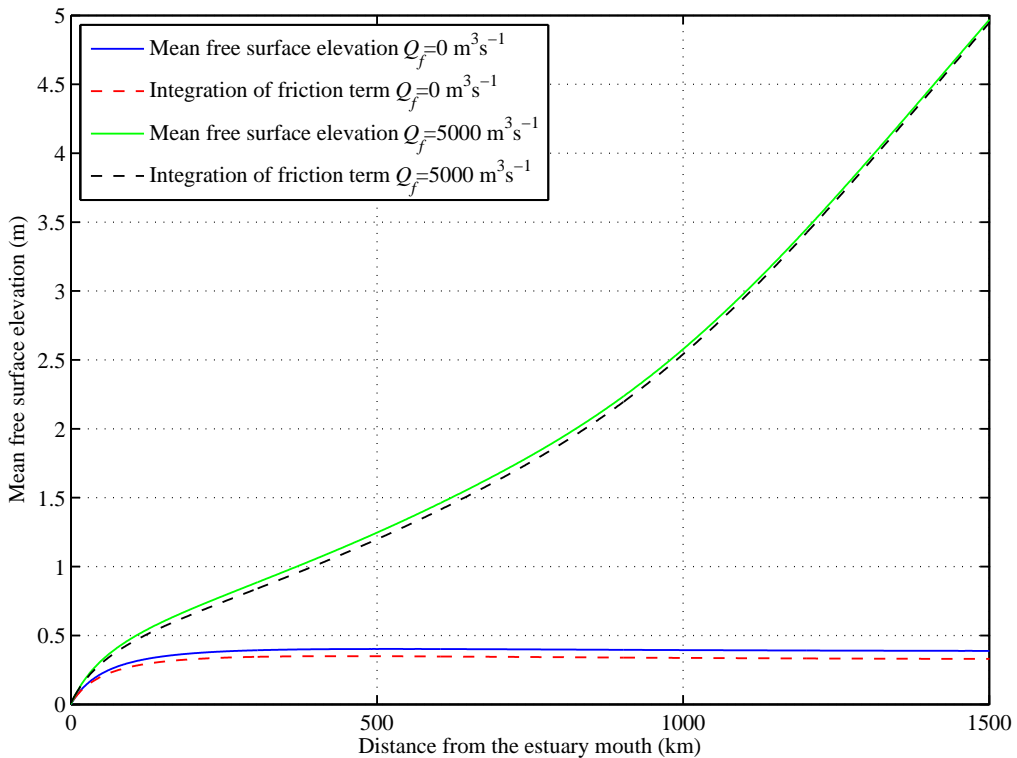
Figure 5.1: Tidally averaged free surface elevation calculated from the numerical model (solid lines) and evaluated through equation (5.18) both with and without river discharge for given values of K=60 $m^{1/3}s^{-1}$, b=352 km, ζ_0=0.2, $\overline{h}$=10 m, $\overline{B_0}$=5000 m, $\overline{B_{min}}$=300 m.

5.4. Results

5.4.1. Analytical Solutions of the New Models

The different damping equations introduced above should be combined with the phase lag, scaling and celerity equations of Table 4.1, to form the system of the hydrodynamic equations:

$$\tan(\epsilon) = \frac{\lambda}{\gamma - \delta} , \qquad (5.20)$$

$$\mu = \frac{\sin(\epsilon)}{\lambda} = \frac{\cos(\epsilon)}{\gamma - \delta} , \qquad (5.21)$$

$$\lambda^2 = 1 - \delta(\gamma - \delta) . \qquad (5.22)$$

In this way we have a new set of four implicit analytical equations that account for the effect of river discharge. As shown in *Savenije et al.* [2008], equations (5.20) and (5.21) can be combined to eliminate the variable ϵ to give

$$(\gamma - \delta)^2 = \frac{1}{\mu^2} - \lambda^2 . \qquad (5.23)$$

A fully explicit solutions for the main dimensionless parameters (i.e., μ, δ, λ, ϵ) can be derived in some cases [*Toffolon et al.*, 2006; *Savenije et al.*, 2008], but an iterative procedure is needed to obtain the solution in general. The following procedure usually converges in a few steps: (1) initially we assume $Q_f = 0$ and calculate the initial values for the velocity number μ, celerity number λ and the tidal velocity amplitude υ (and hence dimensionless river discharge term ϕ) using the analytical solution proposed in *Cai et al.* [2012a] (see Sect. 3); (2) taking into account the effect of river discharge Q_f, the revised damping number δ, celerity number λ, velocity number μ and velocity amplitude υ (and hence ϕ) are calculated by solving equations (5.3), (5.22) and (5.23) using a simple Newton–Raphson method; (3) this process is repeated until the result is stable and then the other parameters (e.g., ϵ, η, υ) are computed.

It is important to realise that the solutions for the dependent dimensionless parameters μ, δ, λ and ϵ are local solutions because they are obtained by the four implicit equations that depend on local quantities that vary along the estuary (i.e., the local tidal amplitude to depth ratio ζ, the local estuary shape number γ and the local friction number χ). To reproduce wave propagation correctly along the estuary, a multi-reach approach has to be used to follow along-channel variation, dividing the estuary in a number of reaches [e.g., *Toffolon and Savenije*, 2011]. With the damping number δ, it is possible to calculate a tidal amplitude η_1 at a distance Δx (e.g., 1 km) upstream by simple explicit integration of the damping number:

$$\eta_1 = \eta_0 + \frac{d\eta}{dx}\Delta x = \eta_0 + \frac{\eta_0 \omega \delta}{c_0}\Delta x . \qquad (5.24)$$

In a Lagrangean reference frame, tidally averaged friction can be estimated by the average of friction at HW and LW, based on the assumption that the water particle

moves according to a simple harmonic, yielding:

$$\overline{\frac{V|V|}{K^2 h^{4/3}}} \approx \frac{1}{2}\left[\frac{V_{HW}|V_{HW}|}{K^2\left(\overline{h}+\eta\right)^{4/3}} + \frac{V_{LW}|V_{LW}|}{K^2\left(\overline{h}-\eta\right)^{4/3}} \right]. \tag{5.25}$$

Substitution of different approximations of the friction term, described in the Sect. 4, into (5.25) and combination with (5.18) ends up with an equal number of analytical solutions for the tidally averaged depth along the estuary:

$$\overline{h}_{new}(x) = \overline{h}(x) + \overline{z}(x), \tag{5.26}$$

which modifies the estuary shape number. Making use of equation (5.26) an iterative procedure can be applied to obtain the tidal dynamics along the estuary accounting for the effect of the residual water level slope.

5.4.2. Comparison among Different Approaches

Table 5.1 summarizes the damping equations with and without the effect of river discharge for the different friction formulations, leading to different forms of the damping equation. The substitution of $\phi = 0$ yields the same damping equations as in Table 4.1 (general case), as it can be derived by exploiting the phase lag and scaling equations [*Cai et al.*, 2012a].

As an illustration, the relation between the dependent dimensionless parameters and the dimensionless river discharge ϕ is shown in Figure 5.2 for given values of $\zeta_0 = 0.1$, $\gamma = 1.5$, $\chi = 2$ and $r_S = 1$. We can see that for increasing river discharge all the analytical models approach the same asymptotic solution, which is due to the fact that the approximations to the quadratic velocity $U|U|$ is close to U^2 when the effect of tide is less important and the current no longer reverses. Actually, we can see that the parameter Γ in the friction term in T1, T2 and T5 (see Table 5.1) tends to $(4/3)\zeta\phi^2/(\mu\lambda)$ when ϕ approaching infinity. Moreover, it can be seen from Figure 5.2 that the performance of the hybrid model is close to the average of Lorentz's and the quasi-nonlinear method, which is to be expected since the hybrid tidal damping represents a weighted average of these two solutions. In addition, we note that the different methods tend to converge for large values of ϕ.

It is important to realise that the different approaches use different expressions for the dimensionless friction f (i.e., equation 2.10) as a result of the variation of the depth over time. While the effect of a variable depth is taken into account in the envelope method, the original Lorentz method assume a constant depth in the friction term, which is the same as considering $\zeta = 0$ in equation (2.10):

$$f_0 = g/\left(K^2\overline{h}^{-1/3}\right). \tag{5.27}$$

The damping equations accounting for time variability, which is related to the term ζ in equation (2.10), are presented in Table 5.1.
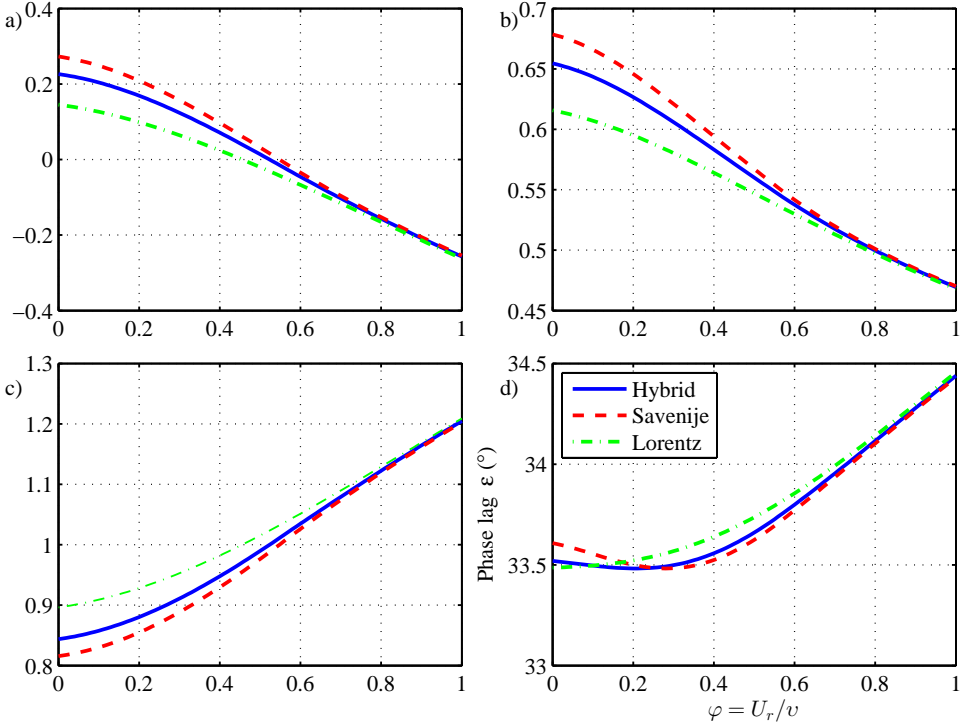
Figure 5.2: The main dimensionless parameters (damping number δ, velocity number μ, celerity number λ and phase lag ϵ) obtained with the different analytical methods as a function of dimensionless river discharge ϕ with $\zeta_0 = 0.1$, $\gamma = 1.5$, $\chi = 20$ and $r_S = 1$.

5.4.3. Sensitivity Analysis

In this section we discuss the effect of changing the frictional and geometrical features of the estuary. Although in principle all the presented methods can be used, in the following we will consider the hybrid model, if not explicitly mentioned.

The relation between the dependent dimensionless parameters (i.e., the damping number δ, the velocity number μ, the celerity number λ and the phase lag ϵ) and the friction number χ for different values of ϕ is shown in Figure 5.3 for given values of $\zeta_0 = 0.1$, $\gamma = 1.5$ and $r_S = 1$. In general, the river discharge intensifies the effect of friction, i.e., inducing more tidal damping (hence less velocity amplitude and wave celerity). The phase lag $\epsilon = \arcsin(\mu\lambda)$ increases with increasing ϕ except for small χ when the values of $\mu\lambda$ are decreased. However, we can see that the curves show an anomaly for very small value of χ. If χ is very small, the river discharge term in the numerator of the damping equation (5.3) is negligible but becomes important in β, defined in equation (5.4). For this case, an increase of the river discharge has an opposite effect, particularly on the phase lag. In fact, for the case of a frictionless estuary ($\chi = 0$) the damping equation (5.3) reduces to

$\delta = \mu^2 \gamma \theta / (1 + \mu^2 \beta)$ in which β is decreased with river discharge.
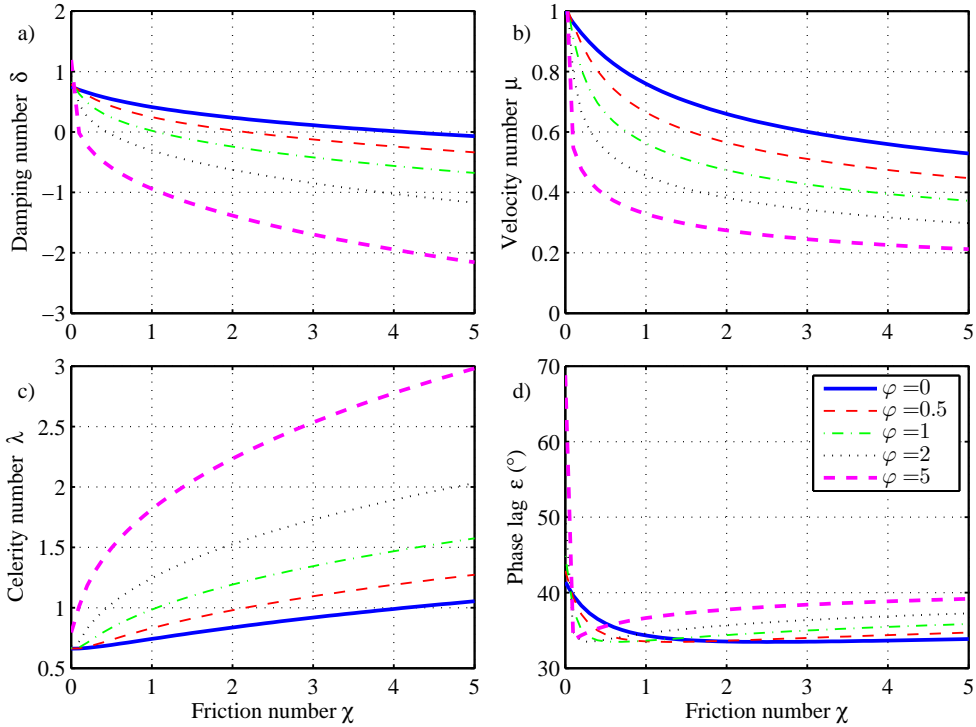
Figure 5.3: Relationship between the main dimensionless parameters and the friction number χ obtained by solving the equations (5.3) (with $\Gamma = \Gamma_H$), (5.22) and (5.23) for different values of the dimensionless river discharge term ϕ with $\zeta_0 = 0.1$, $\gamma = 1.5$ and $r_S = 1$.

The friction number χ is also a function of ζ (see Table 4.1). In order to illustrate the effect of ζ we introduce a modified (time-invariant) friction number χ_0 as:

$$\chi_0 = \chi \left[1 - (4\zeta/3)^2 \right] / \zeta = r_S g c_0 / \left(K^2 \omega \overline{h}^{-4/3} \right). \tag{5.28}$$

Figure 5.4 describes the effect of the dimensionless tidal amplitude ζ for given values of $\chi_0 = 20$, $\gamma = 1.5$ and $r_S = 1$. Larger ζ intensifies the effect of river discharge and friction as well, which induces more tidal damping, less velocity amplitude and wave celerity, and increases the phase difference between HW and HWS (or LW and LWS). For small value of ζ, the phase lag decreases with increasing river discharge, also due to the effect on β.

Figure 5.5 shows the effect of the estuary shape number γ on the main dimensionless parameters for different river discharge conditions ϕ and for given values of the other independent parameters ($\zeta_0 = 0.1$, $\chi_0 = 20$ and $r_S = 1$). In general, the damping number δ and the velocity number μ decrease with river discharge,
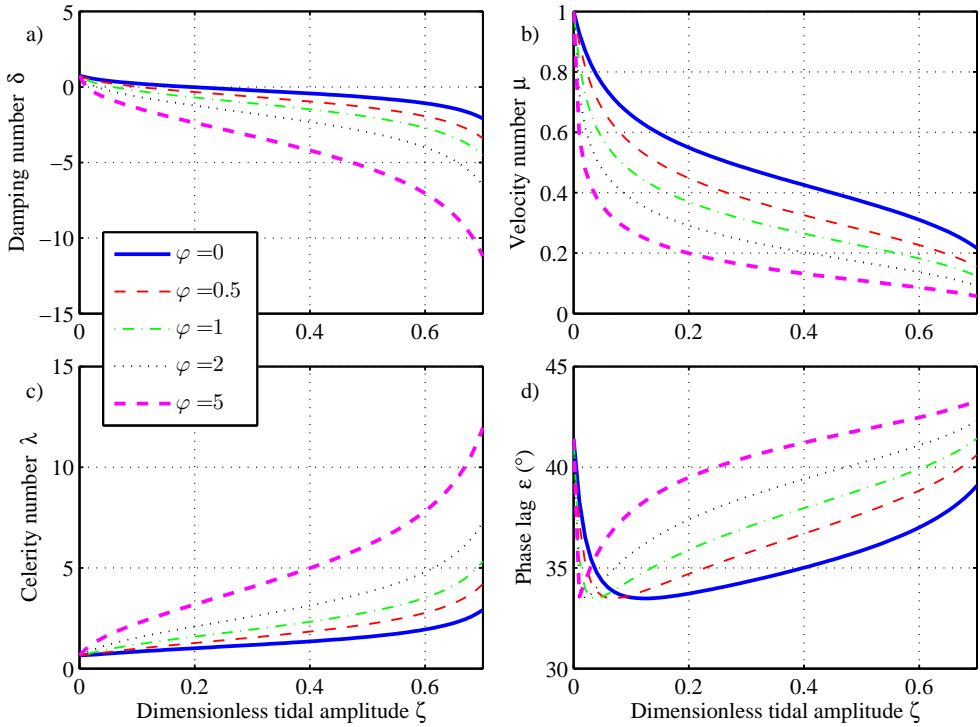
Figure 5.4: Relationship between the main dimensionless parameters and the dimensionless tidal amplitude ζ obtained by solving the equations (5.3) (with $\Gamma = \Gamma_H$), (5.22) and (5.23) for different values of the dimensionless river discharge term ϕ with $\chi_0 = 20$, $\gamma = 1.5$ and $r_S = 1$, where χ_0 is defined with equation (5.28).

which means more tidal damping and less velocity amplitude. On the other hand, the celerity number λ is increased (hence slower wave celerity) due to increasing river discharge. For the phase lag ϵ, we can see from Figure 5.5d that it decreases with river discharge for small values of γ while it increases for larger values of γ. *Cai et al.* [2012a] found the same relationship between the main dimensionless parameters and the friction number χ, which confirms our point that including river discharge acts in the same way as increasing the friction.

From an analytical point of view, it is easy to show that the influence of river discharge on the tidal dynamics is very similar to that of the friction number χ. Referring for sake of simplicity to the quasi non-linear model and considering an artificial friction number χ_r due to river discharge, the damping equation (5.3) can
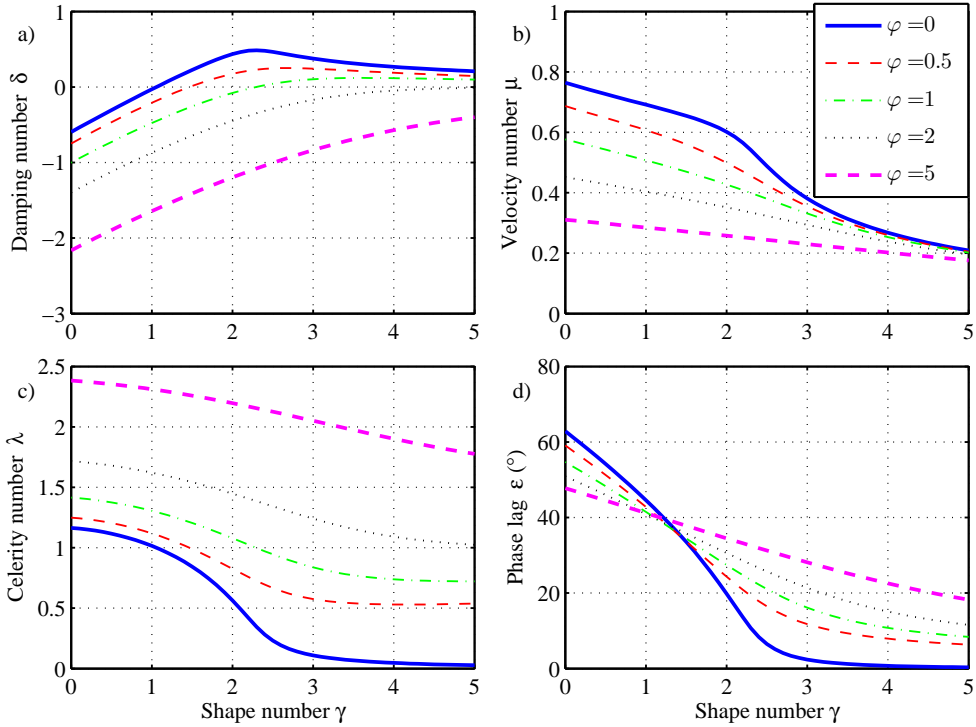
Figure 5.5: Relationship between the main dimensionless parameters and the estuary shape number γ obtained by solving the equations (5.3) (with $\Gamma = \Gamma_H$), (5.22) and (5.23) for different values of the dimensionless river discharge term ϕ with $\zeta_0 = 0.1$, $\chi_0 = 20$ and $r_S = 1$.

be written, with equation (5.6) for the case $\phi < \mu\lambda$, as

$$\delta = \frac{\mu^2}{1 + \mu^2 \beta} \left[\gamma\theta - (\mu\lambda)^2 \chi \left(1 + \frac{8}{3} \zeta \frac{\phi}{\mu\lambda} + \left(\frac{\phi}{\mu\lambda} \right)^2 \right) \right] = \frac{\mu^2}{1 + \mu^2 \beta} \left[\gamma\theta - (\mu\lambda)^2 \chi_r \right]. \tag{5.29}$$

This relationship shows that the effect of river discharge is basically that of increasing friction by a factor that is a function of ϕ. Expressing the artificial friction number as $\chi_r = \chi + \Delta\chi_r$ provides an estimation of the correction of the friction term

$$\frac{\Delta\chi_r}{\chi} = \frac{8}{3} \zeta \frac{\phi}{\mu\lambda} + \left(\frac{\phi}{\mu\lambda} \right)^2, \tag{5.30}$$

which is needed to compensate for the lack of considering river discharge. In fact, increasing ϕ is analogous to changing χ, and the expected non-physical adjustment of the Manning–Strickler coefficient K can be estimated for models that do not consider Q_f.

5.4.4. Comparison with Numerical Results

To investigate the performance of the analytical hybrid solutions, the results have been compared with a one-dimensional numerical model. Since we used equation (5.19) to describe the width convergence along the estuary, the estuary shape number accounting for width convergence becomes a function of distance:

$$\gamma_b = \frac{c_0\left(\overline{B_0} - \overline{B_{\min}}\right)\exp(-x/b)}{b\omega\left[\overline{B_{\min}} + \left(\overline{B_0} - \overline{B_{\min}}\right)\exp(-x/b)\right]} . \tag{5.31}$$

When accounting for river discharge, it is necessary to include depth divergence (i.e., the residual water level slope, which is particularly important if the bed is horizontal)

$$\gamma_d = -\frac{c_0}{\omega}\frac{1}{\overline{h}}\frac{d\overline{h}}{dx} . \tag{5.32}$$

Hence the combined estuary shape number reads:

$$\gamma = \gamma_b + \gamma_d . \tag{5.33}$$

Figure 5.6 compares the performance of two analytical models, i.e., considering depth divergence (indicated by 'div') and without considering depth divergence (denoted by 'nodiv'), against the numerical results (Q_f=0 and 5000 m^{3}s^{-1}) for given tidal amplitude to depth ratios at the estuary mouth (ζ_0=0.2 and ζ_0=0.5). We can see from Figure 5.6 that the performance of the analytical models is the same in the seaward part, where the effect of river discharge is small compared to tidal flow. Thus the usual assumption that river discharge and residual slope on tidal propagation is negligible in this part of the estuary is reasonable. For the case without river discharge, it can be seen that the analytical model performs slightly better when including depth divergence due to residual water level slope, especially in the upper reach of the estuary (this is due to the nonlinearity of the friction term). On the other hand, if river discharge is included, the analytical model requires taking account of depth divergence to accurately simulate the tidal damping. As the tidal amplitude to depth ratio ζ increases, the numerical simulations indicate that the deviation from the numerical results increases if we neglect the residual slope. Including depth divergence, the analytical model performs much better. However, the correspondence with numerical result is not perfect due to the fact that the analytical model does not account for wave distortion when the tide propagates upstream. More detailed comparion between analytical and fully nonlinear numerical results are presented in the Supplement[2].

5.4.5. Application to Real Estuaries

Using the damping equation (5.3) (in the hybrid version, hence $\Gamma = \Gamma_H$), the analytical model has been compared to observations made in the Modaomen and

---

[2]Auxiliary materials are available in the online version at http://www.hydrol-earth-syst-sci.net/18/287/2014/hess-18-287-2014-supplement.pdf
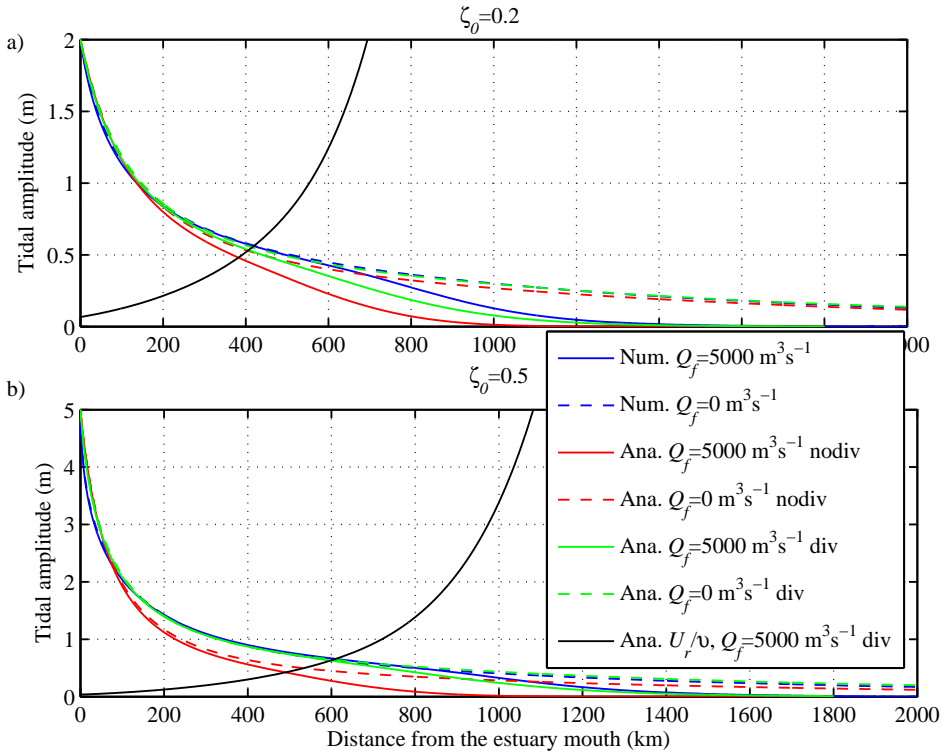
Figure 5.6: Comparison between different analytical models and numerical results for given values of K=60 $m^{1/3}\,s^{-1}$, b=352 km, $\overline{h}$=10 m, $\overline{B_0}$=5000 m, $\overline{B_{min}}$=300 m, ζ_0=0.2 (a) or ζ_0=0.5 (b). The drawn black line represents the river velocity to tide velocity amplitude ratio. The label 'nodiv' indicates the models without considering the residual water level slope, while 'div' denotes the models accounting for it using the approach described in Sect. 5.

Yangtze estuaries in China, where the influence of river discharge in the upstream part is considerable. The Modaomen estuary forms the downstream part of the West River entering the Pearl River Delta with an annual river discharge of 7115 m³ s⁻¹ at Makou [*Cai et al.*, 2012b]. The Yangtze estuary drains the Yangtze River basin with an annual mean river discharge of 28 310 m³ s⁻¹ at Datong [*Zhang et al.*, 2012].

The computation depends on the three independent variables, i.e., γ, χ_0 and ϕ. Given the flow boundary conditions (i.e., the tidal amplitude at the seaward boundary and river discharge at the landward boundary) and the geometry of the channel, the values of γ, χ_0 and ϕ can be computed. Hence, the set of four implicit analytical equations (5.3) (with $\Gamma = \Gamma_H$), (5.20), (5.21) and (5.22) can be solved by simple iteration. The tidal amplitude is obtained by numerical integration of the damping number δ over a length step (e.g., 1 km).

Table 5.2 presents the geometry and flow characteristics (considering two different cases for independent calibration and verification of the model) of the Modaomen

and Yangtze on which the computations are based. The convergence length of the cross-sectional area, which is the length scale of the exponential function, is obtained by fitting equation (1.2), where the parallel branches separated by islands are combined, as recommended by *Nguyen and Savenije* [2006] and *Zhang et al.* [2012]. The calibrated parameters including the storage width ratio r_S and the Manning–Strickler friction K are presented in Table 5.3. In general, the storage width ratio r_S ranges between 1 and 2 [*Savenije*, 2005, 2012]. It is noted that a relatively small roughness value of $K = 70\,\mathrm{m^{1/3}\,s^{-1}}$ (Table 5.3) was used in the Yangtze estuary, which is due to the fact that it is a silt-mud estuary, while the bed consists of sands in the Modaomen estuary. The reason for a small roughness value of $K = 78\,\mathrm{m^{1/3}\,s^{-1}}$ used in the middle reach of the Modaomen estuary (43–91 km) is probably due to the effect of parallel branches [see *Cai et al.*, 2012b].

Table 5.2: Geometric and flow characteristics of the estuaries studied.

Estuary	Reach (km)	Depth $\bar{h}$ (m)	Convergence length a (km)	Tidal amplitude at the mouth (m)		River discharge Q_f (m³ s⁻¹)	
				Calibration	Verification	Calibration	Verification
Modaomen	0–43	6.3	106				
	43–91	7	infinite	1.31	1.09	2259	2570
	91–150	10.3	110				
Yangtze	0–34	7	42				
	34–275	9	140	1.8	2.3	13 100	17 600
	275–600	11	200				

Table 5.3: Calibrated parameters of the estuaries studied.

Estuary	Reach (km)	Storage width ratio r_S (–)	Manning–Strickler friction K (m$^{1/3}$s^{-1}), $Q_f > 0$	Manning–Strickler friction K (m$^{1/3}$s^{-1}), $Q_f = 0$
Modaomen	0–43	1.5	48	45
	43–91	1.4	78	75
	91–150	1.3	35	30
Yangtze	0–34	1.8	70	70
	34–275	1	70	70
	275–600	1	45	26

Figure 5.7 shows the longitudinal computation of the tidal amplitude, the travel time (both at HW and LW) and damping number applied to the Modaomen estuary. Observations of tidal amplitude and travel time of the tidal wave on 8–9 February 2001 were used to calibrate the model, while the observed data on 5–6 December 2002 were used for verification. Both the model with river discharge and the model without river discharge can be made to fit the observations if a suitable friction coefficient is used, as discussed in the previous section. However, such calibrations yield significantly lower values of the Manning–Strickler coefficients upstream. For the model without river discharge we would have required an unrealistically low Manning–Strickler value of $K = 30\,\mathrm{m^{1/3}\,s^{-1}}$ to fit the data in the upstream part of Modaomen estuary (91–150 km). In Figure 5.7, the new model accounting for the effect of river discharge is compared to the original model with the same roughness, but without river discharge. In the lower part of the estuary the models behave the same (e.g., see the dimensionless damping number in Figure 5.7c, f), but behave differently in the upper reach where the river discharge is dominant. Without considering river discharge, the model underestimates tidal damping upstream.
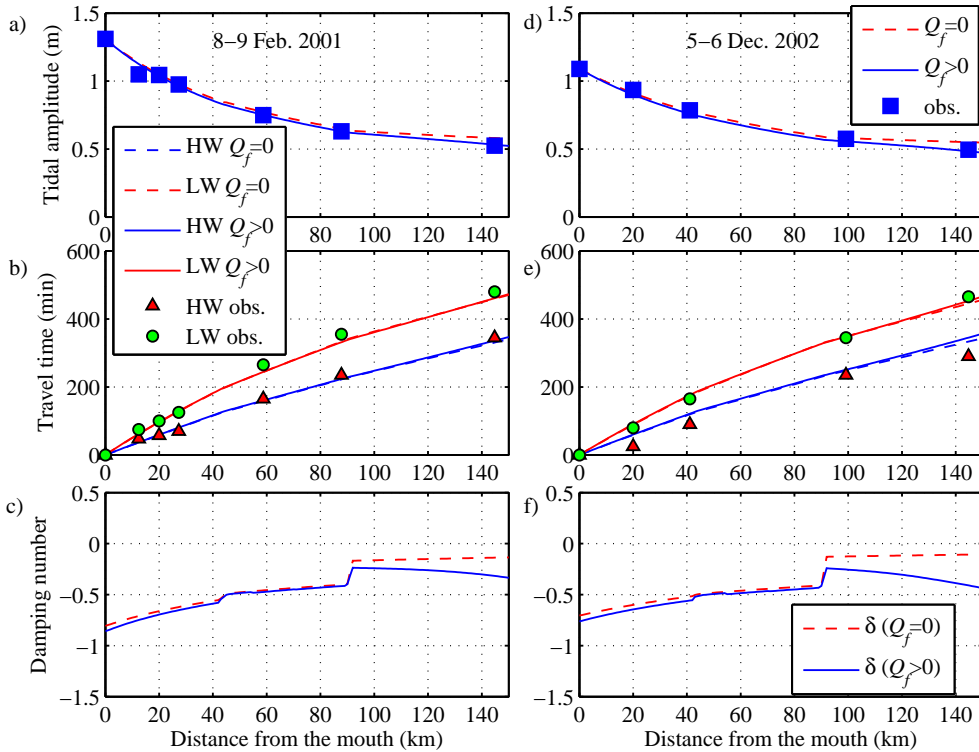
Figure 5.7: Comparison of analytically calculated tidal amplitude (a, d), travel time (b, e) with measurements and comparison of two analytical models to compute the dimensionless damping number (c, f) on 8–9 February 2001 (calibration) and 5–6 December 2002 (validation) in the Modaomen estuary. The dashed line represents the model where river discharge is neglected. The continuous line represents the model accounting for the effect of river discharge. Both models used the same friction coefficients calibrated while considering river discharge.

In Figure 5.8, we can see that the analytically calculated tidal amplitude in the Yangtze estuary is in good correspondence with the observed data on 21–22 December 2006 (calibration) and 18–19 February 2003 (verification). For the travel time, the correspondence with observations at HW is very good, but the correspondence for LW shows a big deviation from the measurements, with an underestimation of the celerity for LW. The reason for the deviation should probably be attributed to significant tidal wave distortion due to the strong river discharge, which is critical for the assumption that the celerities at HW and LW times are symmetrical compared with the tidal average wave celerity (see equation A.58 in Appendix A.6). Without considering the river discharge, a much higher and unrealistic roughness (implying a lower value of $K = 26 \, \text{m}^{1/3} \, \text{s}^{-1}$) would be necessary in the upstream part of the estuary (275–600 km) to compensate the influence of river discharge.
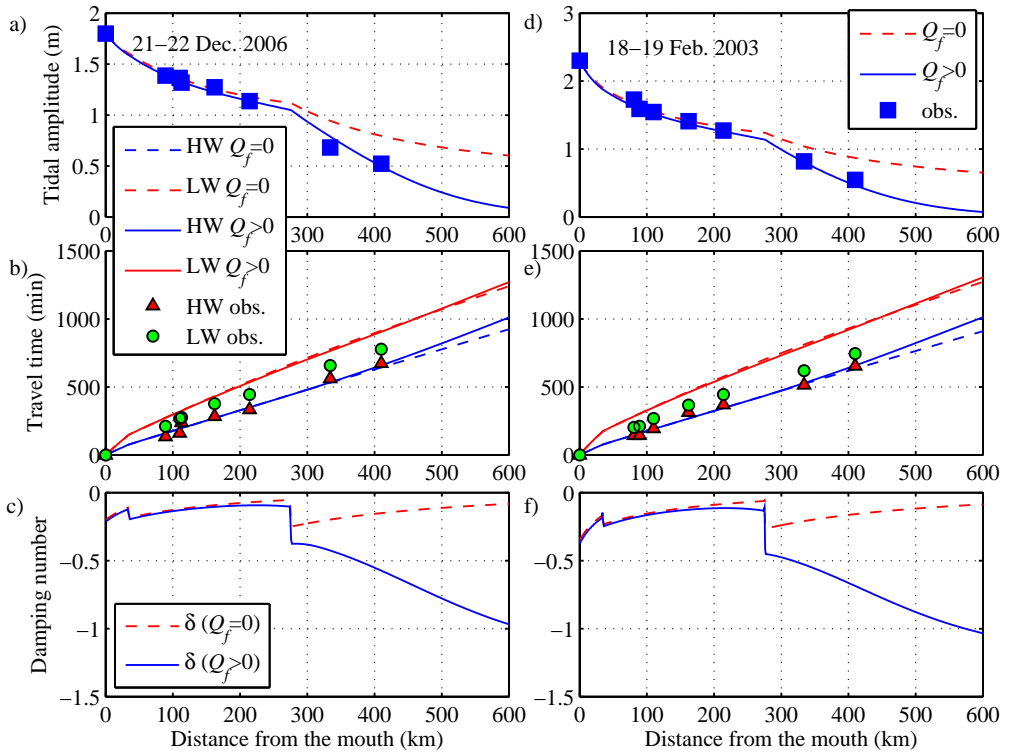
Figure 5.8: Comparison of analytically calculated tidal amplitude (a, d), travel time (b, e) with measurements and comparison of two analytical models to compute the dimensionless damping number (c, f) on 21–22 December 2006 (calibration) and 18–19 February 2003 (validation) in the Yangtze estuary. The dashed line represents the model where river discharge is neglected. The continuous line represents the model accounting for the effect of river discharge. Both models used the same friction coefficients calibrated while considering river discharge.

5.5. Conclusions

In this chapter, we have extended the analytical framework for tidal hydrodynamics proposed by *Cai et al.* [2012a] by taking account of river discharge. With the envelope method [*Savenije*, 1998], different friction formulations considering river discharge can be used to derive expressions for the envelopes at HW and LW and subsequently to arrive at the corresponding damping equations. When combined with the phase lag equation, the scaling equation and the celerity equation, these damping equations can be iteratively solved for the dimensionless parameters μ, δ, λ and ϵ, which are related to tidal velocity amplitude, tidal damping, wave celerity, and phase lag, respectively. Thus, for given topography, friction, tidal amplitude at the seaward boundary and river discharge at the landward boundary, we can reproduce the main tidal dynamics along the estuary.

Unlike previous studies [e.g., *Godin*, 1985, 1999] that neglect higher-order term,

the envelope method retains all terms although it still requires a small tidal amplitude to depth ratio. This allows for including river discharge in a fully analytical framework. It is also worth recognising that the friction term has two nonlinear sources, the quadratic velocity $U|U|$, and the variation of the hydraulic radius (approximated by the flow depth h) in the denominator [*Parker*, 1991]. Lorentz's friction formulations disregarded the tidally varying depth and only focus on the quadratic velocity. By using the envelope method, we are able to take this second nonlinear source into account and end up with a more complete damping equation accounting for river discharge.

We also note that the averaged water level tends to rise landward and that this effect has a considerable influence on tidal wave propagation, particularly when accounting for the effect of river discharge, since river discharge affects depth convergence and friction at the same time. An iterative analytical method has been proposed to include the residual water level slope into the analysis, which significantly improved the performance of the analytical model.

With respect to e.g. *Cai et al.* [2012a], where we did not consider the effect of river discharge, this method is an improvement that is important especially in the upstream part of the estuary where the influence of river discharge is considerable. This is clearly demonstrated by the application of the analytical model to two real estuaries (Modaomen and Yangtze in China), which shows that the proposed model fits the observations with realistic roughness value in the upstream part, while the model without considering river discharge can only be fitted with unrealistically high roughness values.

5

6

A coupled analytical model for salt intrusion and tides in alluvial estuaries

In this chapter we develop a coupled analytical model for salinity and tidal propagation in estuaries where the cross-sectional area varies exponentially. A simple analytical model for tidal dynamics has been used to estimate the tidal excursion, which has an important influence on the salt intrusion process since it determines the extreme salinities (i.e., salinity distribution for high water slack and low water slack). The objective of the coupling is to reduce the number of calibration parameters, which subsequently strengthens the reliability of the salt intrusion model. Moreover, the fully analytical solution for hydrodynamics allows immediate estimation of the tidally averaged depth and friction coefficient for given water level recordings and salinity measurements. This is particularly useful when a geometric survey is not available. The coupled model has been applied to 6 estuaries in Malaysia and the results show that the correspondence between analytical estimations and observations is very good. Thus, the coupled model may become a useful tool to obtain a first estimate of salt intrusion in estuaries based on a minimum amount of information required.

6.1. Introduction

The longitudinal distribution of salinity and the maximum salt intrusion length in an estuary are important environmental concerns for policy makers and managers since they influence water quality, water utilization and agricultural development in estuarine environments and the potential use of water resources in general. To

assess the effects of geometry, fresh water discharge and tide on the salinity distribution in an estuary, predictive analytical models can be useful, which do not require as much data as numerical model and the parameters used are relatively easy to obtain. Such analytical models have been proposed by many researchers, such as *Prandle* [1981], *Savenije* [1986, 1989, 1993b, 2005, 2012], *Lewis and Uncles* [2003], *Gay and O'Donnell* [2007, 2009], *Kuijper and Van Rijn* [2011]. These solutions are based on the steady-state conservation of mass equation which indicates that the dispersive and advective transports of salt are in equilibrium and the effective longitudinal dispersion coefficient incorporates all mixing mechanisms, where the dispersion coefficient along the estuary axis is either constant [e.g. *Gay and O'Donnell*, 2007] or variable [e.g. *Van der Burgh*, 1972; *Savenije*, 1986]. In this chapter we build on the salt intrusion theory developed by *Savenije* [1986, 1989, 1993b, 2005, 2012], which has been applied successfully to 17 different estuaries worldwide [*Savenije*, 2005, 2012], even in some multi-channel estuaries [*Nguyen and Savenije*, 2006; *Zhang et al.*, 2011]. Recently, this method has been tested in 6 previously un-surveyed Malaysian estuaries and the analytical results show good agreement with observations [*Gisen et al.*, 2014].

It should be noted that many predictive analytical models are derived under tidal average (TA) conditions, while the salt intrusion reaches its maximum and minimum at high water slack (HWS) and low water slack (LWS), respectively. Hence the salinity distribution curve for the TA situation should be shifted landward or seaward over half of the tidal excursion to obtain the curves for the HWS and LWS [e.g. *Savenije*, 2005]. The method requires the tidal excursion as an additional calibration parameter (i.e., the distance travelled by a moving particle between LWS and HWS), which is usually assumed to be constant along the estuary. In this chapter, we propose coupling the salt intrusion model developed by *Savenije* [1986, 1989, 1993b, 2005, 2012] to a hydrodynamic model proposed by *Cai et al.* [2012a] and *Cai and Savenije* [2013], where a simple analytical solution for the tidal dynamics can be used to predict the velocity amplitude and hence the longitudinal tidal excursion.

It is important to note that for given friction, geometry and tidal forcing at the seaward boundary, the hydrodynamics model proposed by *Cai et al.* [2012a] can be used to reproduce the main tidal dynamics (i.e., tidal damping, velocity amplitude, wave celerity and phase lag) along the estuary by solving a set of four dimensionless equations. On the contrary, if observed tidal damping (estimated from water level recordings) and velocity amplitude (estimated from salinity measurements at HWS and LWS) are known, it is possible to predict some important hydraulic parameters (e.g., the tidally averaged depth and friction) by rewriting the set of hydraulic equations.

The chapter is organized as follows. In the following section, we briefly introduce the theory for the salt intrusion model in a convergent estuary for the TA situation. The coupled model for predicting salt intrusion at HWS and LWS is described in section 6.3. Section 6.4 presents the comparison of analytically computed axial salinity distribution with salt intrusion measurements from 6 estuaries in Malaysia and the method for predicting tidally averaged depth and friction. Final conclusions

are drawn in section 6.5.

6.2. Salt Intrusion Model

The tidally averaged cross-sectional mass flux of salt F can be expressed as [e.g. *Savenije*, 2005, 2012]:

$$F = -|Q_f|S - \overline{A}D\frac{\partial S}{\partial x}, \tag{6.1}$$

where x is the longitudinal coordinate measured in landward direction, Q_f is the fresh water discharge, S the tidally averaged salinity, $\overline{A}$ the tidally averaged cross-sectional area, D the longitudinal dispersion coefficient. The first term on the right-hand side of equation (6.1) represents the advective flux, which is always negative (since x points in upstream direction), while the second term represents the dispersive flux, which flows from regions of high salinity to low salinity (note $\partial S/\partial x$ is negative in upstream direction).

We seek the solution for the concentration of longitudinal salinity in a convergent estuary, where the cross-sectional area can be described by an exponential function (1.2).

In a steady state situation where there is no net mass flux of salt (i.e., $F = 0$), equation (6.1) can be rearranged as:

$$\frac{dS}{S} = -\frac{|Q_f|}{\overline{A}D}dx. \tag{6.2}$$

It should be noted that the longitudinal dispersion coefficient D is in principle variable. Different assumptions for D as a function of x can be made [See *Prandle*, 1981].

Savenije [1986, 1989, 1993b, 2005, 2012] adopted Van der Burgh's relation to account for the variable dispersion coefficient along the estuary axis:

$$\frac{\partial D}{\partial x} = -\widehat{K}\frac{|Q_f|}{\overline{A}}, \tag{6.3}$$

which in combination with (6.2) yields the following equation [*Savenije*, 2005, 2012]:

$$D/D_0 = (S/S_0)^{\widehat{K}}, \tag{6.4}$$

where $\widehat{K}$ is the dimensionless Van der Burgh's coefficient.

Integration of equation (6.3) in combination with equations (1.2) and (6.4) leads to the averaged salinity along an estuary [*Savenije*, 2005, 2012]:

$$\frac{S}{S_0} = \left(1 - \frac{\widehat{K}|Q_f|a}{\overline{A}_0 D_0}[\exp(x/a) - 1]\right)^{1/\widehat{K}}. \tag{6.5}$$

Making use of the dimensionless parameters

$$S^* = \frac{S}{S_0}, \quad \gamma = \frac{c_0}{\omega a}, \quad D^* = \frac{|Q_f|c_0}{D_0 A_0 \omega}, \quad x^* = \frac{x\omega}{c_0}, \tag{6.6}$$

equation (6.5) can be scaled as:

$$S^* = \left(1 - \frac{D^* \widehat{K}}{\gamma}[\exp(x^*\gamma) - 1]\right)^{1/\widehat{K}}, \tag{6.7}$$

where S^* is dimensionless salinity that is normalized by the salinity at the estuary mouth, γ is the estuary shape number representing the convergence of an estuary, D^* is the dimensionless dispersion at the downstream boundary condition, x^* is the dimensionless longitudinal coordinate that is scaled by the frictionless wavelength in prismatic channels and c_0 is the classical wave celerity of a frictionless progressive wave defined in (2.9). Here the asterisk denotes a dimensionless variable.

   The salt intrusion length (i.e., the distance from the estuary mouth to the location where the water is totally fresh) can be determined by setting $S^* = 0$ in equation (6.7):

$$L^* = \frac{1}{\gamma} \ln\left(\frac{\gamma}{D^* \widehat{K}} + 1\right), \tag{6.8}$$

or

$$L = a \ln\left(\frac{D_0 \overline{A_0}}{\widehat{K} a |Q_f|} + 1\right) = a \ln\left(\frac{D_0 \overline{B_0 h_0}}{\widehat{K} a |Q_f|} + 1\right). \tag{6.9}$$

6.3. Coupled Model for Salt Intrusion

6.3.1. Analytical Solution for Tidal Excursion E

   Since tidal dynamics in convergent estuaries can be reproduced reasonably well by one-dimensional analytical solutions, in principle the output of such model can be used to predict the longitudinal tidal excursion E, defined as [*Savenije*, 2005, 2012]:

$$E = 2v/\omega, \tag{6.10}$$

where v is the velocity amplitude and ω is the tidal frequency. In this chapter, we adopted the hybrid model proposed by *Cai et al.* [2012a] and *Cai and Savenije* [2013] for estimating the velocity amplitude v (hence the tidal excursion E) as this model offers the best prediction when compared with numerical results (see chapters 3 and 4).

6.3.2. Coupled Equations for Salt Intrusion at HWS and LWS

   The assumption that the salt intrusion curves for the HWS and LWS situations can be obtained by shifting the curve for the TA situation upstream or downstream

over half the tidal excursion was first proposed by *Van der Burgh* [1972] and subsequently was demonstrated by *Savenije* [1986, 1989, 1993b, 2005, 2012]. Hence the envelope curves for HWS and LWS are given by:

$$S^{*HWS}(x^*) = S^{*TA}(x^* + E^*/2) , \qquad (6.11)$$

$$S^{*LWS}(x^*) = S^{*TA}(x^* - E^*/2) , \qquad (6.12)$$

where E^* is the dimensionless tidal excursion scaled by the frictionless tidal wave length, defined as:

$$E^* = \frac{E\omega}{c_0} = 2\frac{\upsilon}{c_0} . \qquad (6.13)$$

Unlike previous studies that usually assumed the tidal excursion is independent of x and needs to be calibrated, the proposed analytical model for tidal hydrodynamics can be used to predict a variable velocity amplitude υ (and hence tidal excursion E) for given tidal amplitude at the seaward boundary, estuary shape and friction.

6.4. Results

6.4.1. Application to Malaysia Estuaries

Figure 6.1 shows the locations and the sketches of the 6 estuaries in Peninsular Malaysia to which the coupled analytical model has been applied. Most of the estuaries are located on the west coast with only one on the east coast. The tidal behaviour differs between the west and east, where it is semi-diurnal on the west and a combination of diurnal and semi-diurnal on the east. The topography of the catchments draining on the estuaries also varies, with more mountainous area in the Perak and Kurau, and more flat land in the others. Data collection was carried out from June to August 2012 and February to March 2013 during the dry period at spring tide. The collected data were water level, river cross-section and salinity by a moving boat method.

In Figure 6.2 the variations of the cross-sectional area, width and averaged depth along the axes of the studied estuaries are shown. We see that the geometric parameters can be well fitted by the exponential functions (1.1) and (1.2). In general, it can be seen from Figure 6.2 that each of estuary can be divided into two reaches. The first reach near the estuary mouth has a shorter convergence length (indicated by a_0 and b_0) while the second reach has a longer convergence length (indicated by a_1 and b_1). The point where the geometry changes is the inflection point indicated by x_1 (see also Figure 6.1), where the subscript 1 indicates values at the inflection point. The characteristic geometrical values of the 6 studied estuaries are summarized in Table 6.1, where $< \bar{h} >$ represents the spatially averaged depth.

Figure 6.3 shows the computed tidal amplitude against the available tidal observations obtained with a hybrid model using a variable depth along the estuary. Since the first reach of the estuaries studied is usually short (few kilometres inland)
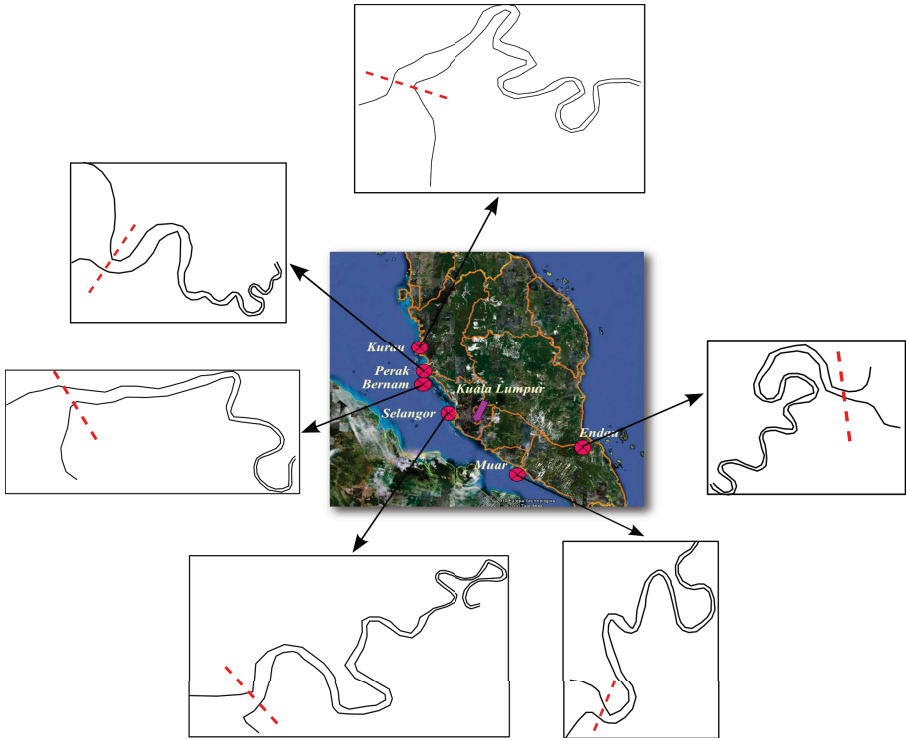
Figure 6.1: Locations of the 6 studied estuaries in Peninsular Malaysia (data obtained from Google Map). The dashed red lines represent the approximated location of the topographical inflection point.

and no observed tidal data is available in this reach, we assumed the tidal propagation in this reach is in ideal condition. Hence, the main tidal dynamics in this short distance is uniform and identical to the values at the inflection point x_1. It is worth noting that the tidal excursion tends to decrease landward while the tidal amplitude increases in Bernam (Figure 6.3a) and Perak (Figure 6.3e). This is mainly due to the depth divergence in landward direction. In Figure 6.4 we present the variation of the estuary shape number for the depth, defined as $\gamma_d = c_0/(\omega d)$ and the phase lag ϵ along the estuary. As the depth increases, we see that in these two estuaries the phase lag approaches 0 asymptotically, which suggests that the estuary tends to become a frictionless standing wave system [*Cai and Savenije*, 2013]. In fact, according to the dimensional scaling equation (identical to T2 in Table 4.1)

$$v = \frac{r_S \eta c \sin(\epsilon)}{\bar{h}},$$ (6.14)

we can derive a formula that determines the damping for the velocity amplitude:

$$\frac{1}{v}\frac{\mathrm{d}v}{\mathrm{d}x} = \frac{1}{\eta}\frac{\mathrm{d}\eta}{\mathrm{d}x} + \Delta,$$ (6.15)

Table 6.1: Geometric characteristics of studied estuaries

Estuaries	x_1 (km)	$\overline{A_0}$ (m²)	$\overline{A_1}$ (m²)	a_0 (km)	a_1 (km)	b_0 (km)	b_1 (km)	d_0 (km)	d_1 (km)	$\overline{h_1}$ (m)	$<\overline{h}>$ (m)
Bernam	4.3	15800	4500	3.4	25	2.9	16.7	-19.7	-50.3	3.6	5.2
Selangor	2.8	2200	1200	3.5	13.4	2	13.4	-4.7	infinity	3.75	3.6
Muar	3.9	3300	1600	5.3	118	2	30.8	-3.2	-41.7	6	7.9
Kurau	3.6	1800	700	3.6	62	1.5	28	-2.6	-51.1	5.2	5.7
Perak	4	20500	10000	5	40	2.7	21	-5.9	-44.2	4.45	6.4
Endau	4.8	6600	2100	4	80	1.7	36	-3	-65.5	6.44	7.1

with

$$\Delta = \Delta' - \frac{1}{\overline{h}}\frac{\mathrm{d}\overline{h}}{\mathrm{d}x} = \frac{1}{c}\frac{\mathrm{d}c}{\mathrm{d}x} + \frac{1}{\sin(\epsilon)}\frac{\mathrm{d}\sin(\epsilon)}{\mathrm{d}x} - \frac{1}{\overline{h}}\frac{\mathrm{d}\overline{h}}{\mathrm{d}x}. \tag{6.16}$$

where Δ is the error made if we assume that $\frac{1}{v}\frac{\mathrm{d}v}{\mathrm{d}x} = \frac{1}{\eta}\frac{\mathrm{d}\eta}{\mathrm{d}x}$ [which is in fact an assumption made for open ended estuaries in the envelope method, see *Savenije*, 2012]. The last term on the right-hand side relates to the depth gradient, which is equal to $-1/d$ (considered constant). This term is implicitly taken into account by using the cross-sectional area convergence a rather than the width convergence b (see Appendix A.1). So if the method uses the cross-sectional area convergence, then the error made in the envelope method is Δ' while if the width convergence is used the error is Δ.

In Figure 6.5 we compare the error term Δ' and the convergence term $1/a_1$ (i.e., $\frac{1}{A}\frac{\mathrm{d}\overline{A}}{\mathrm{d}x}$) along the estuary. We see that the error term Δ' can be negligible compared with $1/a_1$ in Selangor (Figure 6.5b) while in other estuaries it is comparable with $1/a_1$. In particular, Δ' is even bigger than $1/a_1$ in Muar and Kurau. As a result, the potential error Δ' could be considerable. However, this error is usually compensated by the calibrating the friction coefficient in the analytical model [see *Savenije*, 2012, 59–62].

Making use of the computed longitudinal velocity amplitude from equation (4.21), the tidal excursion can be estimated from equation (6.10) (also presented in Figure 6.3 on the right-hand vertical scale). Subsequently, the tidal excursion can be applied in the salt intrusion model in order to simulate the longitudinal salinity distribution in the studied estuaries. Table 6.2 presents the calibrated parameters for the hydrodynamics model (i.e., the Manning-Strickler friction coefficient K and Storage width ratio r_S) and salt intrusion model (the Van der Burgh coefficient $\widehat{K}$ and tidal dispersion coefficient at the estuary mouth D_0). As can be seen from Figure 6.6, the results show that the analytically computed salinity distribution at HWS and LWS is in good agreement with the observed values. This suggests that the proposed coupled analytical model is applicable and useful. The tidal excursion is no longer a calibration parameter but determined on the basis of observed water levels. The reduced degrees of freedom strengthen the reliability and performance of the salt intrusion model.

We also examine the performance of the explicit analytical model (i.e., equations (4.20) and (4.21)) using a spatially averaged depth $<\overline{h}>$ presented in Table 6.1. The results also show good agreement with the observed tidal amplitude in

6
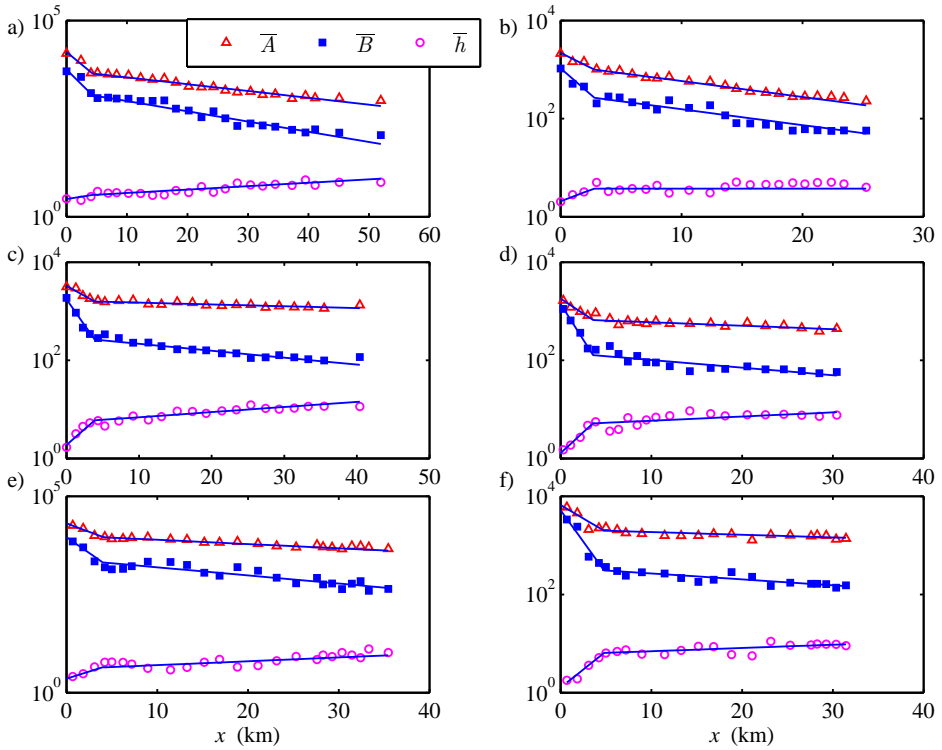
Figure 6.2: Semi-logarithmic plot of cross-sectional area $\overline{A}$ (m²), width $\overline{B}$ (m) and averaged depth $\overline{h}$ (m) along the estuary axis with fitted trend lines (a: Bernam; b: Selangor; c: Muar; d: Kurau; e: Perak; f: Endau).

6 estuaries while exploiting the same Manning-Strickler friction coefficient as the hybrid model using a variable depth. For further details on the comparison between computed tidal amplitude and observations and the resulting salt intrusion for TA, HWS and LWS, readers can refer to the Appendix A.8.

The coupled model is subsequently used to explore the effect of depth variation (such as dredging for navigational channel) on salt intrusion in 6 estuaries studied. We assumed that all the calibrated parameters (e.g., K, r_S and $\widehat{K}$), the tidal forcing in the seaward boundary, the river discharge and the estuary shape (i.e., a_0 and a_1) remain the same and the river bed is horizontal. Based on the empirical relation for the tidal dispersion coefficient at the mouth obtained by *Savenije* [2005, P166], the other assumption we made is that D_0 is proportional to the spatially averaged depth multiplied by the square of velocity amplitude at the mouth, i.e., $D_0 \propto < \overline{h} > \sqrt{v_0}$. Figure 6.7 shows the effect of deepening on salt intrusion length (TA, HWS and LWS) based on the coupled model. It can be seen from Figure 6.7 that the salt intrusion length is increased with increasing depth since it is a monotonically
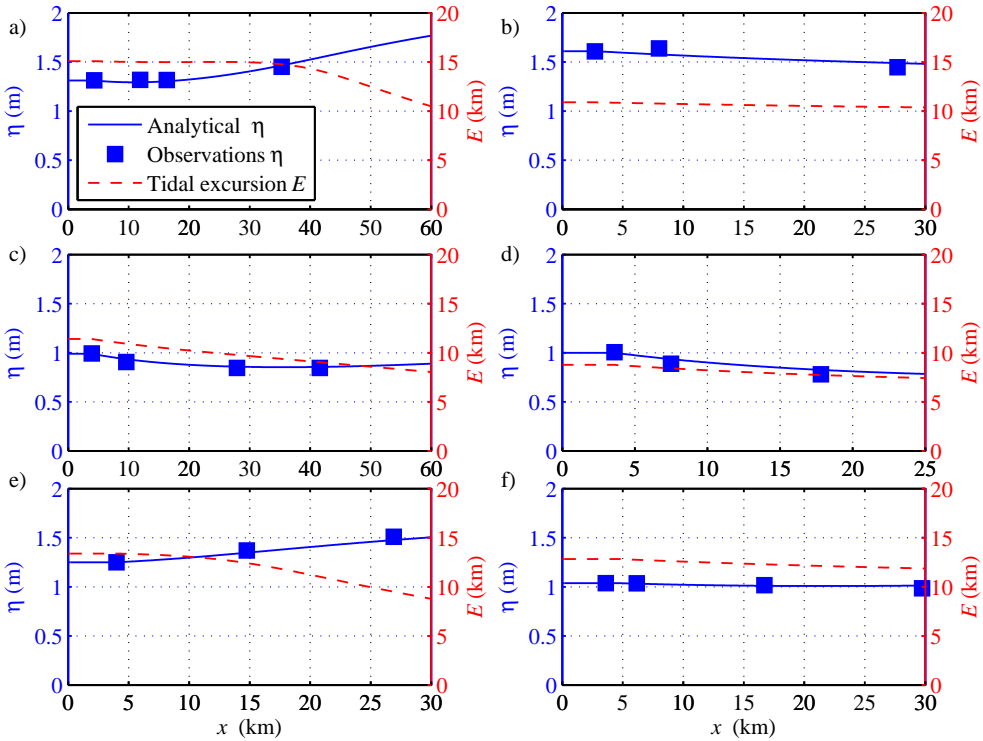
Figure 6.3: Comparison between computed and observed longitudinal tidal amplitude in 6 studied estuaries (a: Bernam; b: Selangor; c: Muar; d: Kurau; e: Perak; f: Endau) based on a hybrid model using a variable depth along the estuary.

increasing function of depth (see equation (6.9)). We also see that the effect of depth increase on the salt intrusion length is not linear: the influence on the TA situation is different from those in the HWS and LWS situations. In particular, we noted that a maximum tidal excursion (the vertical distance between HWS and LWS in Figure 6.7) is reached at a critical depth in Bernam, Selangor and Perak. A further increase of depth reduces the tidal excursion. We termed this as 'over-amplification' in chapter 3. This is mainly due to the nonlinear effect of the depth on the velocity amplitude (hence tidal excursion) in the hydraulic system (T1)—(T4c) in Table 4.1. As can be seen from Figure 6.8, in these three estuaries the velocity amplitude reaches its maximum value at a critical depth beyond which the velocity amplitude is reduced. A similar phenomenon can be observed for the influence of depth on tidal amplitude (see Figure 6.8). Both the damping of the velocity amplitude and tidal amplitude follow equation (6.15). The fact that the amplification patterns of Bernam, Selangor and Perak are substantially different is an indication that Δ has a significant value in these estuaries. For more detailed information about over-amplification, readers can refer to *Cai et al.* [2012a] and *Cai*
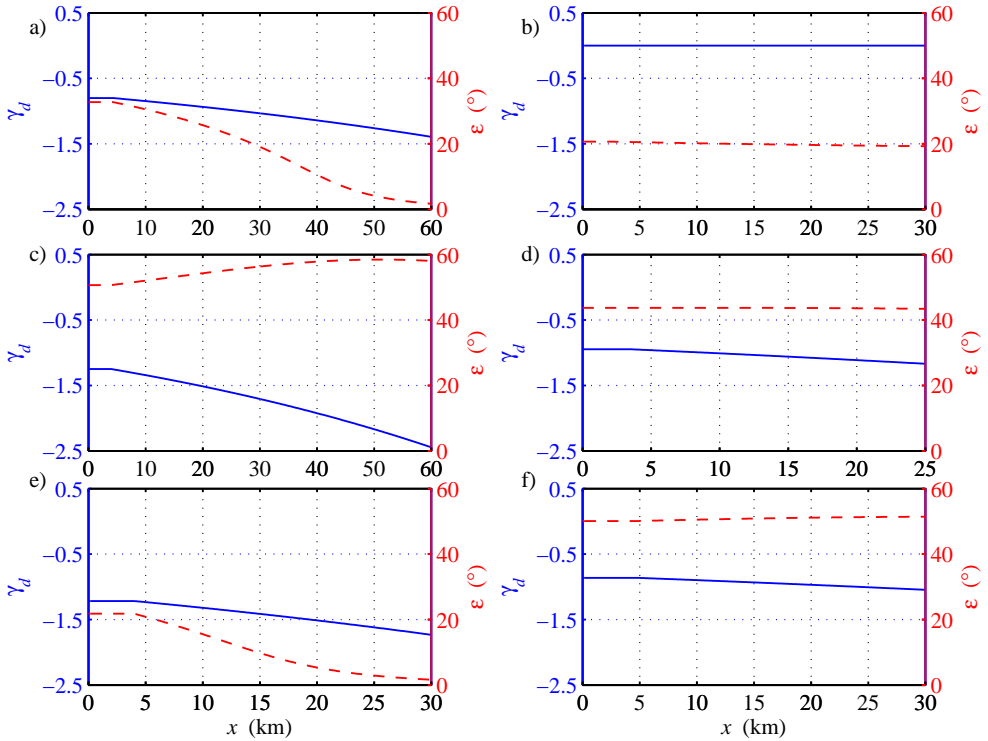
Figure 6.4: Longitudinal variation of the depth divergence γ_d and phase lag ϵ in 6 studied estuaries (a: Bernam; b: Selangor; c: Muar; d: Kurau; e: Perak; f: Endau).

and Savenije [2013].

6.4.2. Estimation of Tidally Averaged Depth and Friction Coefficient in an Estuary with (near) Constant Depth

Observations of tidal damping and salt intrusion are usually done independently. In the previous section 6.4.1 we showed that the computed tidal excursion E from an analytical hydrodynamics model can be used to reduce the number of calibration parameters in a salt intrusion model. Inversely, if observed salinity (or tidal excursion) and tidal damping are known, we can use equations (T1)—(T4c) in Table 4.1 to estimate the unknown tidally averaged depth and Manning-Strickler coefficient. In this case the average depth and the depth convergence are assumed to be unknown, so we have to assume that $a \approx b$.

With available water level recordings along an estuary, it is possible to estimate the damping of tidal amplitude, which is defined as:

$$\delta_H = \frac{1}{\eta}\frac{\mathrm{d}\eta}{\mathrm{d}x}. \tag{6.17}$$
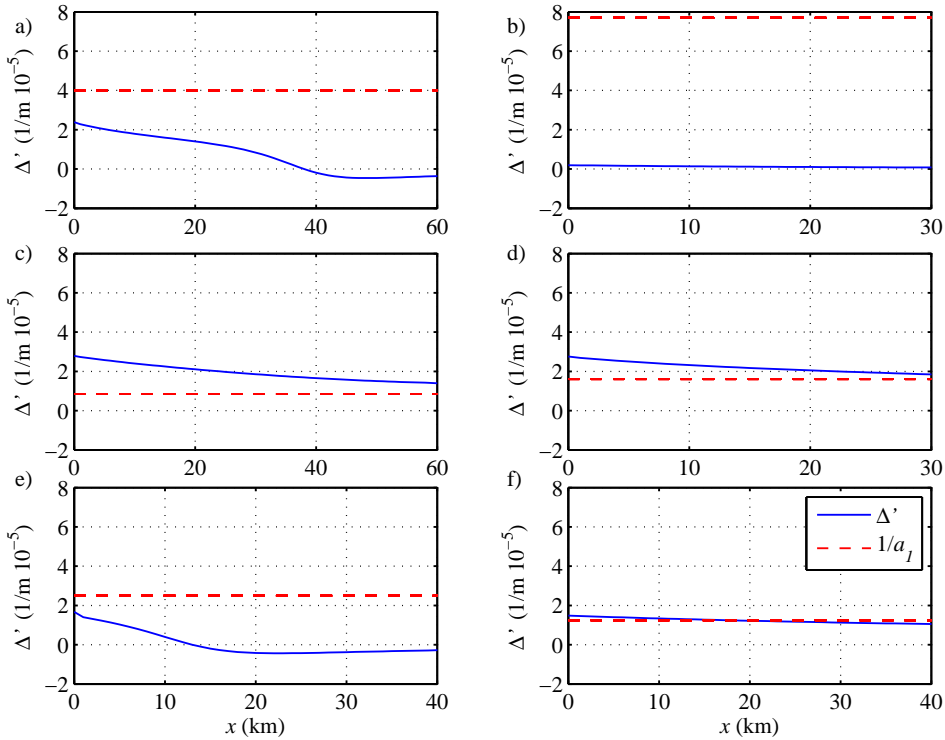
Figure 6.5: Longitudinal variation of the error term Δ' caused by the assumption made in the envelope method in 6 studied estuaries (a: Bernam; b: Selangor; c: Muar; d: Kurau; e: Perak; f: Endau). The red dashed line represents the convergence term $1/a_1$.

The tidal damping can be estimated for a reach of Δx with pressure recorders (temporary divers or tidal stations) at location 1 and 2:

$$\delta_H = \frac{1}{\left(\eta_1 + \eta_2\right)/2} \frac{\eta_2 - \eta_1}{\Delta x}, \qquad (6.18)$$

where η_1 is the tidal amplitude in the seaward part while η_2 is the tidal amplitude Δx upstream.

On the other hand, the tidal excursion E can be estimated by fitting the salinity model to observations at HWS and LWS moments against the distance. Figure 6.9 shows the process of estimating tidal excursion. We firstly fixed the salt intrusion curve at TA by calibrating the parameters of $\widehat{K}$ and D_0 since they determine the general shape of the salt intrusion curve. To obtain the curves at HWS and LWS, the TA curve has been shifted upstream or downstream over half of the tidal excursion ($E/2$), where here we assumed that E is independent of x. The tidal excursion E is calibrated until the best fit is obtained (i.e., with maximum coefficient of de-

Table 6.2: Inputs and calibrated parameters used for the coupled analytical model

Estuaries	Date	S_0 (kg/m^{-3})	η_0 (m)	T (s)	Q_f (m^{3}s^{-1})	K (m$^{1/3}$s^{-1})	Storage width ratio r_S	$\hat{K}$	D_0 (m^{2}s^{-1})	E_1 (km)
Bernam	21/06/2012	29	1.3	44400	23	70	1.1	0.2	154	15
Selangor	24/07/2012	25	1.6	44400	39	40	1.1	0.3	280	11
Muar	03/08/2012	24	1	44400	11	45	1.1	0.25	100	11
Kurau	27/02/2013	26	1	44400	28	30	1.1	0.55	216	8.8
Perak	13/03/2013	18	1.25	44400	132	65	1.1	0.15	75	13
Endau	27/03/2013	29	1	44400	6	60	1.1	0.45	30	13

termination R^2). It then follows from equation (6.10) that the averaged velocity amplitude $\upsilon = E\omega/2$. Such a calibration method was also adopted by *Gisen et al.* [2014] to calibrate the salt intrusion model in 6 Malaysian estuaries.

The phase lag ϵ can be eliminated by combining equations (T1) and (T2), which yields [*Savenije et al.*, 2008]:

$$(\gamma - \delta)^2 = \frac{1}{\mu^2} - \lambda^2. \tag{6.19}$$

When including the error term Δ from (6.15) accounting for the difference between the damping of tidal amplitude and the damping of velocity amplitude, the celerity equation (T3) in Table 4.1 becomes:

$$\lambda^2 = 1 - \delta\left(\gamma + \Delta\frac{c_0}{\omega} - \delta\right). \tag{6.20}$$

The two equations (6.19) and (6.20) can then be combined into a single, second-order equation of the tidally averaged depth $\bar{h}$ when rewriting the equation in a dimensional form, where b has been used to replace a in $\gamma = c_0/(\omega b$:

$$\frac{g\left(2\delta_H^2 b^2 - 3\delta_H b - \delta_H b^2\Delta + 1\right)}{r_S\omega^2 b^2}\bar{h}^2 + \bar{h} - \frac{r_S g\eta^2}{\upsilon^2} = 0, \tag{6.21}$$

which gives the positive solution of tidally averaged depth as:

$$\bar{h} = \frac{-1 + \sqrt{1 + 4g^2\eta^2\left(2\delta_H^2 b^2 - 3\delta_H b - \delta_H b^2\Delta + 1\right)/\left(\omega^2 b^2 \upsilon^2\right)}}{2g\left(2\delta_H^2 b^2 - 3\delta_H b - \delta_H b^2\Delta + 1\right)/\left(r_S\omega^2 b^2\right)}, \tag{6.22}$$

where the expression underneath the square root sign is non-negative.

Substitution of the corresponding dimensionless parameters in wave celerity equation (6.20) yields the expression for wave celerity:

$$c = c_0\omega\sqrt{\frac{b}{\omega^2 b - \delta_H c_0^2 + \delta_H^2 c_0^2 b - \delta_H c_0^2 b\Delta}}. \tag{6.23}$$

Next, the phase lag ϵ can be directly calculated by the dimensional phase lag equation (T1):
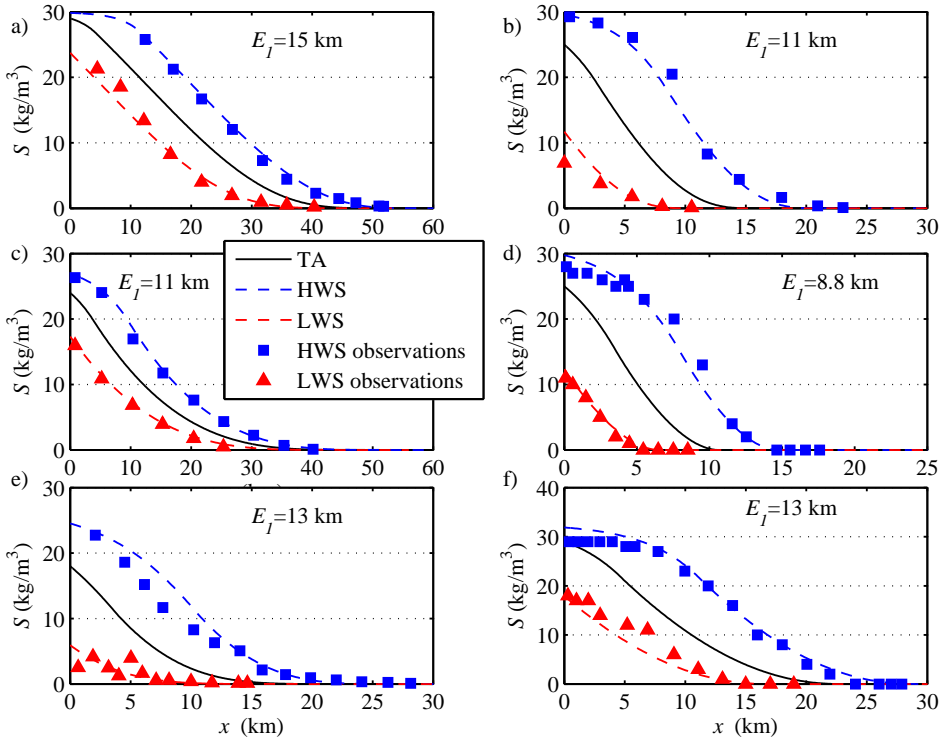
Figure 6.6: Comparison between computed and observed salinity curves at HWS and LWS in 6 studied estuaries (a: Bernam; b: Selangor; c: Muar; d: Kurau; e: Perak; f: Endau) where the tidal excursion is computed with a hybrid model using a variable depth along the estuary. E_1 represents the tidal excursion at the inflection point x_1.

$$\tan(\epsilon) = \frac{\omega b/c}{1 - b\delta_H} . \tag{6.24}$$

Finally, we can estimate the Manning-Strickler friction factor K with the dimensional damping equation (T4c) in Table 4.1 (including the error term Δ):

$$\delta_H \left[1 + \frac{g\eta}{cv\sin(\epsilon)} \right] = \frac{1}{b} - f\frac{v}{hc} \left[\frac{2}{3}\sin(\epsilon) + \frac{8}{9\pi} \right] + \Delta, \tag{6.25}$$

where f is the friction factor defined in (2.10).

After some algebra, it is possible to obtain the expression for K:

$$K = \sqrt{\frac{gv[6\sin(\epsilon) + 8/\pi]}{\overline{h}^{-4/3}c\left[9 - 16\left(\eta/\overline{h}\right)^2\right]\left\{1/b + \Delta - \delta_H\left[1 + \frac{g\eta}{cv\sin(\epsilon)}\right]\right\}}} . \tag{6.26}$$

6
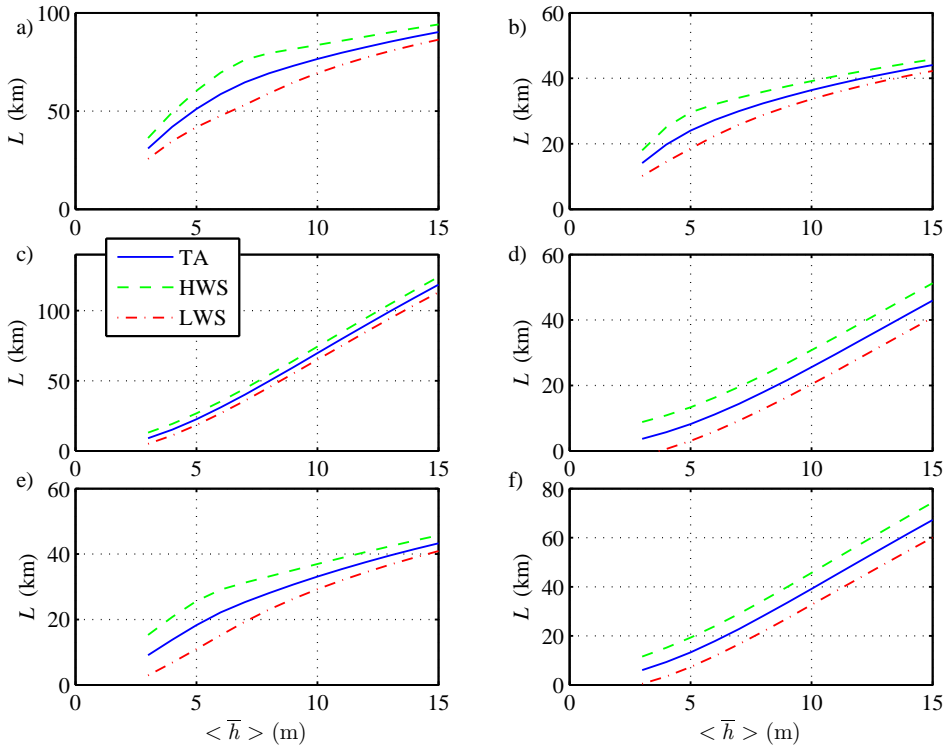
Figure 6.7: The influence of the tidally averaged depth $< \overline{h} >$ on the salt intrusion length L for TA, HWS and LWS in 6 studied estuaries (a: Bernam; b: Selangor; c: Muar; d: Kurau; e: Perak; f: Endau).
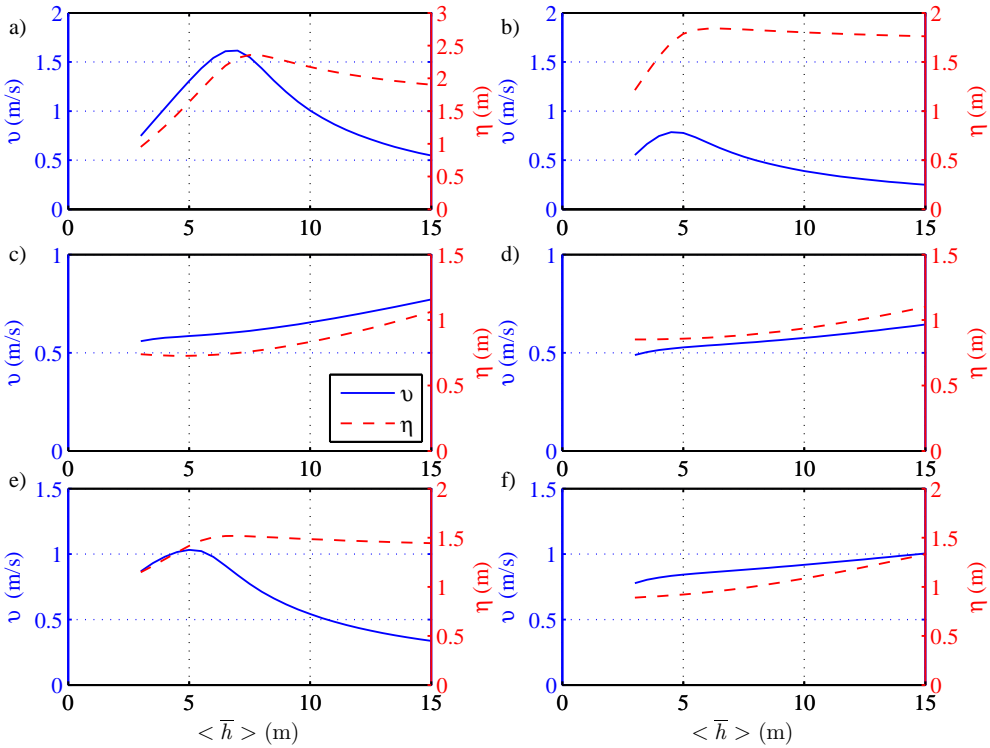
Figure 6.8: The influence of the tidally averaged depth $<\overline{h}>$ on the velocity amplitude υ and the tidal amplitude η at the location of maximum salt intrusion length L in 6 studied estuaries (a: Bernam; b: Selangor; c: Muar; d: Kurau; e: Perak; f: Endau).

It is worth noting that even if observed water level data are not available, it is still possible to have a first estimate of these hydraulic parameters by performing the explicit equations presented in in this section. This is made possible by assuming that the estuary functions more or less as an ideal estuary with constant properties (e.g., tidal amplitude, tidal excursion, friction etc.) (see Appendix A.9).

We adopted the width convergence for the second reach (i.e., longer convergence length b_1 in Table 6.1) and estimated the damping factor δ_H from equation (6.18) . Combining these parameters with predicted velocity from salinity measurements, explicit equations (6.22), (6.23), (6.24) and (6.26) can be exploited to obtain a first-order estimate of tidally averaged depth $\overline{h}$, wave celerity c, phase lag ϵ and Manning-Strickler friction coefficient K if we assume $\Delta \approx 0$.

The results for the depth and friction coefficient estimations are presented in Figures 6.10 and 6.11. The spatially averaged values of these predictive hydraulic parameters are presented in Table 6.3. In Figure 6.10 we see that the estimated results correspond well with the observed depth in Bernam, Selangor, Perak and
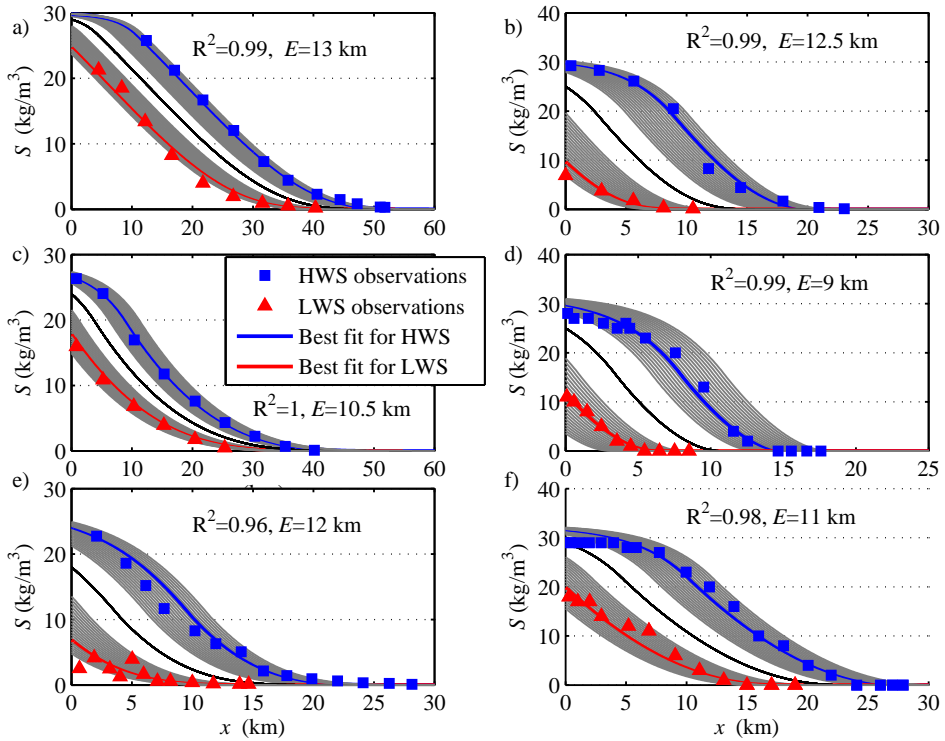
Figure 6.9: Curve fitting of the salinity measurements at HWS and LWS in 6 studies estuaries (a: Bernam; b: Selangor; c: Muar; d: Kurau; e: Perak; f: Endau). The black line indicates the calibrated salt intrusion curve at TA. The horizontal distance between blue and red lines represents the estimation of tidal excursion E. The gray lines show the curve fitting using a wide range of E (5—15 km).

Endau estuary. On the other hand, the model apparently underestimated the tidally averaged depth in the Muar and Kurau estuary. For the estimated friction coefficient, we can see from Figure 6.11 that the predicted values are in reasonable agreement with the corresponding values by calibration. The underestimation of depth in Muar and Kurau could be caused by assuming $\Delta \approx 0$. Since the depth convergence in (6.16) can be combined with the width convergence into the cross-sectional area convergence [see *Savenije*, 2012, 59—62], we also presented the estimated depth based on the cross-sectional area convergence a1 presented in Table 6.1 (see Figures 6.11 and 6.11). The remaining deviation from the observed depth may be caused by the error term Δ' in equation (6.16) or observational errors. As can be seen from Figure 6.10c the performance of equation (6.22) in Muar is much better when including the depth convergence, which suggests that the underestimation of depth is mainly due to the significant increase of depth along the estuary. On the other hand, we see that the correspondence between estimated and observed depth in Kurau (see Figure 6.10d) becomes only slightly better when accounting

for the depth convergence. This indicates the error term Δ' could have substantial influence on the estimated depth in Kurau.

Table 6.3: Estimation of the spatially averaged estuary parameters

Estuaries	δ_H	E (km)	η (m)	υ (m/s)	$\overline{h}$ (m)	c (m/s)	ϵ (∘)	K (m$^{1/3}$s^{-1})
Bernam	1.82E-06	13	1.34	0.91	3.66	6.62	21	62
Selangor	7.74E-07	12.5	1.58	0.88	3.69	6.86	18	58
Muar	-6.61E-06	10.5	0.89	0.74	3.94	5.13	36	54
Kurau	-1.72E-05	9	0.84	0.63	3.16	3.69	37	45
Perak	7.26E-06	12	1.43	0.84	6.39	23.79	10	60
Endau	-1.63E-06	11	1.02	0.77	5.66	6.71	35	48

To explore the sensitivity of the estimated depth $\overline{h}$ to the error Δ', we derive the gradient:

$$\frac{\mathrm{d}\overline{h}}{\mathrm{d}\Delta'} = -\frac{\alpha_2}{2\sqrt{\alpha_1 - \alpha_2\Delta'}(\alpha_3 - \alpha_4\Delta')} + \frac{\left(-1 + \sqrt{\alpha_1 - \alpha_2\Delta'}\right)\alpha_4}{(\alpha_3 - \alpha_4\Delta')^2}, \tag{6.27}$$

with

$$\alpha_1 = 1 + 4g^2\eta^2\left(2\delta_H^2 a^2 - 3\delta_H a + 1\right)/\left(\omega^2 a^2 \upsilon^2\right), \tag{6.28}$$

$$\alpha_2 = 4g^2\eta^2\delta_H a^2/\left(\omega^2 a^2 \upsilon^2\right), \tag{6.29}$$

$$\alpha_3 = 2g\left(2\delta_H^2 a^2 - 3\delta_H a + 1\right)/\left(r_S\omega^2 a^2\right), \tag{6.30}$$

$$\alpha_4 = 2g\delta_H a^2/\left(r_S\omega^2 a^2\right). \tag{6.31}$$

In Figure 6.12 we show how the estimated depth $\overline{h}$ develops as a function of Δ' and the corresponding gradient according to (6.27) for given spatially averaged parameters δ_H, η, υ presented in Table 6.3. It can be clearly seen from Figure 6.11 that in Bernam and Selangor the estimated $\overline{h}$ is insensitive to the error term Δ' (small values of $|\mathrm{d}\overline{h}/\mathrm{d}\Delta'|$) while in other estuaries the sensitivity to Δ' could be rather high (big values of $|\mathrm{d}\overline{h}/\mathrm{d}\Delta'|$). The Δ' that corrspondens to the observed $<\overline{h}>$ is also shown in Figure 6.12, where we see the corresponding values of $|\mathrm{d}\overline{h}/\mathrm{d}\Delta'|$ in Muar and Kurau are actually big. Further study to reduce the influence of Δ' should be explored in the future.

6.5. Conclusions

In this chapter, we propose a coupled model for tide and salt intrusion. The fully analytical hydrodynamics model proposed by *Cai et al.* [2012a] and *Cai and Savenije* [2013] has been used to estimate the tidal excursion along the salt intrusion length. Subsequently, the salt intrusion curve at TA can be shifted by half a tidal excursion to reproduce the curves at HWS and LWS. Such a coupling approach
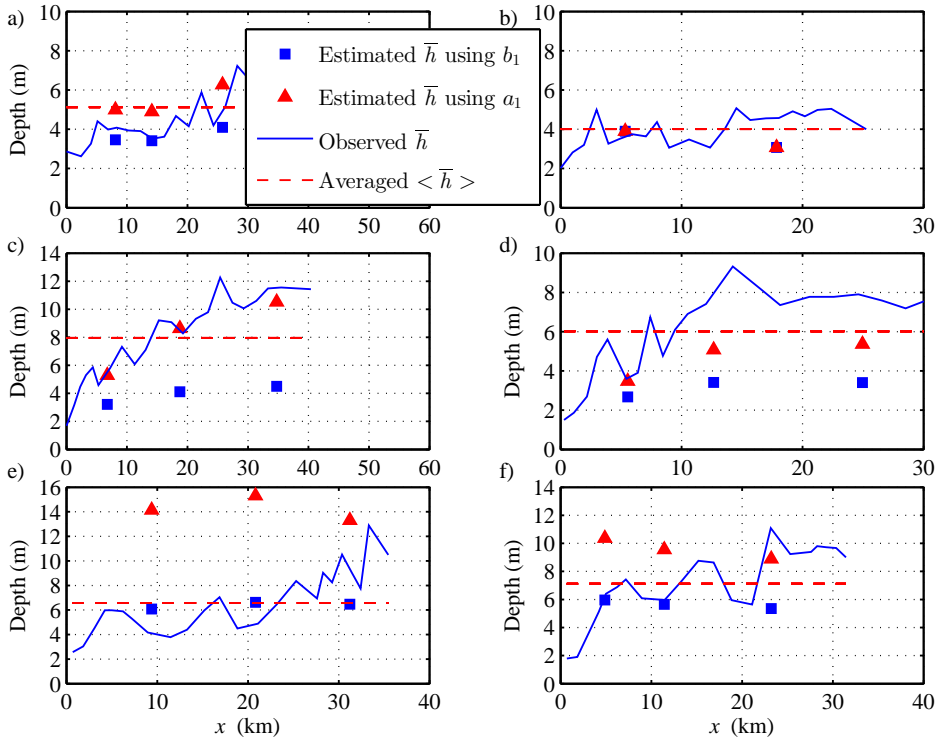
Figure 6.10: Comparison between the estimated depth from equation (6.22) (blue squares using b_1 and red triangles using a_1) and observations (blue lines) in Malaysian estuaries (a: Bernam; b: Selangor; c: Muar; d: Kurau; e: Perak; f: Endau).

reduces the number of calibrated parameters (i.e., the tidal excursion E), which reduces the degree of freedom and subsequently strengthens the reliability of the salt intrusion model. The application of the coupled analytical model in 6 estuaries in Malaysia shows good correspondence against measurements, which suggests that the proposed model can be a useful method for analyzing salt intrusion with minimum information available. Moreover, the coupling with the hydrodynamics model enables us to investigate the potential influence of deepening (such as dredging) on the maximum salt intrusion length.

For given tidal water level recordings and observed salinity at both HWS and LWS situations, it is even possible to obtain a first estimate of the average depth and the friction coefficient by manipulating the set of hydraulic equations (T1)—(T4c) in Table 4.1. This method could be very useful in situations where there are not sufficient data (e.g., detailed geometry) available to set up a hydraulic model, or as a first-order estimate of estuary depth and friction.
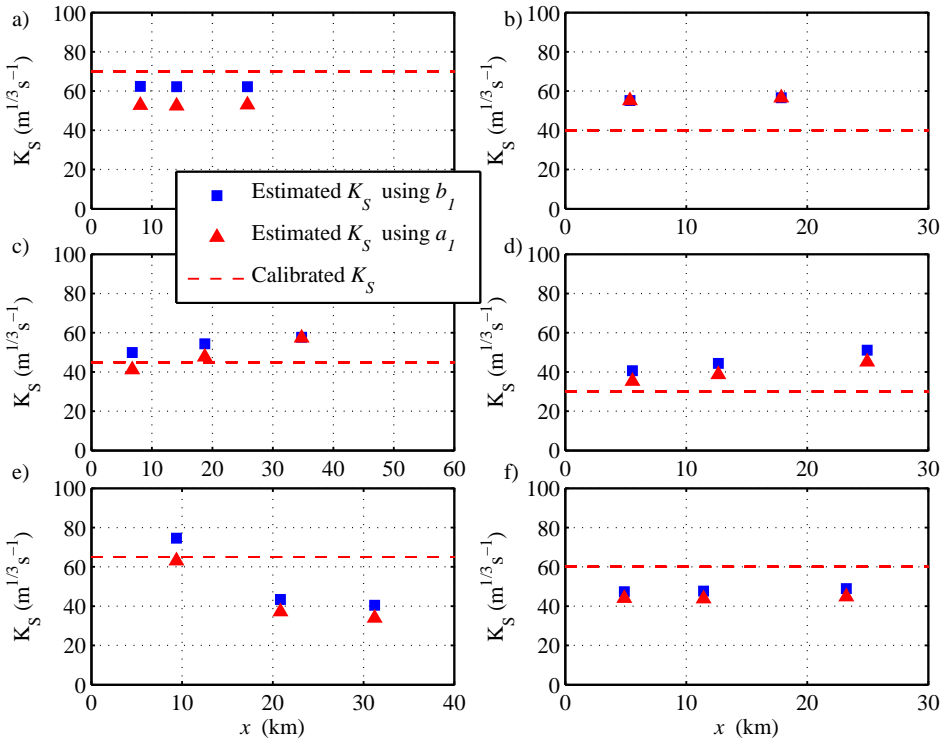
Figure 6.11: Comparison between the estimated Manning-Strickler friction coefficient from equation (6.26) (blue squares using b_1 and red triangles using a_1) and calibrated values in studied estuaries (a: Bernam; b: Selangor; c: Muar; d: Kurau; e: Perak; f: Endau).
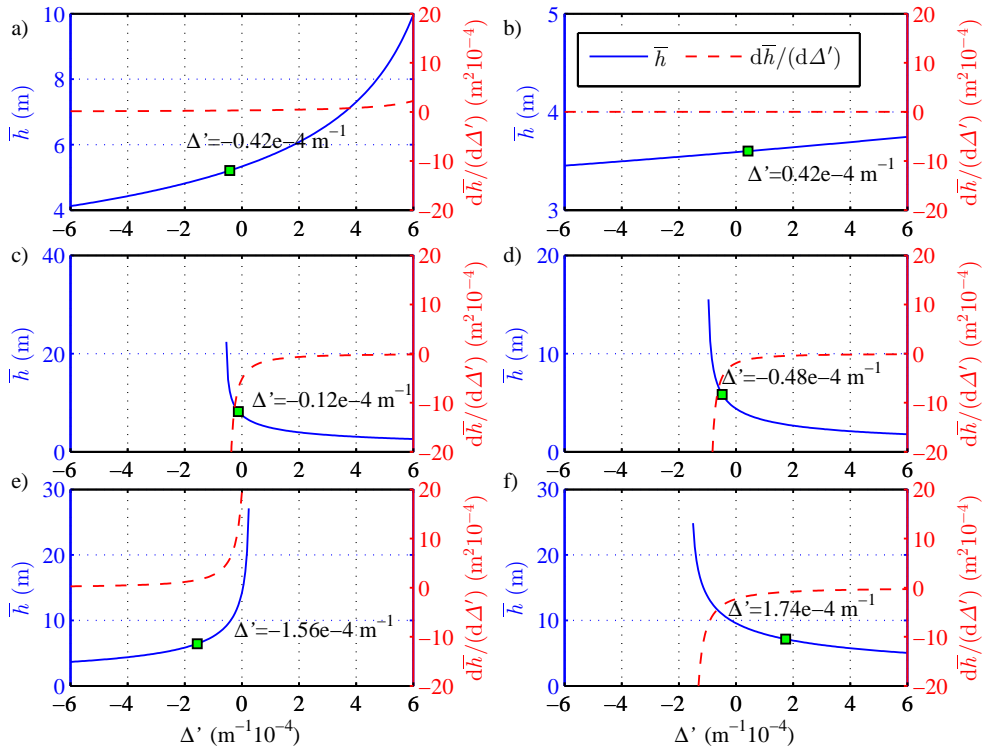
Figure 6.12: Blue line and the left scale show the dependence of $<\overline{h}>$ on Δ' according to equation (6.22). Red dashed line and the right scale show the sensitivity analysis of the estimated spatially average depth $<\overline{h}>$ to the error term Δ' in studied estuaries (a: Bernam; b: Selangor; c: Muar; d: Kurau; e: Perak; f: Endau). The green symbols represent Δ' for the observed $<\overline{h}>$

7

Conclusions and further research

This thesis has laid out a new analytical framework for tidal damping in convergent estuaries, which aims to enhance our understanding of tidal process and to develop a simple yet reliable analytical model to predict the most relevant features of the tidal wave along the estuary. One of the most important factors of tidal dynamics, the friction, was clarified in a Lagrangean reference frame. This approach allows for retention of the nonlinear friction term. We realize that friction is in principle a function of tidal amplitude and depth and hence it varies along the estuary. To account for variable friction (hence depth), a multi-reach approach has been adopted to follow along-channel variation of estuarine sections by simply using an explicit integration of the obtained damping number over a short distance (e.g., 1 km). This allows the model to reproduce realistic tidal hydrodynamics in an estuary where both width and depth are exponentially convergent. With the results presented in the previous chapters, the main objectives as mentioned in Chapter 1 have been met and the main conclusions and further research are summarized in this chapter.

7.1. Conclusions

1. Different analytical approaches developed to date can be compared by rewriting the solutions in the form a set of four implicit dimensionless equations for phase lag, velocity amplitude, damping, and wave celerity, as a function of two parameters describing friction and convergence.

2. In principle, all the linear models exploiting Lorenz' linearization are identical.

3. The envelope method that subtracts the envelope expressions at high water and low water can be used to derive damping equations based on a variety of friction term approximations, resulting in as many analytical solutions, and thereby building one consistent theoretical framework.

4. It was demonstrated that the hybrid model as a weighted average of the linearized and the fully non-linearized friction term, with an optimum weight of the linearized friction term being 1/3, and 2/3 of the fully nonlinear friction term, allows for the best predictions when compared with numerical results.

5. Analysis of the asymptotic behaviour of the equations shows that an equilibrium tidal amplitude exits that reflects the balance between friction and channel convergence.

6. The usual assumption of exponential damping for tidal amplitude and velocity amplitude is only valid for two trivial cases: an ideal estuary (where there is no damping) and the frictionless estuary (where does not exist in reality).

7. It is found that an estuary becomes over-amplified when it has a depth larger than the critical depth (condition for maximum amplification). In this case, a further increase of the depth reduces the tidal wave amplification until a frictionless standing wave system is reached asymptotically, where the tidal dynamics is completely determined by the convergence alone.

8. Within one consistent theoretical framework, we demonstrated that the influence of river discharge on tidal damping is similar to that of increasing friction.

9. The residual water level slope resulting from nonlinear friction can have substantial influence on tidal hydrodynamics when including the effect of river discharge.

10. The proposed hydrodynamics model is particularly useful in combination with the salt intrusion model since the coupling reduces the number of calibration parameters and strengthens the reliability of the salt intrusion model.

7.2. Further Research

1. Analytical solution for tidal wave propagation in a semi-closed estuary

It is important to note that a large number of analytical models are already available concerning the tidal hydrodynamics in a semi-closed estuary [e.g. *Van Rijn*, 2011; *Toffolon and Savenije*, 2011; *Winterwerp and Wang*, 2013]. Most researchers linearized the St Venant equations and adopted an effective friction coefficient so that the solutions for the whole estuary are derived. It is suggested to investigate the dynamics of the tidal wave in a semi-closed estuary as dependent on local quantities, such as tidal amplitude, estuary depth, friction, convergence, and as a function of distance to the head of the estuary. A multi-reach approach (similar to the present thesis) could be adopted to follow variations of the estuarine sections along the estuary by simple integration of the obtained damping factor over a distance interval, which is repeated for the entire length of the estuary.

2. Tidal propagation in a branched estuary

   We realized that the simple analytical model for the channel networks proposed by *Hill and Souza* [2006] and *Alebregtse et al.* [2013], exploiting a constant friction coefficient and imposing a closed end upstream boundary, could be further studied by including the effects of width and depth convergence. By developing such an analytical model to multiple branching estuaries, it is possible to provide valuable information about the behaviour of network systems. For instance, the effects of secondary channels on the tidal dynamics in the main channel could be investigated, which is crucial when considering constructing a secondary channel to reduce potential negative effects (such as reducing tidal range).

3. Energy consideration in tidal wave propagation

   As tidal waves propagate along the channel of an estuary, their energy is also transported. Consideration about energy transport and dissipation in estuaries is important as it provides insight into the formation and longitudinal variation of tidal wave propagation as well as its long-term morphodynamic evolution [*van der Wegen et al.*, 2008]. In addition it has direct relation to the exploitation of tidal wave energy (e.g., tidal electricity generation). It is recommended to investigate the tidal wave propagation from the energy point of view, especially how the potential and kinetic energy develop along the estuary.

4. 2D analytical model for tidal wave propagation in a semi-closed basin

   An idealized model for tidal propagation in a semi-closed basin has been proposed by *Roos et al.* [2011] and *Roos et al.* [2011]. The variations of width and depth along the basin are implicitly taken into account by dividing the whole basin into a sequence of different rectangular compartments with uniform depth. It is suggested to study the tidal propagation in such a basin by applying a continuous geometry, hence explicitly accounting for the width and depth convergence. This allows one to understand the wave behaviour in the light of externally defined, dimensionless parameters, describing the friction and channel convergence (geometry).

5. The influence of tidal hydrodynamics on sediment transport in convergent estuaries

   The issue of tidal morphodynamics has been explored by many researchers with both analytical [e.g., *Friedrichs et al.*, 1998; *Wang and Townend*, 2012; *Schuttelaars and De Swart*, 1996; *Schuttelaars and de Swart*, 2000; *Schramkowski and de Swart*, 2002] and numerical models [e.g., *van der Wegen and Roelvink*, 2008; *Todeschini et al.*, 2008; *Huijts et al.*, 2011; *Seminara et al.*, 2010; *Townend*, 2012]. It is worth noting that the present analytical model for tidal hydrodynamics accounts for the influence of river discharge (especially the seasonal variation), which could be potentially of use to investigate the long-term morphodynamic response to the tidal evolution in an estuary with signif-

icant river discharge. This requires detailed observations of the longitudinal tidal damping and estuarine geomtry.

7

A

Appendix

A.1. Derivation of the Quasi-nonlinear Damping Equation by the Envelope method (modified from [*Savenije, 2012, 59–62*])

We can rearrange continuity equation in a Lagrangean approach as follows:

$$\frac{dV}{dt} = r_s \frac{c}{h} \frac{dh}{dt} - \frac{cV}{b} + \frac{cV}{v} \frac{dv}{dx}. \tag{A.1}$$

We shall now make use of the dimensional scaling equation (3.2): $v = r_s \eta c \sin(\epsilon)/\overline{h}$, stating that the damping of the velocity amplitude is almost equal to the damping of the tidal range (including an error term Δ):

$$\frac{1}{v} \frac{dv}{dx} = \frac{1}{\eta} \frac{d\eta}{dx} + \Delta, \tag{A.2}$$

with

$$\Delta = \Delta' - \frac{1}{\overline{h}} \frac{d\overline{h}}{dx} = \frac{1}{c} \frac{dc}{dx} + \frac{1}{\sin(\epsilon)} \frac{d\sin(\epsilon)}{dx} - \frac{1}{\overline{h}} \frac{d\overline{h}}{dx}. \tag{A.3}$$

This error term is zero when the wave celerity c, the phase lag ϵ, the tidally averaged depth $\overline{h}$ and the damping/amplification are constant (implying exponential damping or no damping). This assumption is valid in long estuaries that gradually transform into a river. Making use of this assumption, (A.1) becomes:

$$\frac{dV}{dt} = r_s \frac{c}{h} \frac{dh}{dt} - \frac{cV}{b} + cV \left(\frac{1}{H} \frac{dH}{dx} + \Delta \right). \tag{A.4}$$

The Lagrangean momentum balance equation when written in a Lagrangean reference frame reads:

129

A

$$\frac{dV}{dt} + g\frac{\partial h}{\partial x} + g(I_b - I_r) + g\frac{V|V|}{K^2 h^{4/3}} = 0. \tag{A.5}$$

Combination of (A.4) and (A.5), and making use of the Lagrangean relationship $V = dv/dt$, yields:

$$r_S\frac{cV}{gh}\frac{dh}{dx} - \frac{cV}{g}\left(\frac{1}{b} - \frac{1}{H}\frac{dH}{dx} - \Delta\right) + \frac{\partial h}{\partial x} + I_b - I_r + \frac{V|V|}{K^2 h^{4/3}} = 0. \tag{A.6}$$

To derive an explicit relation for the tidal damping, we shall condition this differential equation for the occurrence of HW and LW. We shall then obtain two differential equations describing the envelopes of the water levels at HW and LW. At HW and LW the special condition applies that $\partial h/\partial t = 0$, and hence:

$$\left.\frac{dh}{dx}\right|_{HW,LW} = \left.\frac{\partial h}{\partial x}\right|_{HW,LW}. \tag{A.7}$$

Using this relation we can write (A.6) completely in Lagrangean derivatives for the conditions of HW and LW. Moreover, since the tidal range H is the difference between h_{HW} and h_{LW}, the Lagrangean gradient of the tidal range is defined by:

$$\frac{dh_{HW}}{dx} - \frac{dh_{LW}}{dx} = \frac{dH}{dx}. \tag{A.8}$$

And similarly because the sum of the two depth is twice the average depth (for a symmetrical wave), which we may assume to be correct if the tidal amplitude to depth ratio is small:

$$\frac{d\,h_{HW}}{dx} + \frac{dh_{LW}}{dx} \approx 2\frac{d\bar{h}}{dx} = 2I, \tag{A.9}$$

where I is the residual water level slope. Finally the following conditions apply for HW and LW if the tidal amplitude to depth ratio is not too large:

$$h_{HW} \approx \bar{h} + \eta, \tag{A.10}$$

$$h_{LW} \approx \bar{h} - \eta, \tag{A.11}$$

where $\eta = H/2$. Moreover, if the velocity has a sinus shape:

$$V_{HW} = v\sin\epsilon, \tag{A.12}$$

$$V_{LW} = -v\sin\epsilon. \tag{A.13}$$

Combination of (A.6), (A.7), (A.10) and (A.12) yields for the condition of HW:

$$\frac{r_S cv\sin\epsilon}{g(\bar{h} + \eta)}\frac{dh_{HW}}{dx} - \frac{cv\sin\epsilon}{g}\left(\frac{1}{b} - \frac{1}{\eta}\frac{d\eta}{dx} - \Delta\right) + \frac{dh_{HW}}{dx} + \frac{(v\sin\epsilon)^2}{K^2(\bar{h} + \eta)^{4/3}} = -I_b + I_r. \tag{A.14}$$

A

This is the differential equation that describes the upper envelope of all water levels in the estuary, because no water level can rise above the point of HW. Similarly for the condition of LW we find the envelope for LW, which is the lower boundary of all the water levels in the estuary:

$$\frac{-r_s cv \sin\epsilon}{g(\bar{h}-\eta)}\frac{dh_{LW}}{dx}+\frac{cv\sin\epsilon}{g}\left(\frac{1}{b}-\frac{1}{\eta}\frac{d\eta}{dx}-\Delta\right)+\frac{dh_{LW}}{dx}-\frac{(v\sin\epsilon)^2}{K^2(\bar{h}-\eta)^{4/3}}=-I_b+I_r.\ \text{(A.15)}$$

Subtraction of these two envelopes yields:

$$\frac{r_s cv\sin\epsilon}{2\bar{h}}\left(\frac{dh_{HW}}{dx}\frac{\bar{h}}{(\bar{h}+\eta)}+\frac{dh_{LW}}{dx}\frac{\bar{h}}{(\bar{h}-\eta)}\right)-\frac{cv\sin\epsilon}{\bar{h}}\left(\frac{\bar{h}}{b}-\frac{\bar{h}}{\eta}\frac{d\eta}{dx}-\Delta\right)+g\frac{d\eta}{dx}+f\frac{(v\sin\epsilon)^2}{\bar{h}}=0,$$

(A.16)

with:

$$f=\frac{g}{K^2\bar{h}^{1/3}}\left(1-\left(\frac{1.33\eta}{\bar{h}}\right)^2\right)^{-1}.\qquad\text{(A.17)}$$

The coefficient 1.33 in this equation follows from a Taylor series expansion of $(h+\eta)^{1.33}\approx h^{1.33}(1+1.33\eta/h)$, if $\eta<h$. Due to the factor 1.33, this equation only makes sense as long as $\eta/h<0.75$ and may only be applied for smaller amplitude to depth ratios. We can see that if the tidal amplitude to depth ratio is small $f\approx g/(K^2\bar{h}^{-1/3})$.

The part between brackets in the first term of (A.16) can be replaced by the residual water level slope I defined in (A.9), provided $\eta/h<1$. Elaboration yields:

$$\frac{\bar{h}}{\eta}\frac{d\eta}{dx}\left(1+\frac{g\eta}{cv\sin\epsilon}\right)=\frac{\bar{h}}{b}-f\frac{v\sin\epsilon}{c}-r_sI-\bar{h}\Delta.\qquad\text{(A.18)}$$

The width and the depth convergence in this equation can be combined into the cross-sectional area convergence. For small values of r_s this leads to the simplified equation:

$$\frac{\bar{h}}{\eta}\frac{d\eta}{dx}\left(1+\frac{g\eta}{cv\sin\epsilon}\right)=\frac{\bar{h}}{a}-f\frac{v\sin\epsilon}{c}-\bar{h}\Delta'.\qquad\text{(A.19)}$$

Regarding the term $\bar{h}\Delta'$. It is zero in a near ideal estuary where: a) there is no bottom slope, b) the tide is modestly damped/amplification or $\frac{1}{v}\frac{dv}{dx}$ is constant, and c) the phase lag is constant. In long coastal plain estuaries this is generally an acceptable assumption. If there is amplification or damping in a coastal plain estuary, then this is generally modest. In that case the term $\bar{h}\Delta'$ is non-zero, but since the gradient of the tidal velocity amplitude is small compared to the convergence length ($\frac{1}{v}\frac{dv}{dx}b<0.1$), $\bar{h}\Delta'$ is still much smaller than h/a. In short (amplified) estuaries, there may be a bottom gradient, a gradient in the phase lag (gradually moving towards a standing wave) and a gradient in the tidal velocity amplitude (gradually reducing to zero). So in short estuaries the $\bar{h}\Delta'$ term may become prominent and

A

may need to be accounted for. In coastal plain estuaries, however, particularly in the downstream part, this term may be disregarded.

Hence, the analytical solution of the St. Venant's equations yields:

$$\frac{1}{\eta}\frac{\mathrm{d}\eta}{\mathrm{d}x}\left(1 + \frac{g\eta}{cv\sin\epsilon}\right) = \frac{1}{a} - f\frac{v\sin\epsilon}{\overline{h}c}\,. \tag{A.20}$$

This is a differential equation describing the damping of the tidal amplitude as a function of the estuary shape, the friction and the residual slope. The subtraction of the two envelopes for HW and LW resulted in a differential equation that describes the tidal range.

Making use of the dimensionless parameters defined in section 2.2, equation (A.20) can be written as:

$$\delta = \frac{\gamma}{2} - \frac{1}{2}\chi\mu^2\,. \tag{A.21}$$

This is the so-called quasi-nonlinear damping equation.

A.2. Derivation of the Linear Tidal Damping Equation by the Envelope Method

Using a Lagrangean approach for the analysis of tidal flow instead of the more common Eulerian one, as proposed by *Savenije* [2005], the continuity equation can be written as

$$\frac{dV}{dt} = r_s \frac{c}{h} \frac{dh}{dt} - \frac{cV}{a} + cV \frac{1}{\eta} \frac{d\eta}{dx}. \tag{A.22}$$

The momentum equation can be written in a Lagrangean reference frame as well, providing the differential equation

$$\frac{dV}{dt} + g \frac{\partial h}{\partial x} + g(I_b - I_r) + g \frac{V|V|}{K^2 h^{4/3}} = 0. \tag{A.23}$$

where I_r is the water level residual slope resulting from the density gradient.

Combination of equations (A.22) and (A.23), and using $V = dx/dt$ yields:

$$r_s \frac{cV}{gh} \frac{dh}{dx} - \frac{cV}{g} \left(\frac{1}{a} - \frac{1}{\eta} \frac{d\eta}{dx} \right) + \frac{\partial h}{\partial x} + I_b - I_r + \frac{V|V|}{K^2 h^{4/3}} = 0. \tag{A.24}$$

If we consider the situation at HW and LW, then the following relations apply. The tidal range H ($H = 2\eta$) is the difference between h_{HW} and h_{LW}:

$$2 \frac{d\eta}{dx} = \frac{dh_{HW}}{dx} - \frac{dh_{LW}}{dx}, \tag{A.25}$$

where $\overline{h}$ is the tidal average water level. Moreover, at HW and LW

$$\frac{\partial h}{\partial t} \Big|_{HW,LW} = 0 \tag{A.26}$$

by definition, and hence

$$\frac{dh_{HW,LW}}{dx} = \frac{\partial h}{\partial x} \Big|_{HW,LW}. \tag{A.27}$$

If the dimensionless tidal wave (scaled by the tidal range) is considered undeformed (which is the case when $\eta/\overline{h} \ll 1$), the damping is symmetrical with respect to the tidal average water level $\overline{h}$, which may still have a residual slope $I = d\overline{h}/dx$ such that

$$\frac{dh_{HW}}{dx} + \frac{dh_{LW}}{dx} \approx 2 \frac{d\overline{h}}{dx} = 2I, \tag{A.28}$$

with

$$h_{HW} \approx \overline{h} + \eta, \qquad h_{LW} \approx \overline{h} - \eta \tag{A.29}$$

These three approximations are not critical to the derivation, and acceptable if $\eta/\overline{h} \ll 1$.

For the tidal velocity at HW and LW the expressions (3.13) can be derived. Furthermore, we have to realize that the celerities of propagation at HW (c_{HW}) and LW (c_{LW}) are not equal (as a result of the different depths), but we may also assume that they are symmetrical compared to the tidal average wave celerity c, and hence that for small tidal amplitudes

$$\frac{c_{HW}}{h_{HW}} \approx \frac{c_{LW}}{h_{LW}} \approx \frac{c}{\overline{h}}, \tag{A.30}$$

$$c_{HW} + c_{LW} \approx 2c. \tag{A.31}$$

In order to compare the solution obtained using *Savenije* [2005] approach with the linear models, we adopt the usual Lorentz's linearization of the bed shear stress [*Lorentz*, 1926],

$$\frac{V|V|}{K^2 h^{4/3}} = \frac{8}{3\pi} \frac{\upsilon}{K^2 \overline{h}^{-4/3}} V. \tag{A.32}$$

Combination of equations (A.24), (A.27), and (3.13) yields the following expression for the envelope curve at HW:

$$\frac{r_s c_{HW} \upsilon \sin(\varepsilon)}{g(\overline{h} + \eta)} \frac{\mathrm{d}\, h_{HW}}{\mathrm{d}\, x} - \frac{c_{HW} \upsilon \sin(\varepsilon)}{g} \left(\frac{1}{a} - \frac{1}{\eta} \frac{\mathrm{d}\, \eta}{\mathrm{d}\, x} \right) +$$
$$+ \frac{\mathrm{d}\, h_{HW}}{\mathrm{d}\, x} + \frac{8}{3\pi} \frac{\upsilon^2 \sin(\varepsilon)}{K^2 \overline{h}^{-4/3}} = -I_b + I_r. \tag{A.33}$$

Similarly, combination of equations (A.24), (A.27), and (3.13) provides the envelope curve at LW:

$$\frac{-r_s c_{LW} \upsilon \sin(\varepsilon)}{g(\overline{h} - \eta)} \frac{\mathrm{d}\, h_{LW}}{\mathrm{d}\, x} + \frac{c_{LW} \upsilon \sin(\varepsilon)}{g} \left(\frac{1}{a} - \frac{1}{\eta} \frac{\mathrm{d}\, \eta}{\mathrm{d}\, x} \right) +$$
$$+ \frac{\mathrm{d}\, h_{LW}}{\mathrm{d}\, x} - \frac{8}{3\pi} \frac{\upsilon^2 \sin(\varepsilon)}{K^2 \overline{h}^{-4/3}} = -I_b + I_r. \tag{A.34}$$

Subtraction of these envelopes, taking into account the assumption of the wave celerity being symmetrical (equations (A.30) and (A.31)), yields the following expression:

$$\frac{r_s c \upsilon \sin(\varepsilon)}{\overline{h}} \left(\frac{\mathrm{d}\, h_{HW}}{\mathrm{d}\, x} + \frac{\mathrm{d}\, h_{LW}}{\mathrm{d}\, x} \right) - 2c\upsilon \sin(\varepsilon) \left(\frac{1}{a} - \frac{1}{\eta} \frac{\mathrm{d}\, \eta}{\mathrm{d}\, x} \right) +$$
$$+ g\frac{\mathrm{d}\, \eta}{\mathrm{d}\, x} + \frac{16}{3\pi} f_L \frac{\upsilon^2 \sin(\varepsilon)}{\overline{h}} = 0, \tag{A.35}$$

where f_L has been defined in (2.15).

The parameters between parentheses in the first term of equation (A.35) can be replaced by $2I$ of equation (A.28), provided $\eta/\overline{h} < 1$. Further elaboration yields

$$\frac{1}{\eta}\frac{d\eta}{dx}\left(\frac{1+\beta}{\beta}\right) = \frac{1}{a} - \frac{8}{3\pi}f_L\frac{v}{\overline{h}c},\tag{A.36}$$

where $\beta = cv\sin(\varepsilon)/(g\eta)$ is a tidal Froude number.

By scaling, the linear damping equation (A.36) reads:

$$\delta = \frac{\mu^2}{1+\mu^2}\left(\gamma - \frac{8}{3\pi}\chi\mu\lambda\right).\tag{A.37}$$

Making use of the trigonometric equation $[\cos(\varepsilon)]^{-2} = 1 + [\tan(\varepsilon)]^2$, the phase lag and scaling equations ((3.3) and (3.2) in section 3.2) can be combined to eliminate the variable ε to give

$$(\gamma - \delta)^2 = \frac{1}{\mu^2} - \lambda^2.\tag{A.38}$$

Introducing the celerity equation (3.4) and equation (A.37) into equation (A.38), we end up with:

$$\lambda\left[\delta\lambda\left(1 - \frac{1}{\mu^2}\right) + \frac{8}{3\pi}\chi\mu\left(1 - \lambda^2\right)\right] = 0,\tag{A.39}$$

which can be simplified for $\lambda \neq 0$. Subsequently, equation (A.39) along with equation (A.37) yields a simple relationship between δ and μ, λ:

$$\delta = \frac{\gamma}{2} - \frac{4}{3\pi}\frac{\chi\mu}{\lambda},\tag{A.40}$$

which is reported as (3.6) in section 3.3.1.

A.3. Derivation of the Tidal Damping Equation Using Dronkers' Friction Formulation by the Envelope Method

Higher order formulation, like that proposed by *Dronkers* [1964], can be represented using Chebyshev polynomials as follows:

$$\frac{V|V|}{K^2h^{4/3}} = \frac{16}{15\pi}\frac{v^2}{K^2\overline{h}^{4/3}}\left[\frac{V}{v} + 2\left(\frac{V}{v}\right)^3\right].\tag{A.41}$$

Here it has been assumed that the effect of the periodic variation of the depth may be disregarded and that the average depth may be used instead, as long as the tidal amplitude to depth ratio is small. Applying equation (A.41) in the derivation of damping equation as described in the Appendix A.2, one can easily obtain the following expression:

$$\delta = \frac{\mu^2}{1+\mu^2}\left(\gamma - \frac{16}{15\pi}\chi\mu\lambda - \frac{32}{15\pi}\chi\mu^3\lambda^3\right). \tag{A.42}$$

After some algebra, it is possible to obtain a simpler relation between δ. μ and λ:

$$\delta = \frac{\gamma}{2} - \frac{8}{15\pi}\frac{\chi\mu}{\lambda} - \frac{16}{15\pi}\chi\mu^3\lambda. \tag{A.43}$$

A.4. Derivation of the Explicit Solution to the Quasi-nonlinear Tidal Damping Equation

Based on the full nonlinear St. Venant equations, *Savenije* [1998, 2001, 2005] determined an analytical expression for tidal damping by subtracting high water (HW) and low water (LW) envelopes:

$$\frac{1}{\eta}\frac{d\eta}{dx}\left[1 + \frac{g\eta}{cv\sin(\epsilon)}\right] = \frac{1}{a} - f\frac{v\sin(\epsilon)}{\overline{h}c}, \tag{A.44}$$

Using the same assumptions made in section 4.3 and introducing a new parameter

$$\beta_Q = \frac{fv_0\sin(\epsilon)}{\overline{h}c}, \tag{A.45}$$

equation (A.44) can be simplified as:

$$\frac{d\eta^*}{dx} = \frac{\eta^*}{\psi a}\left(1 - a\beta_Q\eta^*\right). \tag{A.46}$$

Equation (A.46) can be integrated by separation of variables. Applying the boundary condition $\eta^* = 1$ at $x=0$, integration yields an explicit solution for tidal damping:

$$\eta^* = \frac{1}{a\beta_Q + \left(1 - a\beta_Q\right)\exp\left[-x/(\psi a)\right]} = \frac{1/(a\beta_Q)}{1 - \left[1 - 1/(a\beta_Q)\right]\exp\left[-x/(\psi a)\right]}. \tag{A.47}$$

Introducing the dimensionless parameters defined in Table 4.1, equation (A.47) can be rewritten as:

$$\eta^* = \frac{\gamma/(\widehat{\chi_0}\mu^2\lambda^2)}{1 - \left[1 - \gamma/(\widehat{\chi_0}\mu^2\lambda^2)\right]\exp\left[-\gamma\mu^2 x^*/(1 + \mu^2)\right]}, \tag{A.48}$$

which gives the asymptotic tidal amplitude $\eta^*_{inf} = \gamma/(\widehat{\chi_0}\mu^2\lambda^2)$ when χ^* goes to infinity.

A.5. Derivation of the Explicit Solution to the Linear Tidal Damping Equation

Cai et al. [2012a] adopted the envelope method using the usual Lorentz's linearization for the friction term and derived the linear tidal damping equation:

$$\frac{1}{\eta}\frac{d\eta}{dx}\left[1 + \frac{g\eta}{cv\sin(\epsilon)}\right] = \frac{1}{a} - \frac{8}{3\pi}f\frac{v}{\overline{h}c}, \tag{A.49}$$

A

Following the derivation as described in Appendix A.4, one can easily obtain the following explicit solution of the linear tidal damping equation:

$$\eta^* = \frac{3\pi\gamma/(8\widehat{\chi_0}\mu\lambda)}{1 - \left[1 - 3\pi\gamma/(8\widehat{\chi_0}\mu\lambda)\right]\exp\left[-\gamma\mu^2 x^*/(1+\mu^2)\right]},\qquad(A.50)$$

We can see from equation (A.50) that $\eta^*_{inf} = 3\pi\gamma/(8\widehat{\chi_0}\mu\lambda)$ when x^* approaches infinity.

A

A.6. Derivation of Lorentz's damping equation incorporating river discharge using the envelope method

Using a Lagrangean approach as in *Savenije* [2005, 2012], the continuity equation can be written as:

$$\frac{dV}{dt} = r_s \frac{c}{h}\frac{dh}{dt} - \frac{cV}{b} + cV\frac{1}{\eta}\frac{d\eta}{dx}. \tag{A.51}$$

The momentum equation can also be written in a Lagrangean form, yielding:

$$\frac{dV}{dt} + g\frac{\partial h}{\partial x} + g(I_b - I_r) + g\frac{V|V|}{K^2 h^{4/3}} = 0, \tag{A.52}$$

where I_b is the bottom slope and I_r is the water level residual slope resulting from the density gradient. Combination of these equations, and using $V = dx/dt$, yields:

$$r_s\frac{cV}{gh}\frac{dh}{dx} - \frac{cV}{g}\left(\frac{1}{b} - \frac{1}{\eta}\frac{d\eta}{dx}\right) + \frac{\partial h}{\partial x} + I_b - I_r + \frac{V|V|}{K^2 h^{4/3}} = 0. \tag{A.53}$$

Next, we condition Eq. (A.53) for the situation of high water (HW) and low water (LW). The following relations apply to h_{HW} and h_{LW}:

$$\frac{dh_{HW}}{dx} - \frac{dh_{LW}}{dx} = 2\frac{d\eta}{dx}, \tag{A.54}$$

$$\frac{dh_{HW,LW}}{dx} = \frac{\partial h}{\partial x}\bigg|_{HW,LW}, \tag{A.55}$$

$$\frac{dh_{HW}}{dx} + \frac{dh_{LW}}{dx} \approx 2\frac{d\bar{h}}{dx}, \tag{A.56}$$

with $h_{HW} \approx \bar{h} + \eta$ and $h_{LW} \approx \bar{h} - \eta$. These three equations are acceptable if $\eta/\bar{h} \ll 1$.

The tidal velocities at HW and LW the following expressions can be expressed as

$$V_{HW} \approx v\sin(\epsilon) - U_r, \qquad V_{LW} \approx -v\sin(\epsilon) - U_r, \tag{A.57}$$

where the river flow velocity U_r is negative (it is in ebb direction). Further we assume that wave celerity is proportional to the square root of the depth:

$$\frac{c_{HW}}{\sqrt{h_{HW}}} \approx \frac{c_{LW}}{\sqrt{h_{LW}}} \approx \frac{c}{\sqrt{\bar{h}}}, \tag{A.58}$$

In this example we use Lorentz's linearization Eq. (5.13) of the bed friction [*Lorentz*, 1926], but also take into account the effect of the periodic variation of the hydraulic radius in the denominator of the friction term (i.e., $K^2 h^{4/3}$). Combination

A

of Eqs. (A.53), (A.55), and the first of Eq. (A.57) yields the following envelope for HW:

$$\frac{r_s c_{HW}[v \sin(\epsilon) - U_r]}{g(\overline{h} + \eta)} \frac{dh_{HW}}{dx} - \frac{c_{HW}[v \sin(\epsilon) - U_r]}{g}\left(\frac{1}{b} - \frac{1}{\eta}\frac{d\eta}{dx}\right) + \frac{dh_{HW}}{dx}$$

$$+ \frac{1}{K^2(\overline{h} + \kappa\eta)^{4/3}}\left[\frac{1}{4}L_0 v^2 + \frac{1}{2}L_1 v^2 \sin(\epsilon)\right] = -I_b + I_r \qquad (A.59)$$

where $\kappa = 1$ corresponds to the time-dependent case, while $\kappa = 0$ to the time-independent case. Similarly, for LW, combination of Eqs. (A.53), (A.55), and the second of Eq. (A.57) yields the LW envelope:

$$-\frac{r_s c_{LW}[v \sin(\epsilon) + U_r]}{g(\overline{h} - \eta)} \frac{dh_{LW}}{dx} + \frac{c_{LW}[v \sin(\epsilon) + U_r]}{g}\left(\frac{1}{b} - \frac{1}{\eta}\frac{d\eta}{dx}\right) + \frac{dh_{LW}}{dx}$$

$$+ \frac{1}{K^2(\overline{h} - \kappa\eta)^{4/3}}\left[\frac{1}{4}L_0 v^2 - \frac{1}{2}L_1 v^2 \sin(\epsilon)\right] = -I_b + I_r \qquad (A.60)$$

Subtraction of these envelopes, using a Taylor series expansion of $h^{4/3}$, and taking into account the assumption on the wave celerity yields the following expressions:

$$\frac{r_s c v \sin(\epsilon)}{\overline{h}}\left(\frac{1}{\sqrt{1+\zeta}}\frac{dh_{HW}}{dx} + \frac{1}{\sqrt{1-\zeta}}\frac{dh_{LW}}{dx}\right)$$

$$- \frac{r_s c U_r}{\overline{h}}\left(\frac{1}{\sqrt{1+\zeta}}\frac{dh_{HW}}{dx} - \frac{1}{\sqrt{1-\zeta}}\frac{dh_{LW}}{dx}\right)$$

$$- \left[2cv \sin(\epsilon) + 2cU_r\left(1 - \sqrt{1+\zeta}\right)\right]\left(\frac{1}{b} - \frac{1}{\eta}\frac{d\eta}{dx}\right)$$

$$+ 2g\frac{d\eta}{dx} + f'\left[\frac{L_1 v^2 \sin(\epsilon)}{\overline{h}} - \kappa\frac{2L_0 v^2 \zeta}{3\overline{h}}\right] = 0 \qquad (A.61)$$

with the dimensionless friction factor f' defined as

$$f' = g/\left(K^2 \overline{h}^{-1/3}\right)\left[1 - (\kappa 4\zeta/3)^2\right]^{-1}. \qquad (A.62)$$

The parts between brackets in the first and second terms of Eq. (A.61) can be replaced by the residual water level slope $d\overline{h}/dx$ defined in Eq. (A.56) and $d\tilde{h}/dx$ defined in Eq. (A.54), respectively, provided $\zeta \ll 1$. Elaboration yields:

$$\frac{1}{\eta}\frac{d\eta}{dx}\left(\theta - r_s\frac{\phi}{\sin(\epsilon)}\zeta + \frac{g\eta}{cv \sin(\epsilon)}\right) = \frac{\theta}{b} - r_s\frac{1}{\overline{h}}\frac{d\overline{h}}{dx}$$

$$- \frac{L_1}{2}f'\frac{v}{\overline{h}c} + \kappa\frac{L_0}{3}f'\frac{v\zeta}{\overline{h}c}\frac{1}{\sin(\epsilon)} \qquad (A.63)$$

A

The dimensionless parameters ϕ and θ have been defined in the main text. The first two terms on the right hand side of Eq. (A.63) represent the width and depth convergences and can be written as:

$$\frac{\theta}{b} - r_{\mathrm{S}}\frac{1}{\overline{h}}\frac{\mathrm{d}\overline{h}}{\mathrm{d}x} = \frac{\theta}{b} + \frac{r_{\mathrm{S}}}{d} \approx \frac{\theta}{a}. \tag{A.64}$$

Here, it has been assumed that both θ and r_{S} are close to unity. Substitution of Eq. (A.64) into (A.63) yields

$$\frac{1}{\eta}\frac{\mathrm{d}\eta}{\mathrm{d}x}\left(\theta - r_{\mathrm{s}}\frac{\phi}{\sin(\epsilon)}\zeta + \frac{g\eta}{cv\sin(\epsilon)}\right) = \frac{\theta}{a} - \frac{L_1}{2}f'\frac{v}{hc}$$
$$+ \kappa\frac{L_0}{3}f'\frac{v\zeta}{hc}\frac{1}{\sin(\epsilon)} \tag{A.65}$$

Making use of the dimensionless parameters and adopting the scaling equation $\sin(\epsilon) = \mu\lambda$, Eq. (A.65) reduces to the following expression:

$$\delta = \frac{\mu^2}{1 + \mu^2[\theta - r_{\mathrm{s}}\phi\zeta/(\mu\lambda)]}\left[\gamma\theta - \chi\left(\frac{1}{2}L_1\mu\lambda - \kappa\frac{1}{3}L_0\zeta\right)\right], \tag{A.66}$$

or

$$\delta = \frac{\mu^2}{1 + \mu^2\beta}(\gamma\theta - \chi\mu\lambda\Gamma_{\mathrm{L}}), \qquad \Gamma_{\mathrm{L}} = \frac{L_1}{2} - \kappa\zeta\frac{L_0}{3\mu\lambda}. \tag{A.67}$$

A.7. Derivation of the Mean Free Surface Elevation due to Nonlinear Frictional Effect

Integration of the Lagrangean momentum equation (A.52) over a tidal period leads to:

$$V(t+T) - V(t) + g\frac{\partial}{\partial x}\int_t^{t+T} z\,\mathrm{d}\sigma + g\int_t^{t+T}\frac{V|V|}{K^2h^{4/3}}\mathrm{d}\sigma = 0. \tag{A.68}$$

which can be simplified as:

$$\frac{\partial\overline{z}}{\partial x} = -\overline{\frac{V|V|}{K^2h^{4/3}}}. \tag{A.69}$$

when tidally averaged conditions achieve a regime configuration. Making use of the boundary condition $\overline{z} = 0$ at $x=0$, integration of equation (A.69) yields an expression for the mean free surface elevation:

$$\overline{z}(x) = -\int_0^x \overline{\frac{V|V|}{K^2h^{4/3}}}\mathrm{d}x. \tag{A.70}$$
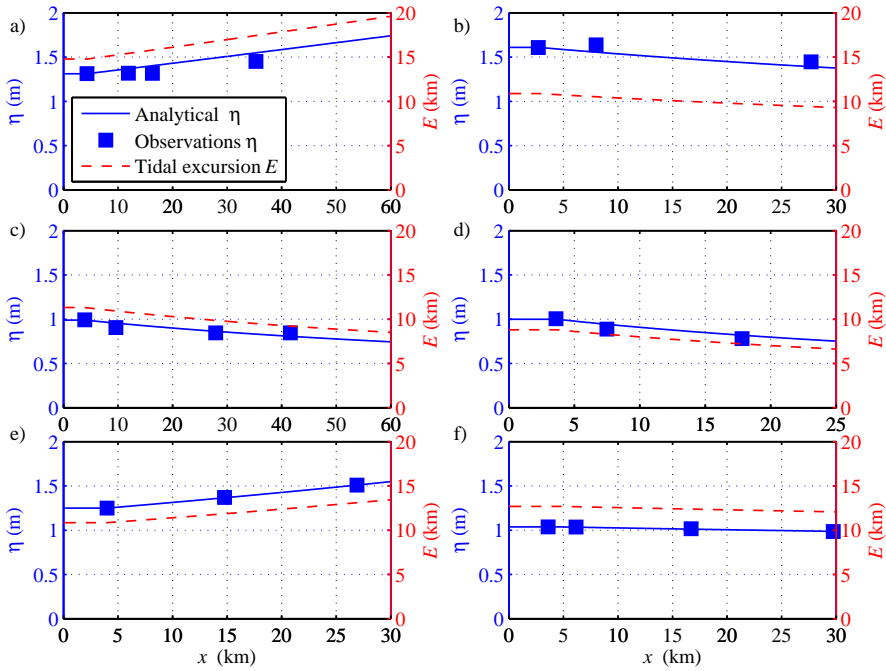
Figure A.1: Comparison between computed and observed longitudinal tidal amplitude in 6 studied estuaries (a: Bernam; b: Selangor; c: Muar; d: Kurau; e: Perak; f: Endau) based on an explicit model using a spatially averaged depth.

A.8. Coupled Analytical Model Using an Explicit Solution for Tidal Dynamics
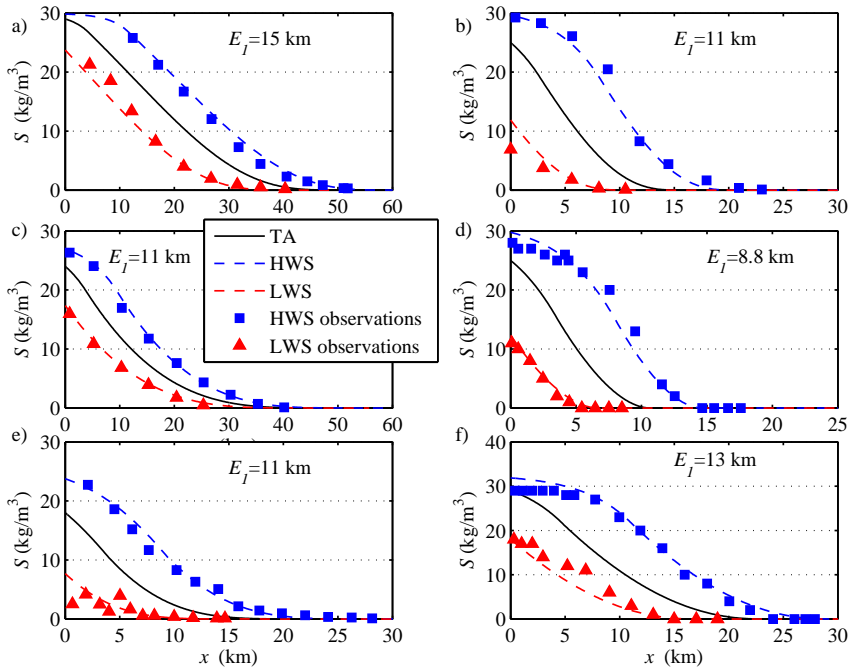
Figure A.2: Comparison between computed and observed salinity curves at HWS and LWS in 6 studied estuaries (a: Bernam; b: Selangor; c: Muar; d: Kurau; e: Perak; f: Endau) where the tidal excursion is computed with an explicit model using a spatially averaged depth. E_1 represents the tidal excursion at the inflection point x_1.

A

A.9. Predictive Hydraulic Equations for an Ideal Estuary

For an ideal estuary where $\delta = 0$ (hence $\lambda = 1$ and $\tan(\epsilon) = 1/\lambda$), substituting $\delta_H = 0$ into equation (6.22) yields an analytical solution for the ideal depth:

$$\overline{h}_I = \frac{r_S \omega b \left(-\omega b + \sqrt{\omega^2 b^2 + 4g^2\eta^2/\upsilon^2} \right)}{2g} , \qquad (A.71)$$

where the subscript I stands for the solution in an ideal estuary.

Then the ideal celerity is given by:

$$c_I = \sqrt{\frac{g\overline{h}_I}{r_S}} = \sqrt{\frac{\omega b \left(-\omega b + \sqrt{\omega^2 b^2 + 4g^2\eta^2/\upsilon^2} \right)}{2}} . \qquad (A.72)$$

Substitution of equations (A.71) and (A.72) into (6.26) ends up with the expression of ideal Manning-Strickler friction coefficient:

$$K_S = \sqrt{\frac{gvb[6\sin(\epsilon_I) + 8/\pi]}{\bar{h}_I^{\,4/3} c_I\left[9 - 16\left(\eta/\bar{h}_I\right)^2\right]}} \,, \tag{A.73}$$

with

$$\sin(\epsilon_I) = \sqrt{\frac{1}{\gamma^2 + 1}} = \sqrt{\frac{\omega^2 b^2}{c_I^2 + \omega^2 b^2}} \,. \tag{A.74}$$

References

Alebregtse, N. C., H. E. de Swart, and H. M. Schuttelaars (2013), Resonance characteristics of tides in branching channels, *J Fluid Mech*, *728, R3*, doi: 10.1017/jfm.2013.319.

Allen, G. P., J. C. Salomon, P. Bassoullet, Y. Dupenhoat, and C. Degrandpre (1980), Effects of tides on mixing and suspended sediment transport in macro-tidal estuaries, *Sediment Geol*, *26*(1-3), 69–90.

Cai, H., H. H. G. Savenije, and M. Tofflon (2012a), A new analytical framework for assessing the effect of sea-level rise and dredging on tidal damping in estuaries, *J. Geophys. Res. Oceans*, *117, C09023*, doi:10.1029/2012JC008000.

Cai, H., H. H. G. Savenije, Q. Yang, S. Ou, and Y. Lei (2012b), Influence of river discharge and dredging on tidal wave propagation; Modaomen estuary case, *J Hydraul Eng*, *138*, 885–896, doi:10.1061/(ASCE)HY.1943-7900.0000594.

Cai, H., H. H. G. Savenije, and M. Toffolon (2014), Linking the river to the estuary: influence of river discharge on tidal damping, *Hydrol. Earth Syst. Sci.*, *18*(1), 287–304, doi:10.5194/hess-18-287-2014.

Cai, H. Y., and H. H. G. Savenije (2013), Asymptotic behavior of tidal damping in alluvial estuaries, *J. Geophys. Res. Oceans*, *118*(11), 6107–6122, doi:10.1002/2013JC008772.

Cartwright, D. E. (1968), A unified analysis of tides and surges round north and east Britain, *Philosophical Transactions of the Royal Society of London*, *A263*, 1–55.

Church, J. A., and N. J. White (2006), A 20th century acceleration in global sea-level rise, *Geophys. Res. Lett.*, *33*(L01602), doi:10.1029/2005GL024826.

Dronkers, J. J. (1964), *Tidal Computations in River and Coastal Waters*, 296-304 pp., Elsevier, New York.

Dyer, K. R. (1997), *Estuaries: A Physical Introduction (2nd Edition)*, 31-40 pp., John Wiley&Sons Ltd, New York.

Friedrichs, C. T. (2010), Barotropic tides in channelized estuaries, in *Contemporary Issues in Estuarine Physics*, edited by A. Valle-Levinson, pp. 27–61, Cambridge University Press, Cambridge, UK.

Friedrichs, C. T., and D. G. Aubrey (1994), Tidal propagation in strongly convergent channels, *J. Geophys. Res. Oceans*, *99*(C2), 3321–3336.

A

Friedrichs, C. T., B. D. Armbrust, and H. E. de Swart (1998), Hydrodynamics and equilibrium sediment dynamics of shallow, funnel-shaped tidal estuaries, *Physics of Estuaries and Coastal Seas*, pp. 315–327.

Garrett, C., and D. Greenberg (1977), Predicting changes in tidal regime - open boundary problem, *J Phys Oceanogr*, *7*(2), 171–181.

Gay, P., and J. O'Donnell (2009), Comparison of the salinity structure of the chesapeake bay, the delaware bay and long island sound using a linearly tapered advection-dispersion model, *Estuar Coast*, *32*(1), 68–87.

Gay, P. S., and J. O'Donnell (2007), A simple advection-dispersion model for the salt distribution in linearly tapered estuaries, *J Geophys Res-Oceans*, *112*(C7).

Giese, B. S., and D. A. Jay (1989), Modeling tidal energetics of the Columbia river estuary, *Estuar Coast Shelf S*, *29*(6), 549–571.

Gisen, J., H. Savenije, R. Nijzink, and A. K. A. Wahab (2014), Testing a 1-D analytical salt intrusion model and its predictive equations in Malaysian estuaries, *Hydrological Sciences Journal*, doi:10.1080/02626667.2014.889832.

Godin, G. (1985), Modification of river tides by the discharge, *J Waterw Port C-Asce*, *111*(2), 257–274.

Godin, G. (1991), Compact approximations to the bottom friction term, for the study of tides propagating in channels, *Cont Shelf Res*, *11*(7), 579–589.

Godin, G. (1999), The propagation of tides up rivers with special considerations on the upper saint lawrence river, *Estuar Coast Shelf S*, *48*(3), 307–324.

Green, G. (1837), On the motion of waves in a variable canal of small depth and width, *Trans. Cambridge Philos. Soc.*, *6*, 457–462.

Hill, A. E., and A. J. Souza (2006), Tidal dynamics in channels: 2. complex channel networks, *J. Geophys. Res. Oceans*, *111*(C11), doi:10.1029/2006JC003670.

Horrevoets, A. C., H. H. G. Savenije, J. N. Schuurman, and S. Graas (2004), The influence of river discharge on tidal damping in alluvial estuaries, *J Hydrol*, *294*(4), 213–228.

Huijts, K. M. H., H. E. de Swart, G. P. Schramkowski, and H. M. Schuttelaars (2011), Transverse structure of tidal and residual flow and sediment concentration in estuaries, *Ocean Dynam*, *61*(8), 1067–1091.

Hunt, J. N. (1964), Tidal oscillations in estuaries, *Geo. J. Roy. Ast. Soc.*, *8*, 440–455, doi:10.1111/j.1365-246X.1964.tb03863.x.

Ippen, A. T. (1966), Tidal dynamics in estuaries, part I:Estuaries of rectangular section, in *Estuary and Coastline Hydrodynamics*, edited by A. T. Ippen, McGraw-Hill, New York.

Jay, D. A. (1991), Green law revisited - tidal long-wave propagation in channels with strong topography, *J Geophys Res-Oceans*, *96*(C11), 20,585–20,598.

Jay, D. A., and E. P. Flinchem (1997), Interaction of fluctuating river flow with a barotropic tide: A demonstration of wavelet tidal analysis methods, *J. Geophys. Res. Oceans*, *102*(C3), 5705–5720, doi:10.1029/96JC00496.

Jay, D. A., K. Leffler, and S. Degens (2011), Long-term evolution of columbia river tides, *J Waterw Port C-Asce*, *137*(4), 182–191.

Kuijper, K., and L. C. Van Rijn (2011), Analytical and numerical analysis of tides and salinities in estuaries; part ii: salinity distributions in prismatic and convergent tidal channels, *Ocean Dynam*, *61*(11), 1743–1765.

Kukulka, T., and D. A. Jay (2003), Impacts of columbia river discharge on salmonid habitat: 1. a nonstationary fluvial tide model, *J. Geophys. Res. Oceans*, *108*(3293), doi:10.1029/2002JC001382.

Langbein, W. B. (1963), The hydraulic geometry of a shallow estuary, *Bulletin of International Association of Scientific Hydrology*, *8*, 84–94.

Lanzoni, S., and G. Seminara (1998), On tide propagation in convergent estuaries, *J Geophys Res-Oceans*, *103*(C13), 30,793–30,812.

Leblond, P. H. (1978), Tidal propagation in shallow rivers, *J. Geophys. Res. Oceans*, *83*(Nc9), 4717–4721.

Lewis, R. E., and J. O. Lewis (1987), Shear-stress variations in an estuary, *Estuar Coast Shelf S*, *25*(6), 621–635.

Lewis, R. E., and R. J. Uncles (2003), Factors affecting longitudinal dispersion in estuaries of different scale, *Ocean Dynam*, *53*(3), 197–207.

Lorentz, H. A. (1926), *Verslag Staatscommissie Zuiderzee (in Dutch)*, Algemene Landsdrukkerij, The Hague, Netherlands.

Lowe, J. A. (2009), *UK climate projections science report: marine and coastal projections*, Met Office Hadley Centre, Exeter, UK.

Luo, X. L., E. Y. Zeng, R. Y. Ji, and C. P. Wang (2007), Effects of in-channel sand excavation on the hydrology of the Pearl River Delta, China, *J Hydrol*, *343*(3-4), 230–239.

Nguyen, A. D., and H. H. G. Savenije (2006), Salt intrusion in multi-channel estuaries: a case study in the mekong delta, vietnam, *Hydrol Earth Syst Sc*, *10*(5), 743–754.

Parker, B. B. (1991), The relative importance of the various nonlinear mechanisms in a wide range of tidal interactions, in *Tidal Hydrodynamics*, edited by B. B. Parker, pp. 236–268, John Wiley, New York.

A

A

Pillsbury, G. B. (1956a), *Tidal Hydraulics (first edition)*, 227-231 pp., Corps of Engineers, Vicksburg, USA.

Pillsbury, G. B. (1956b), *Tidal Hydraulics (revised edition)*, Corps of Engineers, Vicksburg, USA.

Prandle, D. (1981), Salinity intrusion in estuaries, *J Phys Oceanogr*, *11*(10), 1311–1324.

Prandle, D. (1985), Classification of tidal response in estuaries from channel geometry, *Geophys J Roy Astr S*, *80*(1), 209–221.

Prandle, D. (2003), Relationships between tidal dynamics and bathymetry in strongly convergent estuaries, *J Phys Oceanogr*, *33*(12), 2738–2750.

Prandle, D. (2004), How tides and river flows determine estuarine bathymetries, *Prog Oceanogr*, *61*(1), 1–26.

Prandle, D., and M. Rahman (1980), Tidal response in estuaries, *J Phys Oceanogr*, *10*(10), 1552–1573.

Roos, P. C., J. J. Velema, S. J. M. H. Hulscher, and A. Stolk (2011), An idealized model of tidal dynamics in the North sea: resonance properties and response to large-scale changes, *Ocean Dynam*, *61*(12), 2019–2035.

Savenije, H. H. G. (1986), A one-dimensional model for salinity intrusion in alluvial estuaries, *J Hydrol*, *85*(1-2), 87–109.

Savenije, H. H. G. (1989), Salt intrusion model for high-water slack, low-water slack, and mean tide on spread sheet, *J Hydrol*, *107*(1-4), 9–18.

Savenije, H. H. G. (1992a), Lagrangian solution of St Venants equations for alluvial estuary, *J Hydraul Eng-Asce*, *118*(8), 1153–1163.

Savenije, H. H. G. (1992b), Rapid assessment technique for salt intrusion in alluvial estuaries, Ph.D. thesis, International Institute for Infrastructure, Hydraulics and Environment, Delft, The Netherlands.

Savenije, H. H. G. (1993a), Determination of estuary parameters on basis of Lagrangian analysis, *J Hydraul Eng-Asce*, *119*(5), 628–642.

Savenije, H. H. G. (1993b), Predictive model for salt intrusion in estuaries, *J Hydrol*, *148*(1-4), 203–218.

Savenije, H. H. G. (1998), Analytical expression for tidal damping in alluvial estuaries, *J Hydraul Eng-Asce*, *124*(6), 615–618.

Savenije, H. H. G. (2001), A simple analytical expression to describe tidal damping or amplification, *J Hydrol*, *243*(3-4), 205–215.

Savenije, H. H. G. (2005), *Salinity and Tides in Alluvial Estuaries*, 1-190 pp., Elsevier, New York.

Savenije, H. H. G. (2012), *Salinity and Tides in Alluvial Estuaries*, 1-163 pp., completely revised 2nd edition, www.salinityandtides.com.

Savenije, H. H. G., and E. J. M. Veling (2005), Relation between tidal damping and wave celerity in estuaries, *J. Geophys. Res. Oceans*, *110*(C4), doi:10.1029/2004JC002278.

Savenije, H. H. G., M. Toffolon, J. Haas, and E. J. M. Veling (2008), Analytical description of tidal dynamics in convergent estuaries, *J. Geophys. Res. Oceans*, *113*(C10025), doi:10.1029/2007JC004408.

Schramkowski, G. P., and H. E. de Swart (2002), Morphodynamic equilibrium in straight tidal channels: Combined effects of coriolis force and external overtides, *J. Geophys. Res. Oceans*, *107*(C12).

Schuttelaars, H. M., and H. E. De Swart (1996), An idealized long-term morphodynamic model of a tidal embayment, *Eur J Mech B-Fluid*, *15*(1), 55–80.

Schuttelaars, H. M., and H. E. de Swart (2000), Multiple morphodynamic equilibria in tidal embayments, *J. Geophys. Res. Oceans*, *105*(C10), 24,105–24,118.

Seminara, G., S. Lanzoni, N. Tambroni, and M. Toffolon (2010), How long are tidal channels?, *J Fluid Mech*, *643*, 479–494.

Souza, A. J., and A. E. Hill (2006), Tidal dynamics in channels: Single channels, *J. Geophys. Res. Oceans*, *111*(C9).

Todeschini, I., M. Toffolon, and M. Tubino (2008), Long-term morphological evolution of funnel-shape tide-dominated estuaries, *J. Geophys. Res. Oceans*, *113*(C5).

Toffolon, M., and H. H. G. Savenije (2011), Revisiting linearized one-dimensional tidal propagation, *J. Geophys. Res. Oceans*, *116*(C07007), doi:10.1029/2010JC006616.

Toffolon, M., G. Vignoli, and M. Tubino (2006), Relevant parameters and finite amplitude effects in estuarine hydrodynamics, *J Geophys Res-Oceans*, *111*(C10014), doi:10.1029/2005JC003104.

Townend, I. (2012), The estimation of estuary dimensions using a simplified form model and the exogenous controls, *Earth Surf Proc Land*, *37*(15), 1573–1583.

Uncles, R. J. (1981), A note on tidal asymmetry in the Severn estuary, *Estuar Coast Shelf S*, *13*(4), 419–432.

Valle-Levinson, A. (2010), Definition and classification of estuaries, in *Contemporary Issues in Estuarine Physics*, edited by A. Valle-Levinson, pp. 1–10, Cambridge University Press, Cambridge, UK.

Van der Burgh, p. (1972), Ontwikkeling van een methode voor het voorspellen van zoutverdelingen in estuaria, kanalen en zeeen, *Rijkwaterstaat Rapport*, pp. 10–72, in Dutch.

van der Wegen, M., and J. A. Roelvink (2008), Long-term morphodynamic evolution of a tidal embayment using a two-dimensional, process-based model, *J. Geophys. Res. Oceans*, *113*(C3).

van der Wegen, M., Z. B. Wang, H. H. G. Savenije, and J. A. Roelvink (2008), Long-term morphodynamic evolution and energy dissipation in a coastal plain, tidal embayment, *J Geophys Res-Earth*, *113*(F3).

Van Rijn, L. C. (2011), Analytical and numerical analysis of tides and salinities in estuaries; part I: tidal wave propagation in convergent estuaries, *Ocean Dynam*, *61*, 1719–1741, doi:10.1007/s10236-011-0453-0.

Vignoli, G., M. Toffolon, and M. Tubino (2003), Non-linear frictional residual effects on tide propagation, in *Proceedings of XXX IAHR Congress*, vol. A, pp. 291–298, Thessaloniki (Greece), 24–29 August 2003.

Wang, Z. B., and I. H. Townend (2012), Influence of the nodal tide on the morphological response of estuaries, *Mar Geol*, *291*, 73–82.

Winterwerp, J. C., and Z. B. Wang (2013), Man-induced regime shifts in small estuaries-I: theory, *Ocean Dynam*, *63*(11-12), 1279–1292.

Wright, L. D., J. M. Coleman, and B. G. Thom (1973), Processes of channel development in a high-tide-range environment - Cambridge Gulf-Ord River Delta, Western Australia, *J Geol*, *81*(1), 15–41.

Zhang, E. F., H. H. G. Savenije, H. Wu, Y. Z. Kong, and J. R. Zhu (2011), Analytical solution for salt intrusion in the yangtze estuary, china, *Estuar Coast Shelf S*, *91*(4), 492–501.

Zhang, E. F., H. H. G. Savenije, S. L. Chen, and X. H. Mao (2012), An analytical solution for tidal propagation in the yangtze estuary, china, *Hydrol Earth Syst Sc*, *16*(9), 3327–3339.

Summary

The ultimate aim of this thesis is to enhance our understanding of tidal wave propagation in convergent alluvial estuaries (of infinite length). In the process, a new analytical model has been developed as a function of externally defined dimensionless parameters describing friction, channel convergence and river discharge. This model has been used to investigate the potential influence of human interventions such as dredging, land reclamation, and freshwater withdrawal on tidal dynamics. The method allows to reproduce the most relevant features of the tidal wave (tidal amplitude, velocity amplitude, wave celerity and phase lag) along the estuary with a minimum requirement of information, such as geometrical data and the tidal forcing at the estuary mouth.

Analytical solutions to the one-dimensional St. Venant equations for tidal hydrodynamics in convergent alluvial estuaries with negligible river discharge can be cast in the form of a set of four implicit dimensionless equations for phase lag, velocity amplitude, damping, and wave celerity, as a function of two localized parameters describing friction and convergence (dependent on tidal amplitude and depth). This method allows comparison of different analytical approaches by rewriting the different solutions in the same format. In this thesis, both classical and more recent formulations are compared, showing the differences and similarities in view of their specific simplifications. The envelope method that subtracts envelopes at high water and low water can be used to derive damping equations that use different friction approximations, resulting in as many analytical solutions, and thereby building one consistent theoretical framework. It is important to note that a multireach approach has to be adopted to follow variations of the estuarine amplitude and depth along the estuary by simple integration of the damping over a distance interval (e.g., 1 km), which is repeated for the entire length of the estuary.

The asymptotic behaviour of tidal damping has also been investigated. A new asymptotic solution of the tidal amplitude has been found that reflects the balance between friction and channel convergence when the distance from the mouth approaches infinity. As a consequence, the usual assumption that the tidal amplitude and velocity amplitude along the estuary axis can be described by an exponential function appears only to be valid for an ideal or frictionless estuary. We also found that tidal amplification is increased with deepening until a maximum value is reached at a critical depth (corresponding to the maximum tidal amplitude). A further increase of depth reduces the tidal amplification until the frictionless standing wave system is reached asymptotically.

The theoretical framework has subsequently been extended to take into account the effect of river discharge, which allows the analytical solutions to be applicable even in the upstream part of an estuary where the influence of river discharge is not negligible. It is observed that the residual water level slope resulting from asym-

metric friction has substantial influence on tidal wave propagation when including the effect of river discharge. The application to the Modaomen and Yangtze estuaries indicates that the proposed model fits the observations with realistic roughness values upstream, while a model with negligible river discharge can be made to fit observations only with unrealistically high roughness values.

The new hydrodynamics model is particularly useful in combination with a salt intrusion model because the coupling reduces the number of calibration parameters and subsequently strengthens the reliability of the salt intrusion model. The application in 6 Malaysian estuaries shows good correspondence between the computed tidal excursion with observed salinities. Conversely, if observed salinities are known, the hydraulic parameters (depth, friction) may possibly be estimated via an inverse model using observed tidal excursion and tidal amplitudes.

In summary, the new framework for analytical solutions of the tidal hydrodynamics equations is more accurate than the explicit analytical model based on the Lorentz linearization. It has been expanded to include river discharge and the effect of variable depth, and it has been coupled with an analytical salt intrusion model. This analytical framework has been proved to perform well in a wide range of estuaries where it has direct value in allowing the assessment of the consequence of human interventions, such as by dredging or water abstractions. More importantly, it provides direct insight in cause-effect relations which are often nonlinear and it is a valuable educational tool to give insight into the inner functioning of a complex hydrodynamic system.

Samenvatting

Het overkoepelende doel van dit proefschrift is om het begrip van de voortplanting van het getij in taps-toelopende alluviale estuaria te vergroten. Al doende is een nieuwe analytische methode ontwikkeld die gebruik maakt van extern gedefinieerde dimensieloze parameters voor: wrijving, convergentie en rivierafvoer. Deze analytische methode is gebruikt om de mogelijke invloed die menselijk handelen zoals uitbaggering, landaanwinning en wateronttrekking heeft op getijdebeweging. Deze methode is in staat om de meest relevante eigenschappen van de getijdegolf (getijamplitude, snelheidsamplitude, voortplantingssnelheid en faseverschil) te reproduceren op basis van een minimum aan informatie, zoals geometrische gegevens en de getijde amplitude aan de monding van het estuarium.

Analytische oplossingen van de een-dimensionale St. Venant vergelijkingen voor getijdebeweging in taps-toelopende alluviale estuaria met geringe bovenafvoer kunnen worden omgewerkt in vier impliciete dimensieloze vergelijkingen voor het faseverschil, de snelheidsamplitude, de demping, de voortplantingssnelheid, als functie van twee lokale parameters die wrijving en convergentie beschrijven (als functie van diepte en getijamplitude). Met deze benadering kunnen alle analytische methodes in hetzelfde formaat beschreven worden, wat een vergelijking tussen de methoden vergemakkelijkt. In dit proefschrift worden klassieke en recente formuleringen vergeleken, waarbij hun verschillen en overeenkomsten worden belicht alsmede de onderliggende aannames. De omhullenden methode, waarbij de omhullenden van hoog en laag water worden afgetrokken, wordt gebruikt om evenzovele dempingsvergelijkingen te verkrijgen als het aantal verschillende parametrisaties van de wrijvingsterm. Een multi-traject methode wordt gebruikt om de variatie van de diepte en de getijamplitude langs de lengteas van het estuarium te volgen.

Het asymptotisch gedrag van de getijdedemping is eveneens bestudeerd. Een nieuwe asymptotische oplossing voor de getijamplitude is gevonden die de balans tussen wrijving en convergentie weergeeft als de afstand vanaf de monding naar oneindig gaat. Dientengevolge blijkt de algemeen gebruikte aanname dat de demping exponentieel verloopt niet houdbaar en alleen geldig voor het triviale geval van een ideaal of wrijvingsloos estuarium. Wij hebben ook geconcludeerd dat opslingering ten gevolge van verdieping van het estuarium een maximale kritieke waarde bereikt. Verdere verdieping leidt tot een afname van de opslingering tot het systeem asymptotisch een wrijvingsloze staande golf benadert.

Het theoretisch kader is vervolgens uitgebreid door rekening te houden met een substantiële bovenafvoer, waardoor de methode ook analytische oplossingen oplevert in het bovenstroomse deel van een estuarium waar de boevenafvoer niet meer verwaarloosbaar is. Wij concluderen dat door de bovenafvoer de opzet van het waterniveau ten gevolge van de asymmetrie van de wrijvingsterm een substantiële invloed heeft op de getijdevoortplanting. De toepassing in de estuaria

155

van de Modaomen (Pearl river) en de Yangtze laten zien dat het nieuwe model de waarnemingen goed weergeeft met realistische waarden voor de ruwheid in het bovenstroomse deel, terwijl een model dat de bovenafvoer niet in beschouwing neemt dit slechts kan met onrealistisch hoge ruwheden.

De nieuwe methode is bij uitstek geschikt om gecombineerd te worden met een analytisch zoutindringingsmodel omdat het koppelen van de twee modellen het aantal ijkparameters reduceert en aldus de betrouwbaarheid van het zoutindringingsmodel versterkt. De toepassing in zes niet eerder bemeten Maleisische estuaria laat een goede overeenkomst zien tussen de voorspelde en gemeten getijweg. Omgekeerd, als zoutmetingen voorhanden zijn kunnen met deze methode de diepte en de wrijving van het estuarium bepaald worden op basis van de waargenomen getijweg en getijamplitude.

Samengevat is de nieuwe impliciete analytische methode nauwkeuriger dan alle klassieke expliciete methodes gebaseerd op de Lorentz linearisatie. Deze methode is uitgebreid om rekening te houden met de rivierafvoer en variabele diepte. Bovendien is het gekoppeld met een analytisch zoutindringingsmodel waardoor de vrijheidsgraden in de ijking verder worden beperkt. Dit analytisch kader heeft zich bewezen in een breed scala aan estuaria, waar het nuttig is om het effect van menselijke interventies, zoals door uitbaggeren of wateronttrekkingen, te analyseren. Bovendien stelt het ons in staat rechtstreeks oorzaak en gevolg van niet-lineaire betrekkingen te doorzien, en is het daardoor een waardevol onderwijskundig instrument om inzicht te verwerven in het functioneren van het complexe hydrodynamische systeem.

List of Figures

List of Tables

Curriculum Vitæ

Huayang Cai

10-06-1986   Born in Fujian, China.
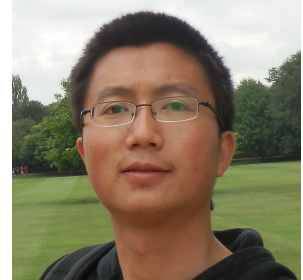
Education

2004–2008   SUN YAT-SEN UNIVERSITY, CHINA
Undergraduate in Geography Science

2008–2010   SUN YAT-SEN UNIVERSITY, CHINA
Master in Physical Geography

Thesis: The influence of river discharge on tidal wave propagation in the Modaomen Estuary, China
supervisor: prof. dr. Qingshu Yang

2010–2014   DELFT UNIVERSITY OF TECHNOLOGY, NETHERLANDS
PhD in Water Resources Section
Thesis: A new analytical framework for tidal propagation in estuaries
promotor: prof. dr. ir. Hubert H. G. Savenije

Short visiting and fieldwork

16.01.2012–16.03.2012   University of Trento, Italy
guest researcher

14.06.2012–07.08.2012   Malaysia
Fieldwork concerning tidal dynamics and salt intrusion

01.08.2013–31.08.2013   HR Wallingford, UK
guest researcher

List of Publications

Journal papers

6. **Cai, H.**, Savenije, H.H.G., Gisen, J.I.A. (2014), *A coupled analytical model for salt intrusion and tides in alluvial estuaries*, Hydrological Sciences Journal, submitted.

5. **Cai, H.**, Savenije, H. H. G., Jiang, C. (2014), *Analytical approach for predicting fresh water discharge in an estuary based on tidal water level observations*, Hydrol. Earth Syst. Sci. Discuss., 11, 7053-7087, doi:10.5194/hessd-11-7053-2014 (open discussion).

4. **Cai, H.**, Savenije, H.H.G., Toffolon, M. (2014), *Linking the river to the estuary: influence of river discharge on tidal damping*, Hydrol. Earth Syst. Sci., 18, 287-304, doi:10.5194/hess-18-287-2014.

3. **Cai, H.**, Savenije, H.H.G. (2013), *Asymptotic behavior of tidal damping in alluvial estuaries*, J. Geophys. Res. Oceans, 118, 1-16, doi:10.1002/2013JC008772.

2. **Cai, H.**, Savenije, H.H.G., Toffolon, M. (2012), *A new analytical framework for assessing the effect of sea-level rise and dredging on tidal damping in estuaries*, J. Geophys. Res., 117, C09023, doi:10.1029/2012JC008000.

1. **Cai, H.**, Savenije, H.H.G., Yang, Q., Ou, S., Lei, Y. (2012), *Influence of river discharge and dredging on tidal wave propagation: Modaomen estuary case*, J. Hydraul. Eng., 138, 885-896, doi:10.1061/(ASCE)HY.1943-7900.0000594.

Conference proceedings

3. **Cai, H.**, Savenije, H.H.G., Kuijper K., *Effect of depth variation on tidal dynamics in the Scheldt estuary*, in the proceedings of the 35th IAHR World Congress, 1-10, Sep. 8-13, 2013 (Chengdu, China).

2. **Cai, H.**, Savenije, H.H.G., Toffolon, M., *The effect of river discharge on tidal dynamics in three alluvial estuaries: Scheldt, Modaomen, Yangtze cases*, in the proceedings of HP1, IAHS-IAPSO-IASPEI Assembly (IAHS), 39-47, Jul. 22-26, 2013 (Gothenburg, Sweden).

1. **Cai, H.**, Savenije, H.H.G., Toffolon, M., *A new analytical framework for assessing the effect of river discharge on tidal damping in estuaries*, in the proceedings of the 7th International Conference on Coastal Dynamics, 261-272, Jun. 24-28, 2013 (Arcachon, France).

Published abstracts

11. **Cai, H.**, H.H.G. Savenije, C. Jiang, *The effect of residual water level slope on tidal propagation in the Yangtze estuary*, European Geosciences Union (EGU), General Assembly, Vienna, Austria, Apr. 27- May 02, 2014.

10. **Cai, H.**, M. Toffolon, H.H.G. Savenije, *Analytical analysis of resonant behaviour in a semi-closed estuary*, European Geosciences Union (EGU), General Assembly, Vienna, Austria, Apr. 27- May 02, 2014.

9. **Cai, H.**, H.H.G. Savenije, M. Toffolon, *A theoretical framework for analyzing the effect of external change on tidal dynamics in estuaries*, American Geosciences Union (AGU), Fall Meeting, San Francisco, Dec. 9-13, 2013.

8. **Cai, H.**, J.I.A. Gisen, H.H.G. Savenije, *Developing a coupled analytical model for analyzing salt intrusion in alluvial estuaries*, American Geosciences Union (AGU), Fall meeting, San Francisco, Dec. 9-13, 2013.

7. **Cai, H.**, H.H.G. Savenije, *Rapid Assessment Techniques for Assessing the Effect of Human Interventions on Tidal Dynamics and Salt Intrusion in Estuaries*, BIT's 3rd Annual World Congress of Marine Biotechnology, Hangzhou, China, Sep. 23-25, 2013.

6. **Cai, H.**, H.H.G. Savenije, M. Toffolon, *Analytical solutions of tidal dynamics in convergent estuaries: a comparison*, European Geosciences Union (EGU), General Assembly, Vienna, Austria, Apr. 7-12, 2013.

5. **Cai, H.**, H.H.G. Savenije, M. Toffolon, *A new analytical framework for understanding the tidal damping in estuaries*, European Geosciences Union (EGU), General Assembly, Vienna, Austria, Apr. 7-12, 2013.

4. **Cai, H.**, M. Toffolon, H.H.G. Savenije, *Application of the lagrangian approach to calculate dispersion coefficient in estuaries*, European Geosciences Union (EGU), General Assembly, Vienna, Austria, Apr. 22-27, 2012.

3. **Cai, H.**, H.H.G. Savenije, *Explicit solution of the tidal damping equation in alluvial estuaries*, European Geosciences Union (EGU), General Assembly, Vienna, Austria, April 22-27, 2012.

2. **Cai, H.**, H.H.G. Savenije, M. Toffolon, *Exploring linear and nonlinear solutions to the tidal hydraulic equations*, European Geosciences Union (EGU), General Assembly, Vienna, Austria, Apr. 3-8, 2011.

1. **Cai, H.**, H.H.G. Savenije, Q. Yang, S, Ou, Y. Lei, *The influence of recent change in river discharge and bathymetry on tidal wave propagation in the Modaomen estuary, China*, European Geosciences Union (EGU), General Assembly, Vienna, Austria, Apr. 3-8, 2011.

Acknowlegements

Huayang Cai
Delft, July 2014